Technical Report Documentation Page

1. Report No.	2. Government Accession No.	3. Recipient's Catalog No.
FAA-RD-74-54		

4. Title and Subtitle	5. Report Date
IMPACT OF SATELLITE AERONAUTICAL CHANNEL ON MODEM SPECIFICATIONS	March 1974
	6. Performing Organization Code
7. Author(s) Phillip A. Bello, Charles J. Boardman, David Chase, Joseph K. DeRosa*	8. Performing Organization Report No. DOT-TSC-FAA-74-1
9. Performing Organization Name and Address CNR, Inc. 20 Wells Ave. Newton MA 02159	10. Work Unit No. (TRAIS) FA411/R4107 11. Contract or Grant No. DOT-TSC-516-1
12. Sponsoring Agency Name and Address Department of Transportation Federal Aviation Administration Systems Research and Development Service Washington DC 20590	13. Type of Report and Period Covered Final Report-Phase I Aug. 1972 - March 1973 14. Sponsoring Agency Code

15. Supplementary Notes

*Under contract to: Department of Transportation
Transportation Systems Center
Kendall Square
Cambridge MA 02142

16. Abstract

This report analyzes the effects of surface-scattered multipath on the performance of ranging and data modems such as might be used on the aircraft-satellite channel of an air-traffic control system. An exact analysis is carried out on the effects of noise and multipath on the one-way ranging errors of a single-sideband tone ranging modem. These results are shown to be applicable at high SNR and direct path/multipath ratios to a double-sideband tone ranging modem whose sideband separation equals the tone separation in the single sideband system. The conventional practice of calculating ambiguity error probabilities with an assumption of Gaussian ranging error distribution is shown to be inapplicable for many situations of practical interest. Computations of ranging and data modem performance for a candidate hemispherical coverage antenna are carried out which lead to the conclusion that there are critical cost trade-offs between modem advanced signal processing and antenna design. Consideration is given to the design trade-offs of a channel prober to collect information useful both for stored-channel playback and channel parameter extraction. The need for additional channel measurements is discussed.

17. Key Words	18. Distribution Statement
Aircraft-Satellite Channel Characterization, Tone Ranging Modem Multipath Performance, Pseudo-Noise Ranging Multipath Performance, Channel Measurement	DOCUMENT IS AVAILABLE TO THE PUBLIC THROUGH THE NATIONAL TECHNICAL INFORMATION SERVICE, SPRINGFIELD, VIRGINIA 22151.

19. Security Classif. (of this report)	20. Security Classif. (of this page)	21. No. of Pages	22. Price
Unclassified	Unclassified	310	

Form DOT F 1700.7 (8-72) Reproduction of completed page authorized

PREFACE

The work documented in this final report is part of an advanced technology task undertaken by the Electromagnetics Division, Communications Branch, of the Technology Directorate at the Transportation Systems Center in support of the Department of Transportation's program to investigate satellite-based air traffic control systems.

Technical associations with Louis A. Frasco and H. David Goldfein of the Transportation Systems Center are hereby acknowledged.

LIST OF ILLUSTRATIONS

Figure		Page
1.1	Utilization of Channel Measurements in Modem Development	1-4
1.2	Channel Characterization Model	1-8
1.3	Important System Function Characteristics	1-10
1.4	Distribution of Multipath Ratio in Azimuth Over Smooth Sea Water	1-17
1.5	RMS and Bias Ranging Errors as a Function of Specular/Scatter Ratio for a Tone Ranging System	1-19
1.6	Distribution of One-Way RMS Ranging Error Over Azimuth for 10^{o} Elevation. Side-Tone Ranging With 8 KHz Tone	1-21
1.7	Probability of Exceeding a Given (Absolute) Ranging Error	1-27
1.8	RMS Ranging Error as a Function of Direct Path/ Scatter Ratio for PN Ranging System	1-31
1.9	Comparison of FSK and DPSK as a Function of γ	1-36
1.10	Distribution of Error Probability for 10^{o} Elevation Angle for Turnstile Antenna of Fig. 1.3	1-38
1.11	Definition of Flat and Total Bandwidths for Equipment Channel	1-47
1.12	Major Functional Blocks of Channel Prober	1-49
1.13	Block Diagram of Prober Demodulator	1-51
1.14	Illustration of Coherent Complex Demodulation Operation	1-54
1.15	Prober Demodulators With Correlators Spaced at One-Half the PN Pulse Width	1-55
1.16	Simultaneous Measurement of Vertical and Horizontal Antenna Channel Characteristics	1-59

LIST OF ILLUSTRATIONS (Continued)

Figure		Page
1.17	Power in Tail of Delay Power Spectrum	1-62
2.1	Channel Model	2-2
2.2	Simplified Block Diagram of Receiver Processing	2-5
2.3	Double-Side-Band Fine Ranging Estimation	2-29
3.1	Multipath Channel Model	3-3
3.2	Code and Carrier Tracking Loops of a PN Ranging Receiver	3-5
3.3	Asymptotic Performance of PN Ranging in Additive Noise Alone	3-13
3.4	Performance of PN Ranging System in the Presence of Flat Fading Multipath Alone	3-17
3.5	Performance of Tone Ranging System in the Presence of Additive Noise Alone	3-20
3.6	Factors Appearing in the Multipath Error Results	3-24
4.1	Interleaving the Encoded Data Block of Length N Over an L Bit Span	4-8
4.2	Interleaving Information Blocks of Length K Over an L Bit Span	4-10
4.3	Coding Gain for the Gaussian Channel	4-13
4.4	Coding Gain for the Independent Slow Fading Rayleigh Channel	4-14
4.5	Block Diagram of a Multiple Rate Encoder (Basic Rate = K/N, Burst Correction Rate = $(K+K_1)/N$)	4-18
4.6	Diagram of Data Combining for a Multiple Rate Code	4-20

LIST OF ILLUSTRATIONS (Continued)

Figure		Page
4.7	Block Diagram for Decoding at R = K/N - Configuration #1	4-23
4.8	Block Diagram for Decoding at R = K/N - Configuration #2	4-24
4.9	Generation of a Burst Correction Signal	4-26
4.10	Block Diagram for Decoding at R = $(K+K_1)/N$ and Recovery of $\underline{I}^{(1)}_{K_1-B}$	4-28
5.1	Definition of Basic Signal Processing Operations in Prober System	5-3
5.2	Channel Playback	5-4
5.3	Transfer Function of Stored Channel for Single Path	5-15
5.4	A Channel Multiplexed Prober Demodulator	5-25
6.1	Representation of Surface Scatter Channel	6-2
6.2	Geometrical Relationships for Scattering in Airplane-Synchronous Satellite Channel Assuming Flat Mean Earth Surface	6-11
6.3	Delay Power Spectrum for Diffuse Scatter	6-19
6.4(a)	Magnitude of Frequency Correlation Function for Diffuse Scatter	6-20
6.4(b)	Angle of Frequency Correlation Function for Diffuse Scatter	6-21
B.1	Relevant to Open Loop Characteristics of PN Ranging Receiver	B-2
D.1	Open Loop Error Voltage, α=0.7, t_d=1.2 bits, θ_m=0	D-6

LIST OF ILLUSTRATIONS (Continued)

Figure		Page
D.2	Open Loop Error Voltage, α=0.7, t_d = 1.2 bits, θ_m=0	D-7
D.3	Code Loop Tracking Error as a Function of Multipath Delay, for Fixed Multipath Phase (α=0.7)	D-8
D.4	Open Loop Error Voltage, α=0.7, t_d=0.5, θ_m=π	D-10
D.5	Phase and Timing Error Trajectories (t_d=0.5) (Points on the Trajectories Corresponding to θ_m=0, $\pi/2$, π, and $3\pi/2$ are Indicated)	D-12
D.6	Receiver Pulse Shapes	D-14
D.7	The Correlation Function R(t)	D-17
D.8	The Correlation Function S(t)	D-18
D.9	Functions Related to Performance in Additive Noise	D-21
E.1	Basic (Complex-Equivalent) Signal Processing Operations in Prober	E-4
E.2	Rearranged Signal Processing Operations of Prober	E-5

TABLE OF CONTENTS

Section		Page
1	INTRODUCTION AND SUMMARY	1-1
	1.1 Relationship Between Modem Development and Channel Characterization	1-3
	1.2 Channel Measurements Available and Needed	1-7
	1.3 Effect of Multipath on Side-Tone Ranging Systems	1-15
	1.3.1 Effect of Multipath on RMS Ranging Error	1-16
	1.3.2 Ambiguity Error Considerations	1-25
	1.4 Effect of Multipath on a Pseudo-Noise Ranging Modem	1-30
	1.5 Effect of Multipath on Data Transmission	1-35
	1.6 Specification of an Airplane-Satellite Channel Prober	1-41
	1.6.1 General Description System Operation	1-45
	1.6.2 Prober Demodulator	1-50
	1.6.3 Horizontal-Vertical Antenna Multiplexing	1-58
	1.6.4 Prober Parameters for Aerosat Channel Probing	1-60
	1.7 Conclusion	1-70
2	EFFECT OF TIME AND FREQUENCY SELECTIVE FADING ON TONE RANGING SYSTEMS: PRELIMINARY ANALYSIS	2-1
	2.1 Channel Model	2-1
	2.2 Representation of Signals	2-4
	2.3 Receiver Processing	2-4
	2.4 Performance With Additive Noise	2-8
	2.5 Performance With Fading and Additive Noise	2-14
	2.6 Inclusion of Effects of Channel Characteristics for an Airplane-Satellite/Link	2-23
	2.7 Use of Single-Side-Band Analysis for a Double-Side-Band System	2-27
3	EFFECT OF TIME AND FREQUENCY SELECTIVE FADING ON A PN RANGING SYSTEM	3-1
	3.1 Introduction	3-1
	3.2 Channel Model	3-2
	3.3 Receiver and Signal Model	3-4
	3.4 Open Loop Error Voltages	3-7
	3.5 High Direct-to-Scatter and High Direct-to-Additive Noise Case	3-11
	3.6 Flat Fading Case	3-14
	3.7 Comparison of Tone and PN Ranging Performance	3-18

TABLE OF CONTENTS (Continued)

Section		Page
	3.7.1 Introduction	3-18
	3.7.2 Performance in the Presence of Additive Noise	3-19
	3.7.3 Performance in the Presence of Multipath	3-21
4	SIGNAL DESIGN CONSIDERATIONS FOR A FAST FADING RICIAN CHANNEL	4-1
	4.1 Introduction	4-1
	4.2 Channel Model Parameters	4-1
	4.3 Modulation Approaches	4-3
	4.4 Advanced Signal Design Concepts	4-6
	4.4.1 Decoding Interleaved Block Codes With Channel Measurement Information	4-7
	4.4.2 Multiple Rate Codes and Adaptive Decoding	4-12
5	THE MEASUREMENT AND REPRODUCTION OF A TIME-VARIANT LINEAR CHANNEL	5-1
	5.1 System Description	5-2
	5.2 Formulation of Prober Output	5-5
	5.3 Operation of Channel Playback	5-13
	5.4 Pseudo-Random Probing	5-16
	5.5 Output SNR of Prober	5-20
	5.6 Analysis of Multiplexed Operation of Channel Prober	5-24
6	STEEPEST DESCENT CHANNEL MODEL	6-1
	6.1 Direct Path Channel	6-1
	6.2 Specular Reflection Channel	6-3
	6.3 Diffuse Scatter Channel	6-6
	6.4 Conclusion	6-26
Appendix A	PROBABILITY DENSITY FUNCTION OF THE PHASE DIFFERENCE BETWEEN TWO CORRELATED NON-ZERO-MEAN COMPLEX GAUSSIAN VARIATES	A-1
Appendix B	OPEN LOOP ERROR VOLTAGES OF A PN RANGING RECEIVER	B-1
Appendix C	ASYMPTOTIC SOLUTION OF THE LOOP TRACKING EQUATIONS OF A PN RECEIVER	C-1

TABLE OF CONTENTS (Continued)

Section		Page
Appendix D	FLAT FADING SOLUTION OF THE TRACKING EQUATIONS OF A PN RECEIVER	D-1
Appendix E	EFFECT OF GROUP DELAY TRACKING ERROR ON PLAYBACK CHANNEL SIMULATION	E-1
Appendix F	EFFECT OF TAP CORRELATOR GAIN AND PHASE INSERTION ON STORED CHANNEL FIDELITY	F-1
Appendix G	SCATTERING FUNCTION FOR GENERAL VELOCITY VECTOR	G-1
Appendix H	REPORT OF INVENTIONS	H-1

LIST OF TABLES

Table		Page
1-1	Azimuth Median One-Way RMS Ranging Error as a Function of Tone Filter Effective Multipath Reduction Factor for a Specific Set of Geometric and Propagation Parameters and Curved Arm Turnstile Antenna	1-23
1-2	Illustration of Variation of Ranging Error With Multipath Spread	1-24
1-3	Table Showing the Maximum Fine Ranging Frequency Allowed in SSB Tone Ranging to Achieve Less Than a Given Ambiguity Error Probability at a Specified Percentage of Azimuth Angles When Ambiguity is Resolved With a 16 KHz Tone	1-29
1-4	Azimuth Median One-Way RMS Ranging Error as a Function of Tone Filter Effective Multipath Reduction Factor for a Specific Set of Geometric and Propagation Parameters and Curved Arm Turnstile Antenna	1-32
1-5	Illustration of Variation of Ranging Error With Multipath Spread	1-33
1-6	Pe as a Function of γ for FSK	1-39
1-7	Pe as a Function of γ for DPSK	1-42
1-8	Pe as a Function of γ for FSK Combined With Advanced Signal Design Concepts	1-43
1-9	Pe as a Function of γ for DPSK Combined With Advanced Signal Design Concepts	1-44
4-1	Error Performance Coding Gain for the Gaussian and Rayleigh Fading Channels	4-15

SECTION 1
INTRODUCTION AND SUMMARY

The effort represented here supports the Department of Transportation's program to provide a satellite-based air traffic control system. In particular, the objective of this study is to develop analysis techniques and measurement procedures to quantitatively describe the impact of the satellite aeronautical channel on modem (modulator-demodulator) specifications.

Satellite-based air traffic control systems are subject to certain serious performance limitations because of the multipath interference due to scattering and reflection off the surface of the earth. Proper design of the ATC system must take account of this multipath. Theoretical analyses characterizing the multipath have been available for some time [1.1], [1.2] (and more recently [1.3]). Recently multipath measurement experiments have been run by Boeing [1.4] for the FAA utilizing a KC-135 jet aircraft and the spinning ATS-5 satellite. The results of the Boeing measurements have been utilized in preparing overall AEROSAT system performance specifications. Additional measurements are recommended in this report to further support the design and development of L-band avionics. This first generation of L-band avionics are intended for experimentation and evaluation with the AEROSAT system and with possible CONUS satellite ATC test beds.

Section 1.1 presents a general approach to the development of modems with the aid of channel measurements, modeling, and simulation. In Section 1.2 a comparison is given between the classes of measurements obtained in the Boeing tests and those needed for system and signal design. Following this, Section 1.3 will present estimated RMS ranging errors and

ambiguity probabilities for tone ranging systems utilizing the "steepest descent" channel model which has been partially validated by the Boeing experiments. The calculations also involve computations of the multipath spread characteristics of the indirect paths and assumptions about antenna discrimination against multipath for candidate antennas. The analyses supporting these results are presented in Section 2. A similar performance analysis for a PN ranging modem is presented in Section 1.4 utilizing the analysis of Section 3.

In Section 1.5 the effect of multipath on the performance of FSK and DPSK modems is presented for the same set of channel and system parameters as the ranging modems. The benefit to be obtained by advanced signal design techniques is also discussed. Section 4 presents the analytical backup to Section 1.5.

Section 1.6 discusses a channel probing technique that will allow the collection of channel characteristics both for statistical analysis and for channel playback simulation at some future time. The analytical background to Section 1.6 is presented in Section 5. Section 6 presents some additional results on the "steepest-descent" model for the multipath and Doppler spread characteristics of the airplane-satellite channel.

Section 1.7 presents some salient conclusions and discusses the consequences of proceeding with candidate hardware development and demonstration tests without further channel measurements.

1.1 Relationship Between Modem Development and Channel Characterization

The most effective approach to the development of optimum modulation and demodulation techniques for a specific class of channels involves a sequence of steps as diagrammed in Fig. 1.1. These steps involve the measurement and modeling of channel characteristics to provide the basis for optimum modem design concepts and the utilization of channel simulators for the development, acceptance testing, and comparative evaluation of implemented modems prior to field testing.

As indicated in Fig. 1.1, the design of the channel measurement experiment involves an initial analytic modeling effort to determine the relationship between significant parameters in the propagation and system function models of the channel. From this modeling effort one may estimate multipath spreads, Doppler spreads, frequency correlation functions, delay power spectra, etc. as a function of propagation channel parameters such as sea state and wavelength and as a function of system parameters such as range, velocity vectors of terminals, antenna patterns, etc. The proper design of the channel probing signal, measurement equipment, and data reduction requires at least that a gross estimate of maximum multipath spread and Doppler spread be available and that the bandwidth be specified over which the channel is to be characterized.

The channel measurement experiment should involve both propagation and system function type measurements in order to validate the initially estimated relationship between the two channel models. It is important to develop such validated

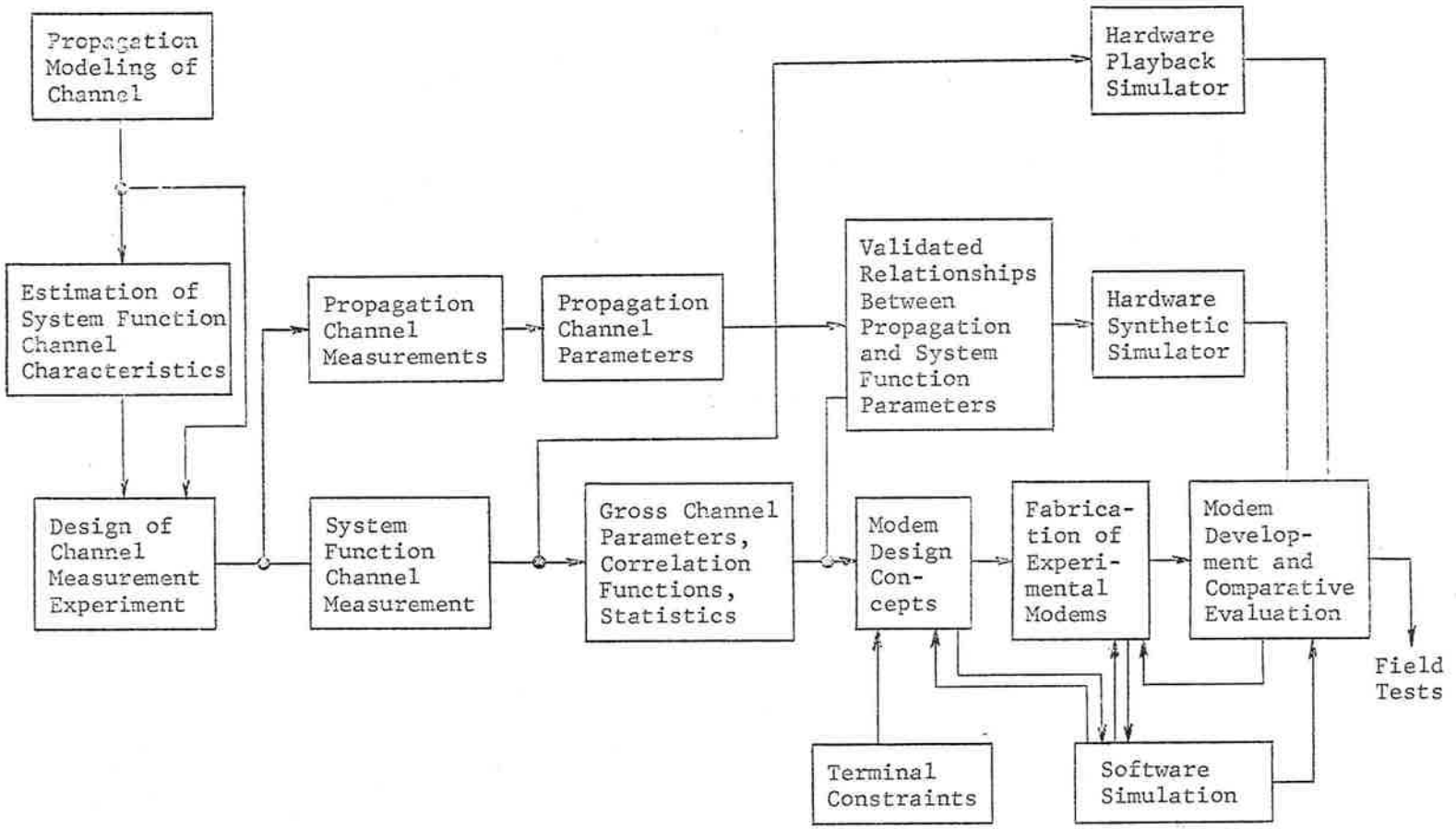

Figure 1.1. Utilization of Channel Measurements in Modem Development

relationships because the time and expense associated with channel measurements prevent the collection of measurements under all physical cases of interest. Thus for example in airplane-satellite channel measurements it is desirable that sea state be measured. If, on the basis of measurements, validated relationships have been developed between, say, sea state and multipath spread, then it will be possible to estimate the effects of other sea states even though such states did not occur in the experiments.

System function channel measurements connected with the multiplicative (distorting) and additive disturbances may be taken separately because of their independence. The signal distortion properties of the channel are characterized by measurements at four levels of increasing complexity:

1. Measurement of gross parameters of system function (e.g., coherence bandwidth, Doppler spread, etc.)
2. Measurement of correlation functions of system functions (e.g., frequency correlation function, delay power spectrum, etc.)
3. Measurement of probability distributions of system functions (e.g., probability distributions of amplitude and phase on a received carrier)
4. Measurement of system functions (e.g., time-variant transfer function and impulse response).

Measurements 1 - 3 in conjunction with terminal constraints, such as bandwidth and power, are useful for bounding the distortions caused by the channel and allow a considerable narrowing of the possible modulation and demodulation techniques to be considered.

In the development of modems both software and hardware simulators are useful. Software simulations are useful during the early stages of modem development where modem concepts are checked out for inclusion in design specifications and where acceptance specifications are developed. They are also useful during the design of the modem by allowing a prediction of performance degradation that would be caused by a proposed design change. The hardware simulator comes into play when modems have been built, both for final checkout and adjustment of the modem prior to acceptance testing, and for the acceptance testing itself.

Two basic types of channel simulators may be identified, each having separate functions in modem development. These two types of simulators are called the synthetic channel simulator and the playback channel simulator. The synthetic channel simulator creates a reproducible channel which has average statistical properties approximating the measurements 1 - 3. Due to the validated relationships between the system function and propagation channel parameters it is then possible to create synthetic channel conditions which would have been observed if sufficient time could have been expended in the channel measurements. For example, in the case of sea states one might deduce that certain sea states not actually observed in the propagation measurements are still reasonably likely and would produce certain multipath structure. The synthetic channel can be set to model this situation.

The playback channel is used to recreate the same instantaneous system functions that were measured in 4 above, with

appropriate measured additive noise, if ordinary thermal noise is not sufficient. Whereas only the approximate statistical behavior is reproduced by the synthetic simulation, the exact instantaneous system function (and representative noise) that existed during the measurements is "played back" by the playback simulation. While the synthetic simulator is of great help in checking out bit-sync tracking and acquisition, and further narrowing the modems of interest through comparative modem performance evaluation under identical conditions, these conditions only approximate the statistical behavior of the actual channel. In order to achieve low error rates in digital communication it is necessary to consider the rare events on the "tails" of probability distributions which cannot be reproduced by the synthetic channel. However, all such rare events which have occurred in the system functions during channel measurements will be accurately reproduced by the playback simulator. Note, moreover, that the playback channel allows a comparative evaluation of modem performance over the same time-bandwidth portion of an actual channel, a feat which is impossible in direct field testing of modems!

1.2 Channel Measurements Available and Needed

Figure 1.2 shows that the input-output characteristics of the aircraft-satellite link are dependent upon geometrical factors (e.g., aircraft position, velocity, and attitude) terminal equipment characteristics (e.g., antenna patterns) and propagation parameters (e.g., reflection coefficient, surface roughness). A useful mathematical model of the aircraft-satellite channel must include relationships between the input-output or

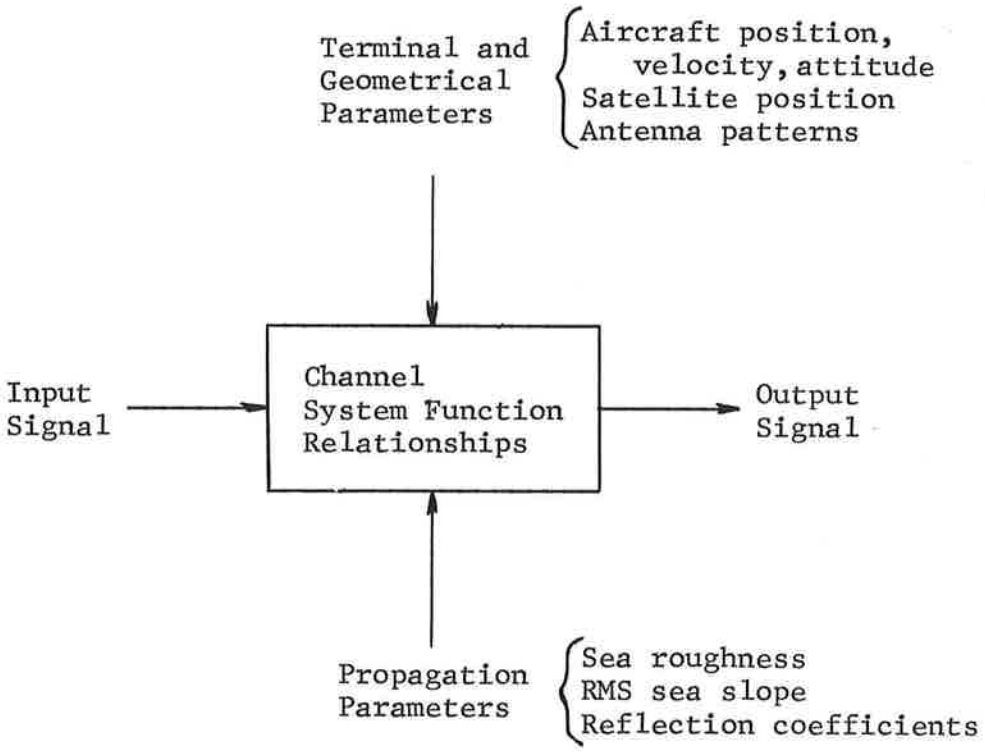

Figure 1.2 Channel Characterization Model

system function characteristics of the link and the geometrical, terminal, and propagation parameters. A basic objective of channel characterization experiments is the validation of such models, because they provide basic tools for modem design in the ATC system.

Figure 1.3 lists various important system function characteristics and notes whether the Boeing experiments investigated them. As discussed in Section 1.1 these input-output characteristics are classed into four groups:

- gross parameters
- second-order parameters
- statistics
- system functions.

In the case of gross channel parameters we have listed five items:

- direct path/multipath received power for an effective omni-antenna
- direct path/multipath received power for candidate operational antennas
- Doppler spread of diffuse multipath
- multipath spread of diffuse multipath
- specular/diffuse multipath ratio.

Knowledge of the ratio of received signal power on the direct path relative to the power received on the indirect paths is clearly of major importance in system design. This ratio depends upon the polarizations of transmitting and receiving antennas, the ratio of antenna gains in the direct path and specular directions, and the reflection coefficients

		BOEING-FAA Experiments
Gross Parameters	Direct path power/multipath power for effective omni-antenna	Yes
	Direct path power/multipath power for candidate operational antennas	No
	Doppler spread	Yes
	Multipath spread	No
	Specular/diffuse multipath ratio	Yes
Second Order Parameters	Doppler power spectrum	Yes
	Delay power spectrum and/or frequency correlation function	No
	Delay-Doppler scatter function	No
Statistics	First order	Yes
	Second order	No
System Functions	Time variant transfer function	No
	Time variant impulse response	No

Figure 1.3 Important System Function Characteristics

at the surface. The Boeing measurements involved two separate antennas, one pointed in the direct path direction and the other approximately* in the specular direction where the multipath is expected to be returned. The receiving multipath antenna on the aircraft was capable of right or left-hand nominal circular polarization and horizontal or vertical linear polarization. Knowing the appropriate antenna and RF amplifier gains the Boeing measurements of received power allow (for small enough sea states*) a determination of the direct path/multipath power that would be received on an omni-antenna of a given polarization characteristics. Within the experimental accuracy of the experiment it has been concluded that the reflection coefficients from the surface of the sea essentially follow the theoretical behavior predicted by Beckmann and Spizzichino [1.5] for diffuse (non-specular) scattering from the sea.

The direct/multipath ratio of immediate importance in signal design is that for an aircraft using a realistic operational-type aircraft antenna. Unfortunately, this type of measurement was not carried out in the Boeing experiments. One may couple ground measurements of candidate antennas with the effective omni-antenna results of the Boeing measurements to infer direct/multipath ratios for an operational antenna. In the following section we shall present such an inference for a

*The multipath antenna was fixed, so that maximum gain was generally not in the specular direction. A gain correction was computed to account for this offset in the measured data.

particular antenna considered to be rather good by Mallinckrodt [1.2]. It will show that while considerable discrimination against multipath can be expected at the higher elevation angles, it cannot be expected at the lower angles. In fact at 10^{o} elevation angle it may happen for some azimuth angles that the antenna will have a higher gain for the multipath than for the direct path.

The gross parameters of Doppler spread and multipath spread associated with the indirect paths are necessary in characterizing bounds on the distortions produced by the aircraft-satellite channel on a particular transmitted signal. Thus in side-tone ranging systems one may estimate a reduction in effective multipath interference by the ratio of the pilot tone filter bandwidth to the Doppler spread when the Doppler spread is much larger than the filter bandwidth. In data transmission by differentially coherent PSK, decorrelation between adjacent bits caused by rapid fading introduces an irreducible error rate. This may be roughly estimated from the Doppler spread. The multipath spread is also important in estimating performance and designing ranging and data modems. For smooth seas the indirect paths will be clustered together in path delay with the minimum path delay relative to the direct path equal to that of the point of mirror reflection at the surface. The frequency selective fading characteristics of the channel will then be wholly determined by the direct/multipath ratio and the direct/specular path delay. <u>However at the lower elevation angles, say 10^{o}, and rough seas such as are found in the North Atlantic in winter, the multipath spread of the indirect paths can be estimated to be larger than the direct-specular point</u>

path delay and have a significant influence on signal distortion and effective signal design.

Boeing has measured Doppler spreads at various elevation angles in conjunction with measurements of RMS sea slopes and reports that the results check rather well with theoretical predictions of Staras [1.1] and Mallinckrodt [1.3] based upon a "steepest-descent" approximation to Beckmann and Spizzichino's [1.5] surface scattering cross/section expression. No multipath spread measurements were undertaken by Boeing. Such measurements should be taken to check the steepest descent model predictions.

We consider now selected second order average characteristics of system functions:

- Doppler power spectrum
- delay power spectrum and/or frequency correlation function
- delay-Doppler scatter function.

These functions are needed for an accurate determination of the time and frequency selective distortion characteristics of the channels and the amount of diversity obtainable from signal design. The Doppler power spectrum is just the spectrum of a received carrier. Such spectra were measured by Boeing and were found to follow the Gaussian shape predicted by the steepest descent model [1.2]. The delay power spectrum describes the intensity of diffuse scattered power as a function

of path delay. The Fourier transform of the delay power spectrum is the complex frequency correlation function which describes the complex correlation between received carriers as a function of their frequency separation. Neither one of these functions was measured by Boeing. The delay power spectrum (which is easier to measure) should be measured and compared to the steepest descent predictions ([1.2], [1.3] and Section 6). The delay-Doppler scatter function, which also has not been measured, describes the distribution of diffuse scatter power at different delays and Doppler shifts.

Knowledge of the average dispersive properties of the aircraft-satellite channel must be complemented by knowledge of the statistics of fluctuations of the received multipath signal, in order to carry out performance analysis. Measurements by Boeing of the envelope of the sum of the direct path and multipath antenna outputs have shown a probability distribution conforming closely to the Ricean distribution which lends support to the complex Gaussian model for the multipath signal.

The most inclusive measurements one may make on a linear channel are the impulse response and transfer function. For a time-variant channel, like the aircraft-satellite channel, these system functions become time variant. It is feasible to measure and tape-record these transfer functions. As pointed out in Section 1.1 the utility of such a measurement and storage on tape is that it is possible to utilize this tape to recreate the channel with hardware or software at some future date. This will allow the testing in the laboratory of many different modem

designs under the same realistic channel conditions without continually mounting field experiments and without making assumptions about channel statistics.

1.3 Effect of Multipath on Side-Tone Ranging Systems

In this section we shall present calculations of the RMS ranging error caused by multipath in side-tone ranging systems. Presently available multipath measurements, such as those of Boeing, while helpful in lending credence to the "steepest-descent" model, do not allow a direct calculation of rms ranging error because no measurements were carried out on

1) direct path/multipath ratios with candidate operational antennas at different elevation angles, and
2) delay power spectra or frequency correlation functions of the multipath channel for various geometrical and propagation parameters.

Calculations of ranging error due to multipath require that certain models, not yet experimentally validated, be assumed to characterize 1) and 2) above. To determine values for direct/multipath ratios for candidate operational antennas we proceed in two steps. First we shall assume that the Boeing measurements have justified the theoretical reflection coefficients for diffuse scatter proposed by Beckmann and Spizzichino [1.6], Mallinckrodt [1.2], and Staras [1.1]. Then we can combine the theoretical reflection coefficients with a measured antenna pattern. This combination of steps has actually been carried out by Mallinckrodt [1.2] for a curved arm turnstile antenna as we have indicated in Fig. 1.4. At a given elevation

angle the multipath (direct/multipath power) ratio is estimated from the equation

$$\Gamma = D + 20 \log \frac{1}{R(\theta)} \triangleq 10 \log_{10} \gamma,$$

where D is the discrimination in dB measured for the antenna between the assumed direct path elevation angle θ and the multipath angle $-\theta$, and $R(\theta)$ is the smooth sea reflection coefficient for the appropriate polarization. At low elevation angles antenna vertical polarization appears to be the dominant mode of propagation. The antenna pattern measurements were carried out with θ fixed and azimuth angle varied. Figure 1.4 shows the multipath ratio expressed as a probability distribution along the azimuth direction for a fixed θ. Note that at $\theta = 10^{o}$, 50% of the azimuth angles had multipath ratios less than 7 dB. At 20^{o} the 50% point increases to around 18 dB.

In order to model the delay power spectra and frequency correlation function of the multipath channel we have used the steepest descent model results given in [1.1], [1.2] and [1.3]. We have also assumed the complex Gaussian model for the diffuse multipath signal, which has been partially validated by the Boeing measurements. With these models it is possible, in principle, to evaluate the ranging error statistics for any ranging modem.

1.3.1 Effect of Multipath on RMS Ranging Error

Section 2 derives results on one-way ranging errors for a single-sideband tone ranging modem that are valid at all SNR, γ, and channel dispersive conditions. It is shown in Section

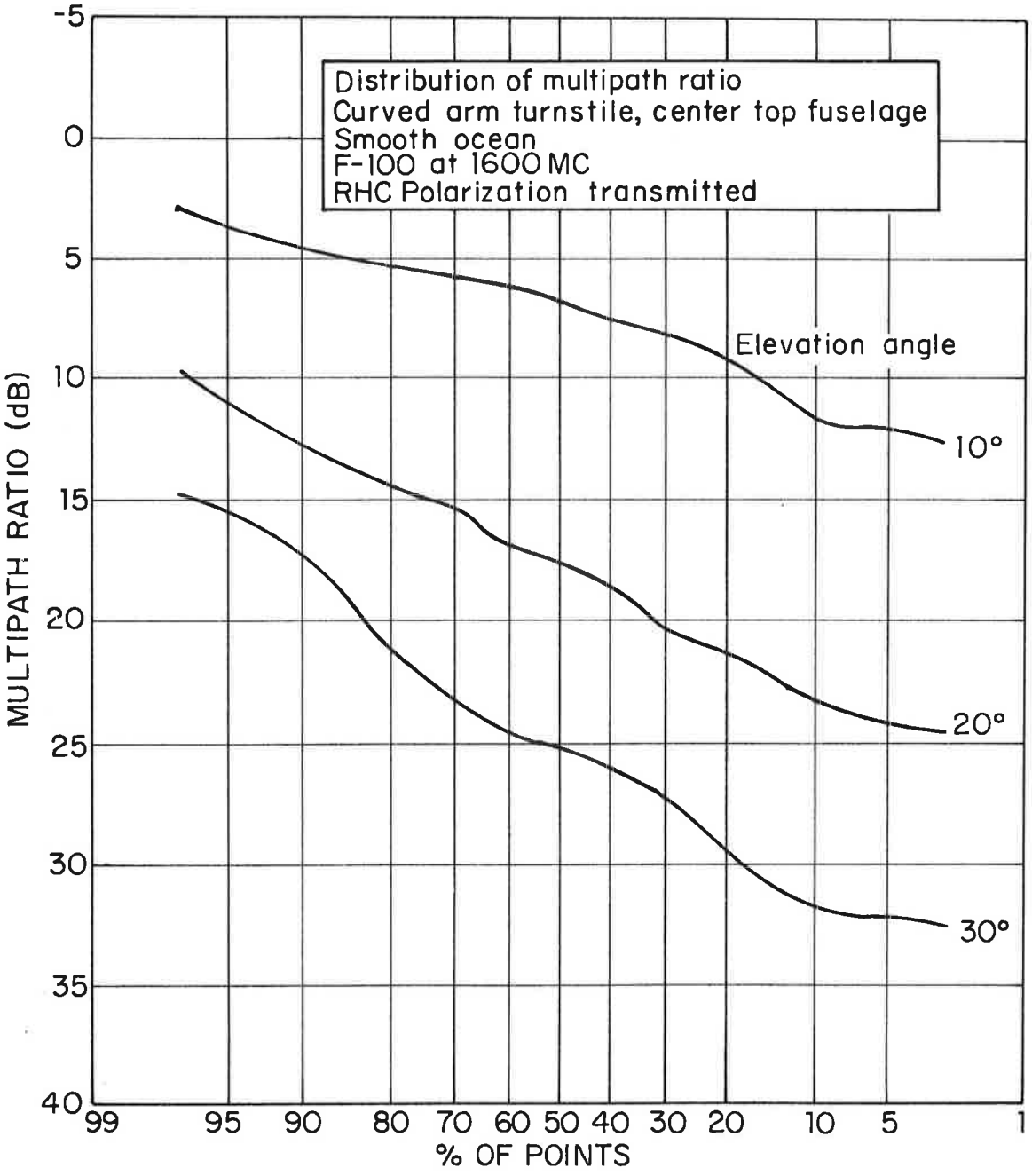

Figure 1.4 Distribution of Multipath Ratio in Azimuth Over Smooth Sea Water

2.7 that at SNR = ∞ and large γ the ranging errors for a double-sideband system with tone frequency F will be very nearly the same as those for a single-sideband system with tone frequency 2F.* To obtain the rms ranging errors it is necessary to operate at such large values of γ at the tone filter outputs that this equivalence of performance will be valid. In the curves to be presented we have used this approximate equivalence at all values of γ for an 8 KHz double-sideband system. Thus at low values of γ (<10 dB) it should be understood that the rms error results are strictly correct only for a single-sideband system using 16 KHz tone frequency spacing.

Figure 1.5 presents calculated rms and bias one-way ranging errors as a function of multipath ratio γ for a 10° elevation angle, assuming an rms sea slope of .1 and an aircraft height of 30,000 ft. No reduction in the strength of the multipath signal by the tone filter is assumed in the results. To approximately take account of such filtering, γ can be increased by the ratio of Doppler spread to tone filter bandwidth. In Fig. 1.5 an 8 KHz ranging tone is assumed. The calculation for a different ranging tone frequency involves the multipath channel's frequency correlation function as discussed in Section 2. It should be

*It is argued, heuristically, that the range errors of the latter system should lower-bound the range errors of the former system.

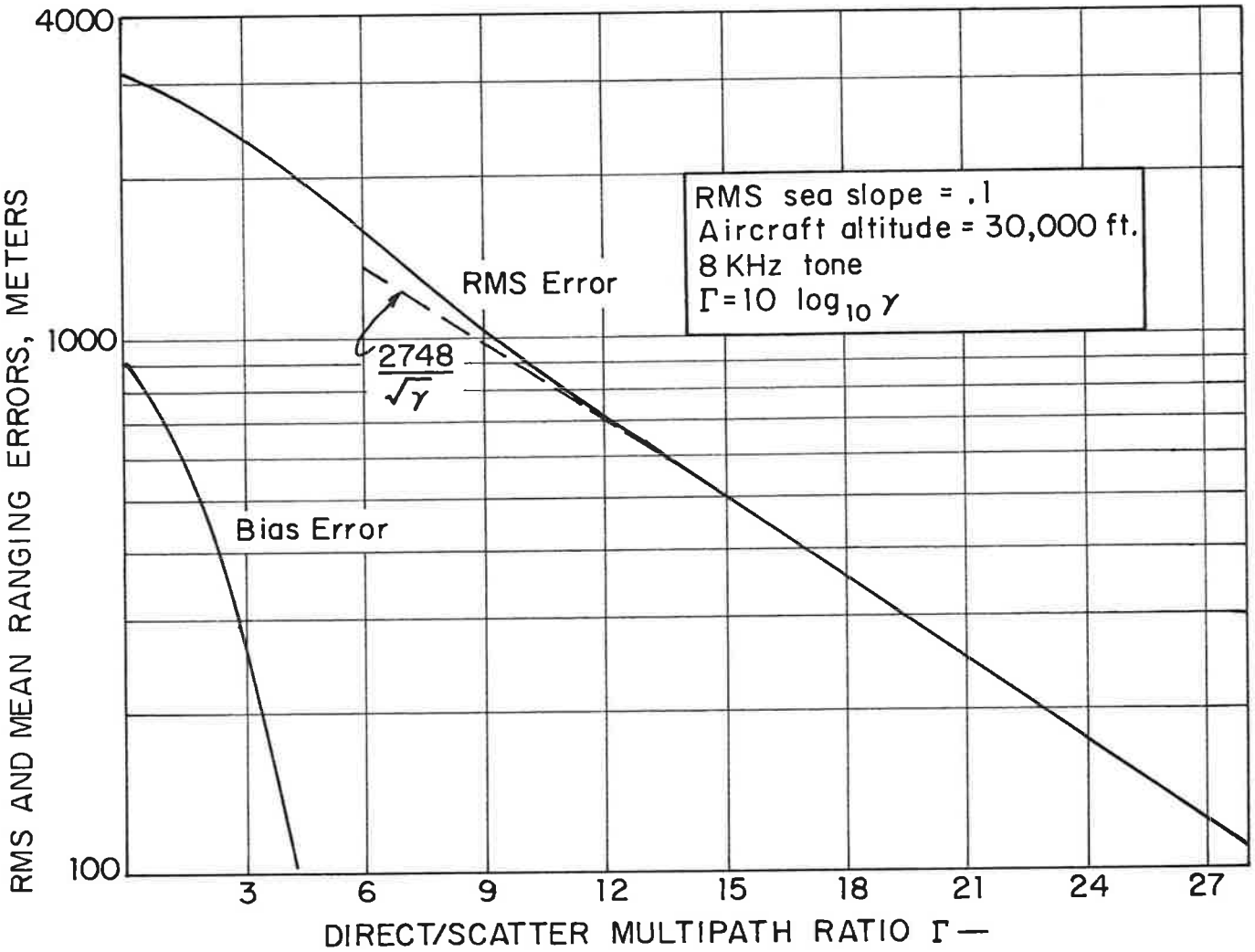

Figure 1.5 RMS and Bias Ranging Errors as a Function of Specular/ Scatter Ratio for a Tone Ranging System

emphasized that the ranging errors shown in Fig. 1.5 are for an ideal system and may be expected to be somewhat worse for a practical system.

We may combine the results of Figs. 1.4 and 1.5 to produce a probability distribution of rms ranging error over the azimuth angle for a 10^{o} elevation angle. This probability distribution is shown in Fig. 1.6 (curve A) together with another probability distribution (curve B) for the case where a 7 dB reduction in effective multipath energy is achieved by a tone filter. Such a reduction could be achieved by a filter time constant of 120 ms with a typical low elevation angle Doppler spread of 40 Hz. Note that the ranging errors far exceed the 100 meter rms value needed to attain the ATC objective of 1 nautical mile position fix [1.6].

In order to achieve a one-way rms error of less than 100 meters for 50% of the azimuth directions another 7-8 dB reduction in effective direct path/multipath power must be achieved in addition to the 7 dB tone filtering improvement of curve B. Another 10 dB beyond this is required (a total of around 24 - 25 dB improvement over curve A!) to achieve a one-way rms error of less than 100 meters for 95% of the azimuth points.

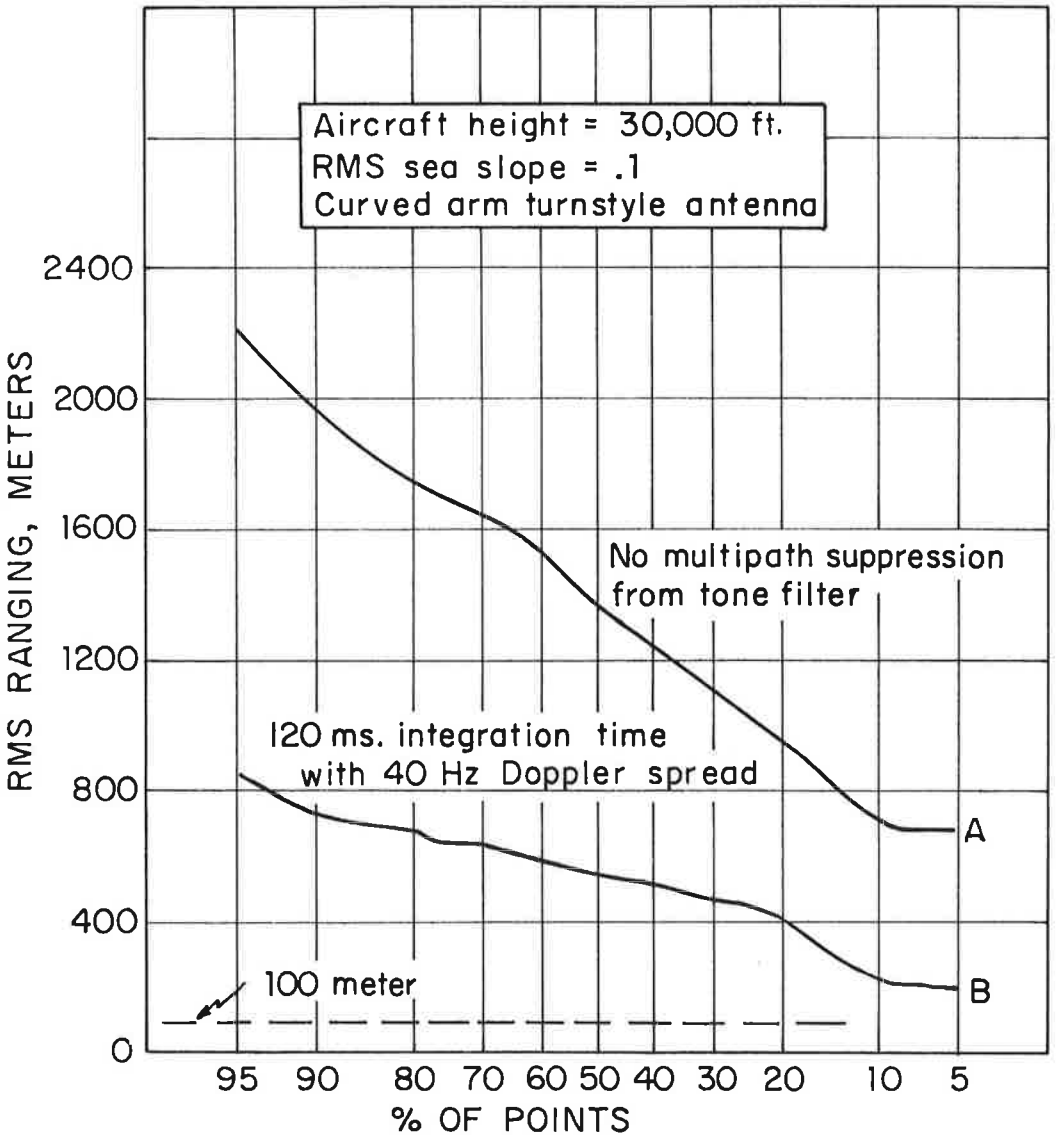

Figure 1.6 Distribution of One-Way RMS Ranging Error Over Azimuth for 10° Elevation. Side-Tone Ranging With 8 KHz Tone

It is worth emphasizing that the ranging error predictions in Fig. 1.6 had to use a theoretical complex frequency correlation function [1.3], since the available experiments (e.g., Boeing) did not provide the means for estimating this correlation function directly or indirectly (i.e., via a Fourier transform of measured delay power spectra of the indirect paths). To illustrate the theoretical dependence of rms ranging error on the multipath spread of the indirect paths we have constructed Tables 1-1 and 1-2.

Table 1-1 presents the one-way median (50%) azimuthal rms ranging error assuming an aircraft equipped with the turnstile antenna of Fig. 1.4 and traveling at an altitude of 20,000 ft. with a 10^{o} elevation angle to the satellite. An rms multipath spread of the indirect paths of 4.00 μsec has been computed for this set of parameters with an rms sea slope of .11, a representative value for the North Atlantic. As in the previous figures, a 16 KHz SSB tone ranging system or an 8 KHz DSB system at large Γ is assumed employed. Table 1-1 shows the decrease in the median azimuthal ranging error as a function of the amount of multipath reduction afforded by the tone filters.

Using these rms ranging errors as reference values we turn to Table 1-2 to describe the variation in ranging error with the multipath spread of the indirect paths. In the theoretical model employed, the multipath spread depends upon the rms sea slope. We have chosen a range of multipath spreads corresponding to rms sea slopes covering the range from .02 to .2. Such a range of rms sea slopes do occur over the North Atlantic. Note that the rms multipath spread varies from .13 to 13.25 μsec. Table 1-2 shows how the percentage of azimuthal

Table 1-1

AZIMUTH MEDIAN ONE-WAY RMS RANGING ERROR AS A FUNCTION OF TONE FILTER EFFECTIVE MULTIPATH REDUCTION FACTOR FOR A SPECIFIC SET OF GEOMETRIC AND PROPAGATION PARAMETERS AND CURVED ARM TURNSTILE ANTENNA

Tone Filter Effective Multipath Reduction Factor	Median Azimuthal RMS One-Way Ranging Errors in Meters
0 dB	1083
6 dB	479
12 dB	232
18 dB	116
24 dB	58

20,000 ft. aircraft altitude

RMS multipath spread = 4.00 μsec
(RMS sea slope = .11)

10^{o} elevation angle

8 KHz DSB tone ranging at large Γ
or 16 KHz SSB tone ranging

Table 1-2

ILLUSTRATION OF VARIATION OF RANGING ERROR WITH MULTIPATH SPREAD

RMS Multipath Spread μ Seconds	Percentage of Azimuth Angles That Have an RMS Ranging Error Exceeding the Median Azimuthal RMS Ranging Error for an RMS Multipath Spread of 4.00 μsec. (for the Curved Arm Turnstile Antenna of Figure 1)
.13	16
.52	18
2.08	32
3.26	43
4.00	50
8.34	80
13.25	90

20,000 ft. aircraft altitude

RMS sea slopes from .02 to .20

10^{o} elevation angle

8 KHz DSB tone ranging for large Γ or 16 KHz SSB system

angles having an rms ranging error exceeding the azimuthal median rms ranging error at 4.00 μsec varies as the multipath spread departs from 4.00 μsec. Thus if one assumed a tone filter multipath reduction factor of 12 dB, Table 1-1 shows that the rms ranging error will be 232 meters. Table 1-2 shows that when the rms multipath spread drops to .13 μsec, the rms ranging error of 232 meters will be exceeded only 16% of the time instead of 50% of the time, as with a multipath spread of 4.00 μsec. On the other hand when the multipath spread increases to 13.25 μsec, an rms ranging error of 232 meters will be exceeded 90% of the time. Thus as the rms multipath of the indirect path swings over a representative set of values, the 232 meter rms ranging error can swing from a low to a high probability of being exceeded. Of course an entirely similar discussion applies to other multipath reduction factors. It is worth noting that achievable multipath reduction factors due to tone filtering are not likely to be large enough to achieve the 100 meter rms error because ATC polling considerations limit the amount of "on-time" to a fraction of a second. Increasing the tone frequency will reduce the rms ranging error. However the proposed 50 kc AEROSAT bandwidth allocation limits the size of the tone frequency. Even considering such an increase in tone frequency, it does not appear that the 100 meter rms error can be achieved for a high percentage of azimuth angles at 10^{o} elevation for the turnstile antenna of Fig. 1.4. It appears that antennas with better multipath discrimination than the turnstile antenna are under development (e.g., [1.12]), and when these new antenna characteristics are available the error calculations, modem performance, and any impact on the conclusions as to the use of tone filters and recommended modems may be modified.

1.3.2 Ambiguity Error Considerations

In Section 1.3.1 the rms ranging error was applied to the fine but ambiguous tone ranging estimate. To resolve these

ambiguities additional tones are used with sufficiently close spacing between tones that the phase between these tones can resolve the ambiguities in the fine ranging estimates. Due to the noise and multipath there is a finite probability that this ambiguity will not be resolved correctly. This occurs when the coarse ranging error exceeds one-half the inherent ambiguity of the fine ranging tone pair. In fact, a series of range measurements may be made with increasing coarseness (larger ambiguity) to achieve the desired ambiguity resolution. Errors may occur at any step of this process when the error in the coarser range measurements exceeds one-half the ambiguity of the finer measurement. In a properly designed system this event should occur with very low probability. Thus we are led in this section to consider the "tails" of the ranging error probability distribution.

The results presented in Section 2 of this report, and particularly in Appendix A make it possible to calculate exact range error probability distributions for the single-sideband tone ranging system. These may then be integrated numerically to find the probability that any given range error is exceeded. As an example, we consider the same geometry and sea state conditions assumed for Fig. 1.5. The same assumptions regarding the delay power spectrum and the complex Gaussian model for the diffuse multipath signal were made as in Section 1.3.1. Figure 1.7 shows plots of the probability that the magnitude of the ranging error will exceed a specified multiple of the RMS ranging error. Each curve is for a different direct/multipath ratio Γ for a 30,000 ft. altitude, 10^{o} elevation angle, and an

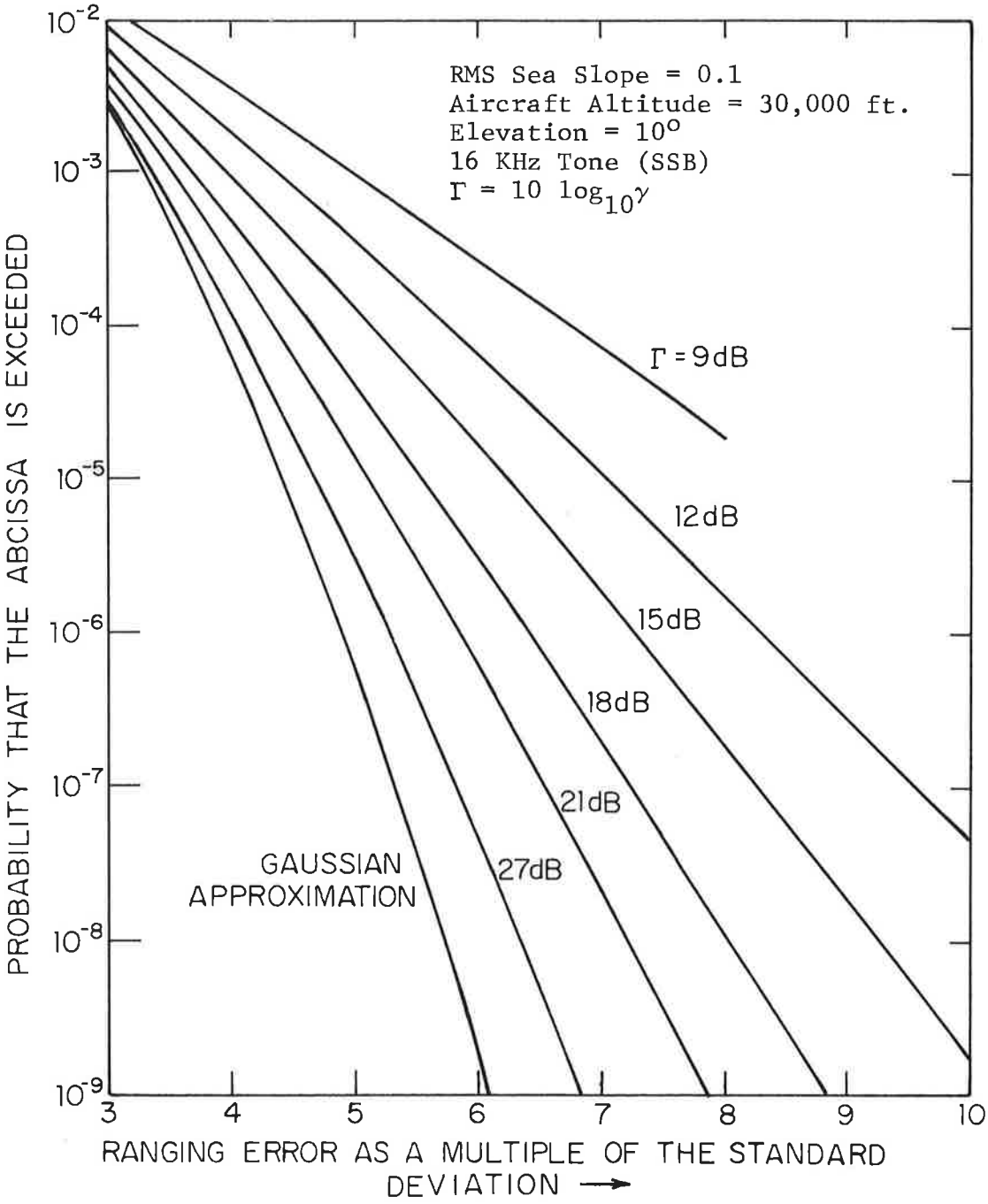

Figure 1.7 Probability of Exceeding a Given (Absolute) Ranging Error

RMS sea slope of .1. The corresponding error probability curve is also shown for a Gaussian probability distribution of ranging error. Note that even for Γ = 21 dB, a prediction of ranging with an assumed Gaussian ranging error distribution can be in considerable error, predicting error probabilities which are too low by an order of magnitude at 10^{-5} and more than two orders of magnitude at 10^{-8}.

To illustrate the influence of ambiguity error on system design we consider the following example. Suppose it was desired to upgrade the 16 KHz SSB system discussed in Section 1.3.1, adding a higher frequency tone to improve fine ranging accuracy and retaining the 16 KHz SSB tone to provide ambiguity resolution. Using Fig. 1.7 it is possible to calculate the maximum tone frequency which may be utilized while achieving a given probability of ambiguity error; results are shown in Table 1-3. In obtaining these results a 7 dB improvement in direct to scatter ratio due to tone filtering is assumed. If, for example, a tone frequency of 70 KHz were required to achieve the fine ranging requirements, an ambiguity error probability of approximately 10^{-3} would be achieved at only 50% of the azimuth angles, while an error probability of 10^{-7} would be achieved for only 10% of the azimuth angles.

Table 1-3

TABLE SHOWING THE MAXIMUM FINE RANGING FREQUENCY ALLOWED IN SSB TONE RANGING TO ACHIEVE LESS THAN A GIVEN AMBIGUITY ERROR PROBABILITY AT A SPECIFIED PERCENTAGE OF AZIMUTH ANGLES WHEN AMBIGUITY IS RESOLVED WITH A 16 KHz TONE

Probability of Ambiguity Error	Percentage of Azimuth Angles for Which Ambiguity Error is Achieved		
	10%	50%	90%
10^{-3}	132 KHz	68 KHz	42 KHz
10^{-4}	108 KHz	52 KHz	32 KHz
10^{-5}	90 KHz	42 KHz	26 KHz
10^{-6}	80 KHz	36 KHz	
10^{-7}	70 KHz	32 KHz	
10^{-8}	64 KHz	28 KHz	
10^{-9}	58 KHz	26 KHz	

1.4 Effect of Multipath on a Pseudo-Noise Ranging Modem

The analysis carried out in Section 3 allows prediction of PN (pseudo-noise) ranging modem performance under the same conditions assumed in Section 1.3 for a tone ranging modem. In Section 1.3 it was assumed initially that the tone filters do not reduce the strength of the multipath signal. In this section we make the equivalent assumption that the loop filter of the receiver code tracking loop passes the multipath component without distortion. Thus Eq. (3.44) of Section 3 has been used to calculate the rms ranging errors shown in Fig. 1.8. The assumed elevation angle, sea slope, and aircraft height are the same as for Fig. 1.8. Details of the PN receiver model may be found in Section 3; the receiver bandpass filter is assumed to be Gaussian with a 3 dB rf bandwidth equal to 1.5 times the PN pulse rate.

Having calculated the ranging error as a function of multipath ratio, the distribution of ranging error (assuming the turnstile antenna of Fig. 1.4) can be plotted as was done for the tone ranging system in Fig. 1.6. However, rather than plotting a new graph, it is simpler to observe that Fig. 1.6 may be used by multiplying the vertical scale by the factor 0.65. This is the ratio between the rms ranging errors of the two systems at any multipath ratio for the assumed system and channel parameters of Fig. 1.6.

To illustrate the theoretical dependence of ranging error on multipath spread we have calculated Tables 1-4 and 1-5 which are the counterparts of Tables 1-1 and 1-2 of the preceding section. Table 1-4 presents the median rms ranging error of the PN system under the same conditions assumed in Table 1-1. These conditions result in a calculated multipath spread of 4.00 μsec. The ranging error is presented as

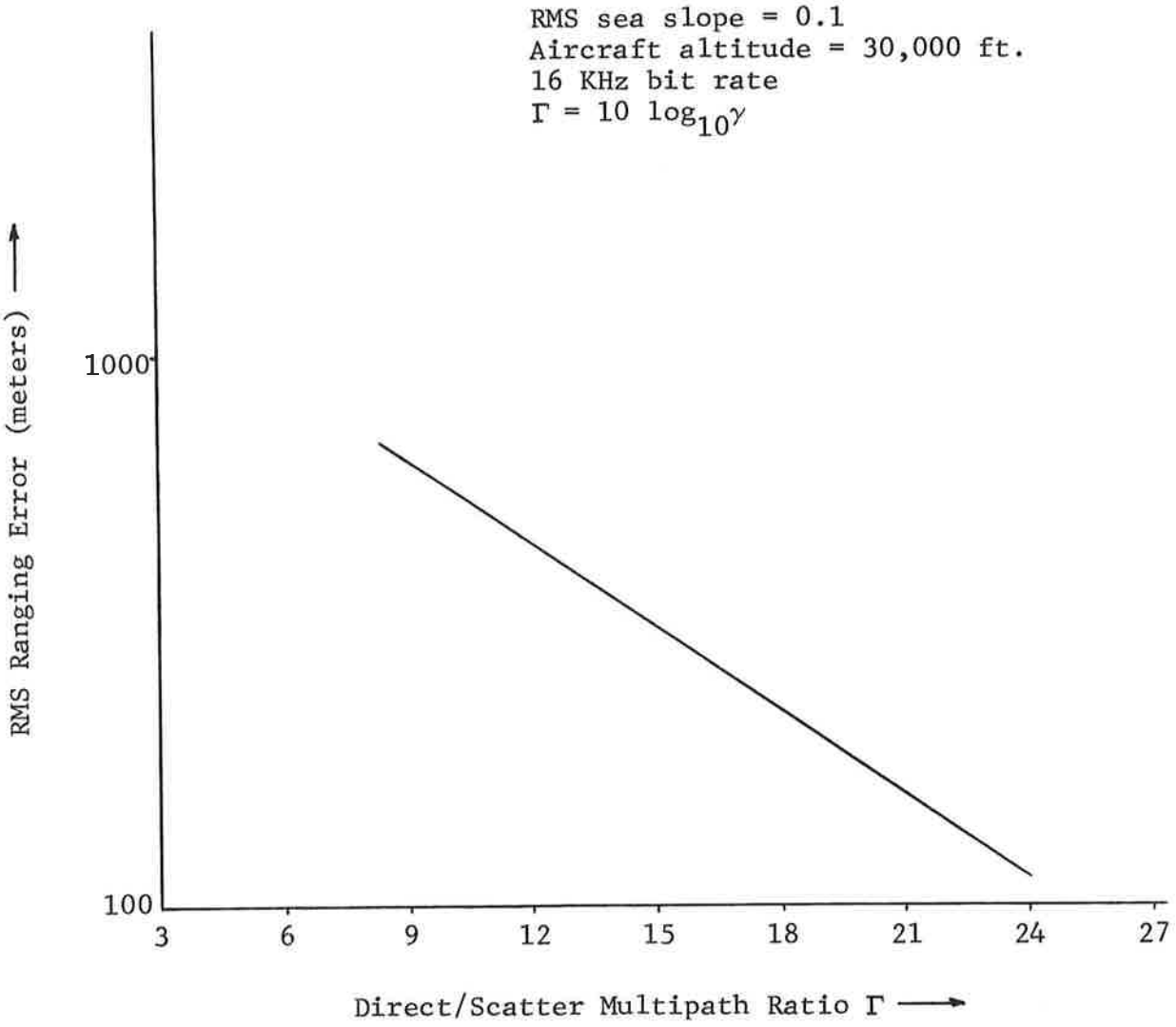

Figure 1.8 RMS Ranging Error as a Function of Direct Path/Scatter Ratio for PN Ranging System

Table 1-4

AZIMUTH MEDIAN ONE-WAY RMS RANGING ERROR AS A FUNCTION OF TONE FILTER EFFECTIVE MULTIPATH REDUCTION FACTOR FOR A SPECIFIC SET OF GEOMETRIC AND PROPAGATION PARAMETERS AND CURVED ARM TURNSTILE ANTENNA

Loop Filter Effective Multipath Reduction Factor	Median Azimuthal RMS One-Way Ranging Errors in Meters
0 dB	534
6 dB	267
12 dB	134
18 dB	67
24 dB	33

20,000 ft. aircraft altitude
RMS multipath spread = 4.00 μsec
(RMS sea slope = .11)
10^{o} elevation angle
16 KHz PN chip rate

Table 1-5

ILLUSTRATION OF VARIATION OF RANGING ERROR WITH MULTIPATH SPREAD

RMS Multipath Spread μ Seconds	Percentage of Azimuth Angles That Have an RMS Ranging Error Exceeding the Median Azimuthal RMS Ranging Error for an RMS Multipath Spread of 4.00 μsec. (for the Curved Arm Turnstile Antenna of Figure 1)
.13	72
.52	68
2.08	55
3.26	51
4.00	50
8.34	72
13.25	84

20,000 ft. aircraft altitude

RMS sea slopes from .02 to .20

10^{o} elevation angle

16 KHz PN chip rate

a function of the multipath rejection achieved by the loop filter--assuming that this filtering does not affect the multipath delay distribution. In this respect, all entries but the first in Table 1-4 are approximate. Using the first entry of Table 1-4 as a reference, Table 1-5 shows the effect of multipath spread on ranging error. It is interesting to note that performance degrades for both larger and smaller multipath spreads. In the tone ranging example considered in Section 1.3 this was not the case; for that system performance improved monotonically with decreasing multipath spread. It should be pointed out that the behavior displayed in Table 1-5 will not occur for all combinations of chip rate, mean delay, and multipath spread.

1.5 Effect of Multipath on Data Transmission

In this section the effect of multipath on the performance of FSK and DPSK modems will be analyzed. This preliminary analysis will show that for the postulated turnstile antenna and a 10^{o} elevation angle the performance specification of less than one error in 100,000 bits can not be met by an FSK modem and can be met by a DPSK modem only 5% of the time. Even with dual diversity the FSK modem can achieve a probability of error below 10^{-5} only 5% of the time and the DPSK modem will meet these specifications only 25% of the time. Fortunately, by the use of an advanced signal design concept the performance specification of 10^{-5} can be met 100% of the time for the given set of conditions outlined below.

An effective direct path signal to noise ratio in a bandwidth equal to the data rate in bps (same as E_b/N_0 energy per bit to noise power density) of 15 dB is assumed for a data rate of 1200 bps. This corresponds to a C/N_0 = 46 dB. A Gaussian Doppler power spectrum is assumed where the correlation coefficient of the fading between successive pulses is assumed equal to .9 (which implies a Doppler spread of B = 172 Hz).* The performance results are plotted as a function of the ratio of direct path/indirect path power denoted by γ as shown in Fig. 1.9. To convert this results to a distribution showing the percent of time the error performance is below a certain value, at an elevation angle of

*We define the Doppler spread as twice the "standard deviation" of the Gaussian power spectrum.

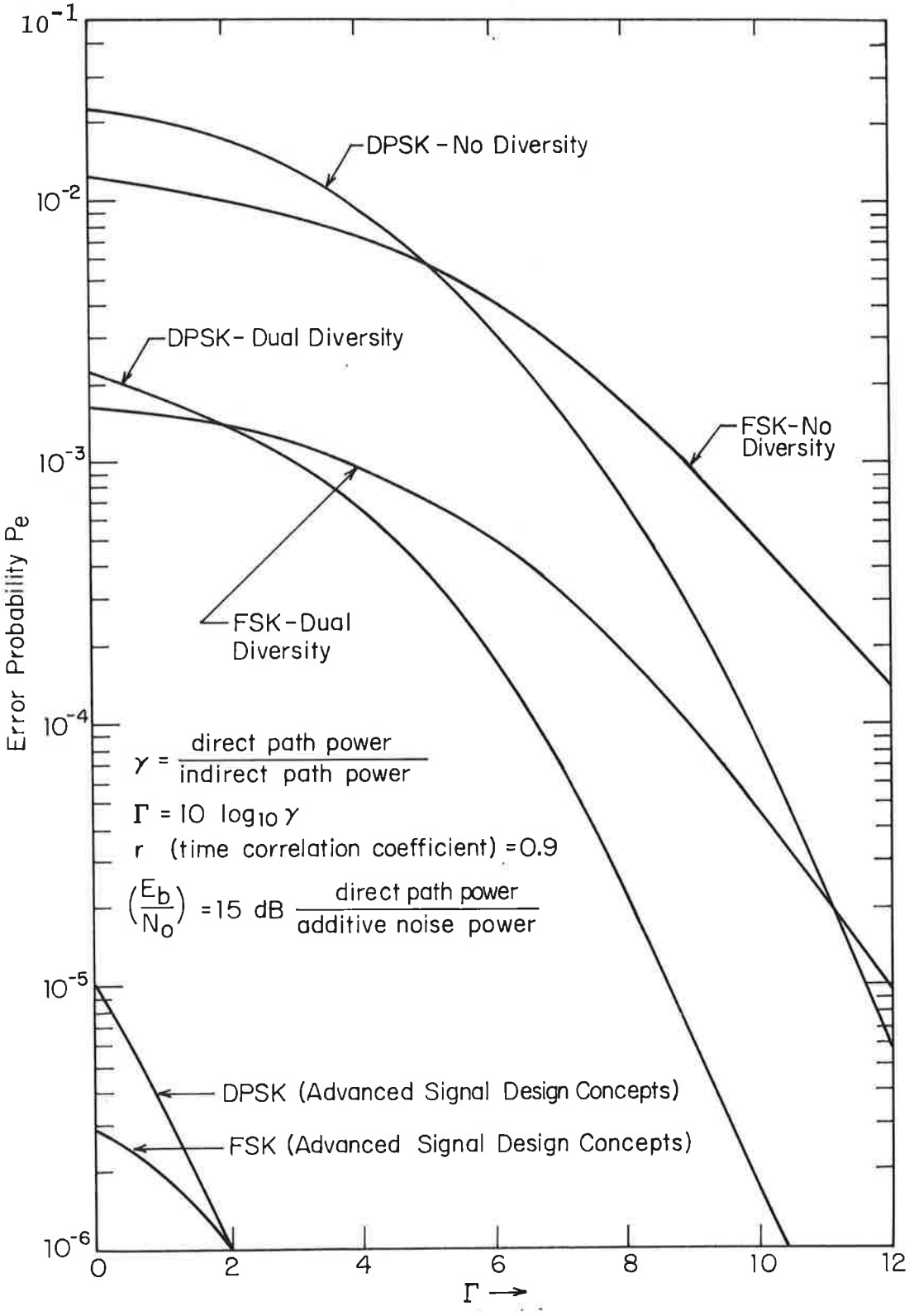

Figure 1.9 Comparison of FSK and DPSK as a Function of γ

10^{o}, the azimuth distribution for the value of γ shown on Fig. 1.4 is used. These error probability distribution results are shown on Fig. 1.10.

It should be noted that these results are just first order estimates, however, they do indicate how critically the error performance depends on particular channel measurement information. This is particularly true for the advanced signal design concepts which employ an efficient form of time diversity to obtain the effects of eighth order diversity at only a loss of 3 dB in direct path SNR (dual diversity loss). The variation in performance as a function of the pulse-to-pulse fading correlation r and the direct path power to additive noise power ratio, $\frac{E_b}{N_0}$, which are held constant on Figs. 1.9 and 1.10, are also critical channel measurement parameters required for evaluating the performance of the various data modems.

The results for an FSK modem can be obtained with the aid of Figs. 4 and 5 of Ref. [1.7] by assuming an SNR = 15 dB for single diversity and SNR = 12 dB for dual diversity. The Doppler spread of 172 Hz is assumed to have a negligible effect on this modulation scheme which enables us to use the slow fading results. Actually, a slight loss in SNR results from filtering and from the possible use of time gating to eliminate the multipath effects. The dual diversity results are obtained assuming independent statistics which can be approximated by combining two pulses spread over a time interval $\gg$ 1/fading bandwidth. Table 1-6 tabulates Pe as a function γ, the ratio of direct to indirect path power. The receiver direct path signal to noise ratio per baud is given by $\frac{E_b}{N_0}$.

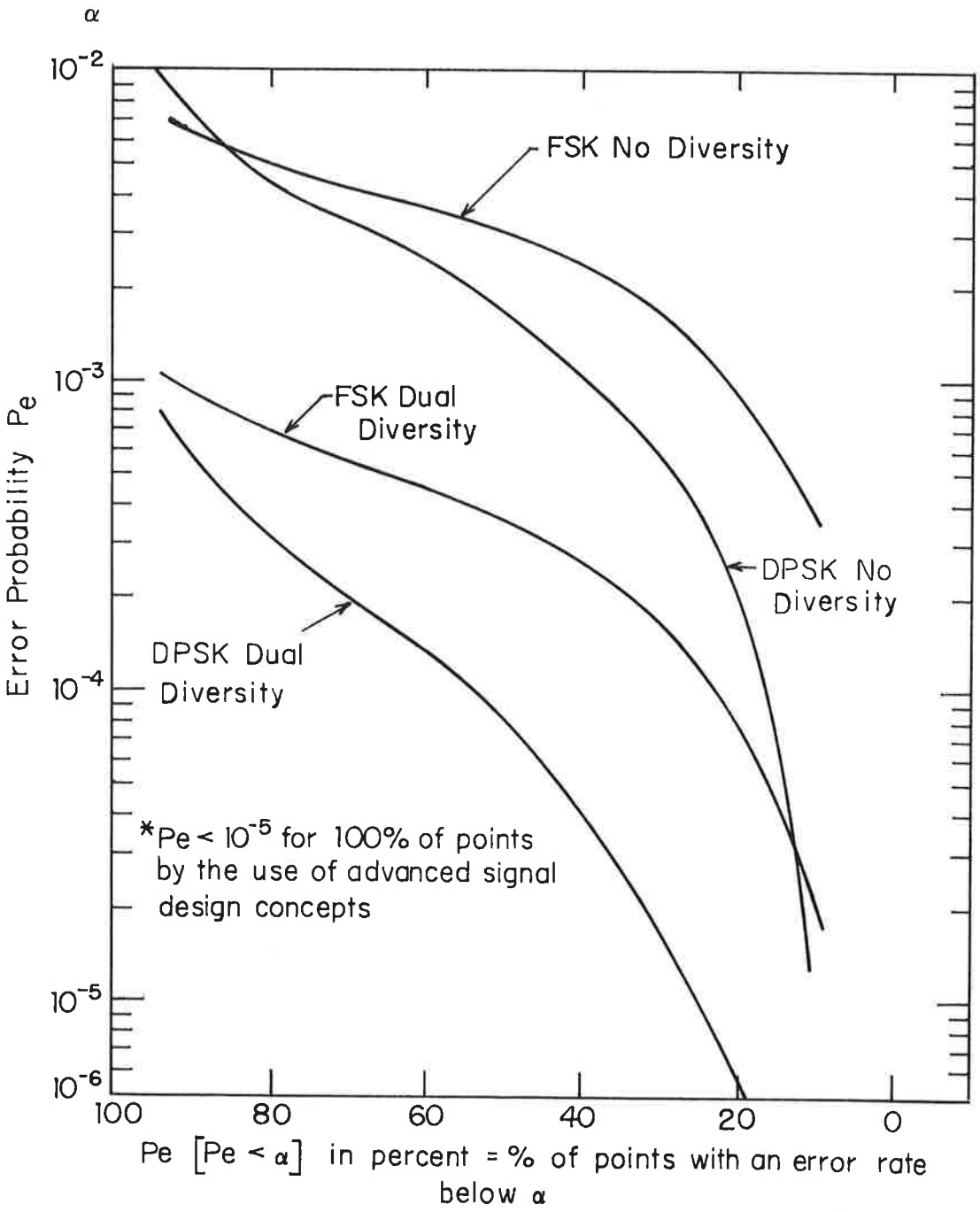

Figure 1.10 Distribution of Error Probability for 10^{o} Elevation Angle for Turnstile Antenna of Fig. 1.3

Table 1-6

Pe AS A FUNCTION OF γ FOR FSK

γ	$\Gamma = 10 \log \gamma$	Pe (FSK) No Diversity $E_b/N_0 = 15$ dB	Pe (FSK) Dual Diversity $E_b/N_0 = 12$ dB
1	0 dB	1.2×10^{-2}	1.5×10^{-3}
2.5	4 dB	8×10^{-3}	10^{-3}
4	6 dB	4×10^{-3}	5×10^{-4}
6.3	8 dB	1.5×10^{-3}	2×10^{-4}
10	10 dB	4×10^{-4}	6×10^{-5}
16	12 dB	10^{-4}	1.2×10^{-5}
22.5	14 dB	1.7×10^{-5}	—

The results for DPSK are obtained by finding an equivalent SNR which includes the decorrelation effects resulting from the assumed Gaussian Doppler power spectrum. This equivalent specular SNR can be shown to be of the form

$$(E_b/N_0)_{eq} = \frac{E_b/N_0}{1 + \frac{(1-r)\frac{E_b}{N_0}}{\gamma}} \qquad (1.1)$$

where E_b/N_0 is the actual direct path SNR ratio (15 dB) and γ is the ratio of specular to diffuse energy.

Since for flat fading DPSK is exactly equivalent to FSK, except for the 3 dB gain, we see that the DPSK and FSK modems are equivalent when

$$10 \log \left[1 + \frac{(1-r)E_b/N_0}{\gamma}\right] = 3 \text{ dB} \qquad (1.2)$$

or

$$\gamma = (1-r)\frac{E_b}{N_0} \qquad (1.3)$$

For E_b/N_0 = 15 dB this cross over point occurs at γ = 5 dB assuming r = .9. For the dual diversity results the direct path signal to noise per baud E_b/N_0 = 12 dB and thus the cross over point is at γ = 2 dB.

The real disadvantage of DPSK as compared to FSK is the irreducible error which results from the time variation. This irreducible error corresponding to a SNR of

$$\left(\frac{E_b}{N_0}\right)_{irr} \Longrightarrow \frac{\gamma}{1-r} \qquad (1.4)$$

which implies that even for $E_b/N_0 \rightarrow \infty$ the minimum error probability obtainable by DPSK for r = .9 and γ = 8 dB is about 2×10^{-4} (this 18 dB SNR is equivalent to 21 dB for FSK). For dual diversity the irreducible signal to noise ratio is still 18 dB and thus an error probability of 10^{-7} can be achieved under the above assumptions. The importance of proper signal design and channel measurement knowledge should be quite evident from these results.

Using the above equation (1.1) to calculate $(E_b/N_0)_{eq}$ and the results of reference [1.8] we tabulate Pe as a function of γ as shown on Table 1-7. To use the results of [1.8] 3 dB must be added to $(E_b/N_0)_{eq}$ to convert the FSK results to DPSK results.

Finally, the results for the advanced signal design concepts are estimated from the calculations of Section 4. While these calculations are approximate, they still indicate the advantages to be gained by the use of advanced signal design concepts. The results of using these signal design concepts with FSK and DPSK modulation schemes are tabulated as Tables 1-8 and 1-9, respectively.

1.6 Specification of an Airplane-Satellite Channel Prober

In Section 1.2 the need for additional channel measurements of the airplane-satellite channel was discussed in detail. With the aid of results in Section 5 and associated appendices, this section develops specifications for a channel prober that will collect the needed channel information.

Table 1-7

Pe AS A FUNCTION OF γ FOR DPSK

γ	$\Gamma = 10 \log \gamma$	Pe (DPSK) No Diversity $E_b/N_0 = 15$ dB		Pe (DPSK) Dual Diversity $E_b/N_0 = 12$ dB	
		$(E_b/N_0)_{equiv}$	Pe	$(E_b/N_0)_{equiv}$	Pe
1	0 dB	8.8 dB	2.2×10^{-2}	7.9 dB	3×10^{-3}
2.5	4 dB	11.5 dB	10^{-2}	9.9 dB	8×10^{-4}
4	6 dB	12.5 dB	3×10^{-3}	10.6 dB	2×10^{-4}
6.3	8 dB	13.25 dB	8×10^{-4}	11 dB	2×10^{-5}
10	10 dB	13.8 dB	10^{-4}	11.4 dB	2×10^{-6}
16	12 dB	14.2 dB	8×10^{-6}	11.6 dB	10^{-7}
22.5	14 dB	14.4 dB	2×10^{-7}	—	—

Table 1-8

Pe AS A FUNCTION OF γ FOR FSK COMBINED WITH ADVANCED SIGNAL DESIGN CONCEPTS

Γ (dB)	E_b/N_0 (SNR Per Pulse)	Pe (Before Processing)	Pe (After Processing)	E_b/N_0 (SNR Per Information Bit)
0	12 dB	2.5×10^{-2}	3×10^{-6}	15 dB
2	12 dB	2×10^{-2}	10^{-6}	15 dB
4	12 dB	1.8×10^{-2}	4×10^{-7}	15 dB

Table 1-9

Pe AS A FUNCTION OF γ FOR DPSK COMBINED WITH ADVANCED SIGNAL DESIGN CONCEPTS

Γ (dB)	Equivalent SNR Per Pulse $(E_b/N_0)_{equiv}$	Pe (Before Processing)	Pe (After Processing)	Equivalent SNR Per Information Bit $(E_b/N_0)_{equiv}$
0	7.9 dB	3×10^{-2}	10^{-5}	10.9 dB
2	9.0 dB	2×10^{-2}	10^{-6}	12 dB
4	10.6 dB	1.2×10^{-2}	10^{-7}	13.6 dB

Particular attention is given to system design so that the prober output can be used for accurate reproduction of the channel's time variant system function in the laboratory. Sections 1.6.1 - 1.6.3 discuss system operation and design in general terms. Section 1.6.4 provides some detailed calculations of system parameters utilizing the results of Section 5.

1.6.1 General Description System Operation

The theoretical foundation for the proposed channel measurement technique goes back to the work of Wiener and Lee [1.9] who noted that if a linear filter is subjected to white noise, the cross correlation function between the input and output is directly proportional to the impulse response of the filter. Price and Green [1.10] made use of this property in the Rake system which involved the continuous measurement of the channel with a periodic noise-like signal. For a periodic white noise input to a linear filter one may readily show that the cross correlation between the input and output results in a function which is proportional to the periodic repetition of the impulse response of the filter. Thus, provided that the period T satisfies the inequality

$$T > L \tag{1.5}$$

where L is the duration of the impulse response, a periodic "white" noise is suitable for probing. Moreover the "white" requirement is not strictly necessary: the probing signal need only be flat over the bandwidth of the filter.

In the proposed prober, the probing signal consists of a $\pm 180^{o}$ phase modulated IF signal with the sequence of phases chosen to agree with the sequence of binary states of a maximal length shift register sequence. We call this a PN-PSK signal. Passage of this signal through the ground station RF and IF amplifiers, the satellite repeater, the propagation media, and the aircraft receiver RF and IF amplifiers, results in a sequence of linear distortions which may be regarded as being caused by two composite channels: an equipment channel and a propagation channel. The equipment channel is assumed to have a composite transfer function H(f), of the general form shown in Fig. 1.11. While the prober design constraints may not allow specifications on H(f), the two bandwidth parameters W and F affect the design of the probing equipment. F is the "flat bandwidth," i.e., the bandwidth over which H(f) exhibits essentially flat amplitude and linear phase response. W is the "total bandwidth," i.e., the bandwidth over which H(f) is significantly different from zero (e.g., 30 dB bandwidth). Due to the fact that the PN-PSK probing signal does not have a flat spectrum, it is shown in Section 5 that one must introduce a factor $(\sin \pi f T_0)^2/(\pi f T_0)^2$ in the apparent measured channel characteristics, where T_0 is the pulse width.

The correlation technique of channel measurement proposed involves a finite number of correlation operations at equi-spaced delays, i.e., the cross-correlation function between the locally generated PN sequence and the receiver probing signal is only taken at a finite uniformly spaced set of delays. Thus a sampled impulse response is actually measured. As with any sampling operation, harmful aliasing

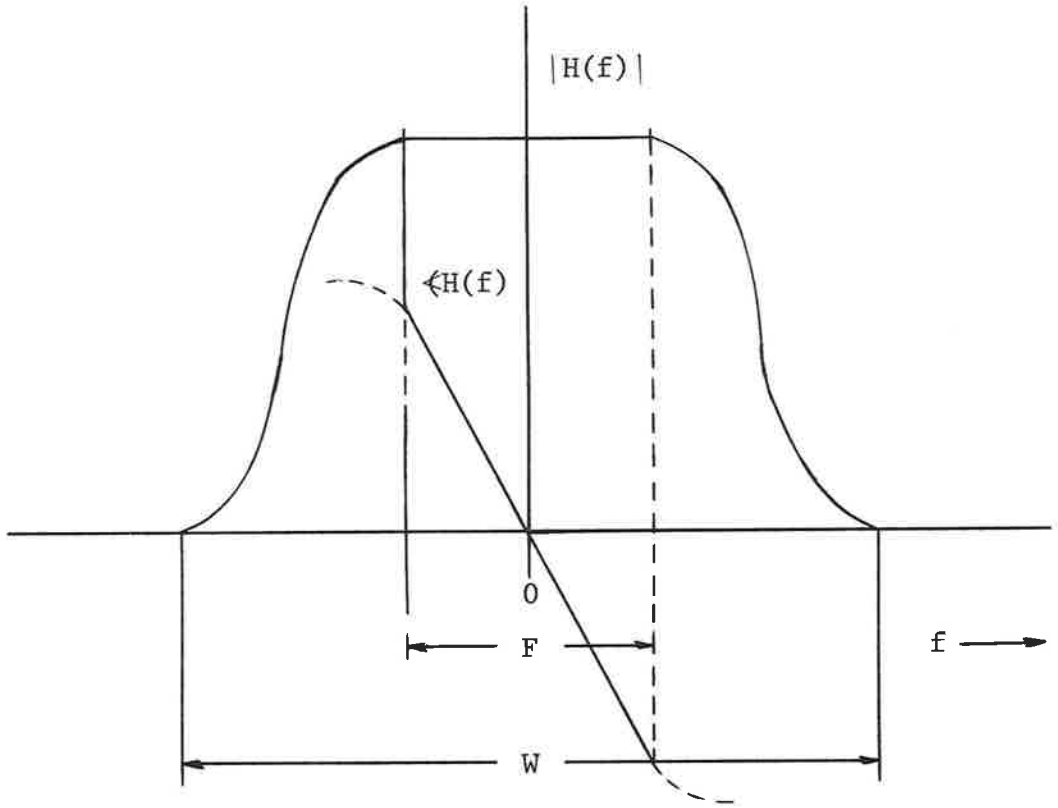

Figure 1.11 Definition of Flat and Total Bandwidths for Equipment Channel

effects must be avoided. If the correlators are separated by Δ in delay, then the transfer function of the sampled impulse response consists of repetitions of the channel transfer function (Fig. 1.11) at multiples of $1/\Delta$ Hz. It is clear that W must be small enough in relation to $1/\Delta$ Hz. If Δ is chosen equal to T_0, the pulse width of the PN sequence, it is generally necessary to provide an IF filter as part of the prober demodulator to reduce W sufficiently so that aliasing effects are tolerable. Note, however, that the number of correlators required is given by

$$N = L/\Delta \tag{1.6}$$

so that cost increases with decreasing Δ and one should not make Δ any smaller than necessary.

A block diagram of the channel prober is shown in Fig. 1.12 which exhibits the major signal processing functions. This specification covers only those blocks in Fig. 1.12 below some selected IF interface, say 70 MHz. Subsequent sections will discuss the individual blocks in more detail.

The impulse response of the propagation channel consists of two distinct parts: a direct path and a continuum of delayed multipath components grouped together and well separated from the direct path. The direct-channel and multipath-channel impulse responses are separately measured as indicated in Fig. 1.12. However the PN-PSK signal received on the direct channel is tracked in delay and Doppler and is used to provide a delay and Doppler reference in measuring the impulse response of the multipath channel.

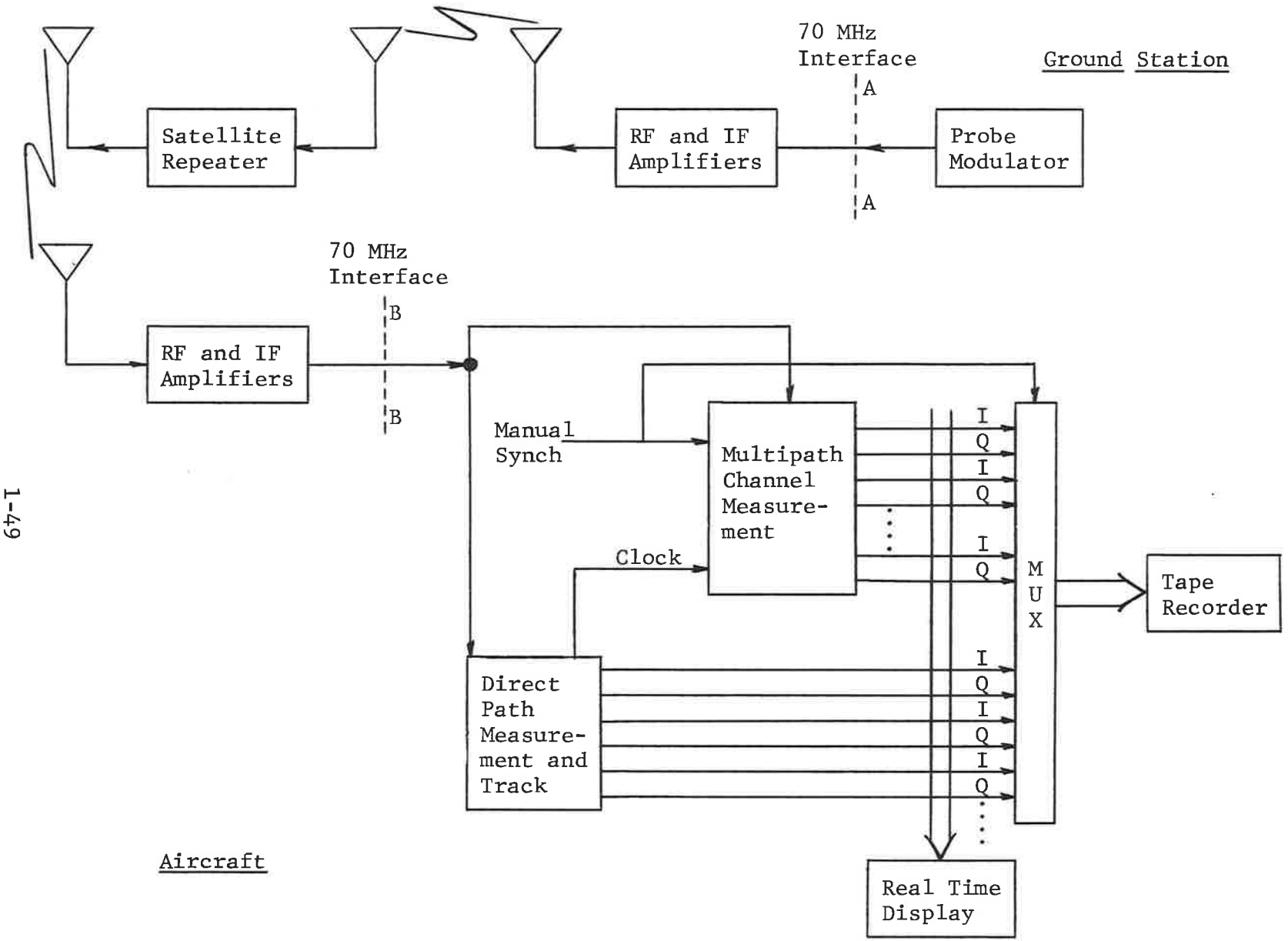

Figure 1.12 Major Functional Blocks of Channel Prober

Prior to data recording it is possible, in principle, to use a manual synch control to adjust the timing of the multipath channel measurement relative to that of the direct path. A real-time display provides a view of the multipath profile as a function of path delay. The manual synch control adjusts this profile so that it is centered properly prior to data recording and will stay well enough centered for the recording period.

The multipath measurement consists of the extraction of the in-phase and quadrature samples of the impulse response. Due to the time-variant nature of the channel these samples are low pass functions of bandwidth equal to the Doppler spread of the channel (referenced to the direct path Doppler shift). This set of low pass functions is sampled and multiplexed to prepare it for analog tape recording. Note that the direct path channel is shown as having several delay samples also. This is necessary because of the smearing effect of the equipment channel. The real-time channel monitor involves the display of the short term average power on each complex tap. An adjustable averaging time should be provided to accommodate different fading rates.

1.6.2 Prober Demodulator

In this section block diagrams and discussions of operation are presented for the prober demodulator. Consider Fig. 1.13 first. A selectable IF filter is shown in case it is desired to adjust the effective flat and total bandwidth parameters F and W in accordance with the probing rate so as to keep the number of correlators as small as possible and to minimize the aliasing effect of the sampled impulse response.

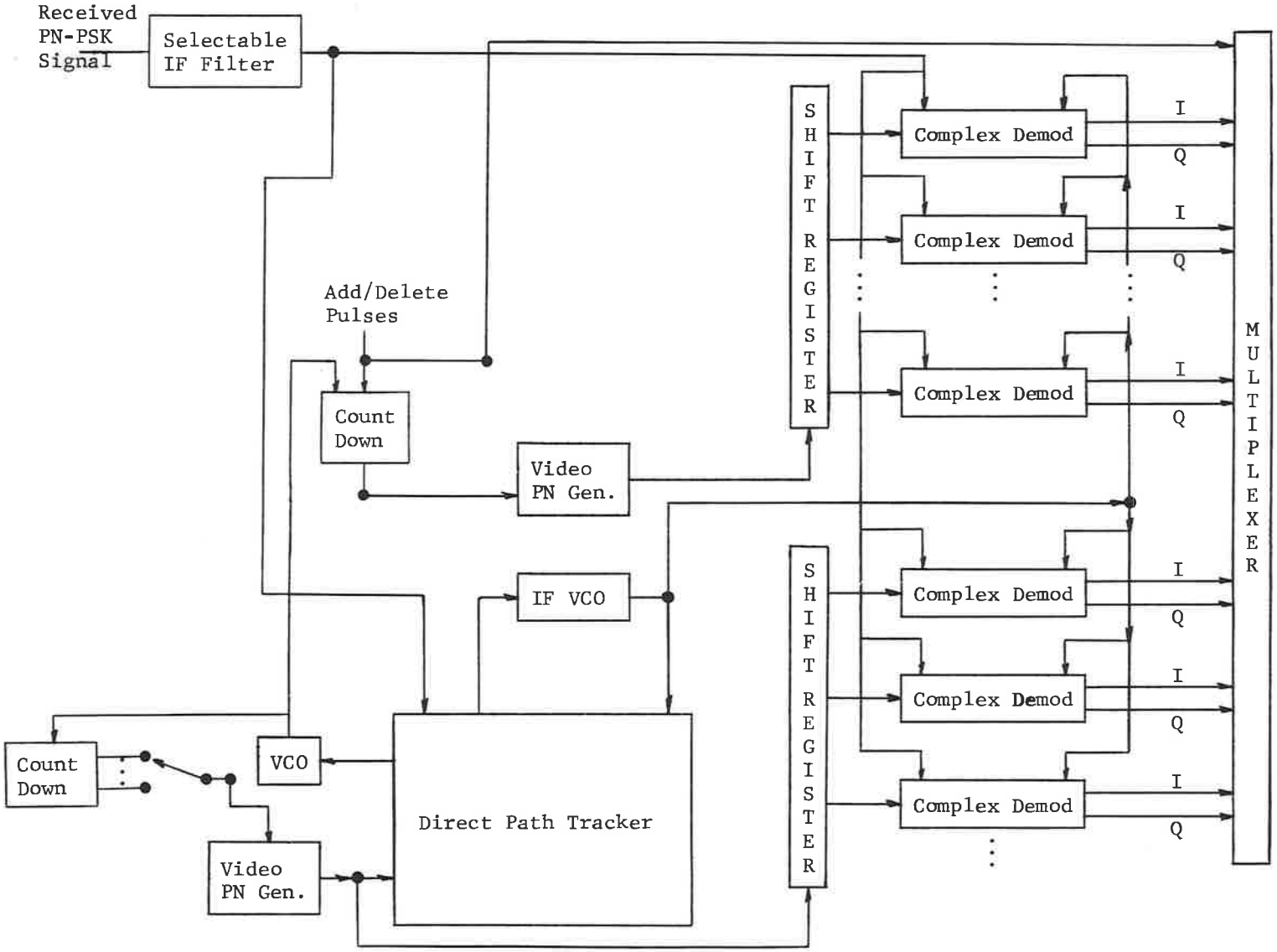

Figure 1-13. Block Diagram of Prober Demodulator

The block labeled "direct-path-tracker" can be identical to a PN ranging modem which tracks the direct path signal. This modem would have two VCO's—one for tracking the PN code and the other for tracking IF phase. The IF-VCO is used as a Doppler reference in complex demodulation of the impulse response samples. The PN-VCO of the direct path tracker and associated count-down circuitry needed for the adjustable PSK rate is used as the basic clock for the video PN-generators of the direct path and the multipath correlation demodulators. These PN generators provide ± 1 sequences following the same maximal-length shift register sequence as used to generate the PN-PSK transmitted signal.

The video PN generator of the multipath channel measurement section has a manual rate control to shift the timing of the multipath PN reference relative to that of the direct path PN reference to account for the delay and changing delay difference between the direct path and the first arriving multipath. The number of PN reference cycles shifted is recorded so that the delay inserted will be known in the data reduction.

To use the manual tracking mode it will be necessary to know the airplane position and velocity approximately. Otherwise an automatic delay difference tracking mode will have to be instituted. In any case, if the delay tracking is carried out in discrete steps, these steps must be sufficiently small compared to a PN bit, as discussed in Appendix E. In this appendix it is shown that the discrete steps in delay produce transients at the output of the playback

channel. The ratio of the strength of the desired output to the peak strength of the transient is given by the expression

$$\rho_1 = \frac{1}{\frac{\pi}{3}\alpha^2 T_0^2 W^2} \tag{1.7}$$

for an input signal with rectangular spectrum of width W and a delay jump of αT_0.

As may be seen in Fig. 1.13 a basic operation performed many times in parallel in the prober demodulator is one of using a set of delayed replicas of the transmitted PN-PSK signals for complex coherent demodulation (identical to complex cross-correlation) of the received PN-PSK signal. Figure 1.14 dissects this basic operation. Two quadrature PN-PSK signals are shown generated by using a video PN signal to modulate the IF-VCO output and 90^o shifted IF-VCO output. The quadrature PN-PSK signals are then used to coherently detect the incoming signal. Two low-pass filters of B Hz bandwidth each are used to extract the low pass detected outputs, called the in-phase and quadrature outputs.

In Fig. 1.13 the cross correlators have been arranged so that the delay between correlators occurs in increments of T_0, the PN pulse width. With this arrangement aliasing can only be made tolerable by using an IF filter as shown in Fig. 1.13, to reduce the total bandwidth W. A change in the PN-PSK probing rate would then require a change in the IF filter. Figure 1.15 shows a configuration in which the correlators are spaced at $T_0/2$ apart in delay. For $\Delta = T_0/2$

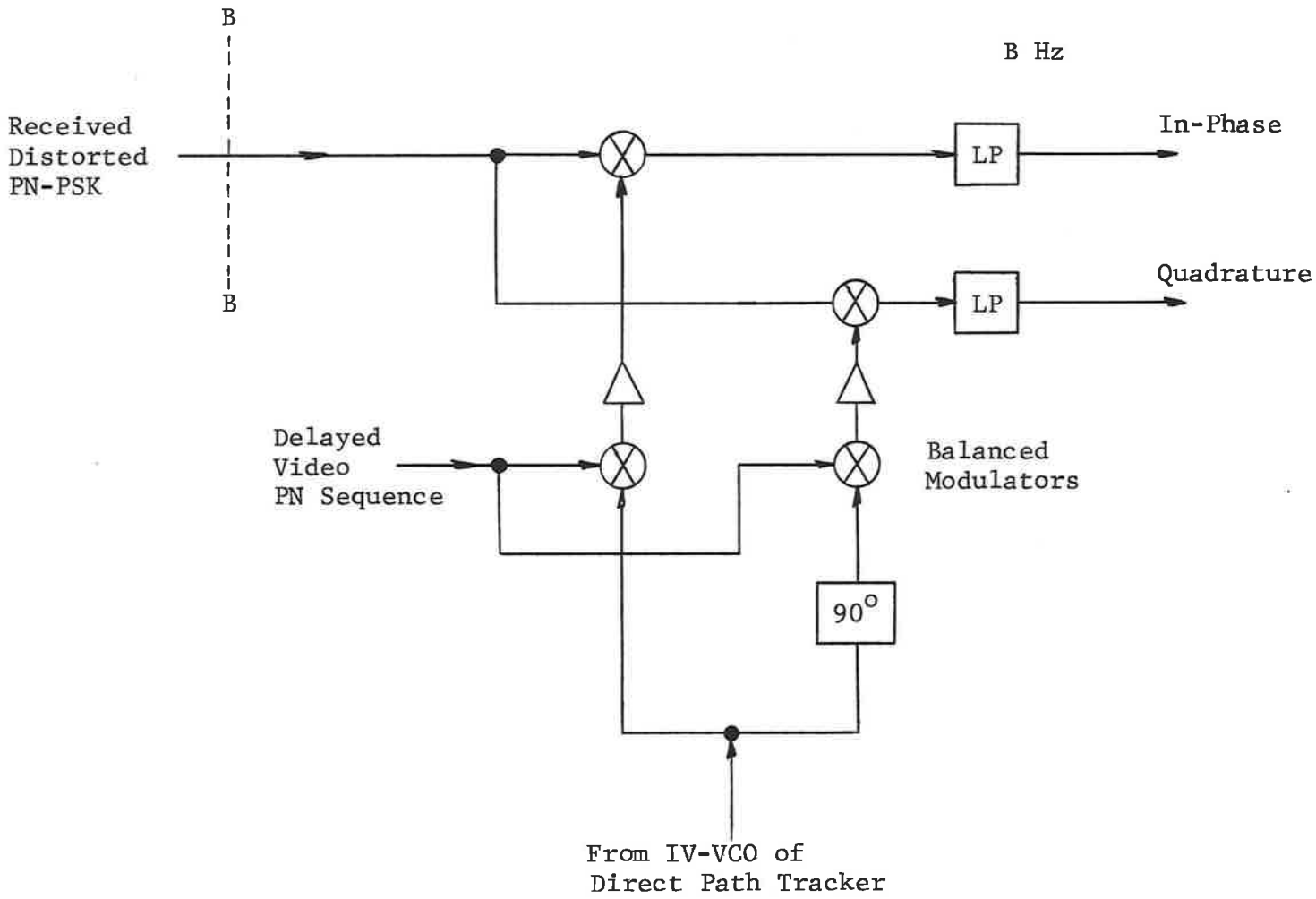

Figure 1.14 Illustration of Coherent Complex Demodulation Operation

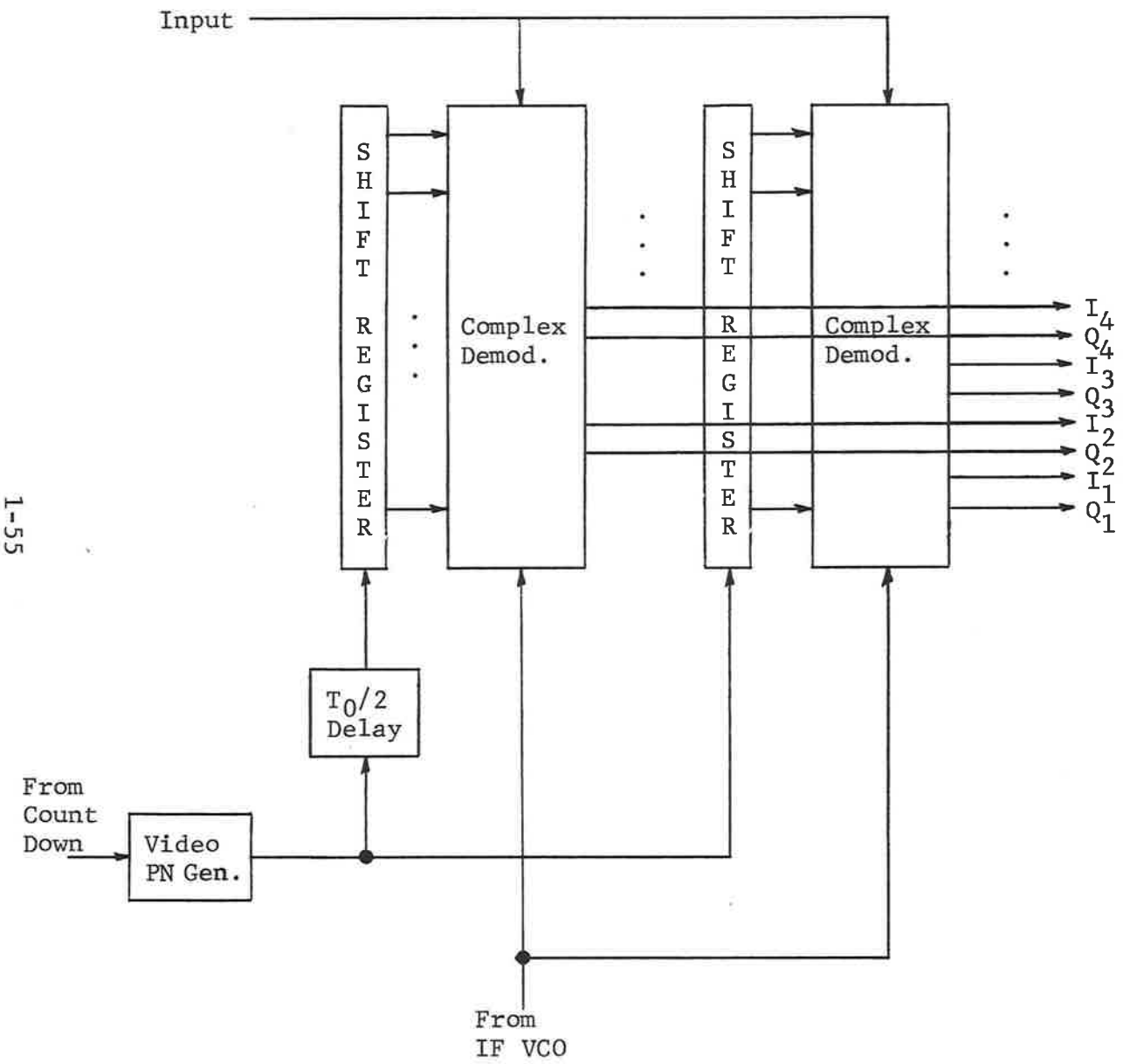

Figure 1.15 Prober Demodulators With Correlators Spaced at One-Half the PN Pulse Width

one may show that the aliasing cross talk will have an average power at least 40 dB below the desired signal in the frequency band $f_0 - 1/4T_0 < f < f_0 + 1/4T_0$. Also the spectrum of the probing signal drops to only 2 dB below band center at the end frequencies. One may obviously generalize this configuration to the case in which the correlators are separated in delay by T_0/p, where p is an integer. For a given multipath spread and PN-PSK pulse rate the number of correlators required increases by a factor of p. However, if the probing rate is reduced by a factor of p, the number of correlators required remains the same.

We now consider the requirements on selection of the output low-pass filters (see Fig. 1.14). The inputs to the low pass filter contain two types of spurious components. Because the PN-PSK signal is a periodic process the input to the low pass filter is given by the sum of a low pass component and a set of undesired components centered at harmonics of the PN fundamental frequency. The bandwidths of these components are equal to the Doppler spread of the channel. The low pass component itself contains not only the desired signal but a spurious cross talk signal due to the side lobes of the PN-PSK autocorrelation function.

In Section 5 expressions are derived for the strengths of the spurious harmonic (Eq. (5.28)) and low pass (Eq. (5.60)) terms. For a rectangular delay power spectrum of length L and a received PN-PSK probing signal of rectangular power spectrum with bandwidth W, the ratio of the strength of the desired to undesired harmonic term is bounded by

$$\frac{P}{P_{harm}} \geq \frac{N}{WL} \qquad (1.8)$$

where N is the number of pulses in one period of the PN sequence.

The ratio of the strength of the desired output to the spurious low pass term is given by

$$\frac{P}{P_{l.p.}} \approx N^2(WT_0^2) \frac{Q(\eta)}{\int Q(\xi)\, d\xi} \tag{1.9}$$

where T_0 is the duration of a PN-PSK pulse, $Q(\xi)$ is the delay power spectrum (profile of scattered power as a function of multipath delay ξ) of the indirect paths, and η is the correlator delay at which the output SNR is being measured.

In addition to the existence of spurious signal term there will be an additive noise term at the filter output. The ratio of output SNR to input SNR is shown (Eq. (5.78)) to be given by

$$\frac{\rho_{out}}{\rho_{in}} = \frac{W}{B_N} \frac{T_0 Q(\eta)}{\int Q(\xi)\, d\xi} \tag{1.10}$$

where B_N is the noise bandwidth of the low pass filter.

While the spurious harmonic terms can be made negligible relative to the desired signal by using a sufficiently small value of B_N, the low-pass spurious term can not. The ratio of the strength of the output noise to the spurious low pass term for the case of a received signal with a rectangular power spectrum is given by

$$\frac{P}{P_{l.p.}}/\rho_{out} = \frac{N^2 B_N}{\rho_{in} W} (T_0 W) \qquad (1.11)$$

If we define the input signal-power to noise-power-density in dB-Hz as P_0 and use the approximation

$$T_0 W \approx 1 \qquad (1.12)$$

we find that

$$\frac{\text{output noise}}{\text{output low pass spurious}} \approx \frac{N^2}{P_0/B_N} \qquad (1.13)$$

where it should be noted that $P_0 = \rho_{in} W$. When $N^2 \gg P_0/B_N$ the spurious low-pass term may be neglected in comparison to the output additive noise.

1.6.3 Horizontal-Vertical Antenna Multiplexing

In order to observe simultaneously the channel characteristics associated with the use of a vertical and horizontal antenna one may provide appropriate switches and additional low-pass filters as indicated in Fig. 1.16. Only one complex coherent demodulation operation is shown for simplicity. An electronic switch alternately connects the outputs of the vertical and horizontal antennas to the RF and IF amplifiers. The switching time is small compared to the duration of the PSK bit and the resting time at each position is equal to one period of the maximal length shift register sequence. Thus the in-phase and quadrature mixer outputs are alternately due to the horizontal and vertical antenna outputs. These alternate outputs are directed to separate low-pass filters by switches synchronized with the antenna switches.

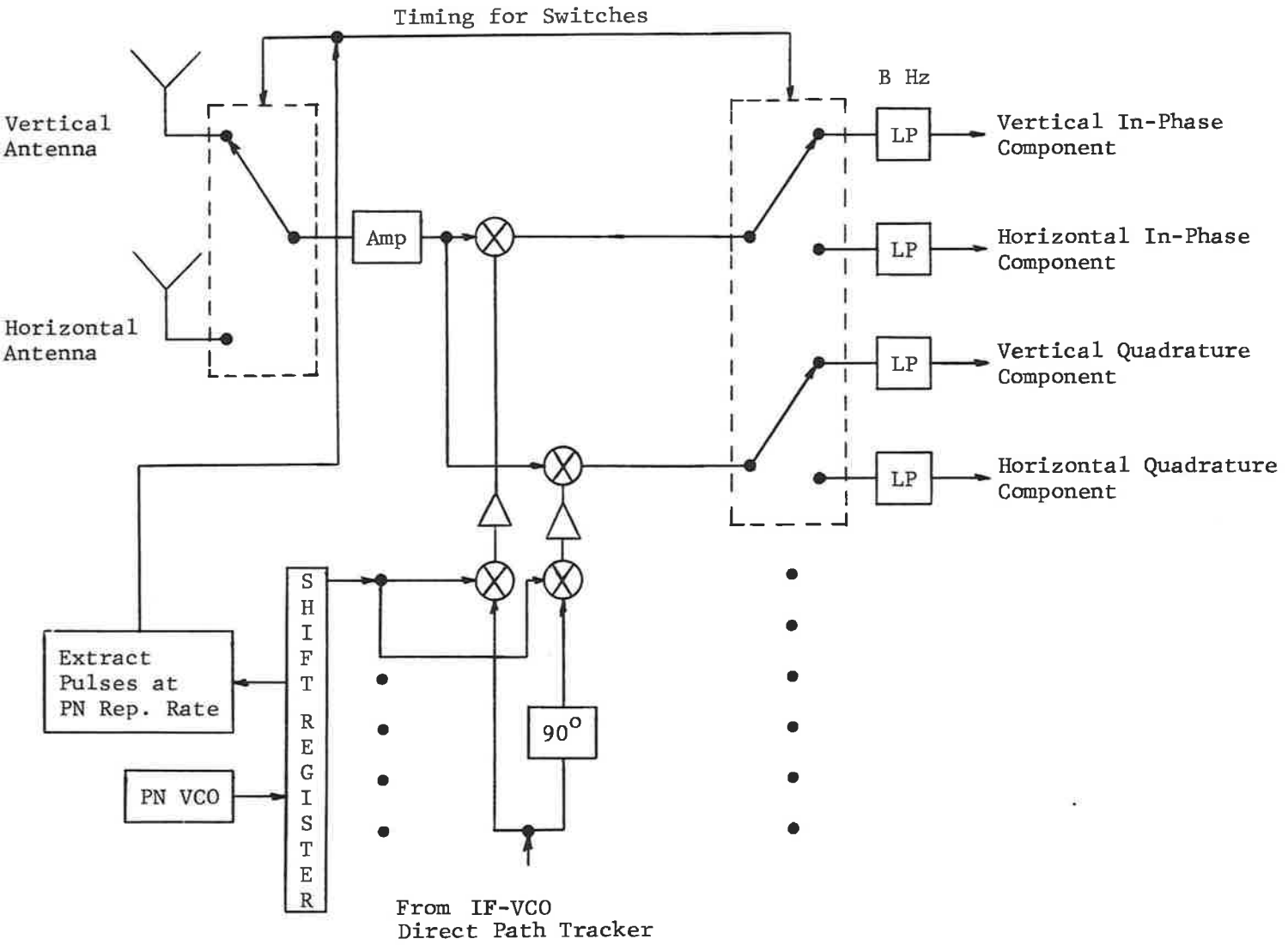

Figure 1.16 Simultaneous Measurement of Vertical and Horizontal Antenna Channel Characteristics

The time constant of the RF and IF amplifiers between the antenna switch and the demodulator should be small compared to the duration of a PN pulse in order to avoid the appearance of cross talk between the measured vertical and horizontal polarized channels. In order to keep this time constant small it is necessary to have the correlators spaced in delay by no more than half of a PN pulse width as in Fig. 1.15.

As discussed in Section 5, the switching process introduces spurious cross talk components at multiples of half the PN-PSK fundamental frequency. The most harmful component generated is at half the PN fundamental frequency and is much stronger than the cross talk terms present when antenna switching is not used. In particular it is shown in Section 5 that this spurious term can be as large as the desired low-pass term and that the output SNR is reduced by a factor of 2 when the multiplexing arrangement of Fig. 1.16 is used.

1.6.4 Prober Parameters for Aerosat Channel Probing

In this section we derive some values of prober parameters for use in probing the aircraft-satellite channel of the Aerosat system. The following system parameters are assumed for the experiment:

Bandwidth: $W = 50$ KHz to 10 MHz

Received SNR: 53 dB Hz for an omni-antenna and direct path

Altitudes: $H = 20{,}000$ to $30{,}000$ feet

Elevation Angle to Satellite: $\theta \geq 10^{o}$

Operating Frequency: L-Band (1.6 GHz)

RMS Sea Slope: $\alpha \leq .2$

Airplane Velocity: V = 400 mph

Design parameters of the prober depend upon the delay and Doppler spreading characteristics of the indirect paths scattered from the ocean's surface. We have used the steepest descent model [1.1], [1.2], [1.3] to infer these characteristics utilizing the system parameters specified above. This model will break down for the lower elevation angles and larger sea slopes but more general calculations, presently being completed, were not available for this report.

As shown in [1.3] and Section 6, for the steepest descent model the Doppler power spectrum for a receiver carrier is Gaussian-shaped with a maximum RMS Doppler spread (two standard deviations of normalized Gaussian shape) given by

$$B = 4\alpha \frac{f_0}{c} v \sin \theta \qquad (1.14)$$

for motion parallel to the surface of the earth. f_0 is the carrier frequency, c is the velocity of light, v is the aircraft velocity, θ is the elevation angle, and α is the RMS sea slope. For a point of reference, 99% of the power in such a Doppler spectrum lies in a bandwidth with limits $f_0 \pm 1.3$ B. Using the quoted system parameters we find that 1.3 B is given by 500, 340, and 170 Hz for elevation angles of $\theta = 30^o$, 20^o, and 10^o, respectively.

The steepest descent model delay power spectrum has more involved analytical expression (see Section 6). Figure 1.17 presents an integration over the delay power spectrum

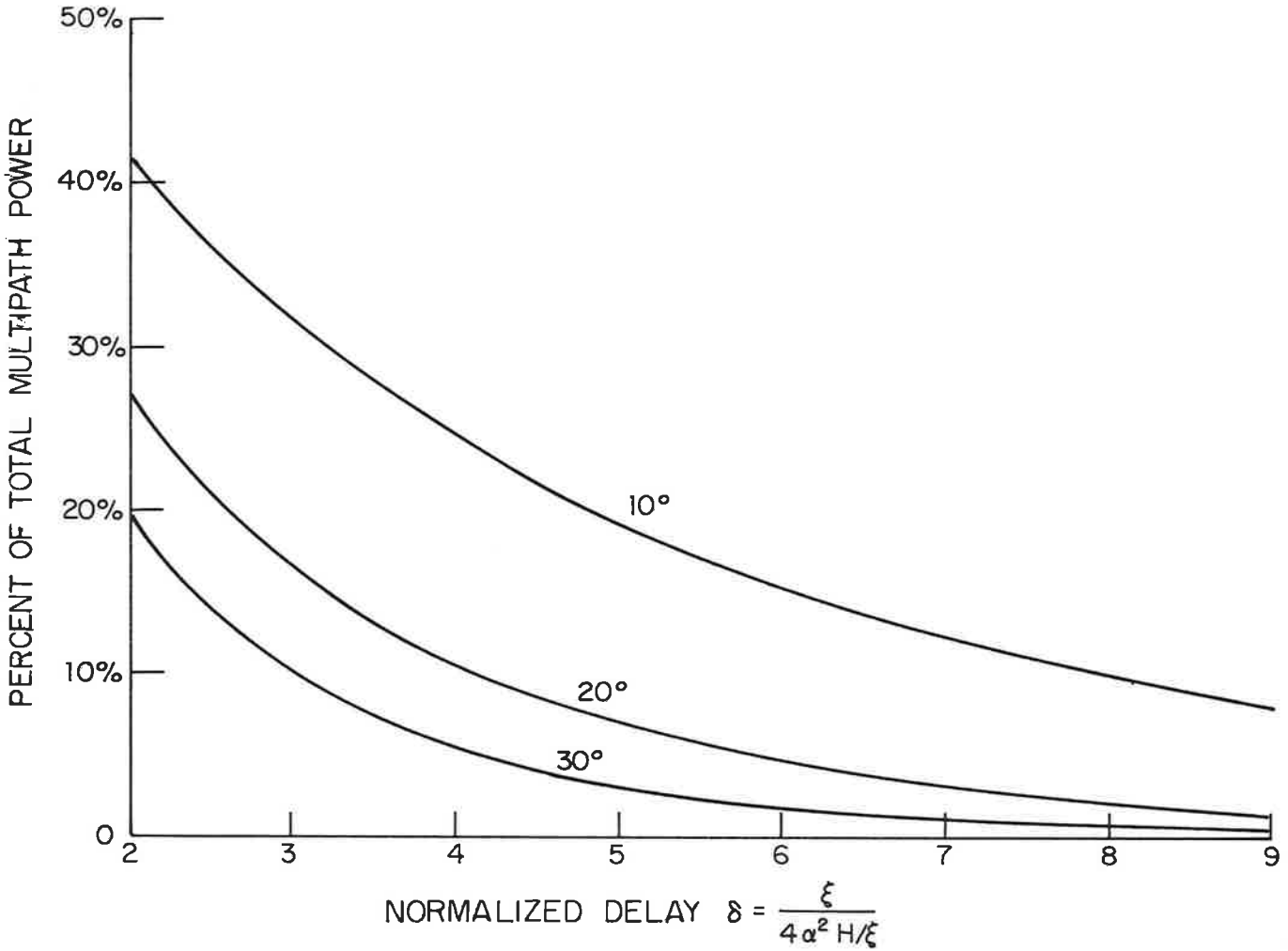

Figure 1.17 Power in Tail of Delay Power Spectrum

starting at different normalized delay values δ for $\theta = 10^{o}$, 20^{o}, and 30^{o}, where

$$\delta = \frac{\xi}{4\alpha^2 H/c} \tag{1.15}$$

in which ξ is the delay relative to the delay at the specular point and H is the aircraft altitude.

The number of correlators required to measure the impulse response of the channel is given by the ratio L/Δ, where L is the "multipath-spread" and Δ is the delay spacing between correlators. While it may be convenient to imagine the impulse response as being confined to a finite interval L, it is clear that an arbitrary criterion must be adopted for L, since $Q(\delta)$ is strictly non-zero over the semi-infinite interval $(0,\infty)$. With the aid of plots such as shown in Fig. 1.17 one may determine the value of δ beyond which there resides some fixed small percentage of the power in the delay power spectrum. For $\theta = 10^{o}$, 20^{o}, 30^{o} the 1% value of δ is given approximately by $\delta_{.01} = 14, 9.5, 6.5$, respectively. Removing the normalization, the number of correlators required to measure 99% of the power in the impulse response becomes

$$N_{.99} = \frac{\delta_{.01} 4\alpha^2 H/c}{\Delta} \tag{1.16}$$

This formula leads to a very large number of taps when the largest values of $\alpha = .2$ and $H = 30{,}000$ feet are used and when it is desired to characterize a large bandwidth (small Δ). Thus to keep the number of correlators practical it is necessary to have the PN-PSK rate adjustable to lower rates when the multipath spread gets too large.

Consider a specific example. Assume that only 100 complex correlators are to be used, $\alpha = .2$, H = 30,000 feet, and $\theta = 10^{o}$. The value of Δ required is then

$$\Delta = \frac{(14)(.16)(30 \times 10^{-6})}{100} = .672 \ \mu\text{sec} \qquad (1.17)$$

The value Δ determines the interval between "samples" of the measured channel impulse response. As pointed out previously a choice of $\Delta = T_0/2$ allows a measured channel with a bandwidth $1/4\Delta$ within which the average aliasing cross-talk will be less than 40 dB and the attenuation of the desired signal 2 dB at band edge. For $\Delta = T_0/2$ the PN-PSK bit rate would be .744 Mbs and the bandwidth characterized 372 Kc.

An alternate choice of $\Delta = T_0$ is permissible but requires the use of an IF filter to control the aliasing cross-talk. An examination of various possible filters to satisfy the conflicting requirement of reducing aliasing cross-talk to less than 40 dB below the desired signal, to cause minimal distortion of the desired transfer function, and to cause small spreading of the measured impulse response (so as not to significantly increase the number of correlators) has resulted in the selection of a fourth-order transitional Butterworth-Thompson filter [1.11] with parameter m = .4 and 3 dB bandwidth equal to $.52/T_0$. With this filter the desired transfer function is attenuated only around 2.2 dB at band edge and the bandwidth characterized is $1/2T_0$ or 744 Kc, twice that for the case $\Delta = T_0/2$ described above. The PN-PSK

bit rate is also twice as large (1.488 Mbs). Calculation shows that the spreading of the impulse response caused by this filter measured at the -40 dB level is less than $4T_0$. Clearly, apart from cost, the case $\Delta = T_0$ is preferable because twice the bandwidth can be characterized for a given multipath spread, or conversely, twice the multipath spread can be accomodated for a given characterizing bandwidth. However, as pointed out in 1.6.3, when time multiplexed horizontal and vertical polarization channel probing is used the filter cannot be employed without introducing cross-talk between measured channels.

Because of the limited received power one may not be able to measure the delay power spectrum very far out on its tail and this may also restrict the number of correlators. Applying Eq. (5.78) with the normalized delay variable shows that the output SNR at a tap having delay δ relative to the specular point is given by

$$\rho_{out}(\delta) \approx \frac{P_0}{B_N} \left(\frac{T_0}{4\alpha^2 H/c}\right) Q(\delta) \qquad (1.18)$$

where B_N is the noise bandwidth of the output low pass filter, $Q(\delta)$ is the delay power spectrum expressed as a function of the normalized variable δ, and P_0 is the received signal power relative to the noise power density. Graphs of $Q(\delta)$ for $\theta = 10^o$, 20^o, 30^o are given in Section 6, Fig. 6.3. The value of P_0 is given by

$$10 \log_{10} P_0 = 53 + \text{multipath antenna gain} - \text{reflection loss from surface} \qquad (1.19)$$

At low elevation angles the reflection loss at vertical polarization is approximately compensated by the gain of proposed multipath antennas, leaving $\log_{10}P_0 = 53$ dB a worst case value.

Since $Q(\delta)$ decreases monotonically with δ, $\rho_{out}(\delta)$ will become too small to make measurement meaningful for sufficiently large values of δ. Consider the case of largest multipath spread, $\theta = 10^o$, $\alpha = .2$, $H = 30{,}000$ feet. For this case a B_N of around 200 Hz is reasonable for the output low pass filters assuming a horizontal aircraft velocity of 400 mph and $f_0 = 1.6$ GHz. Utilizing these parameters

$$\rho_{out} = 208(T_0 10^6)Q(\delta) \tag{1.20}$$

If we select $T_0 = \Delta = .672$ μsec as in our example above, we find that

$$\rho_{out}(\delta) = 140\ Q(\delta) \tag{1.21}$$

At $\delta = 14$, which is the value of delay beyond which 1% of the power exists in the delay power spectrum, we find that $\rho_{out}(\delta_{.01})$ is around 0 dB! The conclusion to be reached here is that more than 100 correlators cannot be justified on the basis of SNR for the worst case multipath measurement.

We turn our attention now to the selection of T the period of the PN sequence and the output low pass filter. There exist two general contradictory restrictions on selection of T. First T must be selected large enough so

that no ambiguities will be introduced by the periodic probing signal, i.e., T must exceed the duration of the channel impulse response including both direct and multipath components. The 99% duration of the multipath as predicted from the steepest descent model for $\alpha = .2$, H = 30,000 feet, $\theta = 10^{o}$ is 67 μsec. This value is undoubtedly only an upper bound to the true value because the steepest descent model, which applies to a flat earth, does not account for the finite illuminated cap of the earth. If we add the delay between the direct path and the specular point, 2H/c sin θ, we obtain a total maximum impulse duration of 77.5 μsec. For the case $\Delta = T_0$ we have found that $T_0 \geq .672$ μsec to keep the number of correlators ≤ 100 for the assumed parameters α, H, θ. The number of bits in one period of the PN sequence must thus exceed

$$N \geq \frac{77.5}{.672} = 115 \qquad (1.22)$$

Since

$$N = 2^{\ell}-1 \qquad (1.23)$$

for a maximal length shift register sequence, the lowest acdeptable value of N is given by 127 which corresponds to $\ell=7$.

The above argument restricted the value of T from being too small. There is another restriction on T which prevents it from being too large. As discussed in Section 1.6.2, the input to the low pass filter contains spurious harmonic

components occuring at multiples of 1/T Hz whose strengths can be as large as the desired signal when the multipath spread is comparable to T (see Eq. (1.8)). Each one of these spurious components has a bandwidth which is of the order of the channel Doppler spread. The Doppler spread increases with elevation angle. At $\theta = 30^{o}$, which is probably the largest elevation angle worth considering where the antenna gains will allow the multipath to be perceptible, the 99% Doppler spread is approximately $\pm$500 Hz relative to the center frequency. Clearly, if T is chosen = 1/1000 the signal/harmonic cross-talk will be less than 20 dB even with ideal rectangular filters. Thus T must be less than 1000 μsec. A value of $T \leq 500$ μsec, corresponding to a nearest harmonic at around 2 Kc should allow the use of moderately complex low pass filter (say fourth-order Butterworth) which will pass the desired component with small distortion and attenuate the nearest harmonic component to negligible values.

A value of $T_0 = 2$ μsec must be considered for the probing equipment because of the existence of an Aerosat tapped delay line simulator which can be used for playback channel simulation. In order to keep the nearest harmonic $\geq$ 2 Kc in this case, a value of N = 255 (ℓ=8) or N = 127 (ℓ=7) would have to be used.

Clearly at the lower elevation angles the Doppler spread will be smaller and thus larger N and T values could be used. It is desirable to use as large an N value as possible because the spurious low pass term discussed in 1.6.2 (see Eq. (1.9)) is thereby reduced relative to the desired term. However, it is pointed out in Section 1.6.2, that if

$$N^2 \gg P_0/B_N \tag{1.24}$$

the spurious low pass term will be negligible with respect to the additive noise. The maximum value of the ratio P_0/B_N will be 1000 which is certainly much less than N^2 even for $N = 127$.

In the case of time-multiplexing the measurement of the vertical and horizontal polarized channels, it will be recalled that the spurious harmonic terms are at multiples of half the PN fundamental frequency. Thus in this case a value of $N = 127$ must be used at $T_0 = 2$ μsec to keep the nearest spurious harmonic around 2 Kc away from D.C.

We consider now the allowable differential phase and gain insertion errors introduced by the set of correlators. These differential phase shifts and gains will cause errors in the reproduction of the measured channel. In Appendix F it is shown that e, the percentage mean-squared error introduced in the reproduced transfer function, is given by

$$e = \sigma_\phi^2 \tag{1.25}$$

where σ_ϕ is the RMS differential phase error. It is also shown that the percentage mean-squared error in the reproduced transfer function introduced by differential gain errors (relative to a mean gain of unity) is given by

$$e = \sigma_\epsilon^2 \tag{1.26}$$

where σ_ϵ is the RMS value of the differential gain error. For uniform distribution of ϕ and ϵ over $|\phi| \leq \phi_{max}$ and $|\epsilon| \leq \epsilon_{max}$ one finds that $\sigma_\phi = \phi_{max}/\sqrt{3}$. Then a value $\epsilon_{max} = .15$ dB and $\phi_{max} = 2^o$ lead to around a value of ϵ of around -34 dB.

1.7 Conclusion

The preceding calculations of ranging and data modem performance suggest strongly that:

1. The level of performance of both side-tone and PN ranging and conventional data modems cannot satisfy the stated requirements of 100 meters RMS ranging error and 10^{-5} error probability, respectively, at low elevation angles for a 50 Kc Aerosat bandwidth and the turnstile antenna of Fig. 1.4.

   For example, with this antenna and an assumed 7 dB of improvement due to tone filtering, an RMS ranging error of around 800 meters may be expected for less than 95% of the azimuth directions at an antenna elevation angle of 10^o with an RMS sea slope of .1. To achieve 100 meters RMS ranging error for the same conditions requires that the antenna discrimination against multipath be improved by 18 dB.

   Thus considerably better antennas are required to meet 100 meter RMS error if conventional modems are used in the 50 Kc Aerosat bandwidth. An increase of the bandwidth available for ranging by an order of magnitude is required to achieve 100 meter RMS ranging error with the turnstile antenna of Fig. 1.4.

2. With regard to data transmission it is shown that for the same set of channel and system parameters quoted above for the ranging modem, an error rate of 10^{-2} or less will be achieved by a DPSK system at 1200 bits/sec for 95% of the azimuth points. For FSK an error rate of 7×10^{-3} is achieved for 95% of the points. On the other hand, the study indicates that with the use of advanced modem techniques an error rate of less than 10^{-5} can be achieved for 100% of the azimuth points for both FSK and DPSK.

It should be abundantly clear that important cost trade-off considerations exist between antenna design and advanced modem design in meeting overall system accuracy goals. The results quoted above are referenced to the turnstile antenna. As soon as data on candidate antennas becomes available, corresponding calculations of ranging error and modem performance will be carried out.

3. To design modems which can meet these requirements requires additional channel parameter information beyond those measured in previous experiments including the FAA-Boeing, ESRO, Dept. of Transportation TSC Balloon Tests, and the Canadian Dept. of Communications. In particular, direct/multipath power ratios for candidate operational antennas and the multipath frequency correlation characteristics of the indirect paths should be measured, especially at low elevation angles.

4. Since the modem design problem is presently an open question, channel measurements should be taken in such a way that the data can be used at some future date for recreating the channel while at the same time providing the necessary channel parameter information for system design. In this way field experiments do not have to be repeated to test modems not available at the time of the field experiments.

5. If modem evaluation tests with modems are carried out it is essential that channel parameter measurements be conducted at the same time so that when poor performance occurs its cause may be related to channel characteristics.

The channel measurement requirements can be satisfied by means of a pseudo-random probing signal and receiver consisting of a set of parallel correlators driven by delayed locally-generated pseudo-random signals as discussed in Section 1.6. The resulting output low-pass signals yield the complex tap gains of a tapped delay line model of the channel. These signals may be analyzed on-line or off-line to determine the channel parameters of interest. They may also be recorded with a standard instrumentation recorder for use at some future date as the driving signals for a tapped delay line in order to recreate the channel's time variant system function for modem testing. The cost of the prober, demodulator, on-line data reduction, and recorder would be a small fraction of the cost of a field demonstration test of modems.

In summary, it is recommended that additional channel measurements be undertaken and coordinated with a laboratory simulation capability for effective modem development and testing. If these recommendations are followed through:

1. It will be possible to develop modem techniques with high probability that they will work effectively under operational conditions. The possible incorrect acceptance of a modem because field tests were not conducted with parallel channel measurements will not occur.

2. It will be possible to identify clearly the reason for failure of modems during field tests and thus formulate approaches for improvement of the modem technique.

3. It will be possible to avoid large-scale production of modems which have high probability of failure, resulting in a large saving to the government.

4. Considerable savings in the money expended for field tests may be expected because the stored channel may be used to test new techniques whenever they occur.

SECTION 1

REFERENCES

[1.1] H. Staras, "Rough Surface Scattering on a Communication Link," Radio Science, Vol. 3, (New Series), No. 6, June 1968, pp. 623-631.

[1.2] A. J. Mallinckrodt, "Ground Multipath in Satellite-Aircraft Propagation," Paper Presented at the Symposium on Application of Atmospheric Studies to Satellite Transmissions (sponsored by the Radio Astronomy Branch of the Ionospheric Physics Lab., AFCRL), Boston, September 1969.

[1.3] P. A. Bello, "Aeronautical Channel Characterization," to be published in IEEE Transactions on Communications, 1973.

[1.4] "Multipath/Ranging Experimental Program Interim Results," Contract DOT FA 09WA-2109, prepared for the F.A.A. by Boeing Co., December 1971.

[1.5] P. Beckmann and A. Spizzichino, The Scattering of Electromagnetic Waves From Rough Surfaces, Pergamon Press, 1963.

[1.6] E. Clausen, et al., "PLACE Final Report," prepared for Goddard Space Flight Center under Contract NAS-5-21101 by Bell Aerospace Corp., June 1970.

[1.7] J. Jay Jones, "Multi-Channel FSK and DPSK Reception With Three-Component Multipath," IEEE Communication Technology, Vol. COM-16, December 1968, pp. 808-821.

[1.8] D. Chase, "A Class of Algorithms for Decoding Block Codes With Channel Measurement Information," IEEE Trans. on Information Theory, Vol. IT-18, No. 1, January 1972.

[1.9] Y. W. Lee, "Statistical Theory of Communications," 1960, Wiley and Sons, p. 342, Section 9.

[1.10] R. Price and P. E. Green, "A Communication Technique for Multipath Channels," Proc. IRE, pp. 555-570, March 1958.

[1.11] Y. Peters and T. Murakaini, "Analysis and Synthesis of Transitional-Butterworth Filters and Bandpass Amplifiers," RCA Review, March 1957.

[1.12] Trygri Olsson, Brian P. Stapleton, "L-Band Orthogonal-Mode Crossed-Slot Antenna and HF Crossed-Loop Antenna," DOT-TSC-NASA-72-2, August 1972 Final Report of Boeing Co.

SECTION 2

EFFECT OF TIME AND FREQUENCY SELECTIVE FADING ON TONE RANGING SYSTEMS: PRELIMINARY ANALYSIS

This section presents a preliminary analysis of the effects of time and frequency selective fading upon tone ranging systems. While we consider the simplest possible tone ranging system, an SSB system involving three tones with one closely spaced pair being used for ambiguity resolution, we show that to a first approximation these analytical results may be used for a double sideband system at high SNR's and γ's. The channel is assumed to consist of the parallel combination of a nonfading channel and a complex Gaussian WSSUS channel [2.1] with associated mean delays and Doppler shifts.

No consideration is given to the measurement of range rate and the range is assumed to change negligibly over the integration time used to provide a range estimate. Finally, we consider only the one-way ranging problem here.

2.1 Channel Model

Figure 2.1 depicts the assumed mathematical model of the channel relating input and output complex envelopes. There is shown a nonfading channel which provides a delay ξ_d, complex gain G_d, and Doppler shift ν_d, in parallel with a fading dispersive channel in which a mean path delay ξ_s, path gain G_s, and Doppler shift ν_s, have been explicitly formalized by separate operations. The time variant transfer function of the fading channel T(f,t) can thereby be normalized to unit strength

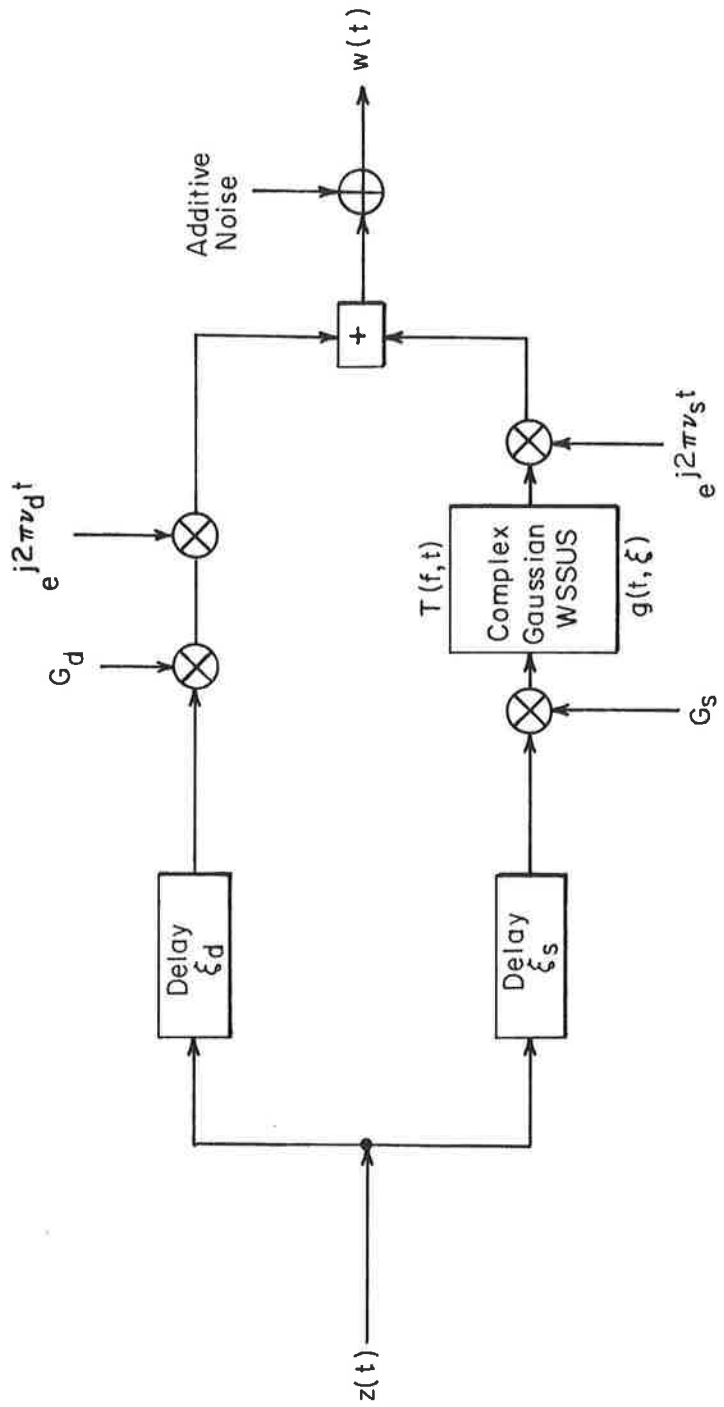

Figure 2.1 Channel Model

$$\overline{|T(f,t)|^2} = 1 \tag{2.1}$$

and to have a spectrum centered at f=0 (i.e., at the carrier frequency). Also the time variant impulse response

$$g(t,\xi) = \int T(f,t)e^{j2\pi f\xi}\, df \tag{2.2}$$

can be shifted in time to have zero "mean" path delay.

The ratio

$$\gamma = \frac{|G_d|^2}{|G_s|^2} \tag{2.3}$$

is called the direct-to-scatter path power ratio. Phase shifts $2\pi\xi_d f_o$ and $2\pi\xi_s f_o$ associated with the carrier frequency have been absorbed into G_d and G_s.

Due to the WSSUS assumption

$$\overline{g^*(t,\xi)g(t+\tau,\eta)} = Q(\tau,\xi)\delta(\eta-\xi) \tag{2.4}$$

where $Q(\tau,\xi)$ is called the tap gain correlation function. Equivalently,

$$\overline{T^*(f,t)T(f+\Omega,t+\tau)} = R(\Omega,\tau) \tag{2.5}$$

where $R(\Omega,\tau)$, the time-frequency correlation function, is the Fourier transform of $Q(\tau,\xi)$

$$R(\Omega,\tau) = \int Q(\tau,\xi)e^{-j2\pi\Omega\xi}\, d\xi \tag{2.6}$$

2.2 Representation of Signals

For the preliminary analysis here, the transmitted signal is assumed to consist of three equal strength sinusoids

$$z(t) = \sum_{k=1}^{3} Ae^{j2\pi f_k t} \tag{2.7}$$

The received signal corresponding to the nonfading path alone is given by

$$AG_d e^{j2\pi\nu_d t} \sum_{k=1}^{3} e^{j2\pi f_k t} e^{-j2\pi f_k \xi_d} \tag{2.8}$$

and the received signal corresponding to the fading path is

$$AG_s e^{j2\pi\nu_s t} \sum_{k=1}^{3} T(f_k,t) e^{j2\pi f_k t} e^{-j2\pi f_k \xi_s} \tag{2.9}$$

Thus the total received signal including additive noise is given by

$$w(t) = A \sum_{k=1}^{3} [G_d e^{j2\pi\nu_d t} e^{-j2\pi f_k \xi_d} + G_s e^{j2\pi\nu_s t} e^{-j2\pi f_k \xi_s} T(f_k,t)] e^{j2\pi f_k t} + n(t) \tag{2.10}$$

2.3 Receiver Processing

Figure 2.2 presents a simplified block diagram showing the signal processing operations in the receiver utilized for estimating path delay and eliminating ambiguities. Since (one-way) range is related to delay by a proportionality constant, no loss in generality results from our consideration of delay rather than range estimation.

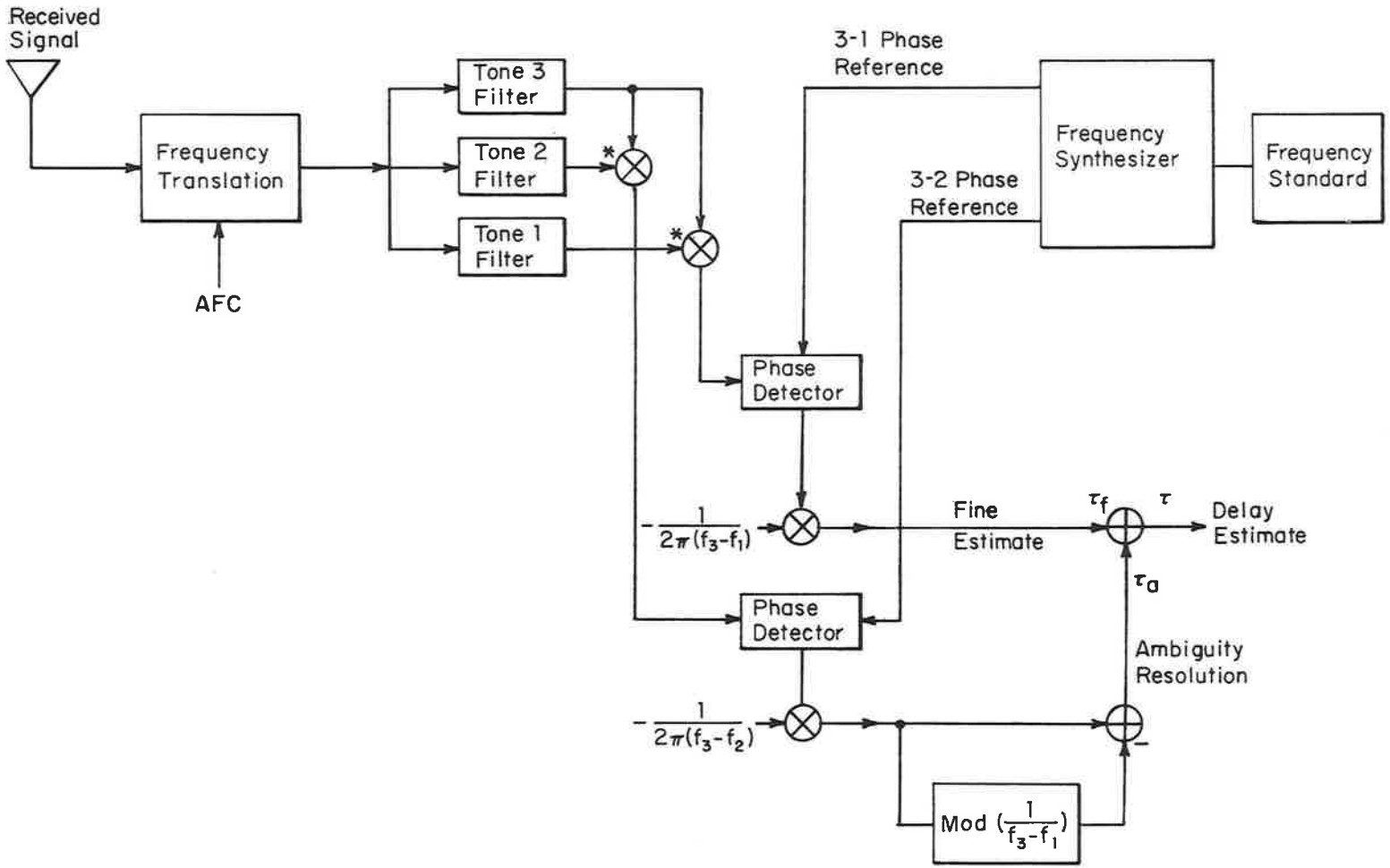

Figure 2-2. Simplified Block Diagram of Receiver Processing

reference at the transmitter. We do not discuss this synchronization problem here but assume that synchronization has been achieved and that no errors occur due to mistiming. Another assumption we make initially is that AFC perfectly compensates for Doppler shifts in the non-fading paths.

At the receiver separate filtering of the received tones occurs at some convenient intermediate frequency (or even at baseband through in-phase and quadrature processing). Tone 3 is the highest frequency and Tone 2 is close enough in frequency to Tone 3 to provide ambiguity resolution. Tone 1* is sufficiently below Tone 3 to provide the desired fine delay estimate. The filters used to extract the tones should be designed to prevent differential phase shifts from occuring with or without residual Doppler tracking error.

Consider the receiver operation in the absence of the fading path and noise, assuming perfect time and frequency synchronization and no phase errors introduced by the tone filters. The result of mixing Tone 3 and Tone 1 filter outputs (to the difference frequency) is given by

$$[AG_d e^{j(2\pi f_3 t - 2\pi f_3 \xi_d)}][AG_d e^{j(2\pi f_1 t - 2\pi f_1 \xi_d)*}]$$

$$= A^2 |G_d|^2 e^{j2\pi(f_3 - f_1)t} \cdot e^{-j2\pi(f_3 - f_1)\xi_d} \qquad (2.11)$$

The local frequency synthesizer driven by the properly synchronized clock provides the reference

---

*In a conventional receiver tone 1 would correspond to the carrier which would be acquired and tracked with a phase locked loop (PLL). The PLL output would be used for coherent detection of tones 2 and 3 and this would be followed by tone filter extraction and comparison with reference tones. In our system all filtering takes place prior to detection and performance should be somewhat better. Also, our system can be analyzed simply.

$$e^{j2\pi(f_3-f_1)t}$$

Consequently the upper phase detector in Fig. 2.2 provides an output

$$-2\pi(f_3-f_1)\xi_d \text{ Mod } (2\pi)$$

which after the multiplication produces a finebut ambiguous delay estimate of

$$\tau_f = \xi_d \text{ Mod } (\frac{1}{f_3-f_1}) \qquad (2.12)$$

The result of mixing Tone 3 and Tone 2 filter outputs is given by

$$A^2|G_d|^2 e^{j2\pi(f_3-f_2)t} \; e^{-j2\pi(f_3-f_2)\xi_d}$$

With the aid of the phase reference from the local frequency synthesizer and carrying through the indicated operations in Fig. 2.2 the ambiguity resolver produces the output

$$\tau_a = \xi_d - \xi_d \text{ Mod } (\frac{1}{f_3-f_1}) \qquad (2.13)$$

assuming $\xi_d < 1/(f_3-f_2)$.

Adding (2.12) and (2.13) produces the correct delay estimate

$$\tau = \tau_f + \tau_a = \xi_d \tag{2.14}$$

2.4 Performance With Additive Noise

In this section we develop expressions for the error in estimating delay of the non-fading path when the fading path is absent and the only non-ideality present is additive noise.

Let the (complex) noise at tone filter k output be denoted by $\eta_k(t)e^{j2\pi f_k t}$. Then the output of the k'th filter is given by

$$w_k(t) = AG_d e^{j2\pi f_k(t-\xi_d)} + \eta_k(t)e^{j2\pi f_k t}$$

$$= AG_d R_k(t)e^{j[2\pi f_k(t-\xi_d) + \phi_k(t)]} \tag{2.15}$$

where

$$R_k(t)e^{j\phi_k(t)} = 1 + \frac{\eta_k(t)}{AG_d} \tag{2.16}$$

and we have absorbed a phase factor exp ($j2\pi f_k \xi$) into $\eta_k(t)$ without loss of generality because $\eta_k(t)$ has a uniform phase distribution and we assume all

the filter additive noise outputs are statistically independent.

For large SNR S_k, i.e.,

$$\frac{1}{\sqrt{S_k}} \equiv \frac{\sqrt{\overline{|\eta_k|^2}}}{AG_d} << 1 \qquad (2.17)$$

only the quadrature component of $\eta_k(t)$ in (2.16) affects the phase, and $\phi_k(t)$ is approximately Gaussianly distributed with

$$\phi_k(t) \approx \frac{\mathrm{Im}\{\eta_k(t)\}}{AG} \quad ; \quad S_k >> 1 \qquad (2.18)$$

The RMS value of $\phi_k(t)$ is then

$$\sqrt{\overline{[\phi_k(t)]^2}} \approx \frac{1}{\sqrt{2S_k}} \quad ; \quad S_k >> 1 \qquad (2.19)$$

When S_k is not large the distribution of $\phi_k(t)$ is non-Gaussian and cannot be expressed in closed form. Single integral expressions are readily obtained.

Assuming no post detection filtering, the delay estimates at the output of the system in Fig. 2.2 are obtained by sampling. Consequently in dealing with the phase detector output we shall find it convenient to suppress the time variables.

The fine delay estimate can be expressed as*

$$\tau_f = -\frac{1}{2\pi(f_3-f_1)}\left[\angle\left\{w_3^*(t)w_1(t)e^{-j2\pi(f_3-f_1)t}\right\} \text{ Mod } 2\pi\right] \qquad (2.20)$$

Using the above definitions,

$$\tau_f = \frac{1}{2\pi(f_3-f_1)}\left(2\pi(f_3-f_1)\xi_d + \phi_1 - \phi_3\right) \text{ Mod } 2\pi$$

$$= \xi_d \text{ Mod } \left(\frac{1}{f_3-f_1}\right) + \frac{1}{2\pi(f_3-f_1)}\left(\phi_1 - \phi_3\right) \text{ Mod } 2\pi \qquad (2.21)$$

Thus determination of the statistics of errors in the fine delay estimate involves evaluation of the probability distribution of $(\phi_1-\phi_3)$. From the previous discussions we see that for high SNR, $\phi_1-\phi_3$ will be approximately zero-mean Gaussian with RMS value

$$\sqrt{\overline{(\phi_1-\phi_3)^2}} \approx \sqrt{\frac{1}{2}\left(\frac{1}{S_1}+\frac{1}{S_3}\right)} = \frac{1}{\sqrt{S}} \qquad (2.22)$$

where S is the common SNR at the outputs of filters 1 and 3.

*All Mod 2π operations are referred to the basic interval $(-\pi, \pi)$.

Although not indicated in Fig. 2.2, it should be clear that because f_2 and f_3 are close in frequency a second fine delay estimate may be obtained by mixing Tone 2 and Tone 1 filter outputs and phase detecting with an appropriate reference. By analogy with the above calculations, this estimate is given by

$$\hat{\tau}_f = \xi_d \text{ Mod } (\frac{1}{f_2-f_1}) + \frac{1}{2\pi(f_2-f_1)} (\phi_1-\phi_2) \text{ Mod } 2\pi \tag{2.23}$$

For the ambiguity delay estimate we see that

$$\tau_a = \tau_o-\tau_o \text{ Mod } (\frac{1}{f_3-f_1}) \tag{2.24}$$

where

$$\tau_o = -\frac{1}{2\pi(f_3-f_2)} [\measuredangle \{w_3^*(t)w_2(t)e^{-j2\pi(f_3-f_2)t}] \text{ Mod } 2\pi$$

$$= \xi_d + \frac{1}{2\pi(f_3-f_2)} (\phi_2-\phi_3) \text{ Mod } 2\pi \tag{2.25}$$

Thus

$$\tau_a = \xi_d-\xi_d \text{ Mod } (\frac{1}{f_3-f_1}) + \frac{1}{2\pi(f_3-f_2)} (\phi_2-\phi_3) \text{ Mod } 2\pi$$

$$- (\frac{(\phi_2-\phi_3) \text{ Mod } 2\pi}{2\pi(f_3-f_2)}) \text{ Mod } (\frac{1}{f_3-f_1}) \tag{2.26}$$

If the estimate $\hat{\tau}_f$ (2.23) is to be resolved in ambiguity it is necessary to form

$$\hat{\tau}_a = \tau_o - \tau_o \text{ Mod } (\frac{1}{f_2 - f_1}) \tag{2.27}$$

The ambiguity error will be zero in τ_a when

$$|(\phi_2 - \phi_3) \text{ Mod } 2\pi| < (\frac{f_3 - f_2}{f_3 - f_1})\pi \tag{2.28}$$

and in $\hat{\tau}_a$ when

$$|(\phi_2 - \phi_3) \text{ Mod } 2\pi| < (\frac{f_3 - f_2}{f_2 - f_1})\pi \tag{2.29}$$

Since $f_2 < f_3$, (2.28) is more stringent.

The system is normally designed to make the probability of an ambiguity error negligible. At high SNR this is seen to imply that

$$\frac{K}{\sqrt{S}} < (\frac{f_3 - f_2}{f_2 - f_1})\pi \tag{2.30}$$

where K is an integer exceeding 6 to have the ambiguity error probability $< 10^{-9}$.

If the ambiguity error is indeed negligible, then the final delay estimates are

$$\tau = \tau_f + \tau_a = \xi_d + \frac{(\phi_1 - \phi_3) \text{ Mod } 2\pi}{2\pi(f_3 - f_1)} \tag{2.31}$$

$$\hat{\tau} = \hat{\tau}_f + \hat{\tau}_o = \xi_d + \frac{(\phi_1 - \phi_2) \text{ Mod } 2\pi}{2\pi(f_2 - f_1)} \tag{2.32}$$

These estimates may be combined to form an improved unbiased estimate $\tilde{\tau}$ as follows

$$\tilde{\tau} = \alpha\tau + (1-\alpha)\hat{\tau} \tag{2.33}$$

where

$$\alpha = \frac{\overline{(\hat{\tau} - \xi_d)(\hat{\tau} - \tau)}}{\overline{(\hat{\tau} - \tau)^2}} \tag{2.34}$$

If f_2 is close to f_3 little error is introduced by setting $\alpha = 1/2$ to form

$$\bar{\tau} = \frac{1}{2}(\tau + \hat{\tau})$$

or when there is no ambiguity error

$$\tilde{\tau} = \xi_d + \frac{1}{2}\left\{\frac{(\phi_1-\phi_3) \text{ Mod } 2\pi}{2\pi(f_3-f_1)} + \frac{(\phi_1-\phi_2) \text{ Mod } 2\pi}{2\pi(f_2-f_1)}\right\} \qquad (2.35)$$

2.5 Performance With Fading and Additive Noise

We consider now the combined fading and additive noise case. Using Eq.(2.10) we find that the complex envelope of the k'th filter output is

$$w_k(t) = AG_d e^{-j2\pi f_k \xi_d}[1 + M_k(t) + \frac{\eta_k(t)}{AG_d}]e^{j2\pi f_k t} \qquad (2.36)$$

where

$$M_k(t) = \frac{G_s}{G_d} e^{-j2\pi f_k(\xi_s-\xi_d)}[e^{j2\pi(\nu_s-\nu_d)t} T(f_k, t) \otimes h_k(t)] \qquad (2.37)$$

and $h_k(t)$ is the impulse response of the k'th filter. Since we have assumed the channel to be complex Gaussian, $M_k(t)$ will also be complex Gaussian and thus have the character of the additive noise term $\eta_k(t)$. However, unlike the set $\{\eta_k(t)\}$, the various $M_k(t)$ will generally be correlated.

To simplify the notation we shall absorb the Doppler difference exponential exp $[j2\pi(\nu_s-\nu_d)t]$ into $T(f_k, t)$, which can be accounted for by simply offsetting the Doppler spectrum of the WSSUS channel by $\nu_s-\nu_d$ Hz. Using this artifice, the cross correlation between M_k and M_ℓ is

$$\overline{M^*_k M_\ell} = \frac{|G_s|^2}{|G_d|^2} e^{-j2\pi(f_k - f_\ell)(\xi_s - \xi_d)} \int R(f_\ell - f_k, \tau) R_h^{k\ell}(\tau)\, d\tau \tag{2.38}$$

where $R(\Omega, \tau)$ is the channels time-frequency correlation function and $R_h^{k\ell}(\tau)$ is the aperiodic cross correlation function of h(t),

$$R_h^{k\ell}(\tau) = \int h_k^*(t) h_\ell(t+\tau)\, dt \tag{2.39}$$

The correlation coefficient between M_k and M_ℓ is

$$r_{k\ell} = e^{-j2\pi(f_k - f_\ell)(\xi_s - \xi_d)} \frac{\int R(f_\ell - f_k, \tau) R_h^{k\ell}(\tau)\, d\tau}{\sqrt{\int R(0, \tau) R_h^{kk}(\tau)\, d\tau \int R(0, \tau) R_h^{\ell\ell}(\tau)\, d\tau}} \tag{2.40}$$

When there is only time selective fading and the filter complex impulse responses are identical

$$R(f_\ell - f_k, \tau) = R(0, \tau) \tag{2.41}$$

$$r_{k\ell} = e^{-j2\pi(f_k - f_\ell)(\xi_s - \xi_d)} \tag{2.42}$$

If by analogy with the previous section we define

$$R_k(t)e^{j\phi_k(t)} = 1 + M_k(t) + \frac{\eta_k(t)}{AG_d} \tag{2.43}$$

Then the same expressions for fine and ambiguity delay estimates apply as in that section. Now, however, the $\{\phi_k\}$ must generally be assumed statistically dependent.

For the case of high SNR and large direct/scatter path power ratio we may use the quadrature approximation

$$\phi_k(t) \approx \text{Im}\ \{M_k(t)\} + \text{Im}\ \{\frac{\eta_k(t)}{AG_d}\}\ . \tag{2.44}$$

so that

$$\tau_f = \xi_d \text{ Mod } (\frac{1}{f_3-f_1}) + \frac{1}{2\pi(f_3-f_1)} \text{ Im } \{M_1(t) - M_3(t) + \frac{\eta_1(t) - \eta_2(t)}{AG_d}\} \tag{2.45}$$

From (2.45) we see that the mean square error in the fine delay estimate is given by

$$\sigma_f^2 = \frac{1}{(2\pi)^2(f_3-f_1)^2}\left[\frac{1}{2}\sigma_{M_{13}}^2 + \frac{1}{S}\right] \tag{2.46}$$

where (using (2.38) and (2.40))

$$\sigma^2_{M_{13}} = \overline{|M_1 - M_3|^2}$$

$$= \frac{1}{\gamma}\sqrt{\int R(0,\tau)R_h^{11}(\tau)\,d\tau \int R(0,\tau)R_h^{33}(\tau)} \qquad (2.47)$$

$$\times\left[\sqrt{\frac{\int R(0,\tau)R_h^{11}(\tau)\,d\tau}{\int R(0,\tau)R_h^{33}(\tau)\,d\tau}} + \sqrt{\frac{\int R(0,\tau)R_h^{33}(\tau)\,d\tau}{\int R(0,\tau)R_h^{11}(\tau)\,d\tau}} - 2\mathrm{Re}(r_{13})\right]$$

For the case of identical filters (2.47) simplifies to

$$\sigma^2_{M_{13}} = \frac{2}{\gamma}\int R(0,\tau)R_h(\tau)\,d\tau\,[1 - \mathrm{Re}(r_{13})] \qquad (2.48)$$

where $R_h(\tau)$ is the aperiodic autocorrelation function of h(t),

$$R_h(\tau) = \int h^*(t)h(t+\tau)\,dt \qquad (2.49)$$

Note that the integral (2.48) can be expressed in the form

$$\int R(0,\tau)R_h(\tau)\,d\tau = \int P(\nu+\nu_d-\nu_s)|H(\nu)|^2\,d\nu \qquad (2.50)$$

where $H(\nu)$ is the transfer function of the complex low-pass filter and $P(\nu)$ is the Doppler spectrum of the fading channel. For a fading spectrum broad compared with the filter bandwidth we may approximate (2.50) by

$$\int R(0,\tau)R_h(\tau)\,d\tau \approx P(\nu_d-\nu_s)W_N \tag{2.51}$$

where W_N is the two-sided noise bandwidth of the filter (we have normalized $H(0) = 1$). Since

$$R(0,0) = \int P(\nu)\,d\nu = 1 \tag{2.52}$$

it follows that

$$P(0) = \frac{1}{B_N} \tag{2.53}$$

where B_N is the two-sided noise bandwidth of the Doppler spectrum. These definitions lead to

$$\int R(0,\tau)R_h(\tau)\,d\tau = \frac{W_N}{B_N} \cdot \frac{P(\nu_d-\nu_s)}{P(0)} \tag{2.54}$$

If the Doppler difference is small compared to B_N and $P(\nu)$ is unimodal and symmetrical, then

$$\int R(0,\tau)R_h(\tau)\,d\tau \approx \frac{W_N}{B_N} \tag{2.55}$$

which leads to the approximation

$$\sigma_f^2 = \frac{1}{(2\pi)^2(f_3-f_1)^2}\left[\frac{W_N}{\gamma B_N}(1 - \mathrm{Re}(r_{13})) + \frac{1}{S}\right] \quad ; \quad P(\nu_d-\nu_s) \approx P(0) \quad ; \quad h_k(t) = h_\ell(t) \tag{2.56}$$

The term $\mathrm{Re}(r_{13})$ can vary between -1 and +1. Note that r_{13} contains the complex exponential $\exp(-j2\pi(f_k-f_\ell)(\xi_s-\xi_d))$. If the frequency selectivity of the fading channel is small enough, then

$$\mathrm{Re}\{r_{13}\} = \cos[2\pi(f_3-f_1)(\xi_s-\xi_d)] \tag{2.57}$$

and $1 - \mathrm{Re}(r_{k\ell})$ can cover the full range between -1, 1.

We may readily determine the requirement for negligible probability of an ambiguity from (2.28). In particular we see that at high ρ and $\gamma B_N / W_N$,

$$K\frac{W_N}{\gamma B_N}(1 - \mathrm{Re}\{r_{23}\}) + \frac{1}{S} < \left(\frac{f_3-f_2}{f_3-f_1}\right)\pi , \tag{2.58}$$

where K is an integer exceeding 6 in order to have the ambiguity error probability $< 10^{-9}$.

Since f_2 and f_3 are close it may be that

$$\mathrm{Re}\{r_{23}\} \approx 1 \tag{2.59}$$

which removes the effect of the fading channel on the ambiguity error probability (at least in the high SNR approximation). However if f_2 and f_3 are closer than the Doppler spectrum width the received tone spectra will overlap into adjacent tone filters. The resulting delay errors may be calculated using the results in this paper.

The above results are readily generalized to include an additional delay estimate with tone pairs 1 and 2.

When the SNR S and γ B_N/W_N are not sufficiently large, the above simplified expressions for measurement error and ambiguity probability must be modified. The analytical problem is that of finding the probability distribution of the phase difference θ between correlated non-zero-mean complex Gaussian vectors. This problem does not seem to have been attacked in the open literature. Appendix A derives a single integral expression for the distribution in the form $W(\theta;r,\beta,\rho_1,\rho_2)$ where ρ_1 and ρ_2 are the SNR's and r exp ($j\beta$) is the complex correlation coefficient of the noises. Our parameters are the direct path/scatter ratio γ; the direct path to additive noise ratio at two tone filter outputs S_1, S_2; the complex correlation coefficient of the scatter components at the two tone filter outputs, r_{12}; and the relative strength of the scatter and additive noise components at the two filter outputs. The relationship between these parameters are as follows:

$$\rho_k = \frac{S_k}{1 + \frac{S_k}{\gamma} \int R(0,\tau) R_h^{kk}(\tau)\, d\tau} \tag{2.60}$$

$$re^{j\beta} = \frac{r_{12}}{\sqrt{\left(1 + \frac{\gamma}{S_1 \int R(0,\tau) R_h^{11}(\tau)\, d\tau}\right)\left(1 + \frac{\gamma}{S_2 \int R(0,\tau) R_h^{22}(\tau)\, d\tau}\right)}} \tag{2.61}$$

where (repeating (2.39) and (2.40))

$$r_{12} = e^{-j2\pi(f_1 - f_2)(\xi_s - \xi_d)} \frac{\int R(f_2 - f_1, \tau) R_h^{k\ell}(\tau)\, d\tau}{\sqrt{\int R(0,\tau) R_h^{11}(\tau)\, d\tau \int R(0,\tau) R_h^{22}(\tau)\, d\tau}} \tag{2.62}$$

in which

$$R_h^{k\ell}(\tau) = \int h_k^*(t) h_\ell(t+\tau)\, dt \tag{2.63}$$

where $h_k(t)$ is the complex impulse response of the k'th filter.

When the Doppler spectrum of the scatter is much wider than the filter bandwidth, the mean Doppler shift is small, the selective fading

over f_2-f_1 is negligible, and the filters are identical, the above relationships simplify to

$$\rho_k = \frac{S_k}{1 + \frac{S_k}{\gamma} \cdot \frac{W_N}{B_N}} \tag{2.64}$$

$$r = \frac{1}{\sqrt{1 + \frac{\gamma}{S_1} \cdot \frac{B_N}{W_N}} \sqrt{1 + \frac{\gamma}{S_2} \cdot \frac{B_N}{W_N}}} \tag{2.65}$$

$$\beta = 2\pi(f_2-f_1)(\xi_s-\xi_d) \tag{2.66}$$

where W_N is the noise bandwidth of the tone filter and B_N is the noise bandwidth ot the Doppler spectrum.

2.6 Inclusion of Effects of Channel Characteristics for an Airplane-Satellite/Link

The previous section has shown that RMS ranging error depends upon the dispersive character of the multipath channel through the correlation coefficient of fluctuations at the tone filter outputs (see Eq. (2.40) and note that we have excluded the exponential in our definition)

$$r(\Omega) = \frac{\int R(\Omega,\tau)R_{hg}(\tau)\, d\tau}{\sqrt{\int R(0,\tau)R_{hh}(\tau)\, d\tau \int R(0,\tau)R_{gg}(\tau)\, d\tau}} \qquad (2.67)$$

where $R_{hh}(\cdot)$, $R_{hg}(\cdot)$, $R_{gg}(\cdot)$ are auto and cross correlation functions of the two tone filter impulse responses and $R(\Omega,\tau)$ is the time-frequency correlation function of the multipath channel.

By using Parseval's theorem one may change the time-domain integrals in (2.67) into frequency domain integrals to produce the alternate expression

$$r(\Omega) = \frac{\int P(\Omega,\nu)H^*(\nu)G(\nu)\, d\nu}{\sqrt{\int P(\nu)|H(\nu)|^2\, d\nu \int P(\nu)|G(\nu)|^2\, d\nu}} \qquad (2.68)$$

where $P(\Omega,\nu)$ is the cross-power spectral density of two received carriers spaced Ω Hz apart at transmission and $H(\nu)$, $G(\nu)$ are the transfer functions of the two tone filters. The cross-power spectrum is related to the time-frequency correlation function by Fourier transformation

$$P(\Omega,\nu) = \int R(\Omega,\tau)e^{-j2\pi\tau\nu}\, d\tau \qquad (2.69)$$

The function $P(0,\nu)$ may be recognized as the Doppler power density spectrum $P(\nu)$, i.e.,

$$P(\nu) = P(0,\nu) \tag{2.70}$$

In [2.3] approximations are derived for $R(\Omega,\tau)$ and $P(\Omega,\nu)$ for the diffuse surface scatter channel of an airplane-satellite link when there is no specular component and the elevation angle to the satellite, θ, is greater than α the rms slope of the surface fluctuations. This approximation, called the "steepest-descent" approximation, has been used by Staras [2.2] to derive time and frequency correlation functions and by Mallinckrodt [2.1] to derive delay power spectra, Doppler power spectra, and delay-Doppler scatter functions for the same channel and under the same restrictions (except that the velocity vector of the airplane was restricted).

The expression for $R(\Omega,\tau)$ derived in [2.3] is given by

$$\begin{aligned} R(\Omega,\tau) &= R_0(F,T) \\ &= q_0(F) \exp\left(-\frac{1}{2}(\pi T)^2\left[\frac{\nu_\theta^2}{1+i2\pi F/\sin\theta} + \frac{\nu_y^2 \sin^2\theta}{1+i2\pi F \sin\theta}\right]\right) \end{aligned} \tag{2.71}$$

where

$$q_0(F) = R_0(F,0) = \frac{1}{\sqrt{(1+i2\pi F/\sin\theta)(1+i2\pi F \sin\theta)}} \tag{2.72}$$

is the frequency correlation function and F,T are normalized frequency shift and time shift variables

$$F = \Omega \cdot 4\alpha^2 H/c \tag{2.73}$$

$$T = \tau \cdot 2\alpha \tag{2.74}$$

In (2.71) ν_x and ν_y are the components of the Doppler shift vector (f_0/c x velocity vector) in the x and y directions. The term ν_θ is the component of the Doppler shift vector which is perpendicular to both the x-z plane and the line-of-sight to the satellite. The parameters H,c are airplane height and the velocity of light. The satellite and aircraft are in the x-z plane with height measured along the z axis.

In [2.3] it is also shown that

$$P(\Omega,\nu) = P_0(F,\omega) = \sqrt{\frac{2}{H}} \frac{1}{\nu_\theta^2 + \nu_y^2 \sin^2\theta + i2\pi F(\nu_\theta^2 + \nu_y^2)}$$

$$\times \exp\left[-2\omega^2\left(\frac{[1 + i2\pi F/\sin\theta][1 + i2\pi F \sin\theta]}{\nu_\theta^2 + \nu_y^2 \sin^2\theta + i2\pi F \sin\theta(\nu_\theta^2 + \nu_y^2)}\right)\right] \tag{2.75}$$

where the normalized Doppler variable ω is given by

$$\omega = \nu \cdot \frac{1}{2\alpha} \tag{2.76}$$

Note that the "steepest descent" approximation leads to a vanishing of the Doppler spread when the aircraft travels in the direction of the line-of-sight to the specular point.

It is interesting to consider some limiting cases. Consider first the case in which the fading is sufficiently slow that the tone filters pass the received fluctuating tones undistorted. Then

$$r(\Omega) = R(\Omega,0) = q(\Omega) = q_0(F) \tag{2.77}$$

where it will be noted that we have normalized

$$R(0,0) = 1 \tag{2.78}$$

Consider the other extreme case where the filters are narrow compared to Doppler spread.

Then in (2.68), $H(\nu)$, $G(\nu)$ must be regarded as impulsive by comparison with $P(\Omega,\nu)$. Thus

$$\int P(\Omega,\nu)H^*(\nu)G(\nu)\, d\nu \approx P(\Omega,0) \int H^*(\nu)G(\nu)\, d\nu \tag{2.79}$$

with analogous approximations for the other two integrals in (2.68). It follows that (2.68) can be approximated by

$$r(\Omega) = \frac{P(\Omega,\nu)}{P(0,0)}\, \rho_f \tag{2.80}$$

where ρ_f is the cross correlation coefficient between the filter impulse responses

$$\rho_f = \frac{\int h^*(t)g(t)\, dt}{\sqrt{\int |h(t)|^2\, dt \int |g(t)|^2\, dt}} \tag{2.81}$$

From (2.75) we see that

$$\frac{P(\Omega,0)}{P(0,0)} = \frac{P_0(F,0)}{P_0(0,0)} = \frac{1}{\sqrt{1 + i2\pi F \dfrac{\nu_\theta^2 + \nu_y^2}{\nu_\theta^2 + \nu_y^2 \sin^2\theta}}} \tag{2.82}$$

It follows that for identical filters we have the limiting approximations

$$r(\Omega) = r_0(F) = \begin{cases} \dfrac{1}{\sqrt{(1+i2\pi F/\sin\theta)(1+i2\pi F\sin\theta)}} & ; \text{ slow fading} \\ \dfrac{1}{\sqrt{1+i2\pi F(\nu_\theta^2+\nu_y^2)/(\nu_\theta^2+\nu_y^2\sin^2\theta)}} & ; \text{ fast fading} \end{cases} \tag{2.83}$$

Note that in the case of fast fading the complex correlation coefficient of the tone filter outputs depends on the direction of motion of the airplane while in the case of slow fading it does not.

2.7 Use of Single-Side-Band Analysis for a Double-Side-Band System

Although the detailed analysis carried out in Section 2 applies to a single side-band system, we show in this section that for small phase fluctuations on the received tones the rms range error for a double-side-band system may be computed as if it were a single-side-band system at twice the tone frequency if the two side-bands each have the same strength as the single-side-band.

The complex envelopes of the received carrier and two side-bands may be expressed as

$$w(t) = AG_d e^{-j2\pi(f_0+\Omega)\xi_d}\left[1 + M_1(t) + \frac{\eta_1(t)}{AG_d}\right]e^{j2\pi\Omega t} \tag{2.84}$$

$$w(t) = BG_d e^{-j2\pi f_0 \xi_d} \left[1 + M_0(t) + \frac{\eta_0(t)}{BG_d}\right] \qquad (2.85)$$

$$w_{-1}(t) = AG_d e^{-j2\pi(f_0-\Omega)\xi_d} \left[1 + M_{-1}(t) + \frac{\eta_{-1}(t)}{AG_d}\right] e^{-j2\pi\Omega t} \qquad (2.86)$$

where the subscripts 1, 0, -1 stand for the upper side-band, carrier, and lower side-band.

The carrier component is invariably extracted with the aid of a phase locked loop and then used as a reference for coherent detection as shown in Fig.2.3. The amount of filtering imposed by the PLL is generally much milder than that of the tone filters because of tracking requirements. In the case of small phase fluctuations, as assumed here, the PLL may be modeled as a linear filter on the phase fluctuations. Then the extracted carrier $\hat{w}$ (t) may be expressed in the form

$$\hat{w}_0(t) = BG_d e^{-j2\pi f_0 \xi_d} e^{j\hat{\phi}_0(t)} \qquad (2.87)$$

where

$$\hat{\phi}_0(t) \approx \phi_0(t) \otimes h(t) \qquad (2.88)$$

in which h(t) is the linear filter representing the phase locked loop and

$$\phi_0(t) \approx \text{Im}\left\{M_0(t) + \frac{\eta_0(t)}{BG_d}\right\} \qquad (2.89)$$

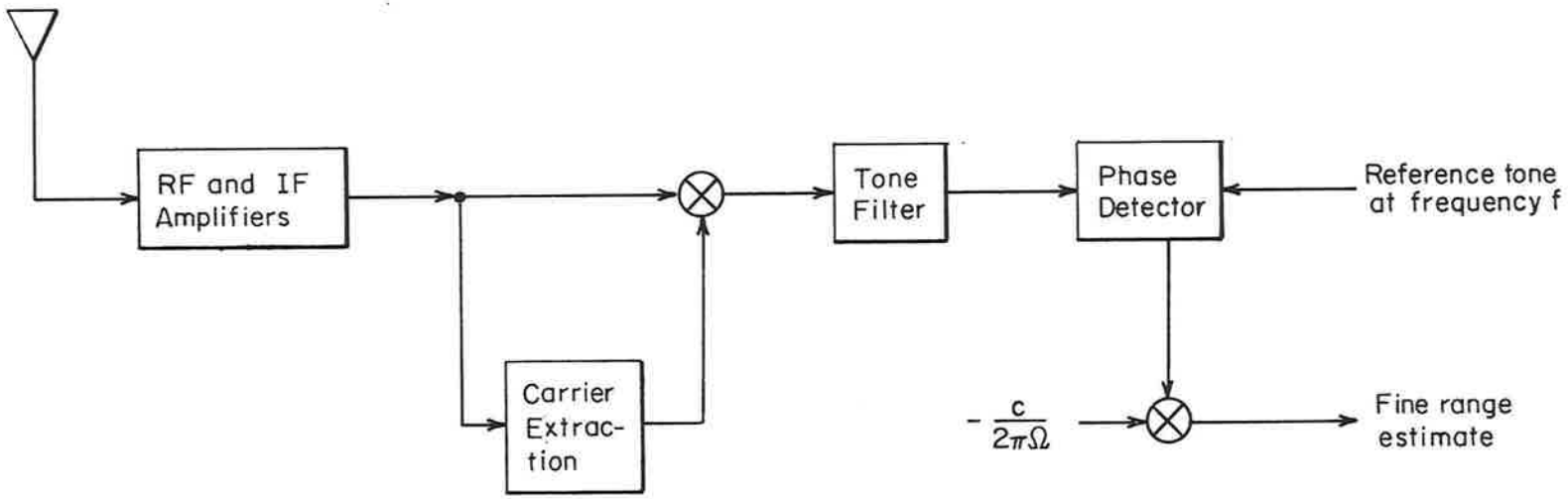

Figure 2.3 Double-Side-Band Fine Ranging Estimation

For small phase fluctuations $w_1(t)$ and $w_{-1}(t)$ may be approximated by

$$w_1(t) \approx AG_d e^{-j2\pi(f_0+\Omega)\xi_d} R_1(t) e^{j\phi_1(t)} e^{j2\pi\Omega t} \tag{2.90}$$

$$w_{-1}(t) \approx AG_d e^{-j2\pi(f_0-\Omega)\xi_d} R_{-1}(t) e^{j\phi_1(t)} e^{-j2\pi\Omega t} \tag{2.91}$$

where

$$R_1(t) = 1 + \text{Re}\ \{M_1(t) + \eta_1(t)/AG_d\} \tag{2.92}$$

$$R_{-1}(t) = 1 + \text{Re}\ \{M_{-1}(t) + \eta_{-1}(t)/AG_d\} \tag{2.93}$$

$$\phi_1(t) = \text{Im}\ \{M_1(t) + \eta_1(t)/AG_d\} \tag{2.94}$$

$$\phi_{-1}(t) = \text{Im}\ \{M_{-1}(t) + \eta_{-1}(t)/AG_d\} \tag{2.95}$$

The input to the tone filter is given by the coherent detector output

$$\begin{aligned} &\text{Re}\ \{w_1(t\ \hat{w}_0^*(t) + w_{-1}^*(t)\hat{w}_0(t)\} \\ &\quad = BA|G_d|^2\ \text{Re}\ \{[R_1(t)e^{j(\phi_1(t)-\hat{\phi}_0(t))} \\ &\qquad + R_{-1}(t)e^{j(\hat{\phi}_0(t)-\phi_{-1}(t))}]e^{j2\pi\Omega(t-\xi_d)}\} \end{aligned} \tag{2.96}$$

In analyzing the output of the tone filter we may select as a new "carrier frequency" the tone frequency Ω. If the complex envelope of the tone filter impulse response is g(t), then the tone filter output complex envelope $z_p(t)$ is given by

$$z_p(t) = BA|G_d|^2 e^{-j2\pi\Omega\xi_d} \left[R_1(t)e^{j[\phi_1(t)-\hat{\phi}_0(t)]} + R_{-1}(t)e^{j[\hat{\phi}_0(t)-\phi_{-1}(t)]}\right] \otimes g(t) \qquad (2.97)$$

For high SNR's (direct/additive and direct/multipath) we may use the approximations (2.92) - (2.95). Thus

$$\begin{aligned} &R_1(t)e^{j(\phi_1(t)-\hat{\phi}_0(t))} \otimes g(t) \\ &\approx (1+\mathrm{Re}\,\{M_1+\eta_1/AG_d\})(1+j\ \mathrm{Im}\,\{M_1+\eta_1/AG_d\}) \otimes g(t) \\ &= 1 + \mathrm{Re}\,\{(M_1+\eta_1/AG_d) \otimes g(t)\} + j\ \mathrm{Im}\,\{M_1+\eta_1/AG_d) \otimes g(t)\} \\ &+ j[\mathrm{Re}\,\{M_1+\eta_1/AG_d\}\ \mathrm{Im}\,\{M_1+\eta_1/AG_d\}] \otimes g(t) \end{aligned} \qquad (2.98)$$

The last term in (2.98) is second order by comparison with the second and third terms. To simplify our calculations we shall replace this second order term with another second order term:

$$j(\mathrm{Re}\ \{M_1 + \eta_1/AG_d\} \otimes g(t))(\mathrm{Im}\ \{M_1 + \eta_1/AG_d\} \otimes g(t)) \tag{2.99}$$

If the fading is slow and the additive noise is negligible the term (2.99) will be identical to the last term in (2.98). In the other cases of interest (2.99) will be smaller than the last term in (2.98). One may reason that our replacement can only reduce the phase fluctuations and resultant rms ranging error. However this reduction will be small percentage-wise for the high SNR case considered here.

With (2.99) we find that

$$g(t) \otimes \{R_1(t)e^{j(\phi_1(t)-\hat{\phi}_0(t))}\} \approx [R_1(t) \otimes g(t)]e^{j[\phi_1(t)-\hat{\phi}_0(t)] \otimes g(t)} \tag{2.100}$$

Similarly for the lower side-band term

$$g(t) \otimes \{R_{-1}(t)e^{j(\hat{\phi}_0(t)-\phi_{-1}(t)}\} \approx [R_{-1}(t) \otimes g(t)]e^{j[\hat{\phi}_0(t)-\phi_{-1}(t)] \otimes g(t)} \tag{2.101}$$

We now define some new functions

$$\phi_1(t) \otimes g(t) = U(t) + V(t) \tag{2.102}$$

$$\phi_0(t) \otimes g(t) = W(t) \tag{2.103}$$

$$\phi_{-1}(t) \otimes g(t) = U(t) - V(t) \tag{2.104}$$

$$G(t) + H(t) = R_1(t) \otimes g(t) \tag{2.105}$$

$$G(t) - H(t) = R_{-1}(t) \otimes g(t) \tag{2.106}$$

Using (2.102) - (2.106) in (2.100) and (2.101) and the resultant in (2.97), we find after applying some trigonometric identities, that the tone filter output is given by

$$z_p(t) = 2BA|G_d|^2 e^{-j2\pi\Omega\xi_d} e^{jV(t)} [G \cos(U(t)-W(t)) + 2jH \sin(U(t)-W(t))] \tag{2.107}$$

The second term in brackets is readily seen to be the product of two first-order terms and thus is of second order. The first term is real and produces no phase fluctuations. The phase error is thus given to first-order by V(t) alone and the ranging error $\epsilon(t)$ by

$$\epsilon(t) \approx \frac{c}{2\pi\Omega} V(t) = \frac{1}{2\pi(2\Omega)} (\phi_1(t) - \phi_{-1}(t)) \otimes g(t) \tag{2.108}$$

which may be recognized as the rms ranging error of a single side-band system utilizing a carrier-side-band separation frequency of 2Ω Hz plus identical tone filters of impulse response g(t). Our heuristic arguments indicate that this system should provide a lower bound to the effects of multipath on ranging error for a double side-band system. However our arguments only apply at high direct path/multipath power and direct path/noise ratios.

SECTION 2

REFERENCES

[2.1] A. J. Mallinckrodt, "Ground Multipath in Satellite-Aircraft Propagation," Paper presented at the Symposium on Application of Atmospheric Studies to Satellite Transmissions (sponsored by the Radio Astronomy Branch of the Ionospheric Physics Lab., AFCRL), Boston, September 1969.

[2.2] H. Staras, "Rough Surface Scattering on a Communication Link," Radio Science, Vol. 3, (New Series), No. 6, June 1968, pp. 623-631.

[2.3] P. A. Bello, "Aeronautical Channel Characterization," IEEE Trans. on Communications, to be published.

[2.4] "Multipath/Ranging Experimental Program Interim Results," Contract DOT FA 09WA-2109, prepared for the F.A.A. by Boeing Co., December 1971.

[2.5] P. Beckmann and A. Spizzichino, The Scattering of Electromagnetic Waves From Rough Surfaces, Pergamon Press, 1963.

[2.6] E. Clausen, et al., "PLACE Final Report," prepared for Goddard Space Flight Center under Contract NAS-5-21101 by Bell Aerospace Corp., June 1970.

[2.7] P. Bello, "Characterization of Random Time-Variant Linear Channels," IEEE Trans. Comm. Systems, December 1963, pp. 360-393.

SECTION 3

EFFECT OF TIME AND FREQUENCY SELECTIVE FADING ON A PN RANGING SYSTEM

3.1 Introduction

This section analyzes the effect of surface scatter multipath and additive Gaussian noise on a PN ranging modem. The assumed channel consists of a fixed component (direct path) and a time-varying component with Gaussian statistics. The receiver structure assumed consists of two phase-locked loops, one tracking the received carrier and one tracking the received PN code. The ranging error is obtained by comparing this derived code timing with a stable reference.

Section 3.2 presents the assumed channel model in more detail, and Section 3.3 presents the assumed receiver structure. Section 3.4 presents a general solution for the open-loop error voltages in the two tracking loops. To obtain explicit solutions for ranging error, two special cases are considered. The first case is that of high direct-to-scatter ratio and high direct-to-additive noise ratio, considered in Section 3.5. In this case an approximate solution is obtained analytically which applies to any multipath channel. The second special case is that of a flat-fading multipath channel in the absence of additive noise, considered in Section 3.6. In this case numerical solutions have been obtained using a computer. These apply for all direct-to-scatter ratios. In Section 3.7 these results are compared with the results obtained in Section 2 for tone ranging systems.

3.2 Channel Model

In this section we define the channel model which will be assumed in the subsequent analysis. The channel is assumed to consist of the parallel combination of a non-fading channel (direct path) and a complex Gaussian WSSUS channel (scatter path).

Figure 3.1 depicts the assumed mathematical model of the channel relating input and output complex envelopes. Direct path delay and attenuation have been set equal to zero; only the relative delay (t_d) and attenuation ($1/\sqrt{\gamma}$) of the multipath channel are shown explicitly. This results in no loss of generality. The time variant transfer function of the fading channel is normalized to unit strength

$$\overline{|T(f,t)|^2} = 1 \tag{3.1}$$

so that the parameter γ is the direct-to-scatter power ratio. Also, the time-variant impulse response

$$g(t,\xi) = \int T(f,t)e^{j2\pi ft}\, df \tag{3.2}$$

can be shifted in time to have zero "mean" path delay.

Due to the WSSUS assumption

$$\overline{g^*(t,\xi)g(t+\tau,\eta)} = Q(\tau,\xi)\delta(\eta-\xi) \tag{3.3}$$

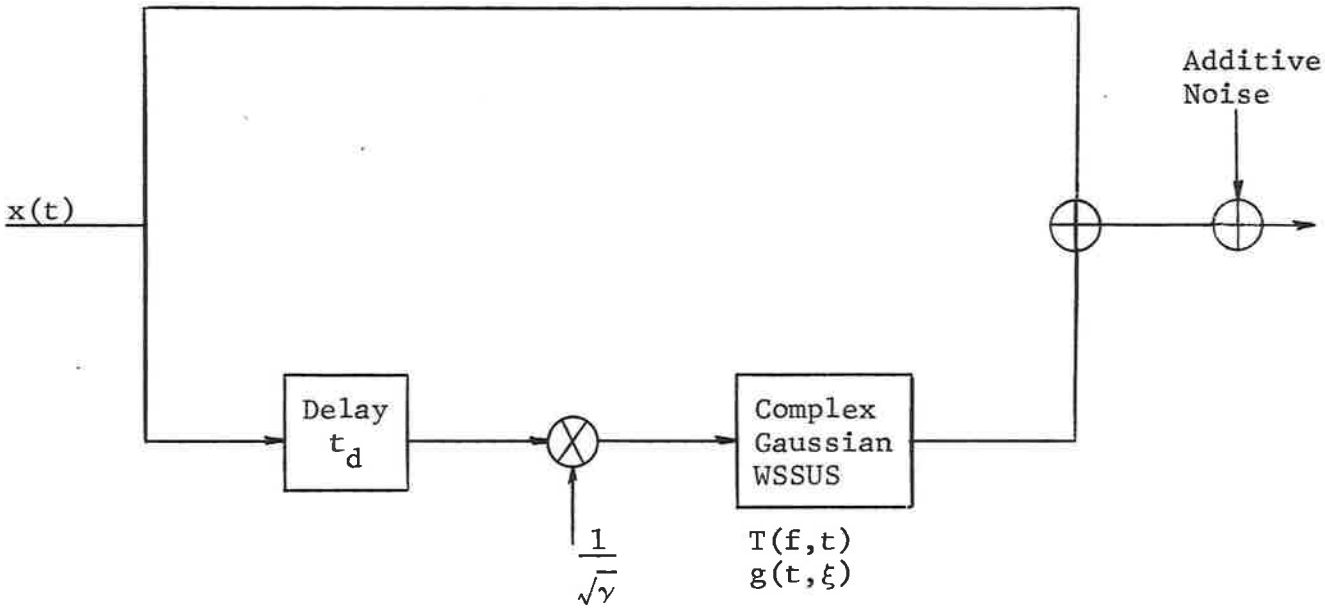

Figure 3.1 Multipath Channel Model

where $Q(\tau,\xi)$ is called the tap gain correlation function. Equivalently,

$$\overline{T^*(f,t)T(f+\Omega,t+\tau)} = R(\Omega,\tau) \tag{3.4}$$

where $R(\Omega,\tau)$, the time-frequency correlation function, is the Fourier transform of $Q(\tau,\xi)$

$$R(\Omega,\tau) = \int Q(\tau,\xi)e^{-j2\pi\Omega\xi}\, d\xi \tag{3.5}$$

Following the channel, Gaussian noise is added to the composite signal, as shown in Fig. 3.1. We will assume the noise is white, with two-sided spectral density $N_o/2$.

3.3 Receiver and Signal Model

The fundamental elements of the PN ranging receiver we have analyzed are a carrier tracking loop and a code tracking loop. The two loops are interdependent, since each provides a reference signal for the other, as shown in Fig. 3.2. Additional circuit elements necessary for acquisition are not shown, since they are not relevant to the present analysis of post-acquisition tracking.

We are assuming a bi-phase-modulated PN signal of the form

$$x(t) \cos \omega_c t \tag{3.6}$$

where $x(t)$ is a sequence of rectangular pulses whose polarity is determined by a suitable binary sequence. Since we set the direct path delay equal to zero, the code loop tracking

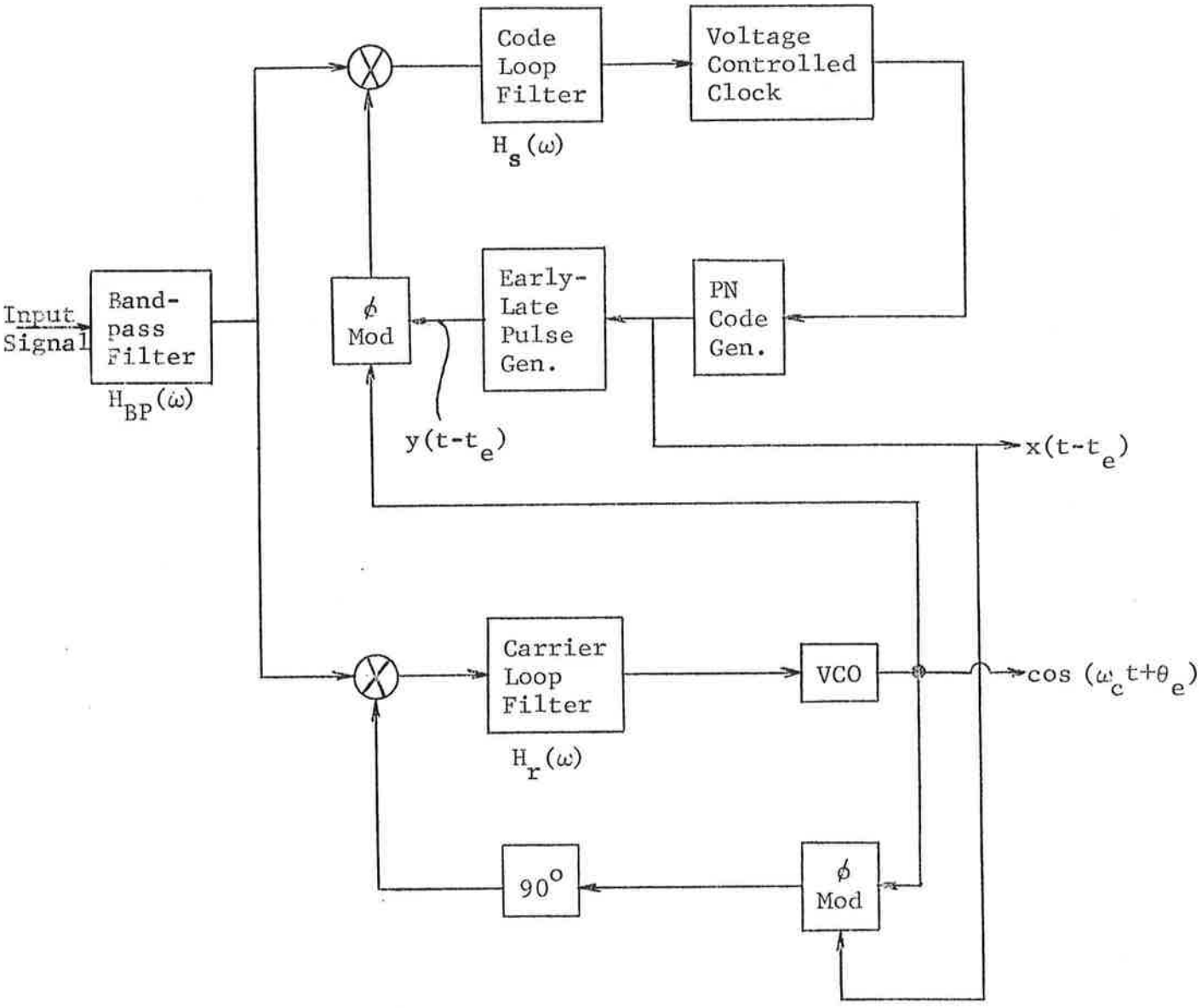

Figure 3.2 Code and Carrier Tracking Loops of a PN Ranging Receiver

error t_e shown in Fig. 3.2 represents the instantaneous ranging error (expressed as a timing error).

We will define the signal-to-noise ratio ρ of a ranging receiver as

$$\rho = \frac{S}{N_o R} \tag{3.7}$$

where

S = signal power (direct path)

R = chip rate of PN sequence

$\frac{N_o}{2}$ = spectral density (two-sided) of the noise

However, in writing the signal in the form of Eq. (3.6), we have set the signal power equal to one-half in order to avoid coefficients in the calculations to follow. In order to preserve the definition of ρ we will define the additive noise density to be

$$\frac{N_o}{2} = \frac{1}{4\rho R} \tag{3.8}$$

Before reaching the receiver tracking loops, the received ranging signal passes through a bandpass filter $H_{BP}(\omega)$. The effect of this filter will be included in the analysis to follow because a real system would always include such filtering. In calculating specific results, we will

assume that the filter transfer function is Gaussian. We will denote the waveform resulting from passing x(t) through the low pass equivalent of $H_{BP}(\omega)$ as r(t). In the presence of a direct path only, the multiplier and low-pass filter in the carrier loop will form the correlation between r(t) and the local code $x(t-t_e)$; we will denote this correlation function by $R(t_e)$:

$$R(t_e) = \int r(t)x(t-t_e)\, dt \tag{3.9}$$

Similarly, the effect of the multiplier and low-pass filter in the code loop will be to generate the correlation function $S(t_e)$:

$$S(t_e) = \int r(t)y(t-t_e)\, dt \tag{3.10}$$

In this and all following equations it will be convenient to use the time variable to represent time measured in fractions of a chip duration 1/R.

3.4 Open Loop Error Voltages

In order to analyze the steady-state behavior of the receiver tracking loops, it is necessary to consider temporarily that the feedback path of each loop has been interrupted after the low-pass filter. In this case the error voltages will be functions of the phase and timing errors θ_e and t_e. We will represent the open-loop error voltages of the carrier and code loops, respectively, as $F(t_e,\theta_e)$ and $G(t_e,\theta_e)$.

Dropping the assumption that the loops are open, we see that in the steady-state both error voltages must be zero, giving a pair of simultaneous equations

$$F(t_e,\theta_e) = 0 \tag{3.11}$$

and

$$G(t_e,\theta_e) = 0 \tag{3.12}$$

Thus, the ranging error analysis considered in this section amounts to solving Eqs. (3.11) and (3.12) for t_e. It should be noted that the solutions presented here are steady-state solutions based on the assumption that the multipath interference changes slowly with respect to the dynamic behavior of the receiver PLL's.

In Appendix B it is shown that the open-loop error voltages may be written as

$$F(t_e,\theta_e) = R(t_e)\sin\theta_e + \frac{1}{\sqrt{\gamma}}\tilde{R}(t_e-t_d)\mathrm{Re}\{z_r(t)e^{-j(\theta_e-\pi/2)}\}$$

$$+ \frac{1}{2}\sqrt{\frac{TB_{Nr}}{2\rho R}}\,n_r(t) \tag{3.13}$$

and

$$G(t_e,\theta_e) = S(t_e)\cos\theta_e + \frac{1}{\sqrt{\gamma}}\tilde{S}(t_e-t_d)\mathrm{Re}\{z_s(t)e^{-j\theta_e}\}$$

$$+ \frac{1}{2}\sqrt{\frac{UB_{Ns}}{2\rho R}}\,n_s(t) \tag{3.14}$$

In each of these equations the first term on the right-hand side is the contribution from the direct path signal while the second term arises from the scatter path and the third is due to the additive noise. Before discussing the latter two, we note that when only the direct path is present, substitution of Eqs. (3.13) and (3.14) into (3.11) and (3.12) yields the expected solution:

$$\theta_e = t_e = 0 \tag{3.15}$$

Returning to the multipath terms of Eqs. (3.13) and (3.14). the functions $\tilde{R}(t)$ and $\tilde{S}(t)$ are defined by

$$\tilde{R}^2(t) = \int\int |H_r(\nu)|^2 R^2(t-\xi) S(\xi,\nu)\, d\xi\, d\nu \tag{3.16}$$

and

$$\tilde{S}^2(t) = \int\int |H_s(\nu)|^2 S^2(t-\xi) S(\xi,\nu)\, d\xi\, d\nu \tag{3.17}$$

where $S(\xi,\nu)$ is the scattering function of the channel and is given by the Fourier transform of $Q(\tau,\xi)$ with respect to τ. The functions $\tilde{R}(t)$ and $\tilde{S}(t)$ may be regarded as average code loop error characteristics for the scatter channel. Also appearing in Eqs. (3.13) and (3.14) are zero-mean Gaussian random processes $z_r(t)$ and $z_s(t)$, normalized so that

$$\overline{|z_r(t)|^2} = \overline{|z_s(t)|^2} = 1 \tag{3.18}$$

In general $z_r(t)$ and $z_s(t)$ are correlated, with a correlation coefficient given by

$$\rho_{rs} = \overline{z_r^*(t) z_s(t)}$$

$$= \frac{\iint S(t_e - t_d - \xi) R(t_e - t_d - \xi) S(\xi, \nu) H_r^*(\nu) H_s(\nu) \, d\xi \, d\nu}{\sqrt{\iint S^2(t_e - t_d - \xi) S(\xi, \nu) |H_s(\nu)|^2 \, d\xi \, d\nu \iint R^2(t_e - t_d - \xi) S(\xi, \nu) |H_r(\nu)|^2 \, d\xi \, d\nu}}$$

(3.19)

Finally, we describe the additive noise terms in Eqs. (3.13) and (3.14). The real random variables $n_r(t)$ and $n_s(t)$ have zero-means and unit variance; they are uncorrelated. Appearing in the coefficients of these terms are the noise bandwidths of the carrier and code loops:

$$B_{Nr} = \int |H_r(f)|^2 \, df \qquad (3.20)$$

and

$$B_{Ns} = \int |H_s(f)|^2 \, df \qquad (3.21)$$

Also we have defined two factors which depend only on the bandpass filter preceding the loop:

$$T = S_x(f) \otimes |H_{BP}(f)|^2 \qquad (3.22)$$

and

$$U = S_y(f) \otimes |H_{BP}(f)|^2 \tag{3.23}$$

where $S_x(f)$ and $S_y(f)$ are the power density spectra of the waveforms $x(t)$ and $y(t)$, respectively.

3.5 High Direct-To-Scatter and High Direct-To-Additive Noise Case

In this section we consider the special case of high direct-to-scatter ratio and high signal-to-additive noise ratio. In Appendix C the closed-loop behavior of the receiver is solved analytically, yielding

$$t_e \doteq \frac{1}{\sqrt{\gamma}} \frac{\tilde{S}(t_d)}{S'(0)} \text{Re}\{z_s(t)\} - \frac{1}{2S'(0)} \sqrt{\frac{UB_{Ns}}{2\rho R}}\, n_s(t) \tag{3.24}$$

Since $\text{Re}\{z_s(t)\}$ is a real, zero-mean Gaussian variable with variance 1/2 and $n_s(t)$ has unit variance, the mean-square timing error is given simply by

$$\overline{t_e^2} = \frac{1}{\gamma} \frac{\tilde{S}^2(t_d)}{2S'^2(0)} + \frac{1}{\left(\frac{\rho R}{B_{Ns}}\right)} \frac{U}{8S'^2(0)} \tag{3.25}$$

and the corresponding rms timing error (as a fraction of a chip) by

$$\sqrt{\overline{t_e^2}} = \left[\frac{1}{\gamma}\left(\frac{\tilde{S}^2(t_d)}{2S'^2(0)}\right) + \frac{1}{\rho_0}\left(\frac{U}{8S'^2(0)}\right)\right]^{1/2} \qquad (3.26)$$

where ρ_0 is the signal-to-additive noise ratio in the bandwidth of the loop filter

$$\rho_0 = \frac{R}{B_{Ns}}\rho = \frac{S}{N_o B_{Ns}} \qquad (3.27)$$

This may be readily converted into rms range error by multiplying by the velocity of light and dividing by the chip rate R.

Equation (3.26) clearly shows the effects of both multipath (first term) and additive noise (second term). Calculation of numerical values for the multipath term depends on the detailed nature of the channel scattering function $S(\xi,\nu)$ through the factor $\tilde{S}(t_e)$. However, the additive noise term depends only on the receiver bandpass filter (through U and $S'(0)$) and the signal-to-noise ratio ρ_0. As an example, we assume that the bandpass filter $H_{BP}(f)$ is Gaussian. (Details necessary for calculating the coefficient of ρ_0 in Eq. (3.26) may be found in Appendix C.) If we also assume that no multipath is present, we may plot the ranging error as a function of ρ_0 for various bandpass filter bandwidths, as shown in Fig. 3.3.

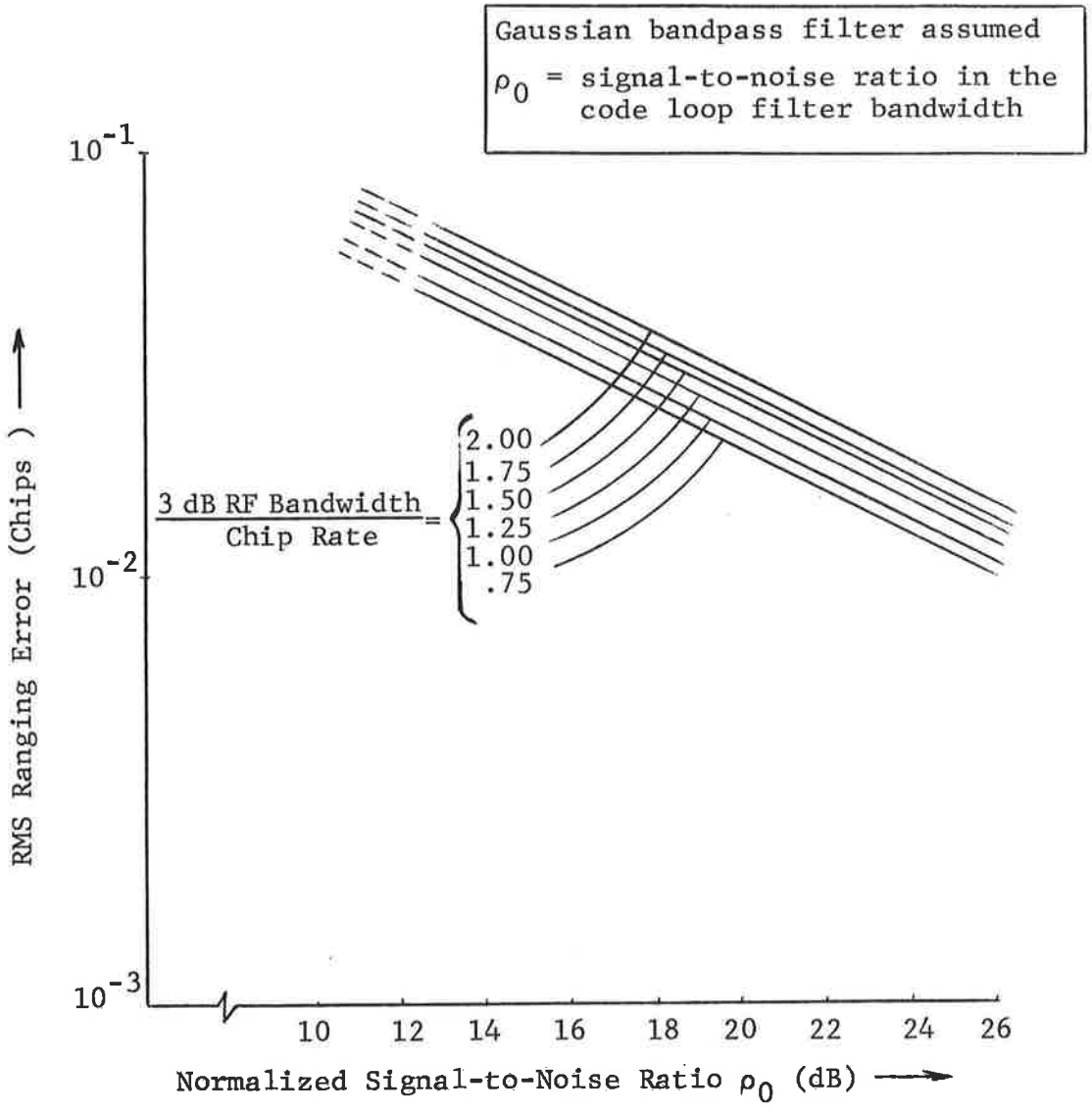

Figure 3.3 Asymptotic Performance of PN Ranging in Additive Noise Alone

3.6 Flat Fading Case

In this section, we consider a second special case: that of "flat" fading in the absence of additive noise. By the term flat fading we will mean simply that the time-varying transfer function $T(f,t)$ may be replaced by its zero-frequency value $T(0,t)$. A direct consequence of this is that the scattering function assumes the simple form

$$S(\xi,\nu) = \delta(\xi)P(\nu) \tag{3.28}$$

where $\delta(t)$ is the unit impulse and $P(\nu)$ is the Doppler power spectrum. Applying this identity to Eqs. (3.16) and (3.17) gives simplified forms for the average code loop characteristics:

$$\tilde{R}(t) = R(t)\left[\int P(\nu)|H_r(\nu)|^2\, d\nu\right]^{1/2} \tag{3.29}$$

$$\tilde{S}(t) = S(t)\left[\int P(\nu)|H_s(\nu)|^2\, d\nu\right]^{1/2} \tag{3.30}$$

A second consequence of Eq. (3.28) is that the correlation ρ_{rs} between the Gaussian variables $z_r(t)$ and $z_s(t)$ becomes

$$\rho_{rs} = \frac{\int P(\nu)H_r^*(\nu)H_s(\nu)\, d\nu}{\sqrt{\int P(\nu)|H_r(\nu)|^2\, d\nu \int P(\nu)|H_s(\nu)|^2\, d\nu}} \tag{3.31}$$

If we make the further assumption that $H_r(\nu)$ and $H_s(\nu)$ are equal, ρ_{rs} becomes equal to unity, implying that the multipath-induced disturbances in both loops ($z_r(t)$ and $z_s(t)$) are identical. As a consequence, we may rewrite the open-loop error voltages (omitting the additive noise contributions) in the form

$$F(t_e,\theta_e) = R(t_e) \sin \theta_e + \alpha R(t_e-t_d) \sin (\theta_e-\theta_m) \tag{3.32}$$

$$G(t_e,\theta_e) = S(t_e) \cos \theta_e + \alpha S(t_e-t_d) \cos (\theta_e-\theta_m) \tag{3.33}$$

In these equations the multipath angle θ_m is uniformly distributed over $(0,2\pi)$ and the multipath amplitude α is Rayleigh with mean-square value

$$\overline{\alpha^2} = \frac{1}{\gamma} \int P(\nu) |H(\nu)|^2 \, d\nu \tag{3.34}$$

where

$$H(\nu) = H_r(\nu) = H_s(\nu) \tag{3.35}$$

When the open-loop error voltages are expressed as in Eqs. (3.31) and (3.32), the closed-loop equations (Eqs. (3.11) and (3.12) may be solved numerically for t_e and θ_e, given

values of α and θ_m. Details of this solution technique are contained in Appendix D. These solutions can then be used to calculate the rms timing error $(\overline{t_e^2})^{1/2}$ by averaging numerically over θ_m and α. The result of this calculation is shown in Fig. 3.4. Note that when the loop filters pass the Doppler spectrum without distortion

$$\int P(\nu)\,|H(\nu)|^2\,d\nu \doteq |H(0)|^2 \int P(\nu)\,d\nu = 1 \quad (3.36)$$

thus the horizontal axis becomes just the direct-to-scatter ratio γ. On the other hand, when the loop bandwidths are much less than the channel Doppler spread

$$\int P(\nu)\,|H(\nu)|^2\,d\nu \doteq P(0) \int |H(\nu)|^2\,d\nu = \frac{B_N}{W_N} \quad (3.37)$$

and the horizontal axis becomes $\gamma(\frac{W_N}{B_N})$ where B_N is the two-sided noise bandwidth of the filter and W_N is the two-sided noise bandwidth of the Doppler spectrum.

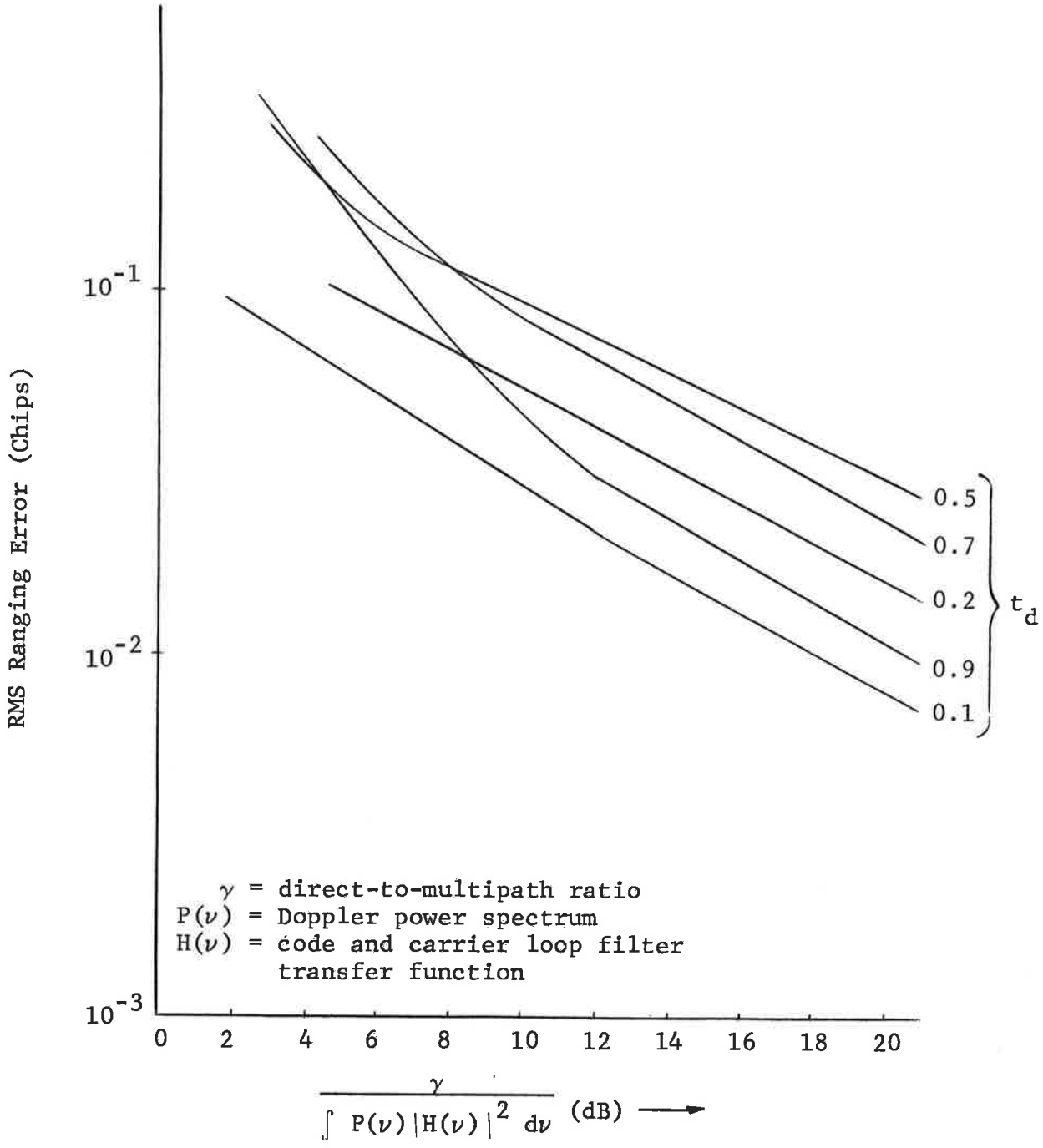

Figure 3.4 Performance of PN Ranging System in the Presence of Flat Fading Multipath Alone

3.7 Comparison of Tone and PN Ranging Performance

3.7.1 Introduction

In Section 2 tone ranging systems were analyzed; the present section has analyzed a PN ranging system under the same conditions. Clearly a comparison of the two systems is now possible. The purpose of this section is to make such a comparison, in so far as it is possible with the present analyses. However, an exact comparison would require that the chip rate of the PN system be specified relative to the tone separation of the tone system with which it is to be compared. Because of the dissimilar nature of the spectra of the two systems, it is difficult to make this specification without a more detailed knowledge of the bandwidth constraints which would apply to the two systems. Therefore, in the comparisons to be presented here, the tone separation and chip rate will be left as parameters, so that either system could be configured to meet a particular operational constraint on bandwidth. Another important constraint which cannot be specified at this point is the channel scattering function $S(\xi,\nu)$; this will of course determine the actual performance of either system in the presence of multipath. It is hoped that the comparison to follow will be useful in spite of the fact that these effects have not been quantified. In the future, when both the channel and the operating constraints are better known, an exact comparison will be possible.

For simplicity the comparison will be made only for the case of high signal-to-additive noise ratio and high direct-to-scatter ratio. Performance with regard to additive noise and

with regard to multipath are considered separately in Sections 3.7.2 and 3.7.3, respectively.

3.7.2 Performance in the Presence of Additive Noise

The asymptotic performance of a PN ranging system in additive noise was plotted as Fig. 3.3. The vertical axis is the rms ranging error as a fraction of the PN chip duration; the horizontal axis is the ratio of signal power to noise power in the bandwidth of the code loop filter.

From Eq. (2.46) we see that the corresponding rms error in the fine delay estimate formed from tones 1 and 3 is

$$\frac{1}{2\pi(f_3-f_1)}\,\frac{1}{\sqrt{S}} \tag{3.38}$$

In this result f_1 and f_3 are the tone frequencies and S is the signal-to-noise ratio at the output of either filter. If we make the rather generous assumption that only a small fraction of the total power need be allotted to other tones for the purpose of ambiguity resolution then each of the tones (f_1 and f_3) contains one-half the total transmitted power. Thus it seems reasonable to identify 2S with the (loop filter) signal-to-noise ratio of the PN system. Figure 3.5 shows Eq. (3.38) plotted with 2S (in dB's) as the horizontal axis; the vertical axis is the rms timing error as a fraction of the reciprocal of the tone separation. This permits direct comparison with Fig. 3.3 when the tone separation (f_3-f_1) is equal to the chip rate of the PN sequence, the total powers are equal, and the tone filter bandwidths are equal to the code loop bandwidth of the PN receiver. Under these conditions the performance of the tone ranging system is equal to that of a PN system with bandwidth approximately 1.25 times the chip rate. Clearly, as far

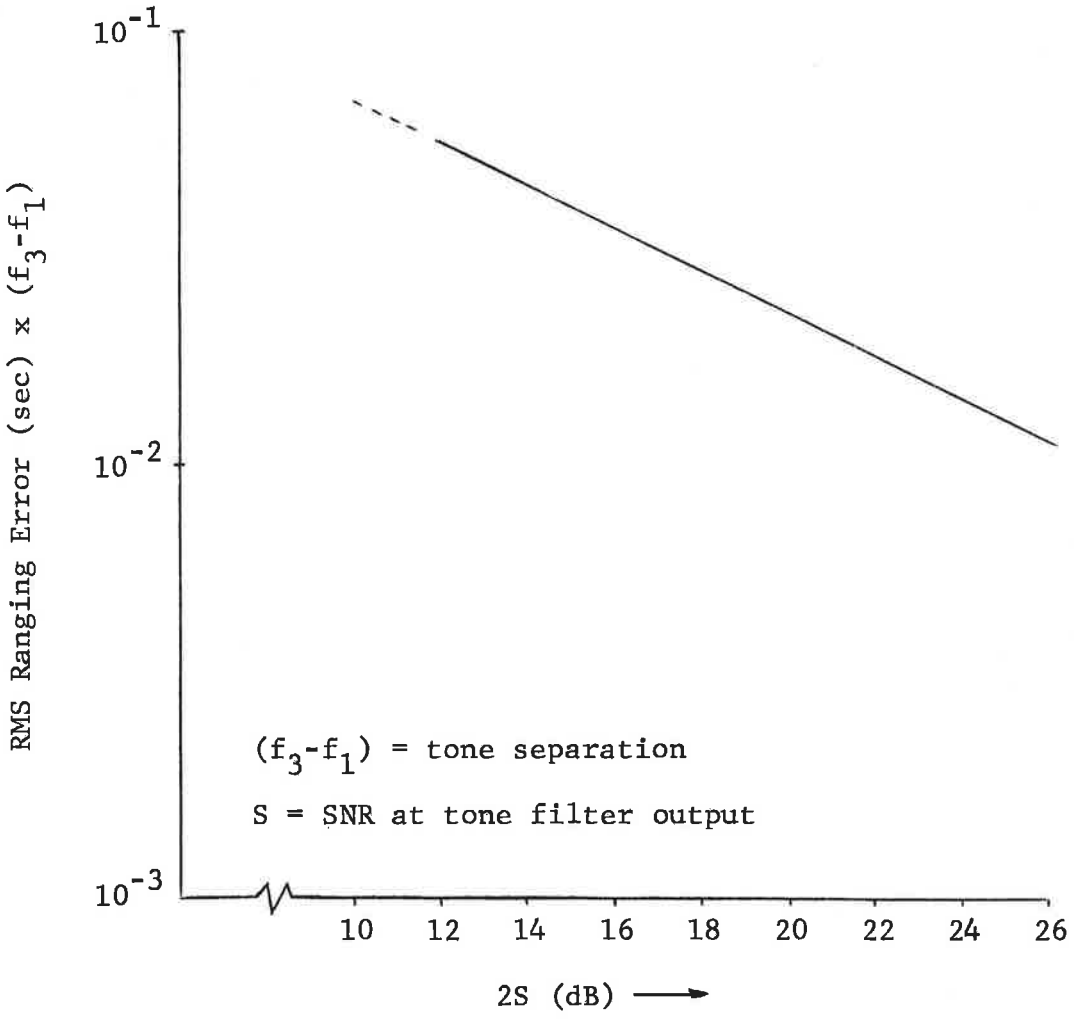

Figure 3.5 Performance of Tone Ranging System in the Presence of Additive Noise Alone

as this measure of performance is concerned, neither system shows a clear advantage.

3.7.3 Performance in the Presence of Multipath

The first term of Eq. (3.25) gives the multipath performance of the PN ranging system for high-direct-to-scatter ratio as a function of a chip. Multiplying by Δ^2 to convert to a timing error and combining with Eq. (3.17) gives

$$\sigma_{PN}^2 = \frac{1}{2\gamma(\frac{1}{\Delta})^2} \iint |H_s(\nu)|^2 \frac{S^2(t_d-\xi)}{S'^2(0)} S(\xi,\nu)\, d\xi\, d\nu \qquad (3.39)$$

To obtain a comparable result for tone ranging we take the multipath term of Eq. (2.46)

$$\sigma_f^2 = \frac{1}{2(2\pi)^2(f_3-f_1)^2} \sigma_{M_{13}}^2 \qquad (3.40)$$

We will assume identical tone filters so that $\sigma_{M_{13}}^2$ is given by Eq. (2.48); combining with Eq. (2.40) we have

$$\sigma_f^2 = \frac{1}{(2\pi)^2(f_3-f_1)^2\gamma} \left[\int R(0,\tau)R_h(\tau)\, d\tau - \right.$$

$$\left. \mathrm{Re}\{e^{-j2\pi(f_1-f_3)(\xi_s-\xi_d)}\} \int R(f_3-f_1,\tau)R_h(\tau)\, d\tau\right] \qquad (3.41)$$

Making use of the transform relationship between $R(\Omega,\tau)$ and $Q(\tau,\xi)$, (Eq. (2.6)), this may be put in the equivalent form

$$\sigma_f^2 = \frac{1}{(2\pi)^2(f_3-f_1)^2\gamma} \mathrm{Re}\{\iint [1-e^{-j2\pi(f_1-f_3)(\xi_s-\xi_d+\xi)}] \; R_h(\tau)Q(\tau,\xi)\, d\xi\, d\tau\} \tag{3.42}$$

which is equivalent to

$$\sigma_f^2 = \frac{1}{2(f_3-f_1)^2\gamma} \iint \frac{\sin^2\pi(f_1-f_3)(\xi_s-\xi_d+\xi)}{\pi^2} S(\xi,\nu)|H(\nu)|^2 \, d\xi\, d\nu \tag{3.43}$$

The similarity between this result and the corresponding result for PN ranging (Eq. (3.39)) is apparent.

In comparing Eqs. (3.43) and (3.39) note that the delay $\xi_s-\xi_d$ appearing in Eq. (3.43) has exactly the same meaning as the delay t_d appearing in Eq. (3.39) except that t_d is normalized to the chip rate $1/\Delta$. Furthermore, it is reasonable to assume that the tone filters will be identical to the code loop filter of the PN receiver since both will be designed to pass the Doppler spread of the direct-path signal. Thus the factor $|H_s(\nu)|^2$ appearing in Eq. (3.39) will be identical to the factor $|H(\nu)|^2$ appearing in Eq. (3.43). So, for a given scattering function, only two factors will distinguish performance of the two systems. First we have the factor $(f_3-f_1)^2$ appearing in the denominator of (3.43) and the factor $1/\Delta^2$ appearing in the

denominator of Eq. (3.39). As discussed previously, we are considering the chip rate $1/\Delta$ and tone separation to be parameters for the purpose of this comparison. However, it is clear that increasing one relative to the other will tend to improve the performance of the corresponding system. (However, there are situations in which increasing the chip rate or tone separation will not result in a net improvement in multipath performance.) Second we have the factor $\frac{1}{\pi^2}\sin^2\pi(f_1-f_3)(\xi_s-\xi_d+\xi)$ appearing in Eq. (3.13) and the factor $S^2(t_d-\xi)/S'^2(0)$ appearing in Eq. (3.39). The great similarity of these two factors is apparent from Fig. 3.6. Of course, the horizontal scale of either factor must be expanded or contracted as the chip rate or tone separation is varied. However, it is clear that for chip rate equal to tone separation the performance of the two systems will be approximately equivalent.

The results in this section may be simplified for the special case wherein it is assumed that the bandwidth of the tone filter or PN code loop filter is much greater than the Doppler spread. Setting $|H_s(\nu)|^2 = 1$ in Eq. (3.39) gives

$$\sigma_{PN}^2 = \frac{1}{2\gamma(\frac{1}{\Delta})^2}\int \frac{S^2(t_d-\xi)}{S'^2(0)}\,Q(\xi)\,d\xi \qquad (3.44)$$

where $Q(\xi)$ is the multipath delay power spectrum. An equivalent result for the tone system is obtained by setting $R_h(\tau) = \delta(\tau)$ in Eq. (3.41), giving

$$\sigma_f^2 = \frac{1}{(2\pi)^2(f_3-f_1)^2\gamma}\left[1 - \mathrm{Re}\left\{R(f_3-f_1,0)e^{j2\pi(f_3-f_1)(\xi_s-\xi_d)}\right\}\right] \qquad (3.45)$$

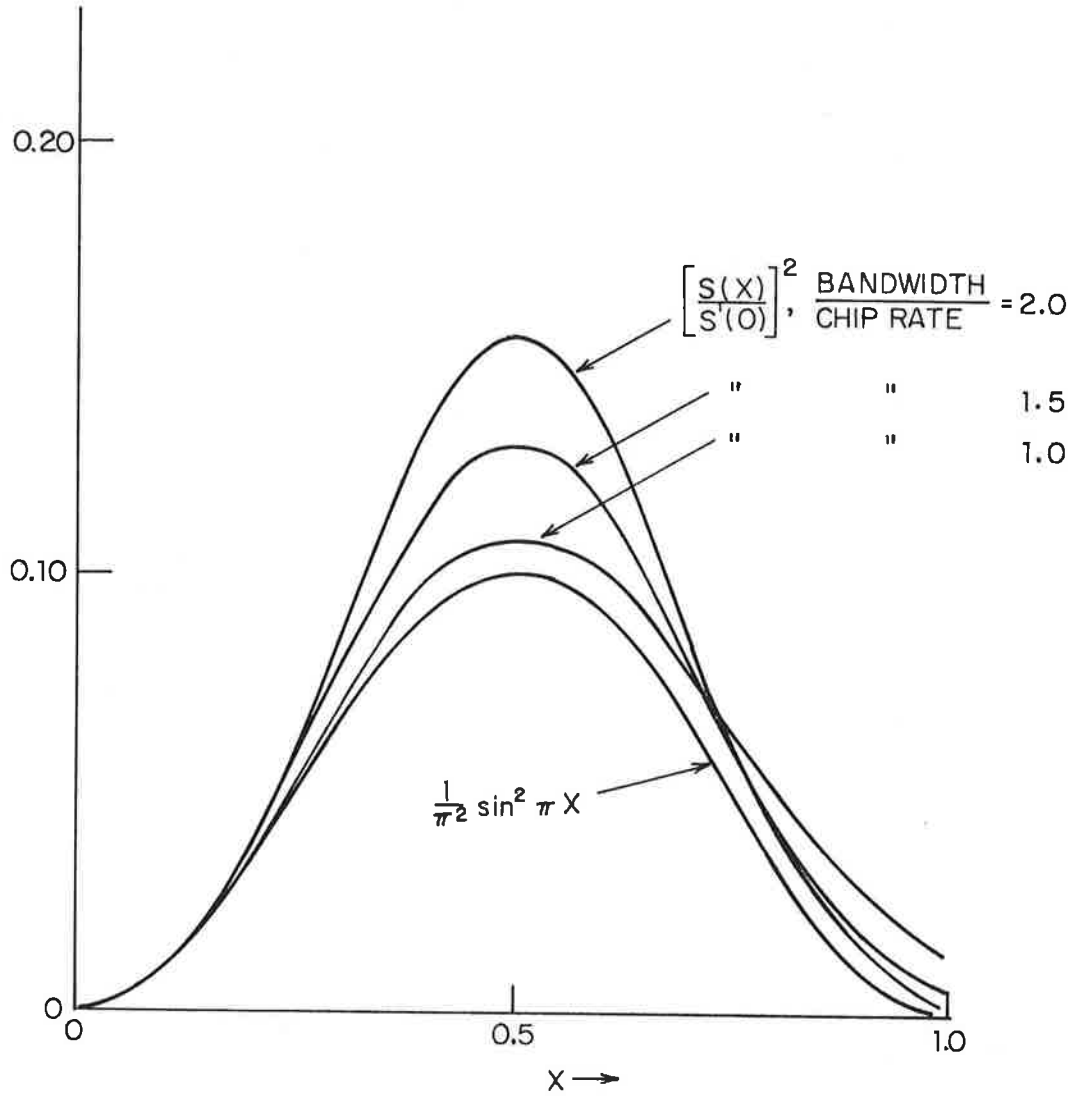

Figure 3.6 Factors Appearing in the Multipath Error Results

SECTION 4

SIGNAL DESIGN CONSIDERATIONS FOR A FAST FADING RICIAN CHANNEL

4.1 Introduction

The problem of obtaining reliable communications over a Rician channel will be addressed. The channel model parameters will be discussed in Section 4.2, some modulation approaches will be discussed in Section 4.3, and advanced signal design concepts (integrated coding and modulation approaches) will be discussed in Section 4.4. In Section 1.5 some assumptions on channel model parameters will be made so that preliminary performance estimates can be made for a narrow-band airplane-satellite channel.

4.2 Channel Model Parameters

A channel model will be assumed which is characterized by the following three parameters:

$\frac{E_b}{N_o}$ = the direct path signal-to-noise ratio in a bandwidth equal to the data rate in bits/sec, or equivalently, the energy per information bit divided by the noise power density.

γ = the ratio of the direct-to-scatter signal-to-noise ratio

= the ratio of direct-to-scatter signal powers

$re^{j\beta}$ = the complex correlation coefficient between successive signaling pulses

The fading will be assumed to be a complex Gaussian and the additive noise will be assumed to have a flat spectrum.

The direct signal-to-noise ratio can be written in terms of the direct energy per signaling pulse E, and the (one-sided) noise power density N_o, as

$$\frac{E}{N_o} = \frac{P_d}{N_o D} \tag{4.1}$$

where P_d is the power received by the direct path and D is the data rate in bits per second. A signaling format of one bit per pulse is assumed so that $E = E_b$. However, when an error correcting code of rate $R < 1$ is utilized and the data rate D is maintained we have

$$\frac{E}{N_o} = \frac{RP_d}{N_o D} = R\left(\frac{E_b}{N_o}\right) \tag{4.2}$$

The received power is still P_d but the energy per signaling pulse is reduced by the factor R due to the increase in signaling bandwidth required to accomodate the code. The direct energy per information bit $E_b = \frac{P_d}{D}$ is fixed regardless of the particular code rate.

The ratio of the direct-to-scatter path γ can vary from $\gamma=0$ for a Rayleigh fading channel to $\gamma \rightarrow \infty$ for a non-fading channel. However, the results will be written in terms of direct path energy that would follow from a link calculation. For our problem a direct path value for P_d/N_o of 46 dB will be assumed.

The correlation coefficient $re^{j\beta}$ between successive signaling pulses follows from the normalized fading spectrum assumed to be given by

$$S(f) = \frac{2}{B\sqrt{2\pi}} e^{-2\left(\frac{f}{B}\right)^2} \tag{4.3}$$

which yields a correlation function

$$R(\tau) = \exp\left(-\frac{1}{2}\pi^2 B^2 \tau^2\right) \tag{4.4}$$

For a pulse length of T

$$r = \exp\left(-\frac{1}{2}\pi^2 B^2 T^2\right) \; ; \beta=0 \tag{4.5}$$

where B is the RMS Doppler spread. Note that if the Doppler spread is defined as the frequency separation between half-power points, we have a half-power fading bandwidth $B_{HP} = B\sqrt{2\ell n(2)} = 1.18B$, which is almost equivalent to the present definition.

4.3 Modulation Approaches

The decision statistic for DPSK modulation can be written in terms of the direct component A, the fading component R, and the additive noise component N, as

$$V = A + R + N \tag{4.6}$$

where the above variables are all complex. Their power values are given by

$$AA^* = P_d \tag{4.7}$$

$$E[RR^*] = P_s \tag{4.8}$$

$$E[NN^*] = \frac{N_o}{T} \tag{4.9}$$

The corresponding previously defined signal-to-noise ratios are

$$\frac{E_b}{N_o} = \frac{TP_d}{N_o} \tag{4.10}$$

and

$$\gamma = \frac{P_d}{P_s} \tag{4.11}$$

The reference statistics for DPSK modulation obtained from the previous baud is given by

$$V' = A + R' + N' \tag{4.12}$$

where N' is independent of N and the complex fading variables R' and R are related by

$$E[R'R^*] = re^{j\beta} \tag{4.13}$$

The effects of the time variations in R can be modeled exactly by assuming

$$R = e^{-j\beta/2}R_0 + Z \tag{4.14}$$

and

$$R' = e^{+j\beta/2}R_0 + Z' \tag{4.15}$$

where R_0 is the completely correlated part of R and R' (apart from a possible phase shift β) and Z and Z' represent zero mean uncorrelated parts (independent for complex Gaussian) of R and R'. Thus we have

$$e^{-j\beta}E[RR'^*] = E[R_0R_0^*] = rP_s \tag{4.16}$$

The variance of independent portions of R is given by

$$E[ZZ^*] = E[(R-R_0)(R^*-R_0^*)] = P_s(1-r) \tag{4.17}$$

For the subsequent calculations we assume $\beta=0$. Using the above results we can reduce the fast fading results to an equivalent slow fading result by noting that

$$V = A + R + N = A + R_0 + Z + N \tag{4.18}$$

where the equivalent direct signal-to-noise ratio is

$$\left(\frac{E_b}{N_o}\right)_{eq} = \frac{P_d}{E[ZZ^*] + E[NN^*]} = \frac{P_d}{P_s(1-r) + \frac{N_o}{T}} \tag{4.19}$$

which can be written in terms of the $\frac{E_b}{N_o}$ and γ

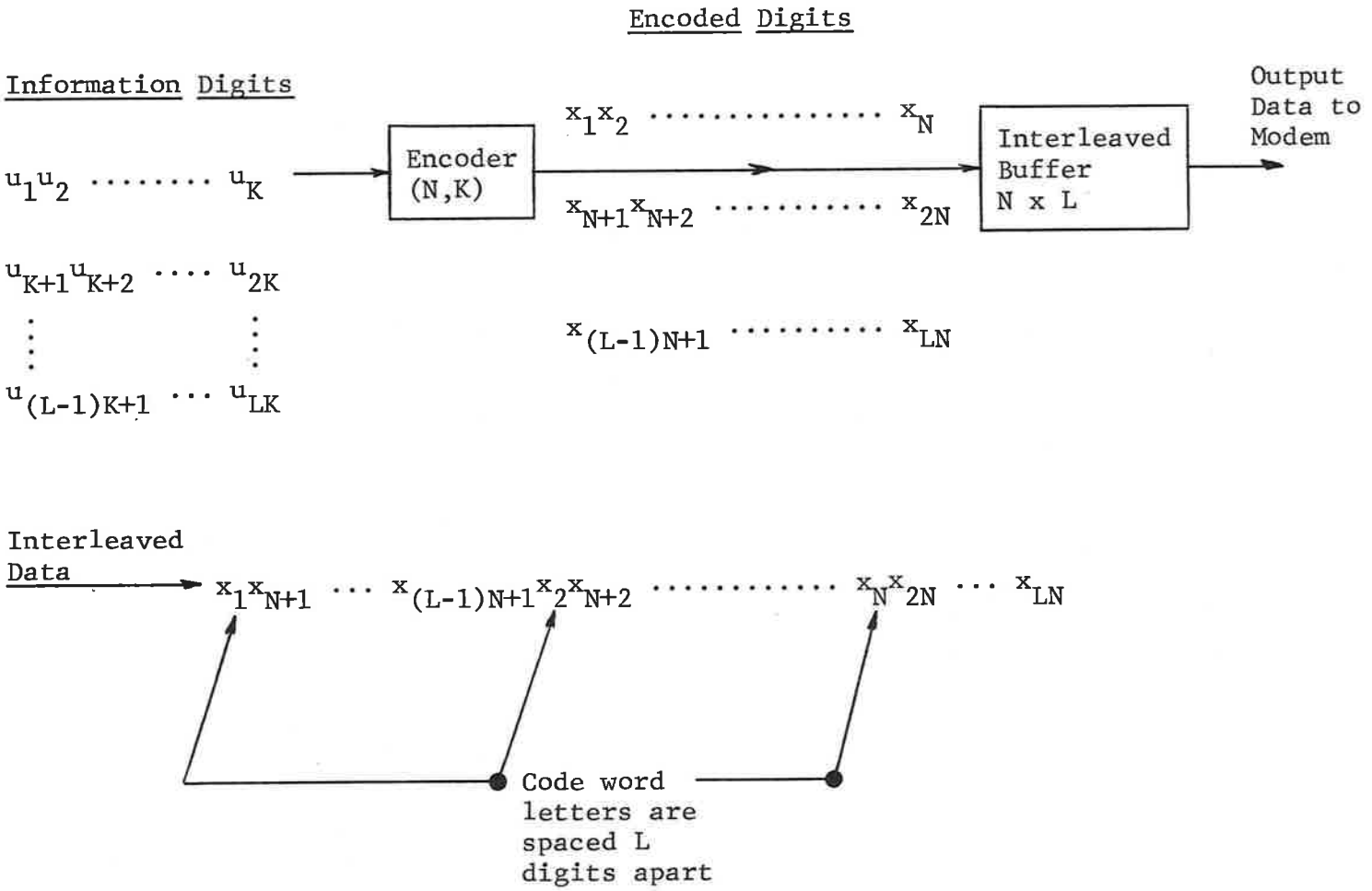

Figure 4.1 Interleaving the Encoded Data Block of Length N Over an L Bit Span

A somewhat more efficient method of interleaving the transmitted data is illustrated on Fig. 4.2 where the information digits rather than the encoded data is interleaved. Part a) of this figure shows a conceptual implementation using L individual (N,K) encoders. Part b) shows an efficient implementation for a cyclic block code whose generation polynomial is given by $g(x) = 1 + g_1x + g_2x^2 + \ldots g_{N-K-1}x^{N-K-1} + x^{N-K}$. The basic storage for this type of interleaver is (N-K)L bits which yields a considerable savings for high rate codes ($R = \frac{K}{N} > \frac{1}{2}$).

Depending on the actual channel parameter, the feasibility of using an interleaver such that code letters are statistically independent will be determined. Actually, even if code letters are partially correlated, decoding with channel measurements can yield a significant gain dependent on the channel parameters to be measured. The extent of this gain is beyond the scope of this preliminary analysis.

Given that code letters are statistically independent we can bound [4.2] the performance of an (N,K) code of minimum distance d by $n_d p^d (1-p)^{N-d} \leq P_e(\text{block}) \leq \binom{N}{d} P_e(\text{dth-order diversity})$ when channel measurement information is used in the decoding process. The raw (before decoding) bit error probability is given by p and n_d represents the number of code words of minimum distance d in the given (N,K) code. The upper bound is written in terms of a coefficient times the error probability of d'th order diversity which has already been derived for the slow fading Rician channel [4.1], [4.3].

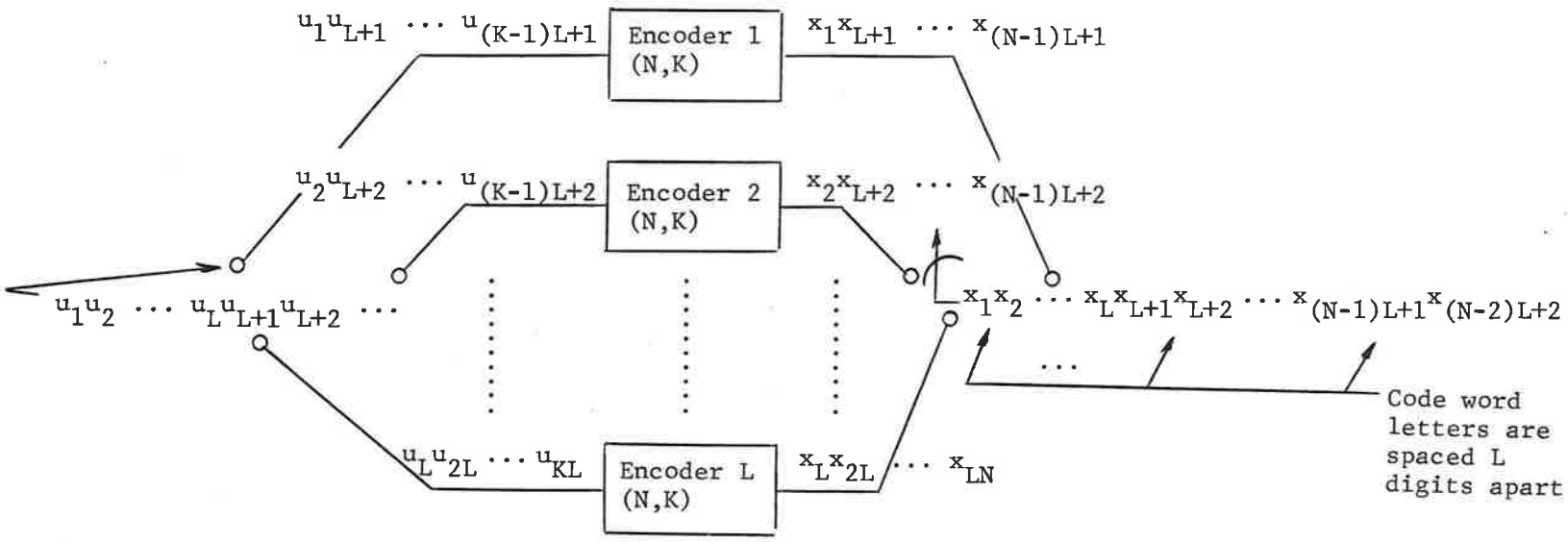

a) Conceptual Implementation

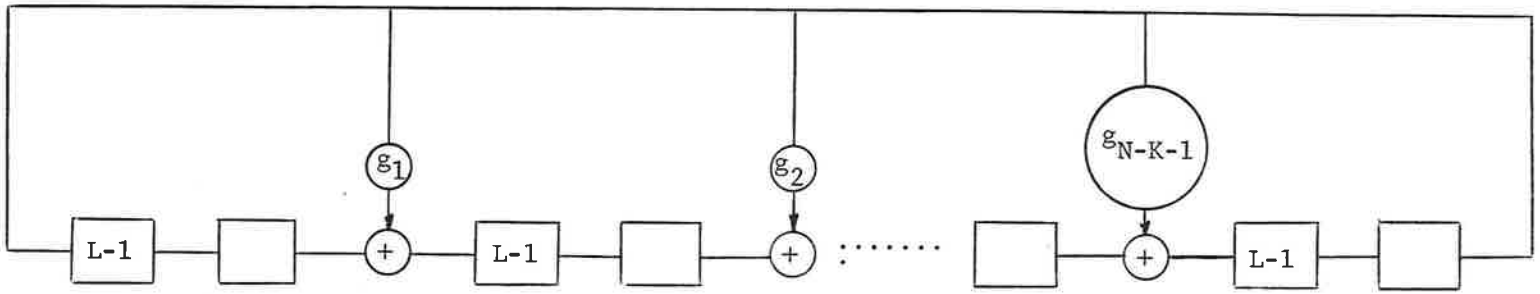

b) Efficient Implementation for a Cyclic Block Code

Figure 4-2. Interleaving Information Blocks of Length K Over an L Bit Span

An approximation to the bit error probability in a given code block is given by

$$P_e \approx \frac{d}{N} n_d P_e(\text{dth-order diversity}) \qquad (4.21)$$

To obtain the above we assume an erroneous code block has d bits of N digits in error and that the block errors result from the n_d nearest neighbor. Intuitively, these assumptions become more realistic as the signal-to-noise increases. However, to obtain the exact performance, computer simulations for a selected code and given decoding algorithm will be necessary.

To use the above approximation for an arbitrary code of rate R we simply have to replace E_b/N_o in the previously derived expressions for a Rician channel with dth-order diversity by

$$\boxed{\left(\frac{E}{N_o}\right)_{eq} = \frac{\left(\frac{E_b}{N_o}\right)R}{1 + \frac{(1-r)}{\gamma}\left(\frac{E_b}{N_o}\right)R}} \qquad (4.22)$$

In the above $\frac{E_b}{N_o} = \frac{P_d}{N_o D}$ which is the direct path signal-to-noise ratio that is actually received whether or not coding is employed. The signal-to-noise ratio per pulse is given by $\left(\frac{E}{N_o}\right)$ and is related to E_b/N_o by (4.2).

In addition to the above expression a first-cut estimate of the performance gain can be obtained by using known simulated results for specific codes. Unfortunately, the results given for decoding with channel measurements are only

for the Gaussian or the Rayleigh fading channel [4.2]. These results are plotted on Figs. 4.3 and 4.4 in terms of p, the raw error before decoding and P_e, the bit error after decoding. The signal-to-noise ratio is held fixed for each comparison and thus the results are a function of E/N_o, rather than $E_b/N_o = (\frac{E}{N_o})(\frac{1}{R})$. The significant point to notice from these results is that the error performance coding gain (p/P_e) are only about a factor 2 to 3 greater than for the Rayleigh fading channel when both channels are compared for the same values of p. (The value of E/N_o is, however, significantly different for a given value of p.) Table 4-1 lists this coding gain as a function of the value of p. These results can be used to predict the performance for the Rician channel (which, depending on γ, is somewhere between the Rayleigh and Gaussian channel) by finding the value of p for a given set of values of E_b/N_o, γ and r and estimating the value of P_e from Table 4-1 or Figs. 4.3 and 4.4. An example of this first cut performance estimate is given in 1.5.

4.4.2 Multiple Rate Codes and Adaptive Decoding

A fairly new coding technique will be discussed in this section which, again, depending on particular channel parameters, may be an important candidate. This particular technique requires considerably less storage than interleaving since code letters need not be statistically independent. Indeed, this technique is quite robust since the decoder adapts to the channel conditions by changing the decoding algorithm to match the estimated error behavior. Actually much of the advantages obtained by feedback communication links are

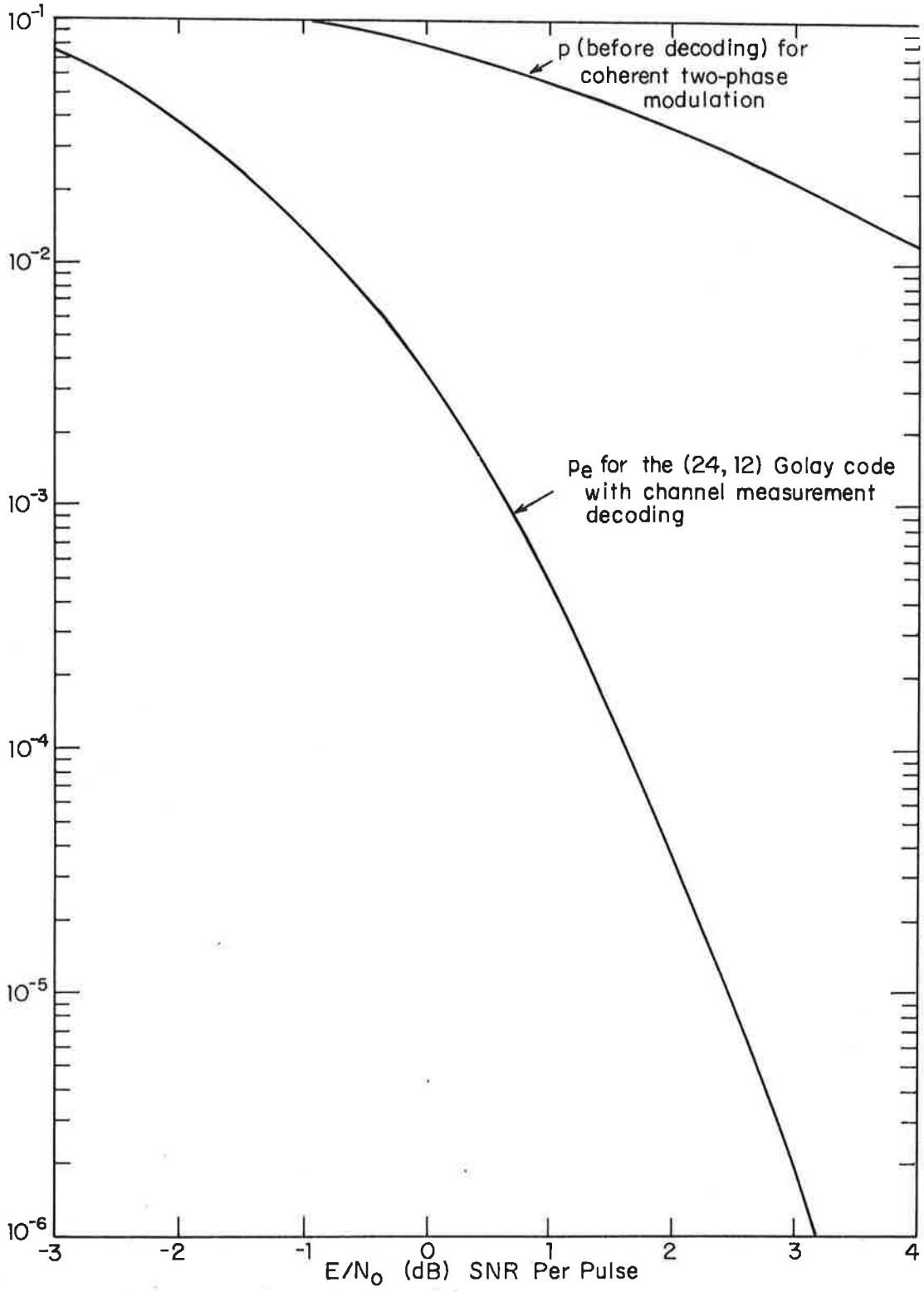

Figure 4.3 Coding Gain for the Gaussian Channel

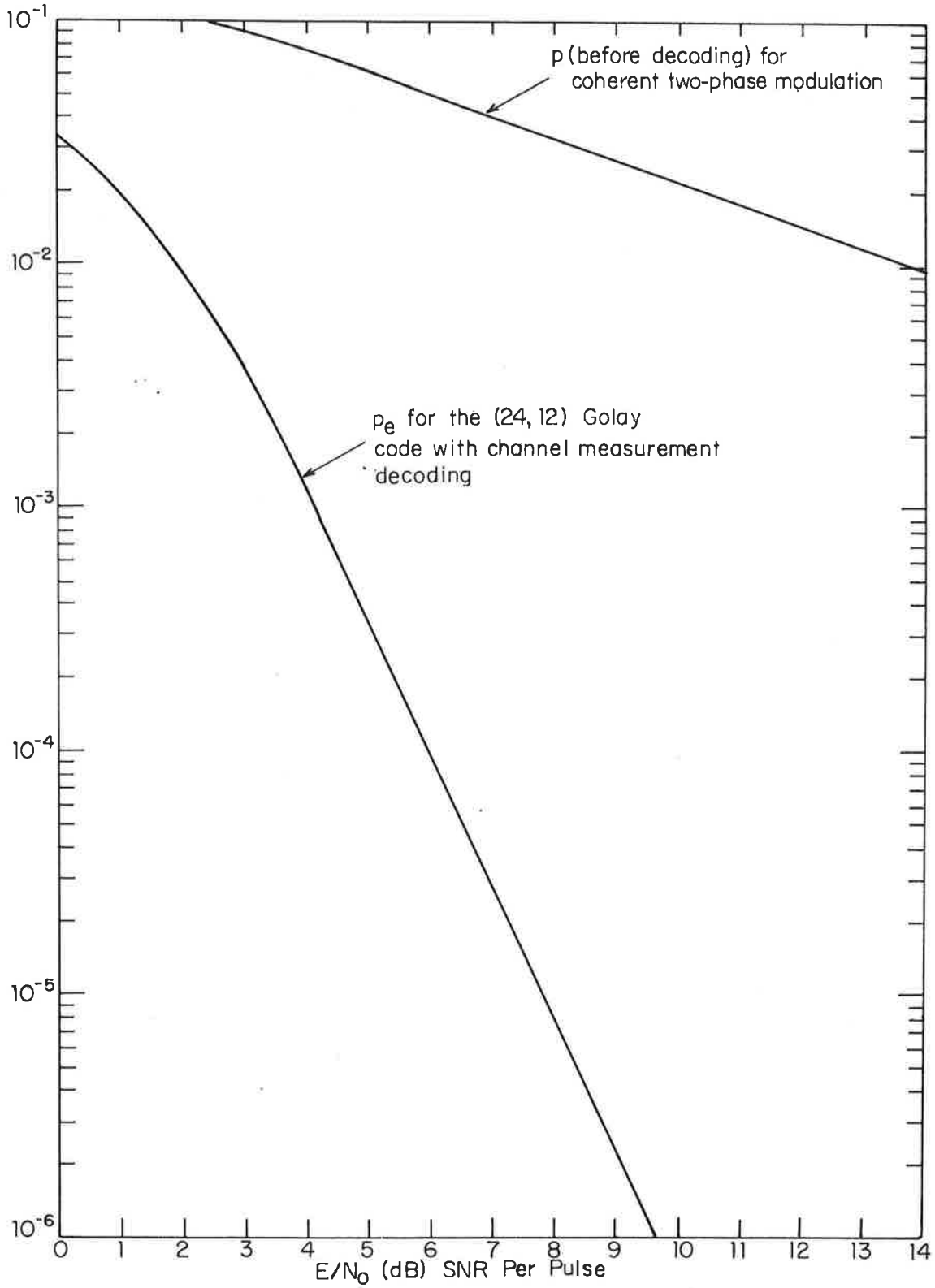

Figure 4.4 Coding Gain for the Independent Slow Fading Rayleigh Channel

Table 4-1

ERROR PERFORMANCE CODING GAIN FOR THE GAUSSIAN AND RAYLEIGH FADING CHANNELS

p	$\frac{p}{P_e}$ Gaussian Channel	$\frac{p}{P_e}$ Rayleigh Fading Channel
10^{-1}	7	14
8×10^{-2}	25	62
6×10^{-2}	85	200
4×10^{-2}	700	1,500
3×10^{-2}	2,500	6,000
2×10^{-2}	14,000	50,000

obtained by this forward error correcting technique which does not require a feedback link. The use of channel measurement information to enhance the effectiveness of these multiple rate codes is also discussed in this section. Since this technique is fairly new [4.4], [4.5], [4.6], [4.7], [4.8], the encoding and decoding procedure as developed by D. Chase in [4.4] will be described in detail in the remainder of this section.

Encoding Procedure

The encoder for a multiple rate code is designed so that, depending on channel conditions, a given code can be decoded in several ways such that various amounts of information digits can be abstracted from it. For example, under normal conditions N/2 information digits are abstracted from a rate 1/2 code of length N. However, if a block of data containing N digits, and N/2 information digits, is lost due to a burst condition, the N/2 information digits are recovered from two later blocks by obtaining an extra N/4 information digit from these two later blocks. Thus, in this example, the code can be decoded as a rate 1/2 (N,N/2) code, as well as a rate 3/4 (N,3/4N) code

In the general case we will assume a basic code of length N with K information digits. This (N,K) code will also have the property that it can be decoded as a higher rate code denoted as an $(N,K+K_1)$ code. The K_1 added information digits have the property that K_1 divides K*, i.e.,

*If this condition is not met we can still use multiple rate codes with u chosen as the smallest integer greater than K/K_1.

$$K = uK_1 \qquad (u \text{ is an integer}) \tag{4.23}$$

and K_1 is less than or equal to the number of parity digits, i.e.,

$$K_1 \leq N-K \tag{4.24}$$

For this case the basic code rate, as viewed by an external interface, is K/N, but during burst correction, it is decoded as a rate $(K+K_1)/N$ code. It should be pointed out that there may be some advantages in treating a code that can be decoded at a basic R = K/N and several other higher rates such as $R_1 = (K+K_1)/N$, $R_2 = (K+K_1+K_2)/N$, etc. However, our primary emphasis will be on a two-state multiple rate code since the complexity grows as the number of decoding rates is increased.

A block diagram of an encoder for a multiple rate code is given in Fig. 4.5 in terms of the parameters N, K, K_1 and u previously defined. The first step is the generation of the basic (N,K) code given by

$$\underline{X}_N = \underline{I}_K, \underline{P}_{N-K} = \underline{I}_K G \tag{4.25}$$

where G is a K x N generator matrix and $\underline{I}_K$ is a 1 x K information vector. Actually, for a cyclic code the generator of $\underline{X}_N$ can be achieved with either a K or (N-K) stage register with the appropriate feedback taps.

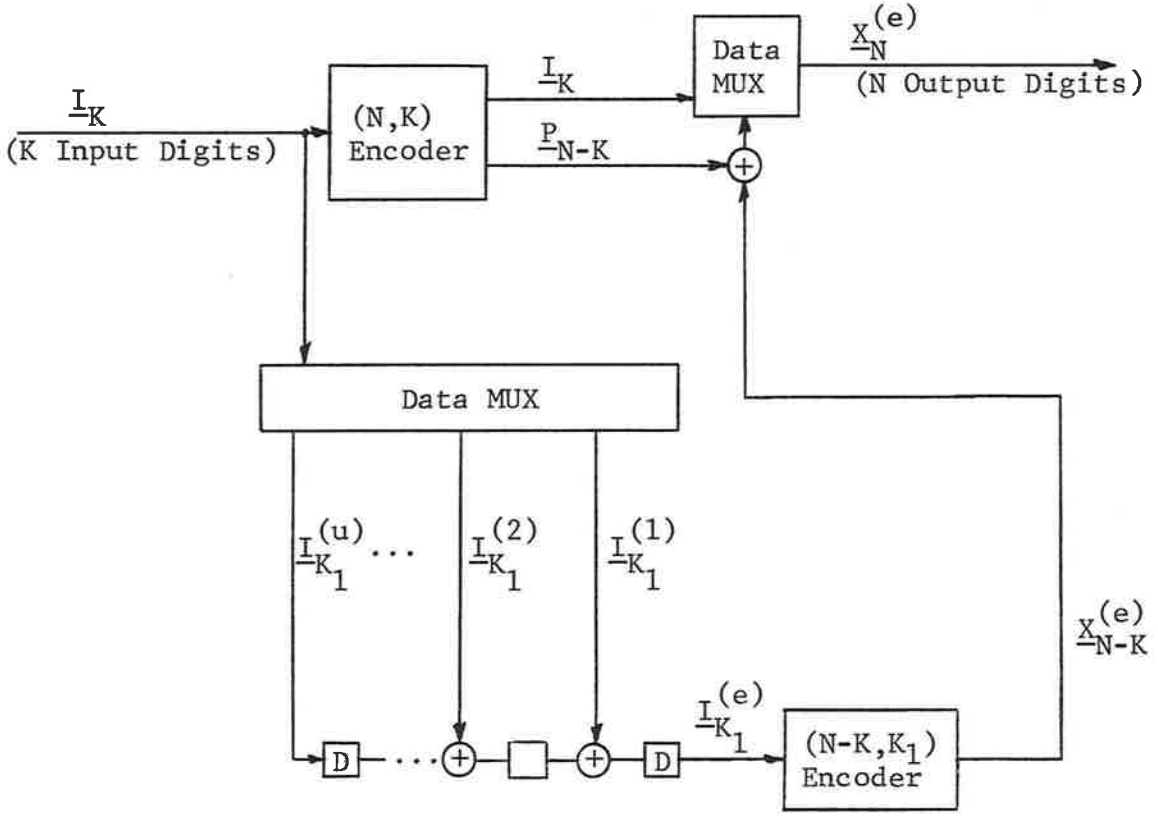

D = $K_1 B$ Bits

B = Number of Blocks of Burst Protection

uD = KB = Total Storage in Information Bits Required for Burst Protection of NB Channel Digits

Figure 4.5 Block Diagram of a Multiple Rate Encoder (Basic Rate = K/N, Burst Correction Rate = $(K+K_1)/N$)

In addition to the basic (N,K) code, an $(N,K+K_0)$ code is generated from several past information blocks. The actual information input to this encoder is given by

$$\underline{I}_{K_1}^{(e)} = \underline{I}_{K_{1-B}}^{(1)} \oplus \underline{I}_{K_{1-2B}}^{(2)} \oplus \ldots \oplus \underline{I}_{K_{1-uB}}^{(u)} \qquad (4.26)$$

where B represents a delay of B code blocks, which is the number of blocks protected against a burst. Thus, the actual input to the $(N-K,K_1)$ encoder contains $I_{K_1}^{(1)}$ from B blocks in the past, $I_{K_1}^{(2)}$ from 2B blocks in the past and finally $I_{K_1}^{(u)}$ from uB blocks in the past as illustrated by the fan for $\underline{X}_N$ shown on Fig. 4.6. The output of this encoder can be written as

$$\underline{X}_{N-K}^{(e)} = \underline{I}_{K_1}^{(e)} G_1 \qquad (4.27)$$

where G_1 is a K_1 x (N-K) matrix used to generate the $(N-K,K_1)$ code.

The final output of multi-rate encoder is given by

$$\underline{X}_N^{(e)} = \underline{X}_N \oplus \underline{O}_K, \underline{X}_{N-K}^{(e)} = \underline{I}_K, \underline{P}_{N-K} \oplus \underline{X}_{N-K}^{(e)} \qquad (4.28)$$

The notation $\underline{O}_K$ is used to represent a sequence of K zeroes which precede $\underline{X}_{N-K}^{(e)}$. The sequence $\underline{X}_N^{(e)}$ contains the original K information digits, intact, but the parity digits are modulo-2 added to $\underline{X}_{N-K}^{(e)}$. This final output code word can be

after the initial delay, a constant flow of data is delivered to the user.

Normal Decoding Mode

A block diagram for the normal mode of operation is given in Fig. 4.7. For simplicity in notation the input to the decoder is assumed error-free.

On this figure we reconstruct $\underline{X}_{N-K}^{(e)}$ from the appropriate portions of the information blocks decoded B, 2B, ..., uB in the past. The reconstruction of $\underline{I}_{K_1}^{(e)}$ is done in the exact manner used in the transmitting section. This particular configuration is attractive due to its analogy to the decoder (especially for half-duplex operation); however, the net storage required by the decoder is (u+1) KB bits. For a typical case u=2 and thus the configuration shown in Fig. 4.7 represents a 50% increase in storage of a configuration requiring only uKB bits of storage. Note that the minimum storage required is uKB since the information sequence is delayed by uB blocks with K information bits per block.

A configuration which minimizes the storage requirements is illustrated in Fig. 4.8. The reconstruction or encoding of $\underline{I}_{K_1}^{(e)}$ now requires a storage of D + 2D + ... + uD which is equal to $(u+1)\frac{u}{2}D = (\frac{u+1}{2})$ KB for u even or odd. This storage is more than the KB bits required for the encoder shown on Fig. 4.5 and for the reconstruction shown on Fig. 4.7. However, configuration #2 does minimize the net storage required even though the technique of just generating $\underline{I}_{K_1}^{(e)}$ does not lead to minimum storage for that particular operation.

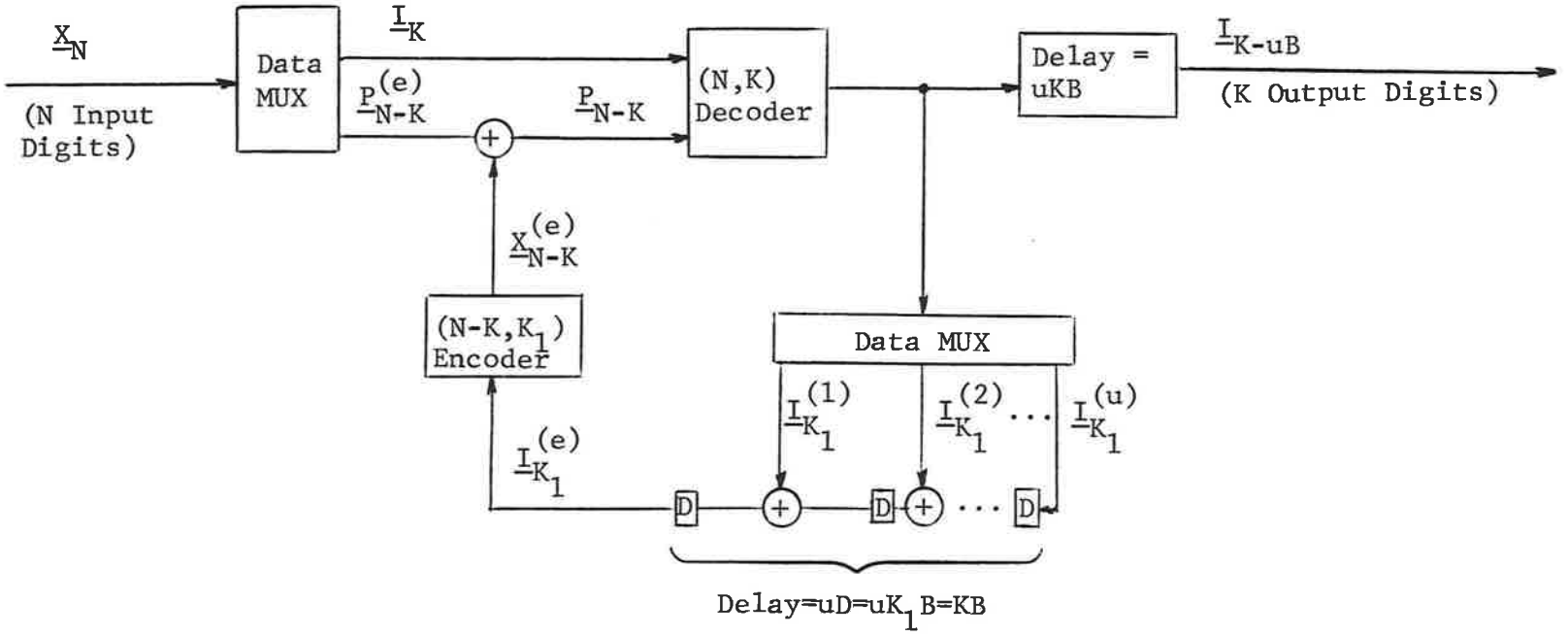

Figure 4.7 Block Diagram for Decoding at R = K/N - Configuration #1

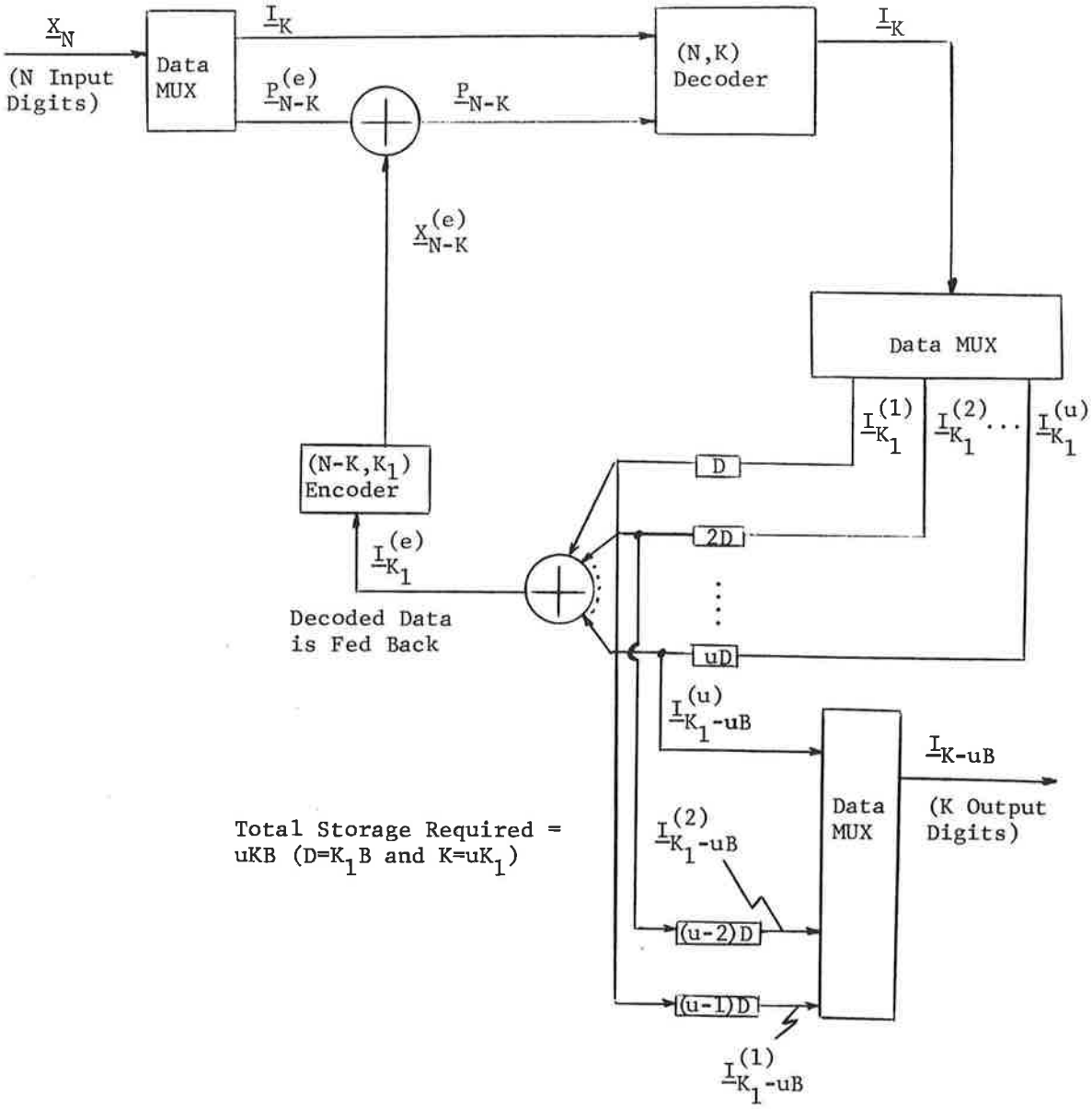

Figure 4-8. Block Diagram for Decoding at R = K/N - Configuration #2

Either configuration shows that in the normal mode we essentially have the performance of an (N,K) decoder. The effect of feeding back incorrect data has been shown in some special cases to have a negligible effect on error propagation. However, this topic deserves further investigation.

Burst Correction Mode

Any time during the normal mode of operation the (N,K) decoder can declare that a given block is likely to be decoded incorrectly and thus correction will then be attempted by the burst correction mode. The data lost in a given block is recovered in u steps from B, 2B, ..., uB future code blocks. To determine which future blocks contain information about the lost block a burst correction signal is generated as shown on Fig. 4.9. The storage requirement necessary for the burst correction signal to appear at the appropriate blocks, which span uB code blocks, is uB bits. Thus, the total storage required for burst trapping decoding is (K+1) uB bits where bursts up to NB channel digits can be corrected.

Since generally the error correction capabilities of the $(N,K+K_1)$ code used for burst correction is less than that possible for the basic (N,K) code a careful optimization is necessary to decide on the criterion for declaring a burst. However, once a burst is declared, one wants to obtain maximum error correcting capability from the $(N,K+K_1)$ decoder. Thus, if available, channel measurement (soft decision) should be utilized to enhance the error correcting capability of this code. The required channel measurement information necessary for decoding need not be delayed since there is no delay in decoding the $(N,K+K_1)$ code. The question as to how

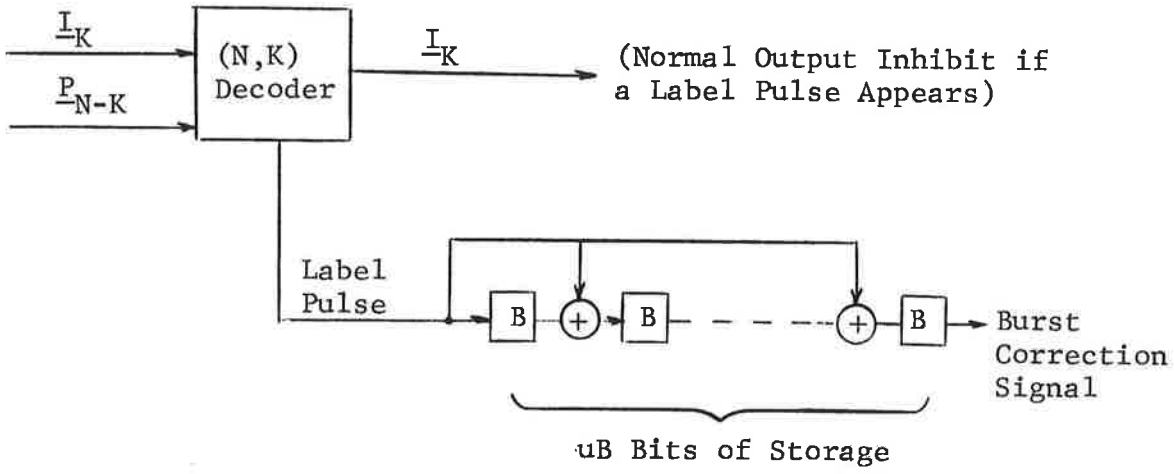

Figure 4.9 Generation of a Burst Correction Signal

effective channel measurement decoding is for the basic (N,K) code is also a subject which requires a certain amount of investigation.

A configuration for burst correction is illustrated on Fig. 4.10 for the case when the first K_1 information digits of the lost block are recovered. This recovered data, $\underline{I}^{(1)}_{K_1\text{-}B}$, is fed forward into a delay line of (u-1)D bits so that it arrives at the data mux #3 after a delay of uD = KB bits which is equivalent to a delay of uB blocks. The lost data are recovered by receiving the first burst correction signal (after B blocks) which opens the first delay line D after data mux #2 and connects the $(N,K+K_1)$ decoder into the receiving circuit. Since $\underline{I}^{(1)}_{K_1\text{-}B}$ is not fed into the $(N\text{-}K,K_1)$ encoder, its code word $\underline{I}^{(1)}_{K_1\text{-}B}G_1$ is not removed from $\underline{P}^{(e)}_{N\text{-}K}$. Note that

$$\underline{X}^{(e)}_{N\text{-}K} = (\underline{I}^{(1)}_{K_1\text{-}B} \oplus \underline{I}^{(2)}_{K_1\text{-}2B} \oplus \ldots \oplus \underline{I}^{(u)}_{K_1\text{-}uB})G_1 \qquad (4.31)$$

which, by the linear properties of a group code, becomes

$$\underline{X}^{(e)}_{N\text{-}K} = \underline{I}^{(1)}_{K_1\text{-}B}G_1 \oplus \underline{I}^{(2)}_{K_1\text{-}2B}G_1 \oplus \ldots \oplus \underline{I}^{(u)}_{K_1\text{-}uB}G_1 \qquad (4.32)$$

Thus, by omitting $\underline{I}^{(1)}_{K\text{-}B}$ from the encoder input, we remove the (N-K) letter code word $\underline{I}^{(1)}_{K\text{-}B}G_1$ from the output. The input to the $(N,K+K_1)$ decoder is then given by

$$\underline{I}_K,\underline{P}_{N\text{-}K} \oplus \underline{I}^{(1)}_{K_1\text{-}B}G_1 \qquad (4.33)$$

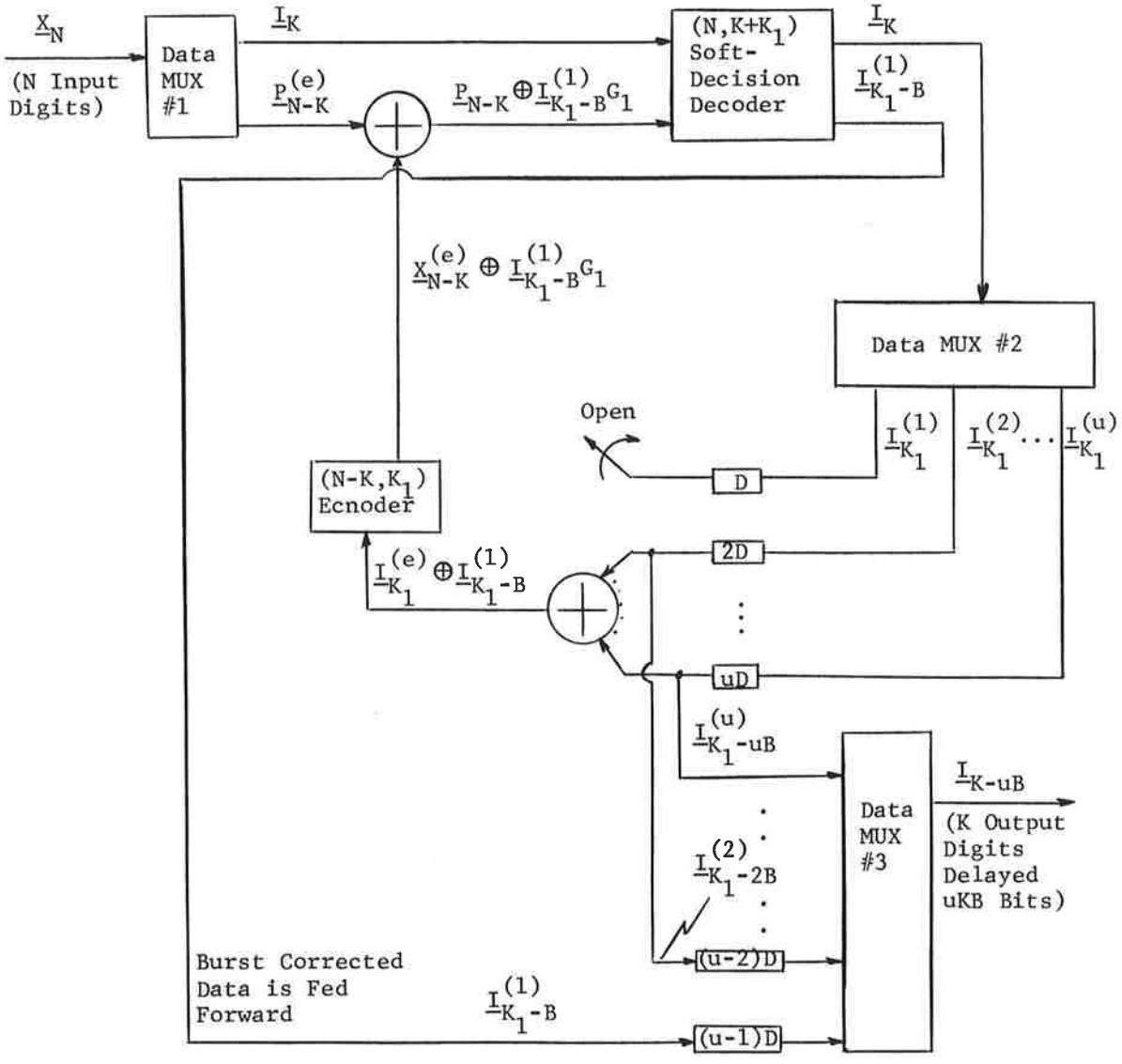

Configuration for Recovery of the First Portion of Block
Labelled B Blocks in the Past

Figure 4-10. Block Diagram for Decoding at $R = (K+K_1)/N$ and Recovery of $\underline{I}^{(1)}_{K_1-B}$

and $\underline{I}_K$ and $\underline{I}^{(1)}_{K-B}$ are recovered

In order to recover the entire code word lost, this process is repeated B times, corresponding to the burst correction signal shown in Fig. 4.9. The second step is the recovery of $\underline{I}^{(2)}_{K_1-2B}$ which is achieved after 2B blocks by opening the 2D delay line after data mux #2 and feeding the burst corrected signal $\underline{I}^{(2)}_{K_1-2B}$ into the (u-2)D delay line before data mux #3. The last step is the recovery of $\underline{I}^{(u)}_{K_1-uB}$ just after uB have been received so that it appears at the input of mux #3 in time to complete the reconstruction of $\underline{I}_{K-uB}$ before the information block is delivered to the user.

For synchronization of the decoder it is not necessary to know when the encoded sequence starts. One can operate the decoder in the $(N,K+K_1)$ mode without feeding back $\underline{X}^{(e)}_{N-K}$ (which is unknown initially) so that the decoder will determine $\underline{I}_K$, which is fed into data mux #2, and $\underline{I}^{(e)}_{K_1}$ which is ignored. After operating in this mode for uB blocks the delay lines following data mux #2 are updated and the decoder can then go into the normal (N,K) decoding mode and feed back a valid estimate of $\underline{X}^{(e)}_{N-K}$. Also, the initial block sync for the $(N,K+K_1)$ code can internally be achieved by the decoder if this signal is unavailable and thus the burst trapping decoder can readily be interfaced with the modem.

REFERENCES

[4.1] J. Jay Jones, "Multi-Channel FSK and DPSK Reception With Three-Component Multipath," IEEE Communication Technology, Vol. COM-16, December 1968, pp. 808-821.

[4.2] D. Chase, "A Class of Algorithms for Decoding Block Codes With Channel Measurement Information," IEEE Trans. on Information Theory, Vol. IT-18, No. 1, January 1972.

[4.3] W. C. Lindsey, "Error Probabilities for Rician Fading Multi-Channel Reception of Binary and N-ary Signals," IEEE Trans. on Information Theory, Vol. IT-10, October 1964, pp. 339-350.

[4.4] D. Chase, et al., "Timation Modulation Study," Contract N00014-71-C-0285, for Naval Research Labs.

[4.5] D. Chase, "Incorporation of Burst Trapping Into CODEM I," Final Report, Contract N62269-70-C-0061 for Naval Air Development Center.

[4.6] S. Y. Tong, "Burst-Trapping Techniques for a Compound Channel," IEEE Trans. on Information Theory, Vol. IT-15, November 1969, pp. 710-715.

[4.7] H. O. Burton, D. D. Sullivan, and S. Y. Tong, "Generalized Burst-Trapping Codes," IEEE Trans. on Information Theory, Vol. IT-17, November 1971, pp. 736-774.

[4.8] D. Chase, "Error Correcting Coding for Navy Spread Spectrum Modem," Final Report, Contract N00014-71-C-0167, for Naval Research Labs.

SECTION 5

THE MEASUREMENT AND REPRODUCTION OF A TIME-VARIANT LINEAR CHANNEL

This section* discusses in some mathematical detail the problem of measuring and reproducing in the laboratory the behavior of a real time-variant linear channel. Such a reproduction can be an extremely powerful tool for the development and comparative evaluation of modems.

The first implementation of such a system was carried out at Fort Monmouth for the HF channel under the direction of B. Goldberg [5.1] as a by-product of the Rake implementation of Price and Green [5.2]. Subsequent implementations were developed under the direction of P. Bello for mobile ground-ground 50 Kc VHF and UHF channels [5.3], [5.4] for the U.S. Army and the Department of Transportation.

In the following discussion a particular method of channel probing and a particular method of channel playback (reproduction) are considered. While the number of possible channel measurement techniques is quite large, the measurement errors for optimized systems are not significantly different (see the comparison of measurement techniques by Bello and Esposito [5.5]). Thus the choice must rest upon practical considerations such as power utilization, efficiency, cost, and complexity, in addition to the basic requirement that the channel measurements be suitable for recreating or playing back the channel at some future date. A consideration

*Part of the material in this section was written by P. Bello under Contract DOT-TSC-84.

of these factors leads to the use of a PN cross-correlation prober for channel measurement and the use of a tapped delay line for channel reproduction as the preferred approaches.

5.1 System Description

Figure 5.1 defines the basic signal processing operations of the probing system. A periodic probing signal with complex envelope $z(t)$ is filtered at the transmitter by IF and RF filters prior to transmission. All the filtering operations in the transmitter are lumped together as one filter, called the transmitter filter, which has impulse response $h_T(t)$. The propagation medium is represented by the complex time-variant impulse response $h(t,\tau)$ and the additive noise by the complex process $n(t)$. All the linear operations in the receiver prior to the correlation operations are lumped together into one receiver filter with impulse response $h_R(t)$. The output of the filter is fed to a number of parallel correlators, only one of which is shown in the figure. Complex notation is used to describe the correlation operation as a multiplication of the receiver filter output by the complex conjugate of a shifted probing signal, followed by a complex low pass filtering operation.

Channel playback is achieved with a tapped delay line as shown in Fig. 5.2. The complex time-varying multipliers are just equal to the low pass filter outputs of the correlators. These outputs are estimates of the impulse response for uniformly spaced values of delay separated by Δ seconds.

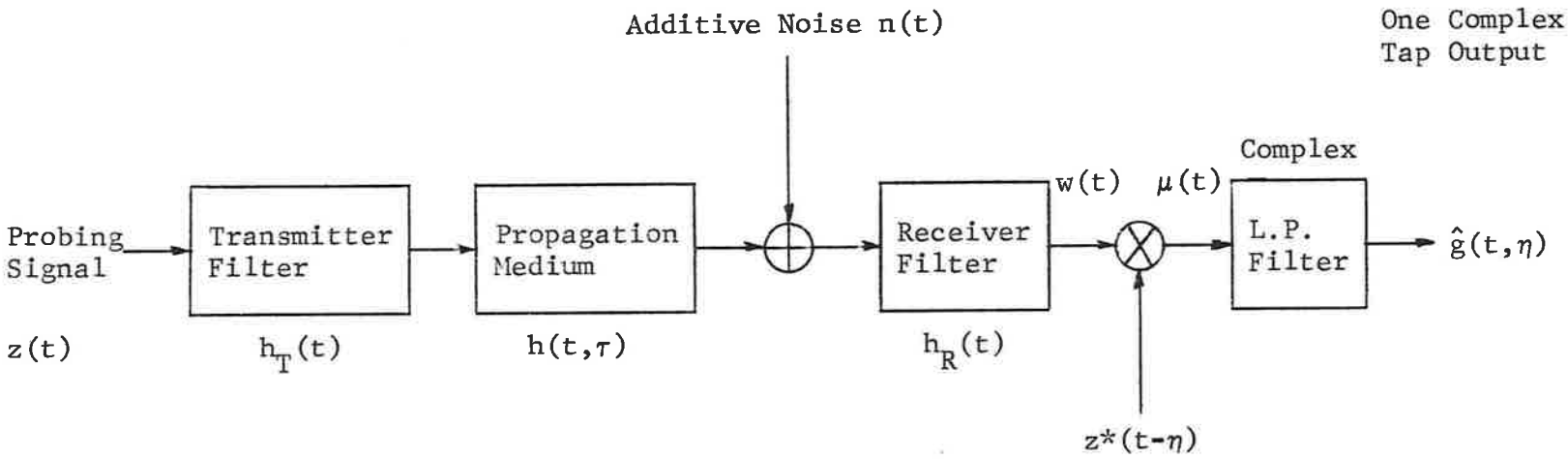

Figure 5.1 Definition of Basic Signal Processing Operations in Prober System

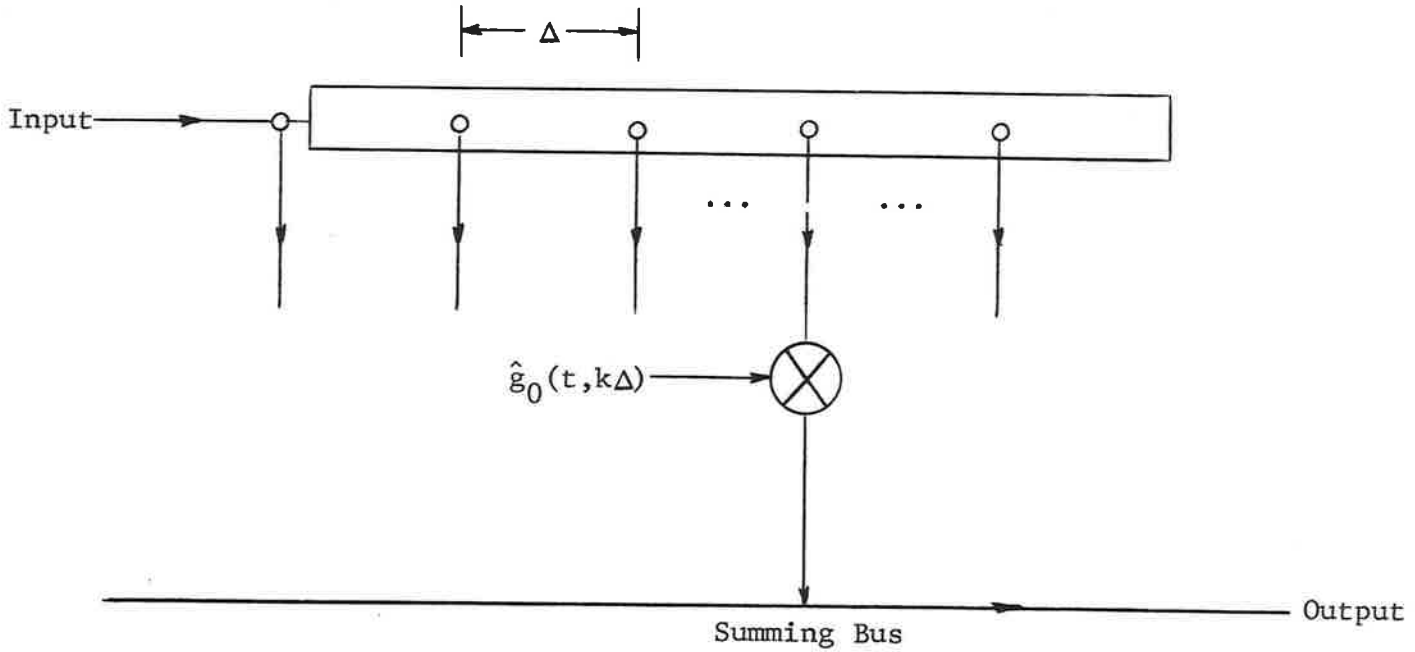

Figure 5.2 Channel Playback

5.2 Formulation of Prober Output

The complex representation of the receiver filter output in the absence of noise is given by the sequence of convolutions

$$w(t) = z(\tau) \otimes h_T(\tau) \otimes h(t,\tau) \otimes h_R(\tau) \qquad (5.1)$$

where $\otimes$ denotes convolution. We assume that the time-constants of $h_T(\ )$ and $h_R(\ )$ are very much smaller than the fading time constant. In this case one may lump the transmitter and receiver filters together, i.e.,

$$w(t) = z(\tau) \otimes e(\tau) \otimes h(t,\tau) \qquad (5.2)$$

where $e(\ )$ is the impulse response of a hypothetical filter, called the "equipment" filter,

$$e(\tau) = h_T(\tau) \otimes h_R(\tau) \qquad (5.3)$$

which represents the combined filtering operations of the transmitter and receiver.

The combination of the equipment filter and the channel impulse response $h(t,\tau)$ may be regarded as an equivalent channel impulse response

$$g(t,\tau) = e(\tau) \otimes h(t,\tau) \qquad (5.4)$$

so that (in the absence of additive noise)

$$w(t) = \int z(t-\tau)g(t,\tau)\, d\tau \qquad (5.5)$$

and the complex low pass filter input is given by

$$u(t) = z^*(t-\eta) \int z(t-\tau)g(t,\tau)\, d\tau$$

$$= \int z^*(t-\eta)z(t-\tau)g(t,\tau)\, d\tau \qquad (5.6)$$

Alternatively, the combination of the equipment filter and the probing signal may be regarded as an equivalent probing signal

$$y(t) = e(t) \otimes z(t) \qquad (5.7)$$

so that (in the absence of additive noise) the received signal

$$w(t) = \int y(t-\tau)h(t,\tau)\, d\tau \qquad (5.8)$$

and the complex low-pass filter output is given by the equivalent form

$$\mu(t) = \int z^*(t-\eta)y(t-\tau)h(t,\tau)\, d\tau \qquad (5.9)$$

The probing signal is assumed to be periodic with period T. Thus the product $z^*(t-\eta)z(t-\tau)$ in (5.6) is also periodic with period T and may be expressed in a Fourier series

$$z^*(t-\eta)z(t-\tau) = \sum C_n e^{j2\pi \frac{n}{T} t} \qquad (5.10)$$

where

$$C_n = \frac{1}{T}\int_{-T/2}^{T/2} z^*(t-\eta)z(t-\tau)e^{-j2\pi\frac{n}{T}t}\,dt$$

$$= X(\eta-\tau, \tfrac{n}{T})e^{-j2\pi\frac{n}{T}\eta} \qquad (5.11)$$

where

$$X(\xi,\nu) = \frac{1}{T}\int_{-T/2}^{T/2} z^*(t)z(t+\xi)e^{-j2\pi\nu t}\,dt \qquad (5.12)$$

is the periodic complex ambiguity function of the probing signal.

Using (5.10) in (5.6)

$$\mu(t) = \sum_n e^{j2\pi\frac{n}{T}(t-\eta)} \int X(\eta-\tau, \tfrac{n}{T})g(t,\tau)\,d\tau \qquad (5.13)$$

Alternatively we note that the product $z^*(t-\eta)y(t-\tau)$ in (5.9) is also periodic with period T and may be expressed in a Fourier series

$$z^*(t-\eta)y(t-\tau) = \sum D_n e^{j2\pi\frac{n}{T}t} \qquad (5.14)$$

where

$$D_n = \frac{1}{T}\int_{-T/2}^{T/2} z^*(t-\eta)y(t-\tau)e^{-j2\pi\frac{n}{T}t}\,dt$$

$$= \frac{1}{T}\int_{-T/2}^{T/2} z^*(t-\eta)\int z(t-x)e(x)\,dx\, e^{-j2\pi\frac{n}{T}t}\,dt$$

$$= \hat{X}(\eta-\tau, \tfrac{n}{T})e^{-j2\pi\frac{n}{T}\eta} \qquad (5.15)$$

where

$$\hat{X}(\xi,\nu) = X(\xi,\nu) \otimes e(\xi) \qquad (5.16)$$

is a delay smeared version of the complex ambiguity function of the probing signal. Thus we have the alternate expression to (5.13) for the correlator output,

$$\mu(t) = \sum_n e^{j2\pi\frac{n}{T}(t-\eta)} \int \hat{X}(\eta-\tau, \tfrac{n}{T})h(t,\tau)\,d\tau \qquad (5.17)$$

Each of the integrals in (5.13) and (5.17) varies with both time and the variable η. The rate of variation with time is controlled by the channel fading rate and equals the Doppler spread of the channel, B_{max}. The phasor $\exp\left[j\frac{2\pi\eta}{T}t\right]$ in (5.13) and (5.17) shifts this spectrum to the frequency n/T Hz. Thus $\mu(t)$ consists of a set of frequency bands centered on multiples of 1/T Hz, the repetition rate of the probing signal.

The strength of the component at n/T Hz, P_n, is given by

$$P_n(\eta) = \iint \hat{X}^*(\eta-\tau_1, \tfrac{n}{T})\hat{X}(\eta-\tau_2, \tfrac{n}{T})\, \overline{h^*(t,\tau_1)h(t,\tau_2)}\, d\tau_1\, d\tau_2 \tag{5.18}$$

Assuming a wide-sense-stationary-uncorrelated scattering (WSSUS) channel

$$\overline{h^*(t,\tau_1)h(t,\tau_2)} = Q(\tau_1)\delta(\tau_2-\tau_1) \tag{5.19}$$

where $Q(\tau_1)$ is the channel's delay power spectrum. Using (5.19) in (5.18),

$$P_n(\eta) = \int |\hat{X}(\eta-\tau, \tfrac{n}{T})|^2 Q(\tau)\, d\tau \tag{5.20}$$

When the smearing effect of $e(\cdot)$ in (5.16) is small and

$$P_n(\eta) \approx \int |X(\eta-\tau, \tfrac{n}{T})|^2 Q(\tau)\, d\tau \tag{5.21}$$

To obtain an estimate of the size of P_n relative to P_0, the strength of the desired signal, we must generally assume specific probing waveforms and delay power spectra.

For the case of a probing signal consisting of a periodic sequence of N bi-phase modulated rectangular pulses of duration T_0 with $(0, 180^o)$ phases following the (1,0) designations of a maximal length shift register sequence, it is readily shown that [5.7] for large N

$$|X(\xi,\nu)|^2 \leq \frac{1}{N} |X(0,0)|^2 \tag{5.22}$$

so that

$$P_n \leq \frac{1}{N} |X(0,0)|^2 \int Q(\tau)\, d\tau \tag{5.23}$$

Consider now the desired term corresponding to n=0 in (5.13) or (5.17):

$$\hat{g}(t,\eta) = \int R(\eta-\tau)g(t,\tau)\, d\tau \tag{5.24}$$

where

$$R(\tau) = X(\tau,0) = \frac{1}{T}\int_0^T z^*(t)z(t+\tau)\, dt = R(\tau+T) \tag{5.25}$$

is the autocorrelation function of the probing signal. Note that the autocorrelation function of the periodic probing signal is also periodic with the same period. Ideally $R(\tau)$ consists of a set of impulses. Then, $\hat{g}(t,\eta)$ would consist of a periodic repetition of $g(t,\tau)$ along the τ axis. It is clear that the period of the ideal probing signal must exceed the duration of $g(t,\tau)$ to avoid overlapping of periodic repetitions of $g(t,\tau)$. Due to bandwidth limitations $R(\tau)$ will not be an impulse train and $\hat{g}(t,\eta)$ will consist of a periodic repetition of smoothed (on η) versions of $g(t,\eta)$. Thus the period T must exceed the duration of this smoothed $g(t,\eta)$. In the realization of the prober T

is always chosen much larger than the duration of the smoothed $g(t,\eta)$ and the correlators sample the non-zero portion of one period along the η axis of $\hat{g}(t,\eta)$. It is then sufficient to deal with a single period of $R(\tau)$, say $R_0(\tau)$, and use samples of

$$\hat{g}_0(t,\eta) = \int R_0(\eta-\tau)g(t,\tau)\, d\tau \qquad (5.26)$$

along the η axis as representations of the correlator outputs for the desired term in (5.13) and (5.17) at n=0.

The strength of the estimated impulse response at a particular value of η is given by (from (5.25))

$$\begin{aligned} P_0 &\approx \int |R(\eta-\tau)|^2 Q(\tau)\, d\tau \\ &\approx Q(\eta) \int |R(\tau)|^2\, d\tau \end{aligned} \qquad (5.27)$$

where we have assumed that the autocorrelation function $R(\tau)$ looks "impulsive" by comparison to $Q(\tau)$. Thus for the PN waveform the ratio of the strengths of the desired term to the n'th undesired term at the correlator output is given by

$$\frac{P_0}{P_n} \geq \frac{Q(\eta)}{\int Q(\tau)\, d\tau} \cdot \frac{\int |R(\tau)|^2\, d\tau}{R^2(0)} \cdot N \qquad (5.28)$$

For a rectangular delay power spectrum of length L and a probing signal of rectangular power spectrum with width W, (5.28) leads to

$$\frac{P_0}{P_n} \geq \frac{N}{WL} \tag{5.29}$$

Assuming that the spurious terms corresponding to $n \neq 0$ in (5.13) and (5.17) have been eliminated by filtering, the set of correlator outputs may be represented conveniently in the impulse sampled form

$$\tilde{g}(t,\eta) = \hat{g}_0(t,\eta)I(\eta) = \Sigma\, \hat{g}_0(t,k\Delta)\delta(\eta-k\Delta) \tag{5.30}$$

where

$$I(\eta) = \Sigma\, \delta(\eta-k\Delta)\ , \tag{5.31}$$

Δ is the sampling interval along the η axis, and $\hat{g}_0(t,k\Delta)$ is the complex representation of the k'th correlator output.

We turn now to a frequency domain analysis and define the Fourier transforms

$$\hat{G}_0(f,t) = \int \hat{g}_0(t,\eta)e^{-j2\pi f\eta}\, d\eta \tag{5.32}$$

$$G(f,t) = \int g(t,\eta)e^{-j2\pi f\eta}\, d\eta \tag{5.33}$$

$$H(f,t) = \int h(t,\eta)e^{-j2\pi f\eta}\, d\eta \tag{5.34}$$

$$P_0(f) = \int R_0(\tau)e^{-j2\pi f\tau}\, d\tau \tag{5.35}$$

$$E(f) = \int e(\tau)e^{-j2\pi f\tau}\, d\tau \tag{5.36}$$

where $\hat{G}_0(f,t)$, $G(f,t)$, and $H(f,t)$ are time-variant transfer functions, $P_0(f)$ is the spectrum of one period of the probing signal autocorrelation function, and $E(f)$ is the transfer function of the equipment filter. From (5.2) and (5.24)

$$G(f,t) = E(f)H(f,t) \tag{5.37}$$

$$\hat{G}_0(f,t) = P_0(f)E(f)H(f,t) \tag{5.38}$$

Using the appropriate sampling theorems the transform of the sampled function $\tilde{g}(t,\eta)$, given by,

$$\tilde{G}(f,t) = \int \tilde{g}(t,\eta)e^{-j2\pi f\eta}\, d\eta \tag{5.39}$$

is expressible as

$$\tilde{G}(f,t) = \frac{1}{\Delta}\sum_n P_0(f - \frac{n}{\Delta})E(f - \frac{n}{\Delta})H(f - \frac{n}{\Delta}, t) \tag{5.40}$$

If aliasing is to be completely avoided then $1/\Delta$ must be larger than the bandwidth of $P_0(f)E(f)H(f,t)$. If $E(f)$ is flat compared to $P_0(f)$ and the rectangular PN sequence is chosen for probing, a choice of Δ = half the pulse width will usually reduce the aliasing to sufficiently low levels.

5.3 Operation of Channel Playback

The impulse response of the tapped delay line in Fig. 5.2 is just equal to the impulse sampled impulse response $\tilde{g}(t,\eta)$, Eq. (5.30). We concern ourselves in this section only with the effectiveness of operation of the tapped delay

line channel playback. For correct prober operation this periodic transfer function should behave just like the propagation medium over a limited bandwidth F about f=0, i.e.,

$$\tilde{G}(f,t) \sim \frac{1}{\Delta} P_0(f)E(f)H(f,t) \quad ; \quad |f| < F/2$$

$$\sim H(f,t) \tag{5.41}$$

or

$$P(f)E(f) = \text{constant} \quad ; \quad |f| < F/2$$

For a single path, i.e.,

$$H(f,t) = 1 \tag{5.42}$$

the stored channel transfer function becomes

$$\tilde{G}(f,t) = \frac{1}{\Delta} \Sigma P_0(f - \frac{n}{\Delta})E(f - \frac{n}{\Delta}) \quad ; \quad H(f,t) = 1 \tag{5.43}$$

This representation of the spectrum $\tilde{G}(f,t)$ is shown in Fig. 5.3. If only the interval $|f| < F/2$ is to be free of aliasing, then the spectral width of $P_0(f)E(f)$, W, must satisfy the inequality

$$W < \frac{2}{\Delta} - F \tag{5.44}$$

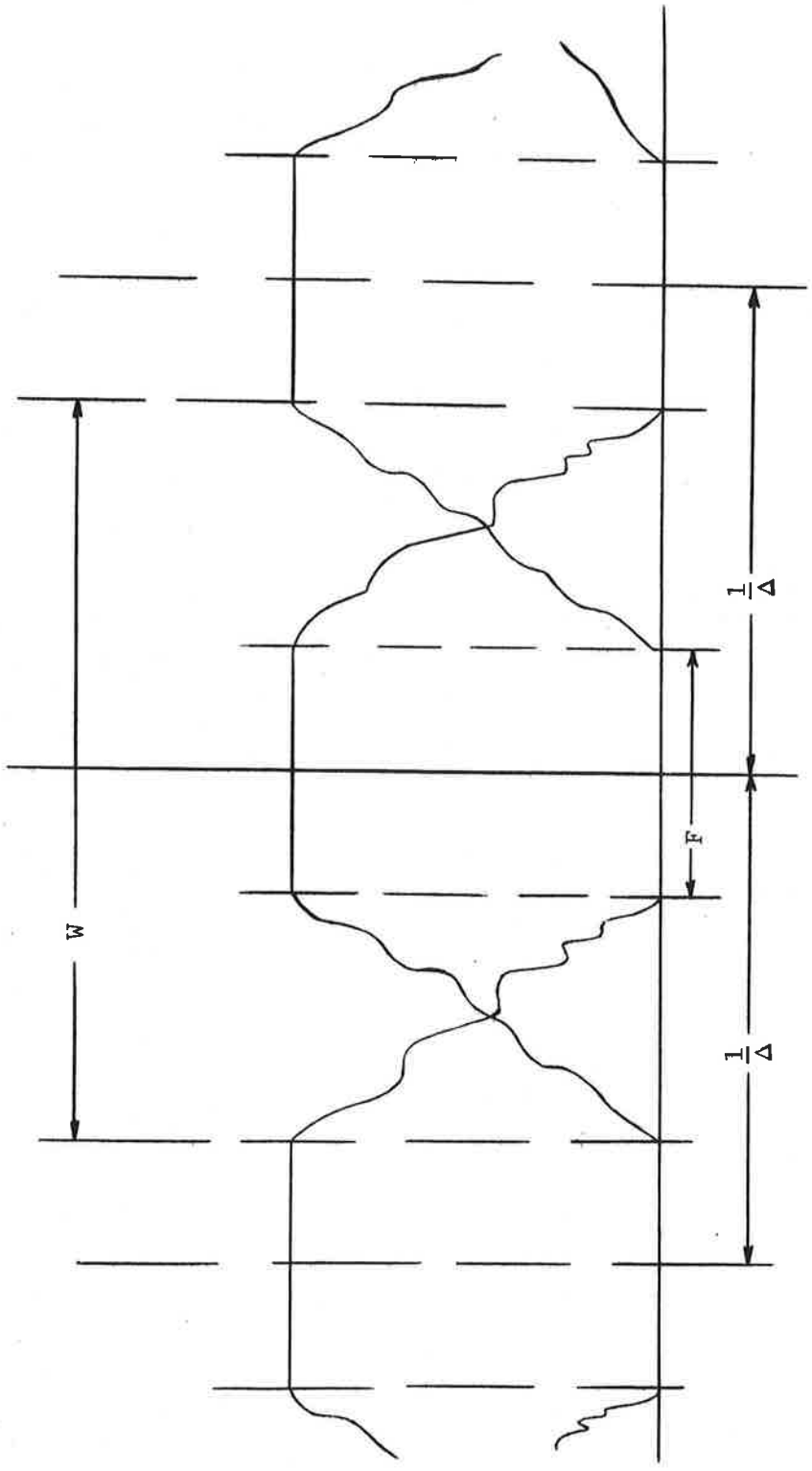

Figure 5-3. Transfer Function of Stored Channel for Single Path

On the other hand if aliasing is to be totally prevented

$$W < \frac{1}{\Delta} \tag{5.45}$$

Since F will be a fraction of $1/\Delta$, (5.44) allows the use of a larger bandwidth probing signal.

In order for the channel playback to work correctly all samples of $\hat{g}_0(t,\eta)$ vs. η of significant size should have been measured by the prober. The duration of $\hat{g}_0(t,\eta)$ vs. η depends upon both the duration of the propagation medium impulse responses and the duration of the time constants associated with the terminal equipment. From Eq. (5.38) we see that the latter time constants are embodied in a single hypothetical filter with transfer function

$$K(f) = P_0(f)E(f) \tag{5.46}$$

and impulse response

$$k(t) = \int K(f)e^{-j2\pi ft}\, dt \tag{5.47}$$

The system designer can control k(t) to have as small duration as possible consistent with the bandwidth constraints (5.44) or (5.45).

5.4 Pseudo-Random Probing

We examine somewhat more closely the case in which the probing signal consists of a periodic sequence of N bi-phase modulated rectangular pulses of duration T_0 with the

$(0, 180^{o})$ phases following the (1,0) designations of a maximal length shift register sequence. Then it is readily calculated that [5.7]

$$R_0(\tau) = \text{Tri}\ (\frac{t}{T_0})(1 + \frac{1}{N}) - \frac{1}{N} \quad ; \quad |t| \leq \frac{NT_0}{2} = \frac{T}{2} \tag{5.48}$$

where we have normalized

$$\frac{1}{T}\int_0^T \overline{|z(t)|^2}\, dt = 1 \tag{5.49}$$

and

$$\text{Tri}(x) = \begin{cases} \{1 - |x|\} & ; \quad |x| \leq 1 \\ 0 & ; \quad |x| > 1 \end{cases} \tag{5.50}$$

From (5.26)

$$\hat{g}_0(t,\eta) = (1 + \frac{1}{N}) \int \text{Tri}(\frac{\eta-\tau}{T_0}) g(t,\tau)\, d\tau - \frac{1}{N}\int g(t,\tau)\, d\tau \tag{5.51}$$

We may compute the relative strengths of these terms for a WSSUS channel [5.6]. These calculations are facilitated by noting that the first integral may be expressed in a different form due to the convolutions comprising $g(t,\tau)$,

$$\text{Tri}(\tfrac{\cdot}{\Delta}) \otimes g(t,\cdot) = k_1(\cdot) \otimes h(t,\cdot)$$

$$= \int k_1(\eta-\tau)h(t,\tau)\, d\tau \qquad (5.52)$$

where

$$k_1(\tau) = \int \text{Tri}(\tfrac{\tau-\xi}{T_0})e(\xi)\, d\xi \qquad (5.53)$$

Neglecting the 1/N in the first term in (5.51), the average strength of this term becomes

$$\iint k_1^*(\eta-\tau_1)k_1(\eta-\tau_2)\, \overline{h^*(t,\tau_1)h(t,\tau_2)}\, d\tau_1\, d\tau_2 \qquad (5.54)$$

The WSSUS property is

$$\overline{h^*(t,\tau_1)h(t,\tau_2)} = Q(\tau_1)\delta(\tau_2-\tau_1) \qquad (5.55)$$

where $Q(\tau_1)$ is the delay power spectrum of the channel. Thus (5.54) becomes

$$\int |k_1(\eta-\tau)|^2 Q(\tau)\, d\tau \qquad (5.56)$$

When there is significant multipath spread, which is the case of interest, $k_1(\cdot)$ should look impulsive compared to $Q(\tau)$ and the above integral should be approximately

$$\int |k_1(\tau)|^2\, d\tau\, Q(\eta) \qquad (5.57)$$

The second integral in (5.51) may be expressed in the form

$$\int g(t,\tau)\, d\tau = \iint e(\xi-\tau)h(t,\xi)\, d\xi\, d\tau$$

$$= \int e(\tau)\, d\tau \int h(t,\xi)\, d\xi \qquad (5.58)$$

and its average strength by

$$\left|\int e(\tau)\, d\tau\right|^2 \int Q(\tau)\, d\tau \qquad (5.59)$$

The ratio of the strength of the first term in (5.51) to the second term is then

$$\rho_C = N^2 \cdot \frac{\int |k_1(\tau)|^2\, d\tau}{\left|\int e(\tau)\, d\tau\right|^2} \cdot \frac{Q(\eta)}{\int Q(\tau)\, d\tau} \qquad (5.60)$$

Let us consider each of these ratio's separately. Each of the integrals in the first ratio may be expressed in the frequency domain:

$$\left|\int e(\tau)\, d\tau\right|^2 = |E(0)|^2$$

$$\int |k_1(\tau)|^2\, d\tau = T_0^2 \int |E(f)|^2\, \mathrm{sinc}^4\, fT_0 df \qquad (5.61)$$

The noise bandwidth of the spectrum $|E(f)|^2 \text{ sinc}^4 fT_0$ is just equal to the ratio

$$\hat{W}_N = \frac{\int |E(f)|^2 \text{ sinc}^4 fT_0 \, df}{|E(0)|^2} \tag{5.62}$$

So that the first ratio in (5.60) is $\hat{W}_N T_0^2$. For a uniformly distributed multipath over a delay spread L the second ratio becomes 1/L. Thus

$$\rho_C = N^2 (\hat{W}_N T_0)(\frac{T_0}{L}) \tag{5.63}$$

In the event that N cannot be increased sufficiently to reduce the spurious second term in (5.51) to a low enough value, one may estimate this second term, which is common to all the taps, and subtract it from each of the correlator outputs. A direct estimate is provided by the output of a correlator which is offset in delay sufficiently to cause the first term to be negligible. Of course this estimate will be noisy and the subtraction will only be useful when the noise level is sufficiently smaller than the second term in (5.37).

5.5 Output SNR of Prober

We assume that the additive noise has a flat power density spectrum over the bandwidth occupied by the probing signal. For simplicity we measure both noise and signal at the output of the receiver filter, i.e., at the correlator input. Thus

$$w(t) = \int z(t-\tau)g(t,\tau)\, d\tau + n(t) \qquad (5.64)$$

If the low pass filter has impulse response $h_L(t)$, then the noise at the typical correlator output is

$$N(t) = \int n(\tau)z^*(\tau-\eta)h_L(t-\tau)\, d\tau \qquad (5.65)$$

and its strength is given by

$$\overline{|N(t)|^2} = \iint \overline{n^*(\tau_1)n(\tau_2)}\; z(\tau-\eta)z^*(\tau_2-\eta)h_L^*(t-\tau_1)h_L(t-\tau_2)\, d\tau_1\, d\tau_2$$

$$= 2N_o \int |z(\tau-\eta)|^2 |h_L(t-\tau)|^2\, dt$$

$$= 2N_o \int |h_L(t)|^2\, dt$$

$$= 2N_o B_N \qquad (5.66)$$

where B_N is the noise bandwidth of the low pass filter and N_o is the one-sided power density of the real additive noise.

The strength of the signal at the correlator output has already been computed as

$$S_{out} \approx Q(\eta) \int |k_1(\tau)|^2\, d\tau \qquad (5.67)$$

The strength of the signal at the receiver filter output is given by

$$S_{in} = \langle \left| \int z(t-\tau)g(t,\tau)\, d\tau \right|^2 \rangle$$

$$= \langle \left| \int y(t-\tau)h(t,\tau)\, d\tau \right|^2 \rangle \qquad (5.68)$$

where we have again arranged convolutions and the $\langle\ \rangle$ denotes time average. The function (see 5.7)

$$y(t) = \int z(t-\tau)e(\tau)\ d\tau \tag{5.69}$$

is the response of the external filter to the probing signal.

Continuing the evaluation in (5.65)

$$S_{in} \int \langle |y(t-\tau)|^2 \rangle\ Q(\tau)\ d\tau \tag{5.70}$$

Note that

$$\langle |y(x)|^2 \rangle = \iint \langle z^*(x-\tau_1)z(x-\tau_2)\rangle e^*(\tau_1)e(\tau_2)\ d\tau_1\ d\tau_2$$

$$= \int R(\tau)\left[\int e^*(t)e(t+\tau)\ dt\right] d\tau \tag{5.71}$$

Returning to the frequency domain and applying Parseval's theorem,

$$\langle |y(x)|^2 \rangle = T_0 \int |E(f)|^2\ \text{sinc}^2 fT_0\ df \tag{5.72}$$

and

$$S_{in} = T_0 \int |E(f)|^2\ \text{sinc}^2 fT_0\ df \int Q(\tau)\ d\tau \tag{5.73}$$

To define the input noise we use a noise bandwidth measure

$$\hat{W}_N = \frac{\int |E(f)|^2 \operatorname{sinc}^2 f\Delta \, df}{|E(0)|^2} \tag{5.74}$$

Since the shape of the transmitted signal will be controlled primarily by E(f) it is clear that we may use

$$\hat{W}_N \approx W_N \tag{5.75}$$

Thus we quickly find the following ratios

$$\rho_{in} = \frac{T_0 |E(0)|^2 \int Q(\tau) \, d\tau}{2N_o} \tag{5.76}$$

$$\rho_{out} = \frac{T_0^2 |E(0)|^2 W_N Q(\eta)}{2N_o B_N} \tag{5.77}$$

$$\frac{\rho_{out}}{\rho_{in}} = \frac{W_N}{B_N} \cdot \frac{Q(\eta) T_0}{\int Q(\tau) \, d\tau} \tag{5.78}$$

For uniformly distributed multipath

$$\frac{\rho_{out}}{\rho_{in}} = \frac{W_N}{B_N} \cdot \frac{T_0}{L} \tag{5.79}$$

We are now in a position to compare the relative strength of the output noise and the spurious term $\frac{1}{N}\int g(t,\tau)\,d\tau$ in (5.51). This ratio will be denoted by ρ_c/ρ_{out}. From (5.63) and (5.79),

$$\rho_c/\rho_{out} \approx \frac{N^2 B_N}{\rho_{in} W_N} = \frac{N^2}{P_0/B_N} \tag{5.80}$$

where P_0 is the input signal-power to noise-power density in dB-Hz and we have used

$$W_N T_0 \approx 1 \tag{5.81}$$

From (5.66) we see that when $N^2 \gg P_0/B_N$ the spurious term $1/N\ (\int g(t,\tau)\,d\tau)$ will be negligible compared to the noise level and, conversely, when $N^2 \ll P_0/B_N$ the spurious term will dominate the additive noise. In this case the spurious term should be subtracted out as discussed at the end of the last subsection.

5.6 Analysis of Multiplexed Operation of Channel Prober

In some applications, such as diversity reception or reception on more than one polarization, it is desirable to measure more than one channel simultaneously. If the spread factor of the channel (product of multipath spread by Doppler spread) is small enough and the SNR is sufficient, it is possible to multiplex a considerable part of the prober demodulator as shown in Fig. 5.4. Each complex correlator output is sequentially connected to one of M output low-pass filters in synchronism with a switch at the receiver input

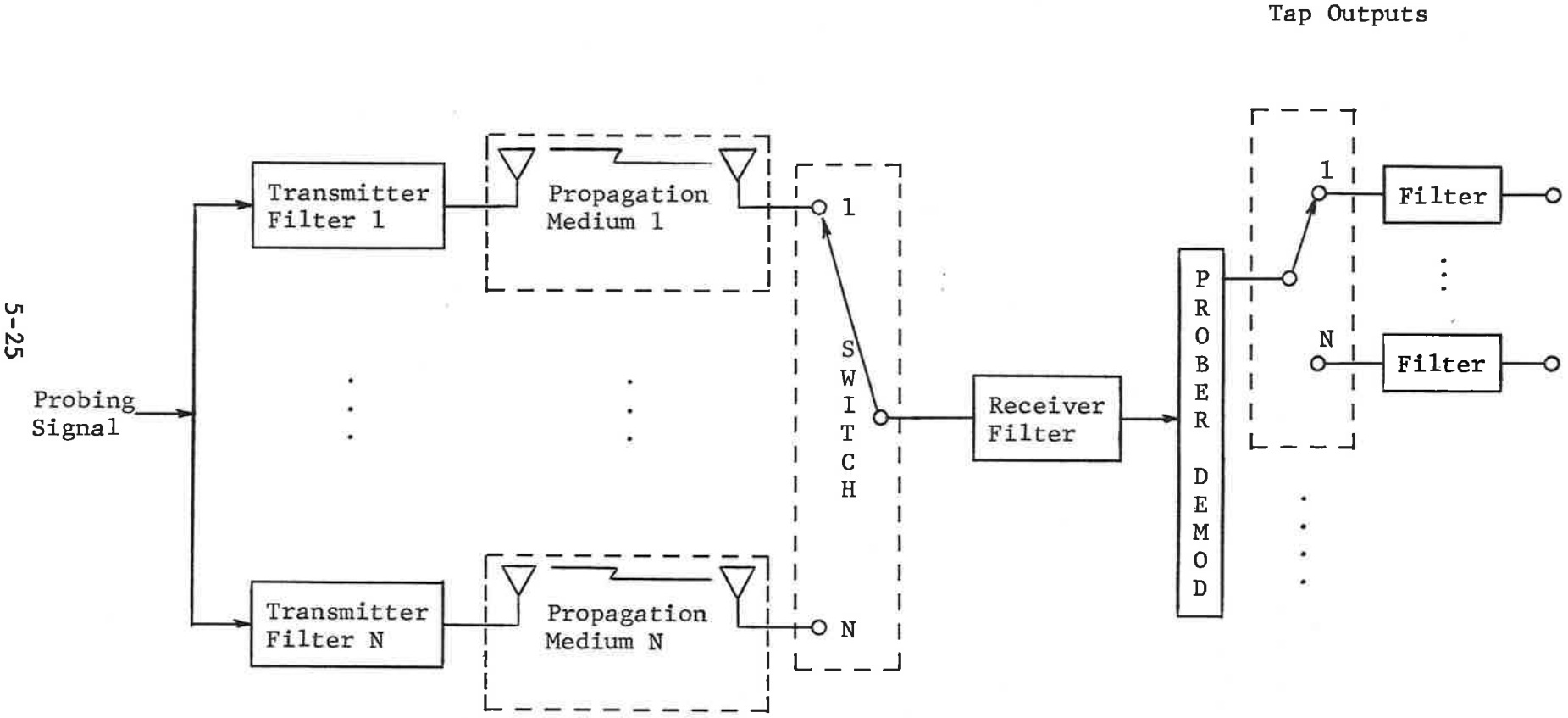

Figure 5.4 A Channel Multiplexed Prober Demodulator

which connects the receiver with one of M receiving antennas corresponding to the M different channels to be measured.

The switch is assumed to work in a time small compared to T_0, the duration of a PN bit, and to switch at a rate equal to 1/T, the repetition rate of the PN probing waveform. To avoid crosstalk between the multiplexed channels introduced by the transients of the receiver filter, this latter filter is assumed to have a time constant sufficiently smaller than T_0.

If we focus our attention on a particular switch position, say position 1, and a reference PN signal with delay η, the complex low pass filter input in the absence of noise may be expressed as (cf. Eq. (5.6))

$$\mu_1(t) = G_1(t)z^*(t-\eta) \int z(t-\tau)g(t,\tau)\, d\tau \quad (5.82)$$

where $G_1(t)$ is a periodic gating function

$$G_1(t) = \sum_m G(t-mMT) \quad (5.83)$$

and

$$G(t) = \begin{cases} 1 & ; \quad 0 < t < T \\ 0 & ; \quad \text{elsewhere} \end{cases} \quad (5.84)$$

and T is the period of the PN sequence.

Bringing the product term outside the integral (5.82) into the integrand, and noting that

$$G_1(t)z^*(t-\eta)z(t-\tau) = \Sigma\, E_p e^{j2\pi \frac{p}{MT} t} \qquad (5.85)$$

i.e., that the product is periodic with period MT and Fourier coefficient

$$E_p = \frac{1}{MT} \int_0^{MT} G_1(t)z^*(t-\eta)z(t-\tau)e^{-j2\pi \frac{p}{MT} t}\, dt$$

$$= \frac{1}{MT} \int_0^{T} z^*(t-\eta)z(t-\tau)e^{-j2\pi \frac{p}{MT} t}\, dt$$

$$= \frac{1}{M} e^{-j2\pi \frac{p}{MT} \eta} X(\eta-\tau, \tfrac{p}{MT}) \qquad (5.86)$$

where, as in Eq. (5.12),

$$X(\xi,\nu) = \frac{1}{T} \int_0^{T} z^*(t)z(t+\xi)e^{-j2\pi\nu t}\, dt \qquad (5.87)$$

is the periodic complex ambiguity function of the probing signal.

Using (5.71) in (5.68)

$$\mu_1(t) = \sum_p e^{j2\pi \frac{p}{MT}(t-\eta)} \frac{1}{M} \int X(\eta-\tau, \tfrac{p}{MT}) g(t,\tau)\, d\tau \qquad (5.88)$$

Each of the integrals in Eq. (5.74) varies with both time and the variable η. The rate of variation with time is controlled by the channel fading rate and is equal to the Doppler spread of the channel, B. The phasor exp $[j2\pi(p/MT)t]$ in (5.74) shifts this spectrum to the frequency p/MT Hz. Thus $\mu(t)$ consists of a set of frequency bands centered on multiples of 1/MT Hz. Note that this is 1/M times the repetition rate of the probing signal.

The strength of the component at p/MT Hz is found to be approximately (see Eq. (5.21))

$$Q_p \approx \frac{1}{M^2} \int |X(\eta-\tau, \tfrac{p}{MT})|^2 Q(\tau)\, d\tau \qquad (5.89)$$

for a WSSUS channel. An examination of this expression reveals that the spurious terms can be comparable in size to the desired term.

The strength of the desired term is decreased by a factor $1/M^2$ as compared to the non-multiplexed case. It may also be shown that the output noise is decreased by 1/M. Thus the output SNR has decreased by 1/M as compared to the non-multiplexed case. Consequently, higher transmitter power is needed in the multiplexed case to achieve the same measurement error against additive noise.

The period of the PN sequence must satisfy the inequality

$$T > L \tag{5.90}$$

to avoid ambiguities in the measurement of the impulse response with a periodic probing signal. With M'th order multiplexing the Doppler spread of the channel B must be less than 1/MT to be able to discriminate against the nearest spurious component at 1/MT Hz with an ideal rectangular low pass filter, i.e.,

$$B < 1/MT \qquad \text{or} \qquad T < \frac{1}{BM} \tag{5.91}$$

In order for both inequalities (5.90) and (5.91) to be satisfied

$$BL < 1/M \tag{5.92}$$

and to use practical filters $BL < 1/2M$.

SECTION 5

REFERENCES

[5.1] B. Goldberg, et al., "Stored Ionosphere," First IEEE Annual Communications Convention Record, June 7-9, 1965, pp. 619 to 622.

[5.2] R. Price and P. E. Green, "A Communication Technique for Multipath Channels," Proc. IRE, pp. 555-570, March 1958.

[5.3] Contract DAAB07-71-C-0019 with Signatron, Inc., Lexington, Mass.

[5.4] Contract DOT-TSC-84 with Signatron, Inc., Lexington, Mass.

[5.5] P. Bello and R. Esposito, "Measurement Techniques for Time Variant Dispersive Channels," Alta Frequenza, No. 11, Vol. XXXIX, 1970, pp. 980-996.

[5.6] P. Bello, "Characterization of Randomly Time-Variant Linear Channels," IEEE Trans. on Communication Systems, Vol. CS-11, No. 4, December 1963, pp. 360-393.

[5.7] R. M. Lerner, "Signals With Uniform Ambiguity Functions," IRE National Convention Record, Vol. 6, Pt. 4, March 1958, pp. 27-36.

SECTION 6
STEEPEST DESCENT CHANNEL MODEL

For the purposes of channel modeling, the airplane-satellite channel may be thought of as the parallel combination of three subchannels, a direct path channel, a discrete specular reflection channel, and a diffuse scatter channel. Thus the complex envelope of the received signal may be expressed as the sum

$$w(t) = w_{dir}(t) + w_{sp}(t) + w_{dif}(t) + \eta(t) \quad (6.1)$$

where $\eta(t)$ is an additive noise term and the subscripts identify the other terms as contributions from the three subchannels in Fig. 6.1. We consider each of these channels in order.

6.1 Direct Path Channel

Excluding tropospheric and ionospheric channel effects, the propagation through the atmosphere between two points is characterized for the airplane-satellite channel simply by means of a (time varying) delay, complex gains associated with antenna patterns, and free space losses. In particular the received signal from the direct path channel is given by

$$w_{dir}(t) = G_{dir} z(t-\tau_{dir}) e^{-j2\pi f_0 \tau_{dir}(t)} \quad (6.2)$$

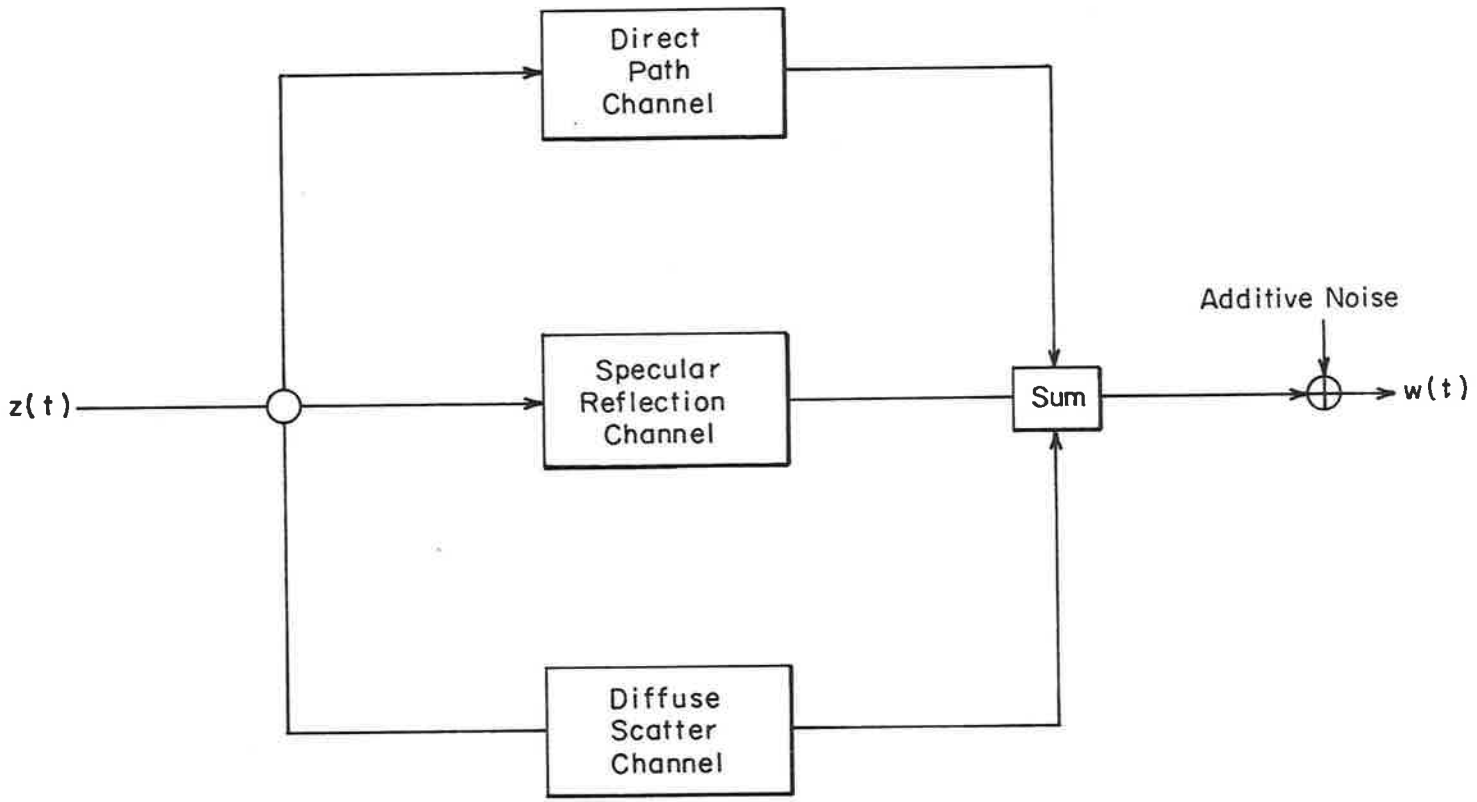

Figure 6.1 Representation of Surface Scatter Channel

where G_{dir} is a slowly varying complex gain due to transmitter and receiver antenna patterns and free space losses, f_0 is the carrier frequency, and $\tau_{dir}(t)$ is the line-of-sight path delay. As far as the modulation $z(t-\tau_{dir})$ is concerned, $\tau_{dir}(t)$ is a slowly varying delay which must be adequately tracked for synchronization in data reception or measured in the case of ranging systems. As far as the exponential term in (6.2) (due to the delayed carrier) is concerned, however, $\tau_{dir}(t)$ produces a rapidly time variant phase shift $2\pi f_0 \tau_{dir}(t)$ and a slowly varying Doppler shift ν_{dir},

$$\nu_{dir} = f_0 \frac{d\tau_{dir}(t)}{dt} = \frac{f_0}{c} V_{dir} \qquad (6.3)$$

where c is the velocity of light and V_{dir} is the rate of change of the path length from transmitter to receiver. Expressions for G_{dir} and τ_{dir} are readily obtained from the geometry, velocity vectors, and antenna characteristics of the transmitter and receiver, and will not be presented here.

6.2 Specular Reflection Channel

The specular reflection channel is used to characterize $w_{sp}(t)$ the received signal due to the average (over the surface heights) field. Assuming a very large scattering surface, this field is focused entirely in the specular direction and behaves, apart from a complex gain, just like a mirror reflection from the surface. Thus

$$w_{sp}(t) = \Gamma G_{sp} z(t-\tau_{sp}) e^{-j2\pi f_0 \tau_{sp}(t)} \qquad (6.4)$$

where Γ is a complex gain that accounts for the electrical and roughness properties of the surface, G_{sp} is a slowly varying complex gain due to complex antenna gains of the transmitter and receiver in the specular direction and free space path losses, and $\tau_{sp}(t)$ is the total path delay from transmitter to specular reflection point to receiver. From a mathematical point of view $w_{sp}(t)$ has the same structure as $w_{dir}(t)$, (6.2). The difference lies in the relative complex gains, delays, and Doppler shifts. A detailed set of delays and Doppler shifts for the direct path and specular channels is given in [6.1] for an airplane to synchronous satellite link.

A useful approximate expression for the time delay difference between the specular reflection and direct path channels for this case of an airplane to synchronous satellite link (accurate down to $\gamma = 15^{o}$ according to [6.1]) is given by

$$\tau_{sp} - \tau_{dir} = \frac{2H}{c} \sin \gamma \tag{6.5}$$

where H is the height of the aircraft. For an aircraft at 20 km and 20^{o} grazing angle this difference is 45 μsec.

The Doppler shift difference

$$\nu_{sp} - \nu_{dir} = f_0 \frac{d}{dt} (\tau_{sp} - \tau_{dir})$$

$$= \frac{f_0}{c} (V_{sp} - V_{dir}) \tag{6.6}$$

where V_{sp} is the rate of change of the transmitter-specular point-receiver path distance, and ν_{sp} is the Doppler shift on the specular reflection channel. The Doppler shift difference is usually quite small. We quote some results from [6.1] for the airplane-satellite channel. For horizontal flight in the great circle plane containing specular point, airplane and satellite, the maximum Doppler shift has a broad maximum between 10^{o}-30^{o} for airplane heights of 10-20 km and airplane velocities of 600-1600 knots. For 1600 knots and 20 km the Doppler shift difference is 5 Hz. Motion at right angles to the great circle plane produces no Doppler shift. Vertical motion of the aircraft will also produce a Doppler shift difference. At L-band (1.6 GHz) and 20 degree grazing angle this Doppler difference is around 3.5 V Hz where V is the vertical velocity in meters/sec.

The importance of the specular component depends on the size of the reflection coefficient Γ and antenna discrimination against energy from the specular direction. Over the North Atlantic it appears that at L-band the surface is rough enough to make the specular reflection channel negligible most of the time. However, at VHF the specular reflection channel can produce a significant output relative to the direct path. The simple surface scattering model provided by the Kirchoff approximation [6.2] will be valid much less in-land than over the sea. At any rate, as the terrain changes in the vicinity of the Fresnel zone, one may expect that $|\Gamma|$ will vary from negligible values to values close to unity (over a lake perhaps).

6.3 Diffuse Scatter Channel

The diffuse scatter channel accounts for all received signals other than those due to the direct path and the discrete specular path. Over the ocean the diffuse scatter paths produce a continuum of infinitesimal contributions to the received signal, and the diffuse channel is generally representable as a random time varying dispersive filter with a time variant impulse response containing no discrete components. (The only exception is in the limiting case of very small RMS slope α, when the diffuse paths concentrate so closely in the specular direction, that the entire diffuse scatter channel may be approximated by a single fluctuating discrete path having the same path delay as the discrete specular component.) In addition, enough statistical regularity exists in the surface fluctuations so that quasi-stationary WSSUS [6.3] models with associated channel correlation functions (e.g., frequency correlation function, Doppler power spectra, delay-Doppler scatter functions) represent useful means of characterization. Moreover, with the aid of the Kirchoff method [6.2], one may obtain meaningful estimates of channel correlation functions for some cases of interest.

Over land the characterization problem is considerably more difficult. The scattering surface exhibits far greater statistical irregularity (desert, foliage, mountains, cities, etc.) and the Kirchoff and small perturbation methods will only be useful for a fraction of the scattering surfaces. While a continuum of return paths is likely, there will be situations where strong localized reflections may occur, such as reflections from man-made metallic structures (e.g., buildings), and natural objects (e.g., mountains). When such localized reflections occur, one must add discrete multipath components to the diffuse channel as defined here.

It is still likely that a quasi-stationary WSSUS channel is useful. However, much more rapid changes in the channel correlation functions are to be expected. In any case the received signal due to the diffuse scatter channel can be represented by

$$w_{dif}(t) = \int z(t-\xi)g(t,\xi)\, d\xi \qquad (6.7)$$

where $g(t,\xi)$ is the impulse response of the diffuse scatter channel.

In this subsection we discuss the evaluation of channel correlation functions for the diffuse scatter channel assuming the Kirchoff model and present some theoretical results for an airplane-synchronous satellite channel.

Two general approaches have been used to determine system function characteristics for the surface scatter link. One approach makes use of normalized scattering cross-sections to directly formulate integral expressions for channel correlation functions (e.g., frequency correlation function $q(\Omega)$, Doppler power spectrum $P(\nu)$, scattering function $S(\xi,\nu)$). This approach has been used by Mallinckrodt [6.4], [6.5], Staras [6.6], Durrani and Staras [6.7], and DeRosa [6.8]. It is implicit in such calculations that the channel may be characterized as a WSSUS channel. The other approach is more basic, starting with the formulation of expressions (usually integrals) for system functions (e.g., time-variant transfer functions) and then proceeding to the averaging required to

determine channel correlation functions. The latter approach provides the means for answering basic questions not obtainable by the scattering cross-section formulation, such as the degree of statistical dependence between signals received on different polarizations, and the validity of the quasi-WSSUS channel model. The more basic formulation has been carried out by DeRosa [6.9].

We first present the simplest non-trivial results derived from the use of scattering cross-sections. These involve the computation of the frequency correlation function $q(\Omega)$, delay power spectra $Q(\xi)$, Doppler power spectrum $P(\nu)$, time correlation function $p(\tau)$, time-frequency correlation function $R(\Omega, \tau)$ and scatter function $S(\xi,\nu)$. Approximate expressions for these functions will be derived for the channel between an aircraft and a synchronous satellite. The results presented here are derived under the same conditions and with the same "steepest descent" approximations as those of Mallinckrodt [6.4], [6.5] who derives expressions for $Q(\xi)$, $P(\nu)$, $S(\xi,\nu)$ and Staras [6.6] who derives expressions for $q(\Omega)$ and $p(\tau)$. The results of these authors are compared and generalized to include an arbitrary direction of the airplane velocity vector and an analytic expression for $R(\Omega, \tau)$.

The earth is assumed to have a flat mean surface with Gaussian distributed surface heights relative to the mean and sufficiently smooth fluctuations to satisfy the requirements of the Kirchoff method. The surface is assumed to be sufficiently rough at L-band so that the specular component is

negligible. Finally it is also assumed that the rms surface slope $\alpha \ll 1$ and the deviation angle $\theta \gg \alpha$. Even with all these assumptions, it appears that these results should provide useful channel information for some L-band oceanic airplane-to-satellite channel over the North Atlantic. It should be realized, however, that the case $\theta \gg \alpha$ will be violated under some conditions of interest in aeronautical communications (in particular, sufficiently low elevation angles or rough surfaces).

From the Kirchoff model of the surface Beckmann [6.2] has obtained the following expression* for the scattering cross-section per unit area

$$\sigma(\vec{r}) = |\Gamma_0|^2 \frac{1}{2\alpha^2 \cos^4\beta} \exp\left(-\frac{\tan^2\beta}{2\alpha^2}\right) \qquad (6.8)$$

where Γ_0 is the appropriate Fresnel reflection coefficient (horizontal or vertical) for a flat ocean, α is the RMS sea slope, and β is the tilt angle of a plane at $\vec{r}$ relative to a tangent plane to the mean surface at $\vec{r}$ required for mirror reflection from transmitter to receiver.

*We have slightly generalized Beckmann's expression by introducing the RMS sea slope α and thus making the answer independent of the spatial correlation function of surface heights.

For a flat mean surface and a satellite very far from the airplane, Fig. 6.2 depicts geometrical relationships for the scattering process. As the origin of the coordinate system we have chosen the point on the mean surface directly below the aircraft, so that the airplane coordinates are (0,0,H) where H is the height of the aircraft. The satellite is assumed to be in the XZ plane, so far from the airplane and scattering surface that rays leaving the airplane and any scattering points on the glistening zone and terminating on the satellite have essentially the same elevation angle θ, as shown in Fig. 6.2. At the specular point, located on the X axis, the grazing angle $\gamma=\gamma_{sp}=\theta$.

Due to our assumed coordinate system we may express $\sigma(\vec{r})$ as a function of the rectangular surface coordinates X, Y, i..e, $\sigma(\vec{r}) = \sigma(X,Y)$. The incremental power transferred from transmitter to receiver normalized to the power received on the direct path for a small area $\Delta x \Delta y$, is given by

$$\frac{\Delta P_S}{P_D} = |\Gamma_0|^2 \frac{\sigma(X,Y) R_0^2}{4\pi R^2 R_2^2} A(X,Y)\ \Delta x\, \Delta y$$

$$\approx |\Gamma_0|^2 \frac{\sigma(X,Y)}{4\pi R^2} A(X,Y)\ \Delta x\, \Delta y \qquad (R_0 \approx R_2) \quad (6.9)$$

where R_0, R, R_2 are the lengths of the direct path, the path from airplane to scattering area element, and the path from scatterer to satellite, respectively; A(X,Y) is the surface illumination pattern of the combined transmitter and receiver antenna gains

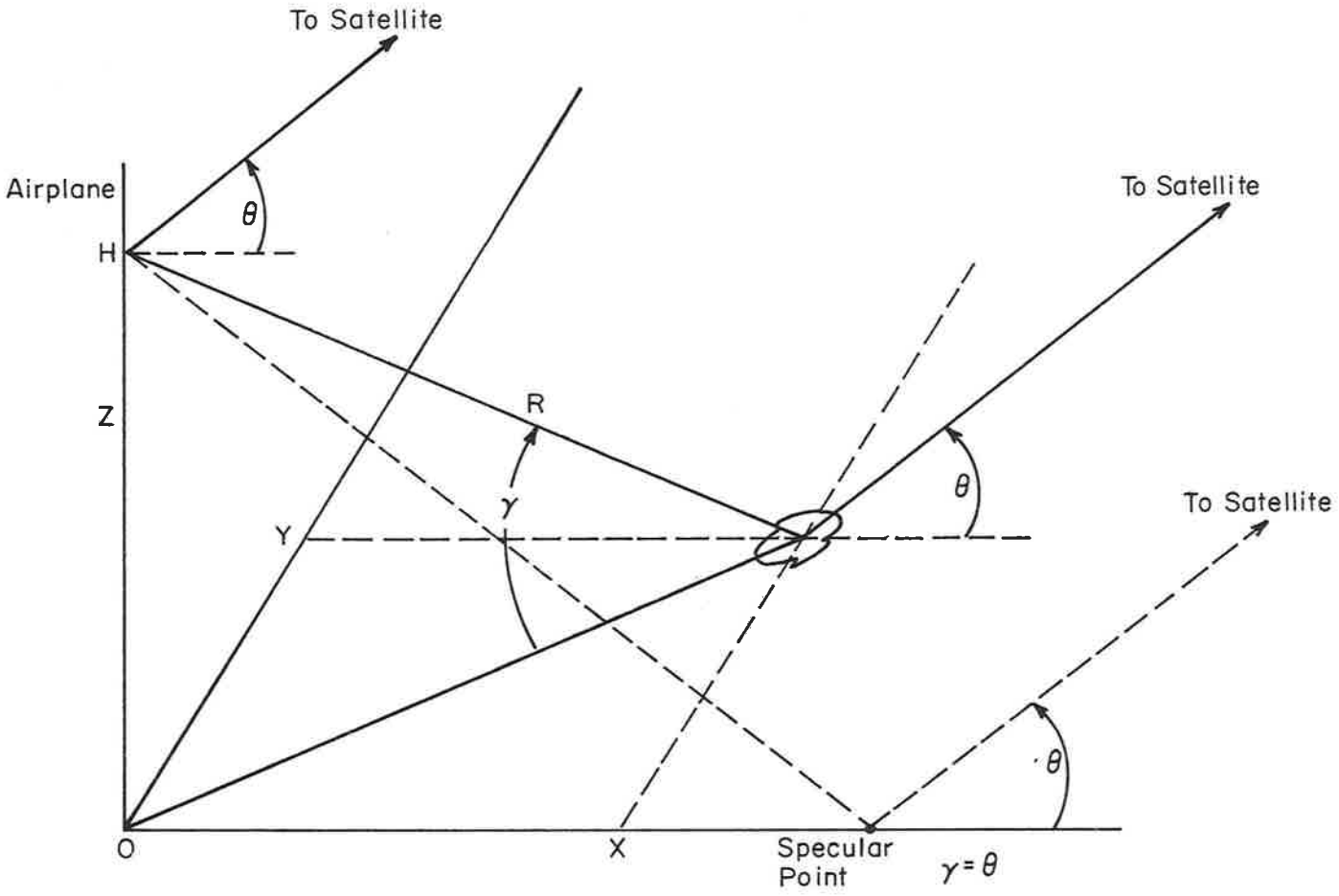

Figure 6.2 Geometrical Relationships for Scattering in Airplane-Synchronous Satellite Channel Assuming Flat Mean Earth Surface

normalized to the direct path gains; and P_S, P_D are the total scattered and direct path powers. The total normalized scattered power is then

$$\frac{P_S}{P_D} = |\Gamma_0|^2 \int\int_{-\infty}^{\infty} W(X,Y)A(X,Y)\, dx\, dy \qquad (6.10)$$

where

$$W(X,Y) = \frac{\sigma(X,Y)}{4\pi(X^2+Y^2+H^2)} \qquad (6.11)$$

For small α, $\sigma(X,Y)$ and $W(X,Y)$, will be concentrated in the vicinity of the specular point $(H/\tan\theta,0,0)$ and will decrease to negligible values rapidly outside the glistening zone. The "steepest descent" approximations used in Mallinckrodt[6.4], [6.5] and Staras [6.6]and also in the simple derivations to be given here, represent the argument of the exponent in W(X,Y) by the leading nonvanishing terms in a Taylor series expansion of the surface coordinates about the specular point (Mallinckrodt used rectangular coordinates and Staras used polar coordinates). Any expressions multiplying the exponential terms are represented by their value at the specular point. This approximation should be useful when $\theta >> \alpha$.* With this approximation

*It is readily shown that in the plane Y=0, $\beta = \frac{\theta-\gamma}{2}$. Thus when $\beta = \frac{\theta}{2}$, there can be energy scattered to the receiver by areas at infinity on a plane surface. Of course on a spherical earth γ=0 corresponds to the points at which planes through the airplane are tangent to the earth. In the former case the glistening zone extends to infinity and in the latter case it is still so large as to violate the conditions required for the use of (6.9). If $\alpha << \theta$ one may argue that the power returned at values of β which violate (6.9) will be negligible. However the authors are not aware of any critical analysis to determine simple criteria for use of (6.9).

$$W(X,Y) = W(X)W(Y) = \frac{1}{2\alpha H \csc^2\theta \sqrt{2\pi}} \exp\left(-\frac{(X - H \operatorname{ctn}\theta)^2}{8\alpha^2 H^2 \csc^4\theta}\right)$$

$$\times \frac{1}{2\alpha H \sqrt{2\pi}} \exp\left(-\frac{Y^2}{8\alpha^2 H^2}\right) \qquad (6.12)$$

which may be recognized as the product of the probability density function of two normally distributed random variables, the "X" variable having mean H ctn θ and standard deviation $2\alpha H \csc^2\theta$ and the "Y" variable having zero mean and standard deviation $2\alpha H$. Use of (6.12) in (6.10) shows that when the surface illumination pattern varies little over the glistening region

$$\frac{P_S}{P_D} \approx |\Gamma_0|^2 \, A(H/\tan\theta, 0) \qquad (6.13)$$

We consider now the case wherein (6.13) applies and determine expressions for channel correlation functions. To determine the Doppler power spectrum $P(\nu)$, delay power spectra $Q(\xi)$, or delay-Doppler scatter function $S(\xi,\nu)$, one may associate a single delay and Doppler shift and a particular power density with each differential area of the surface.* By expressing the Doppler shift ν as a function of X and Y, and regarding X, Y as random variables, the probability density function of ν will be identical

*Since the sea surface is moving this is clearly an approximation (to be included among all the others). However one may show that little error can be introduced in the estimate of $P(\nu)$, $Q(\xi)$ and $S(\xi,\nu)$ by this approximation in airplane communication channels.

to the desired Doppler power spectrum, normalized to unit area. The factor $|\Gamma_0|^2 A(H/\tan\theta, 0)$ may then be applied to correct the height of $P(\nu)$. An exactly analogous procedure will be used to derive $Q(\xi)$ and $S(\xi,\nu)$ as probability density functions of the random variable ξ and the point variable (ξ,ν). The Fourier transforms of $P(\nu)$, $Q(\xi)$, $S(\xi,\nu)$, $p(\tau)$, $q(\Omega)$, and $R(\Omega,\tau)$, respectively may be regarded as characteristic functions of the variables ν, ξ, (ν,ξ).

If $\vec{V}$ is the velocity vector of the airplane, it is seen that the Doppler shift associated with the received signal from a scattering element is given by

$$\frac{f_0}{c}\vec{V}\cdot\left(\frac{\vec{R}}{R}\right) = \frac{f_0}{c}\left(V_x\frac{X}{R} + V_y\frac{Y}{R} - V_z\frac{H}{R}\right) \qquad (6.14)$$

where $\vec{R}$ is a vector extending from the airplane to the scattering element. The Doppler shift relative to that produced by an element at the specular point is

$$\nu = \frac{f_0}{c}V_x\left(\frac{X}{R} - \cos\theta\right) + \frac{f_0}{c}V_y\frac{Y}{R} + \frac{f_0}{c}V_z(\sin\theta - \frac{H}{R}) \qquad (6.15)$$

Following the procedure described above, ν is to be regarded as a random variable related to the random variables X and Y by Eq. (6.15). The probability density function of ν is the normalized Doppler power spectrum. Before determining the density function

of F we approximate F by leading terms in a Taylor series expansion of the right-hand side of (6.15). The approximations used are identical with those used in deriving the Gaussian approximation to W(X,Y), (6.12). There is no point in seeking any more accuracy in representing ν. All the expansions that are used depend upon the expansion of either R or 1/R,

$$R = \sqrt{H^2+X^2+Y^2} = \frac{H}{S}\left[1 + CS\left(\frac{X}{H} - \frac{C}{S}\right) + \frac{S^4}{2}\left(\frac{X}{H} - \frac{C}{S}\right)^2 + \frac{S^2}{2}\left(\frac{Y}{H}\right)^2 + \ldots\right] \tag{6.16}$$

$$\frac{1}{R} = \frac{S}{H}\left[1 - CS\left(\frac{X}{H} - \frac{C}{S}\right) - S^2\left(\frac{S^2}{2} - C^2\right)\left(\frac{X}{H} - \frac{C}{S}\right)^2 - \frac{S^2}{2}\left(\frac{Y}{H}\right)^2 + \ldots\right] \tag{6.17}$$

where we have used the notation

$$S = \sin\theta \tag{6.18}$$

$$C = \cos\theta \tag{6.19}$$

Use of (6.16) in (6.15) then shows that

$$\nu = \frac{f_0}{c}\left[V_x S^3 + V_z CS^2\right]\left(\frac{X}{H} - \frac{C}{S}\right) + \frac{f_0}{c} V_y S \frac{Y}{H} + \ldots \text{ (higher order terms)} \tag{6.20}$$

To be consistent with the approximations to R involved in the steepest descent approximations used to derive (6.12) we neglect the higher order terms in (6.20). Then ν regarded as a random variable is represented as the linear combination of two independent zero mean Gaussian random variables. It follows from elementary statistics that ν will also be a zero mean Gaussian random variable with variance equal to the sum of the variances of the individual random variables. Thus the Doppler power spectrum is

$$P(\nu) = \frac{\sqrt{2}}{B_{RMS}\sqrt{\pi}} \exp\left[-\frac{2\nu^2}{B_{RMS}^2}\right] \tag{6.21}$$

where we have defined the RMS Doppler spread as <u>twice</u> the standard deviation,

$$B_{RMS} = 4\left(\frac{f_0}{c}\right)\alpha\sqrt{(V_x \sin\theta + V_z \cos\theta)^2 + V_y^2 \sin^2\theta} \tag{6.22}$$

Note that $V_x \sin\theta + V_z \cos\theta$ is the velocity component in the x-z plane at right angles to the specular direction. Thus the steepest descent approximation leads to a zero Doppler spread when the aircraft moves along the line-of-sight to the specular point. In practice this means that the Doppler spread is small but non-vanishing and determined by second order terms in the expansion (6.20).

The time correlation function $p(\tau)$ is the Fourier transform of (6.21).

$$p(\tau) = \exp\left[-\frac{1}{2}(\pi\tau B_{RMS})^2\right] \tag{6.23}$$

Mallinckrodt computed $P(\nu)$ for airplane motion in the X direction (i.e., $\bar{V} = (V_x,0,0)$ and in the Y direction ($\bar{V} = (0,V_y,0)$). For these special cases $P(\nu)$ in (6.21) agrees with Mallinckrodt's results (note that his $s = \sigma/L = \alpha\sqrt{2}$ and fix

typo's which left out $\sqrt{2}$ on p. 27 of [6.5]). Staras [6.6] computed $p(\tau)$ for the cases of motion in the direction of each coordinate axis, i.e., $(V_x,0,0)$, $(0,V_y,0)$, $(0,0,V_z)$. Our result (6.23) when specialized to these cases agrees with his calculations for the two cases $\vec{V} = (V_x,0,0)$ and $\vec{V} = (0,0,V_z)$. For airplane motion in the Y direction, however, his results differ from ours. The reason for the difference may be shown to be equivalent to the inclusion of the second order term $(\sim Y(X - \frac{C}{S} H))$ in the Taylor expansion of Y/R in (6.15) about the specular point Y=0, $X = \frac{C}{S} H$. If the steepest descent argument is valid, the inclusion of this second order term will yield different but not necessarily better approximations to the exact $p(\tau)$.

We consider now the computation of the delay power spectrum. From the geometry in Fig. 6.2 one may determine that the delay of a scattered signal from an area element at X, Y relative to the delay of scattered signals from the specular direction is given by

$$\xi = \frac{1}{c} \left(\sqrt{H^2+X^2+Y^2} - X \cos \theta - H \sin \theta\right) \qquad (6.24)$$

Using (6.16) it is found that

$$\xi = \frac{H}{c} \frac{\sin \theta}{2} \left(\sin^2\theta \left(\frac{X}{H} - \text{ctn } \theta\right)^2 + \frac{Y^2}{H^2}\right)$$

$$+ \ldots \text{ higher order terms} \qquad (6.25)$$

Neglecting the higher order terms we see that the path delay ξ, regarded as a random variable, may be expressed as the sum of squares of two independent zero-mean Gaussian random variables.

The density function and characteristic function of such a random variable are readily computed in closed form. The results are

$$Q(\xi) = \frac{1}{4\alpha^2 H/c} \exp\left(-\left[\frac{\sin\theta + 1/\sin\theta}{8\alpha^2 H/c}\right]\xi\right) I_0\left(\frac{\left[\frac{1}{\sin\theta} - \sin\theta\right]}{8\alpha^2 H/c}\,\xi\right) \tag{6.26}$$

$$q(\Omega) = \overline{e^{-i2\pi\Omega\xi}} = \frac{1}{\sqrt{\left[1 + i4\pi\Omega\left(\frac{2H}{c}\,\frac{\alpha^2}{\sin\theta}\right)\right]\left[1 + i4\pi\Omega\left(\frac{2H}{c}\alpha^2\sin\theta\right)\right]}} \tag{6.27}$$

which provide the normalized delay power spectrum and frequency correlation function of the diffuse channel (referenced to the specular path delay). Aside from a factor of $1/\pi$ in front and a scale factor on ξ, the $Q(\xi)$ computed by Mallinckrodt ([6.5], Eq. (26)), is the same as (6.26). Also Staras [6.6] has obtained the result (6.27), (complete the integration in his Eq. (23a)). Plots of $Q(\xi)$ and $q(\Omega)$ as a function of the normalized variable $\xi/4\alpha^2(H/c)$ are presented in Figs. 6.3 and 6.4 for several elevation angles.

The time-frequency correlation function of the channel is just the joint characteristic function of the random variables, ξ, ν. Thus

$$R(\Omega,\tau) = \overline{e^{-i2\pi\Omega\xi} e^{i2\pi\tau\nu}} \tag{6.28}$$

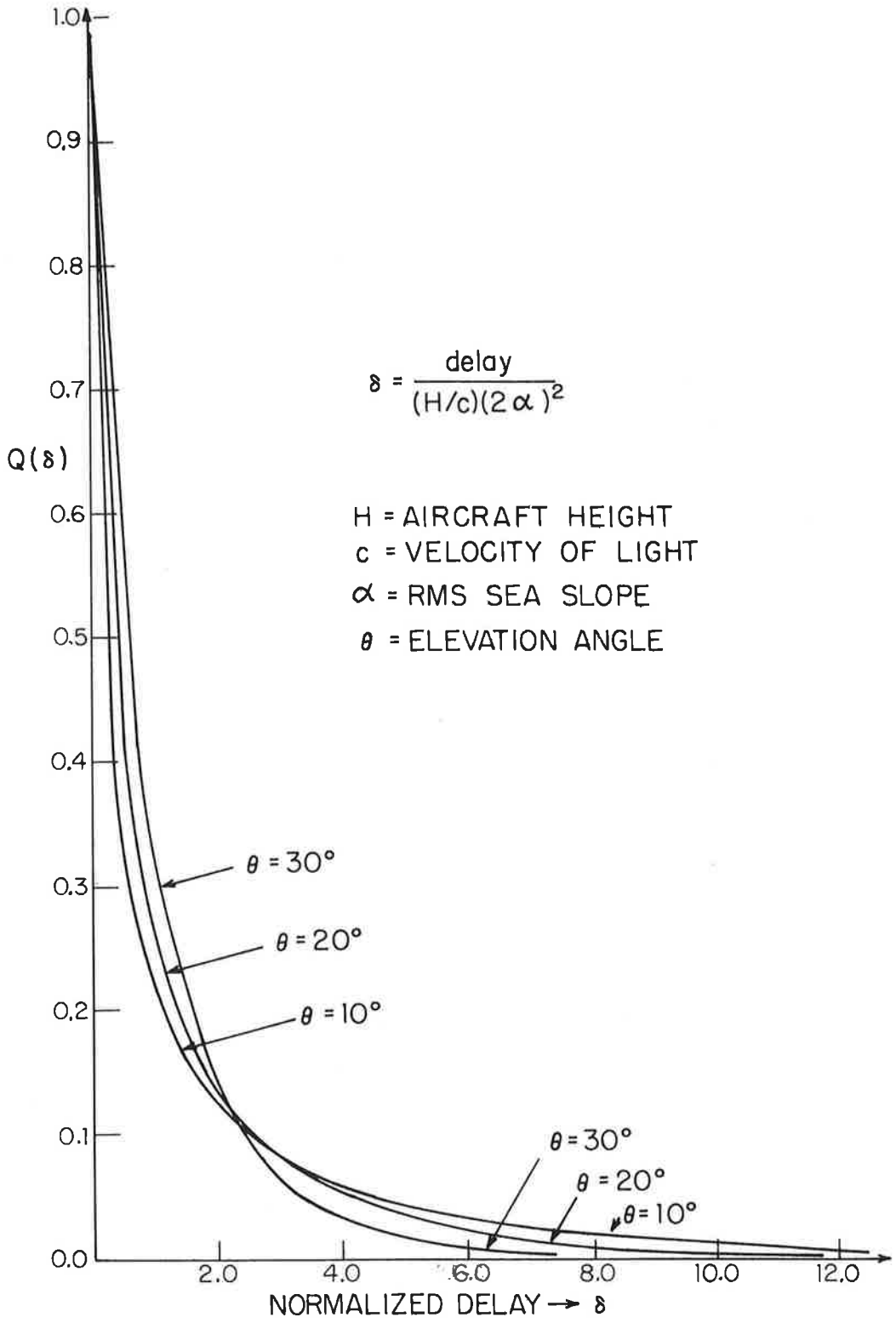

Figure 6-3. Delay Power Spectrum for Diffuse Scatter

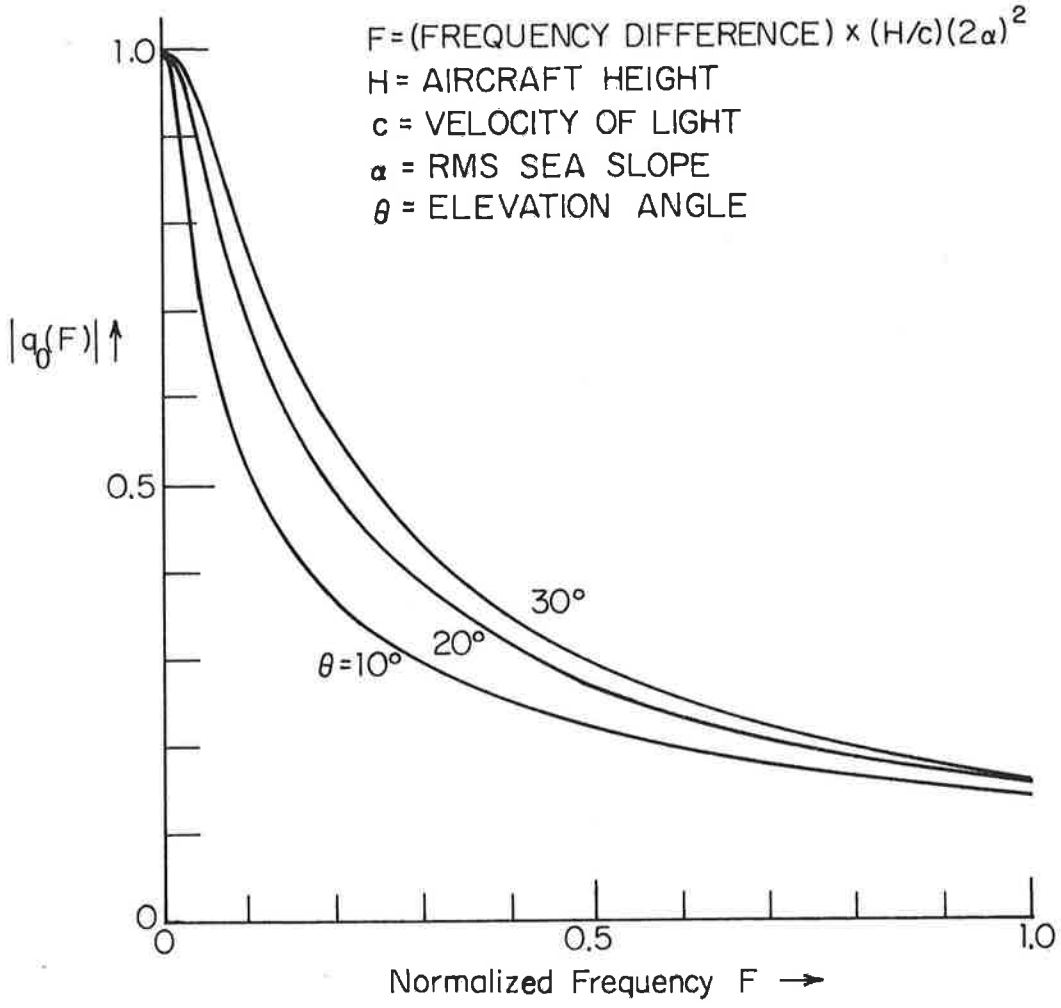

Figure 6.4(a) Magnitude of Frequency Correlation Function for Diffuse Scatter

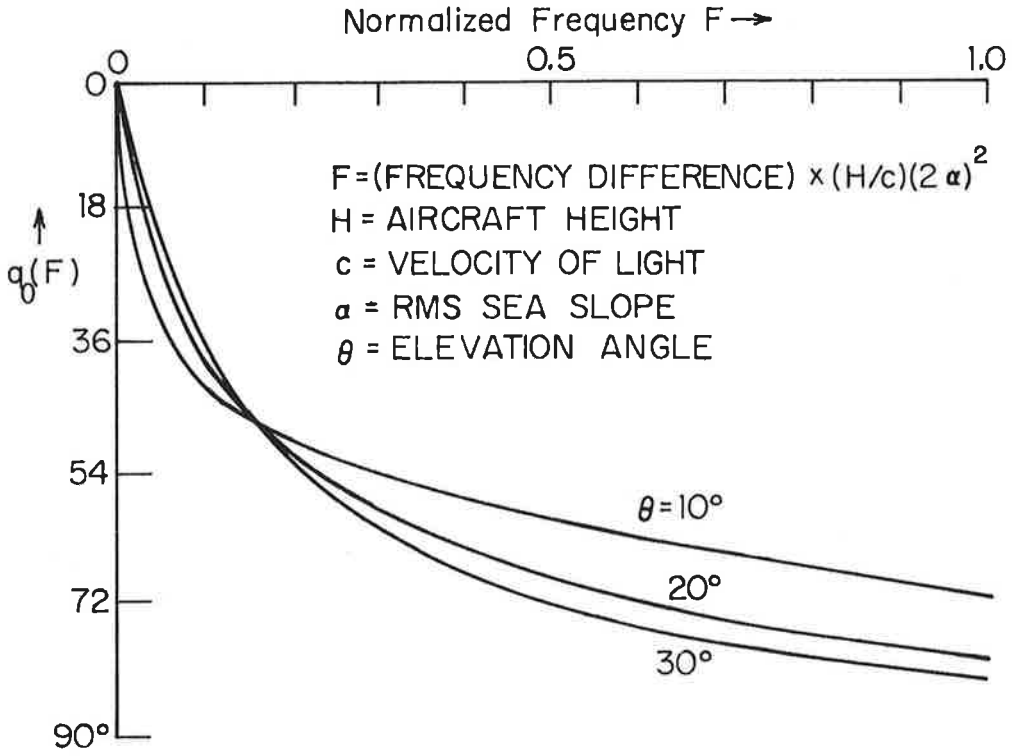

Figure 6.4 (b) Angle of Frequency Correlation Function for Diffuse Scatter

where ξ,ν are given in terms of the X,Y variables. It is convenient to deal with normalized variables

$$\delta = \frac{\xi}{4\alpha^2 H/c} \tag{6.29}$$

$$\omega = \frac{\nu}{2\alpha} \tag{6.30}$$

$$x = \frac{\sin^2\theta}{2\alpha}\left(\frac{X}{H} - \text{ctn }\theta\right) \tag{6.31}$$

$$y = \frac{1}{2\alpha} \cdot \frac{Y}{H} \tag{6.32}$$

The variables x,y are zero-mean Gaussian with unit variances. In terms of normalized variables, Eqs. (6.20) and (6.25) show that

$$\delta = \frac{\sin\theta}{2}\left(\frac{x^2}{\sin^2\theta} + y^2\right) \tag{6.33}$$

$$\omega = \nu_\theta x + \nu_y \sin\theta\, y \tag{6.34}$$

where

$$\nu_\beta = \frac{f_0}{c} V_\beta \tag{6.35}$$

is the Doppler shift as measured along an axis in the β direction (ν_θ is the Doppler shift $\nu_x \sin\theta + \nu_z \cos\theta$ corresponding to the velocity component in the x-z plane at right angles to the line-of-sight to the specular point).

Consistent with the normalizations (6.29), (6.30) we used the normalized shift variable

$$F = \Omega 4\alpha^2 H/c \tag{6.36}$$

$$T = \tau 2\alpha \tag{6.37}$$

Thus (6.28) becomes

$$R_0(F,T) = \overline{e^{-i2\pi F\delta} e^{i2\pi T\omega}} \tag{6.38}$$

If (6.33) is used in (6.38) it is trivial to show that

$$R_0(F,T) = q_0(F) \exp\left(-\frac{1}{2}(\pi T)^2\left[\frac{\nu_\theta^2}{1+i2\pi F/\sin\theta} + \frac{\nu_y^2 \sin^2\theta}{1+i2\pi F \sin\theta}\right]\right) \tag{6.39}$$

where

$$q_0(F) = \frac{1}{\sqrt{(1 + i2\pi F/\sin\theta)(1 + i2\pi F \sin\theta)}} \tag{6.40}$$

is the frequency correlation function for the normalized variable.

The Fourier transform of $R(\Omega,\tau)$ along the τ axis $P(\Omega,\nu)$ is the cross power spectral density between two received carriers separated by Ω Hz in frequency. This function is of direct interest in the evaluation of tone ranging systems where range

estimates depend upon the phase difference between filtered sidebands spaced in frequency. The Fourier transform is readily carried out to yield (in normalized variables)

$$P_0(F,\omega) = \sqrt{\frac{2}{H}} \frac{1}{\sqrt{\nu_\theta^2 + \nu_y^2 \sin^2\theta + i2\pi F \sin\theta(\nu_\theta^2 + \nu_y^2)}}$$

$$\exp\left[-2\omega^2\left(\frac{[1 + i2\pi F/\sin\theta][1 + i2\pi F \sin\theta]}{\nu_\theta^2 + \nu_y^2 \sin^2\theta + i2\pi F \sin\theta(\nu_\theta^2 + \nu_y^2)}\right)\right] \tag{6.41}$$

To obtain the scattering function one may Fourier transform $P_0(F,\omega)$ along the F axis or, more simply, regard δ,ω as new random variables related to the variables x,y, by (6.33) and (6.34). Note that for each pair δ,ω there can be as many as two pairs of x,y values $(x_1(\delta,\omega), y_1(\delta,\omega))$, $(x_2(\delta,\omega), y_2(\delta,\omega))$ which satisfy these equations. Since the Jacobian of this transformation is given by

$$J(\delta,\omega) = \frac{\partial x}{\partial \delta}\frac{\partial y}{\partial \omega} - \frac{\partial y}{\partial \delta}\frac{\partial x}{\partial \omega} \tag{6.42}$$

the density function $S_0(\delta,\omega)$ is given in terms of $W_0(x,y)$ the density function of x,y, by

$$S_0(\delta,\omega) = J(\delta,\omega)[W_0(x_1(\delta,\omega), y_1(\delta,\omega)) + W_0(x_2(\delta,\omega), y_2(\delta,\omega))] \tag{6.43}$$

We present the general expression for $S_0(\delta,\omega)$ in Appendix G. For the velocity vector in the XZ plane ($\nu_\theta \neq 0$, $\nu_y = 0$) one readily finds that

$$S_0(\delta,\omega) = \frac{1}{\pi\nu_\theta \sin\theta} \frac{1}{\sqrt{\frac{2\delta}{\sin\theta} - \frac{\omega^2}{\nu_\theta^2 \sin^2\theta}}} \exp\left(\frac{\omega^2}{2\nu_\theta^2 \tan^2\theta} - \frac{\delta}{\sin\theta}\right)$$

$$; \ \omega^2 < 2\delta \sin\theta \ \nu_\theta^2 \qquad (6.44)$$

For the velocity vector along the y axis $S_0(\delta,\omega)$ has the same form as (6.44) with ν_θ replaced by ν_y. For the general velocity vector it is rather more involved, as shown in Appendix G. Note that $S_0(\delta,\omega)$ in (6.44) vanishes for $\omega^2 > 2\delta\nu_\theta^2 \sin\theta$ and becomes infinite at $\omega^2 = 2\delta\nu_\theta^2 \sin\theta$. More generally, Appendix G shows that $S_0(\delta,\omega)$ vanishes for $\omega^2 > 2\delta(\nu_\theta^2 + \nu_y^2) \sin\theta$ and becomes infinite for $\omega^2 = 2\delta(\nu_\theta^2 + \nu_y^2) \sin\theta$. Expressions differing from (6.44) only by multiplicative constants and scale factors have been derived by Mallinckrodt [6.4], [6.5] for the velocity vector in the X or Y direction.

Channel correlation functions are particularly useful when they lead to a more complete statistical description of the channel as the case of the complex Gaussian WSSUS channel. To explain simply the conditions leading to Gaussian statistics (the discussion may be made rigorous) we note heuristically that a transmitted signal of bandwidth W cannot resolve path delays less than 1/W apart. The locus of surface scatterers causing channel path delays lying between ξ and $\xi + 1/W$ is an elliptical ring. If the surface area of the ring extends over

a large enough surface area to encompass many correlation lengths of the surface fluctuations, then, via Central Limit Theorem type arguments (and representation of the channel as a tapped delay line for a bandlimited signal [6.3], [6.10]), one may argue that the channel will act upon the input signal as if it were a Gaussian WSSUS channel. Moreover, as DeRosa has shown [6.9] when the surface is sufficiently rough to make the specular component negligible the symmetry conditions required for the complex Gaussian property are automatically satisfied. The maximum bandwidth required for the Gaussian WSSUS property to hold appears to be much bigger than needed in aeronautical communications, at least when the roughness condition is valid.

6.4 Conclusion

The analytic expressions for channel correlation functions presented above were derived under a restricted set of conditions:

a) one terminal so far from the earth that rays to the other terminal and glistening zone appear parallel

b) elevation angle to far-terminal $\theta \gg$ rms surface slope α

c) rough surface

d) small surface curvature for validity of Kirchoff method

e) no wave shadowing or multiple scattering effects.

Restrictions a), b), and c) can be eliminated by using more general scattering cross-section formula with more general geometry. But due to the complexity involved a computer

is needed to obtain channel correlation functions. The simplest general results may be obtained for the scattering function because it involves only the computation of the Jacobian of the transformation from surface coordinates to delay-Doppler coordinates. Such general results have been programmed by DeRosa [6.9].

Restrictions d) and e) cannot be readily relaxed by existing analytical approaches. Clearly at low enough grazing and elevation angles d) and e) will become violated. Unfortunately low grazing angles are of considersble interest because of the reduced multipath discrimination provided by the nominally hemispherical coverage antennas proposed for use on air-traffic control systems. Thus the need for channel characterization experiments is clearly indicated in order to gather necessary data for system design.

SECTION 6

REFERENCES

[6.1] P. Horn, et al., "Theoretical Study of Multipath Effects in an Aeronautical Satellite System," Final Report on Contract 1064/70CG (RFQ 1737), by Messerschmidt-Bialkow Blohm GMBH for European Space Research and Technology Centre, System Study Division, Noordwijk, Holland.

[6.2] P. Beckmann and A. Spizzichino, The Scattering of Electromagnetic Waves From Rough Surfaces, Pergamon Press, 1963.

[6.3] Bello, P. A., "Characterization of Random Time-Variant Linear Channels," IRE Trans. on Comm. Systems, Vol. CS-11, pp. 360-393, December 1963.

[6.4] A. J. Mallinckrodt, "Ground Multipath in Satellite-Aircraft Propagation," Paper Presented at the Symposium on Application of Atmospheric Studies to Satellite Transmissions, (sponsored by the Radio Astronomy Branch of the Ionospheric Physics Lab., AFCRL), Boston, September 1969.

[6.5] A. J. Mallinckrodt, "Propagation Errors," Notes for UCLA Short Course, Satellite Based Navigation Traffic Control and Communications to Mobile Terminals, September 14-25, 1970.

[6.6] H. Staras, "Rough Surface Scattering on a Communication Link," Radio Science, Vol. 3 (New Series), No. 6, June 1968, pp. 623-631.

[6.7] S. H. Durrani and H. Staras, "Multipath Problems in Communication Between Low-Altitude Spacecraft and Stationary Satellites," RCA Review, March 1968, pp. 77-105.

[6.8] J. K. DeRosa, "On the Determination of the Delay-Doppler Scattering Function for a Ground-to-Aircraft Link," 1970 Canadian Symposium on Communications, November 12-13, 1970.

[6.9] J. K. DeRosa, "The Characterization of Multipath and Doppler Fading in Earth Scatter Communication, Navigation and Radar Links," Doctorate Thesis at Northeastern University, Boston, Mass., June 1972. Paper in preparation.

[6.10] T. Kailath, "Sampling Models for Linear Time-Variant Filters," M.I.T. Research Lab. of Elec., Cambridge, Mass., Report No. 352, May 1959.

Appendix A

PROBABILITY DENSITY FUNCTION OF THE PHASE DIFFERENCE BETWEEN TWO CORRELATED NON-ZERO-MEAN COMPLEX GAUSSIAN VARIATES

In this section we derive a single integral expression for the probability density function of the phase difference between two correlated non-zero-mean complex Gaussian variates.

Our starting point is the joint density function of two zero-mean complex Gaussian variates z_1, z_2:

$$W_0(z_1, z_2) = \frac{\rho_1^2 \rho_2^2}{\pi^2 (1-r^2)} \exp\left[- \frac{\rho_1^2 |z_1|^2 + \rho_2^2 |z_2|^2 - 2\rho_1\rho_2 \, \mathrm{Re}(re^{j\beta} z_1 z_2^*)}{1-r^2} \right] \tag{A.1}$$

where

$$re^{j\beta} = \frac{\overline{z_1^* z_2}}{\sqrt{\overline{|z_1|^2}\;\overline{|z_2|^2}}} \tag{A.2}$$

is the complex correlation coefficient between the complex Gaussian variates and

$$\overline{|z_1|^2} = 1/\sigma_1^2 \tag{A.3}$$

$$\overline{|z_2|^2} = 1/\sigma_2^2 \tag{A.4}$$

are the average magnitude squared.

The joint density function for non-zero mean complex Gaussian variates, z_1, z_2, is obtained from (A.1) by replacing z_k by $z_k-\alpha_k$; k = 1,2 where the generally complex α_k is the mean of z_k. Since we allow the fluctuating parts of z_1, z_2 to have different strengths and arbitrary correlation coefficients, no loss in generality results in our analysis by letting $\alpha_k = 1$. Thus

$$W_1(z_1, z_2) = \frac{\rho_1\rho_2^2}{\pi^2(1-r^2)} \exp\left[-\frac{\rho_1^2|z_1-1|^2+\rho_2^2|z_2-1|^2 - 2\rho_1\rho_2 \operatorname{Re}\{re^{j\beta}(z_1-1)(z_2^*-1)\}}{1-r^2}\right] \tag{A.5}$$

Note that with the normalization to unit mean value, the quantities ρ_1^2, ρ_2^2 become signal-to-noise ratios.

To obtain the joint density function of the phases and amplitudes, $W(R_1, R_2, \phi_1, \phi_2)$, where

$$z_k = R_k e^{j\phi_k} \quad ; \quad k = 1, 2 \tag{A.6}$$

we change from rectangular to polar coordinates and find that

$$W(R_1, R_2, \phi_1, \phi_2) = R_1R_2W_1(R_1e^{j\phi_1}, R_2e^{j\phi_2}) \tag{A.7}$$

Using this transformation and the further transformation

$$\psi = \phi_2 - \phi_1$$

$$\phi_1 = \varphi \tag{A.8}$$

where ψ is the phase difference of interest to this analysis.

$$W_2(R_1, R_2, \phi, \psi) = \frac{\rho_1^2 \rho_2^2 R_1 R_2}{\pi^2 (1-r^2)} \exp\left(-\frac{\rho_1^2 + \rho_2^2 - 2\rho_1\rho_2 r \cos\beta}{1-r^2}\right) x$$

$$\exp\left[-\frac{1}{1-r^2}\left(\rho_1^2 R_1^2 + \rho_2^2 R_2^2 - 2\rho_1\rho_2 R_1 R_2 r \cos(\psi-\beta)\right)\right] x \tag{A.9}$$

$$\exp\left[\frac{2}{1-r^2}\left|[\rho_1^2 - \rho_1\rho_2 r e^{j\beta}]R_1 + [\rho_2^2 - \rho_1\rho_2 r e^{-j\beta}]R_2 e^{j\psi}\right|\cos(\phi + \delta)\right]$$

where

$$\delta = \measuredangle\left[(\rho_1^2 - \rho_1\rho_2 r e^{j\beta})R_1 + (\rho_2^2 - \rho_1\rho_2 r e^{-j\beta})R_2 e^{j\psi}\right] \tag{A.10}$$

Note that ϕ appears only in the last exponential in (A.9). With the aid of the integral

$$\frac{1}{2\pi}\int_{-\pi}^{\pi} e^{A\cos(\phi+B)}\,d\theta = I_0(A) \qquad (A.11)$$

where $I_0(\cdot)$ is a modified Bessel function, we find that we can carry out the integration

$$W(R_1, R_2, \psi) = \int W_2(R_1, R_2, \phi, \psi)\,d\phi \qquad (A.12)$$

which yields

$$W(R_1, R_2, \psi) = \frac{2\rho_1^2\rho_2^2 R_1 R_2}{\pi(1-r^2)} \exp\left(-\frac{\rho_1^2+\rho_2^2-2\rho_1\rho_2 r\cos\beta}{1-r^2}\right) x$$

$$\exp\left[-\frac{1}{1-r^2}(\rho_1^2R_1^2+\rho_2^2R_2^2-2\rho_1\rho_2R_1R_2r\cos(\psi-\beta))\right]$$

$$I_0\left[\frac{2}{1-r^2}\left|[\rho_1^2-\rho_1\rho_2\,re^{j\beta}]R_1+[\rho_2^2-\rho_1\rho_2\,re^{-j\beta}]R_2e^{j\psi}\right|\right] \qquad (A.13)$$

The density function of ψ, $W(\psi)$, may be represented as the double integral

$$W(\psi) = \int_0^\infty\int_0^\infty W(R_1, R_2, \psi)dR_1dR_2 \qquad (A.14)$$

Using (A.13) in (A.14) and making the change of variables

$$\rho_1 R_1 = W \cos\theta \tag{A.15}$$

$$\rho_2 R_2 = W \sin\theta \tag{A.16}$$

we find that

$$W(\psi) = \frac{1}{\pi(1-r^2)} \exp\left(-\frac{\rho_1^2 + \rho_2^2 - 2\rho_1\rho_2 r\cos\beta}{1-r^2}\right) x \tag{A.17}$$

$$\int_0^{\pi/2} \sin 2\theta \int_0^{\infty} W^3 I_0(2W\sqrt{\alpha}) e^{-pW^2}\, dW\, d\theta$$

where

$$\alpha(\theta,\psi;r,\beta,\rho_1,\rho_2) = \frac{1}{[1-r^2]^2} \left|(\rho_1 - \rho_2 re^{j\beta})\cos\theta + (\rho_2 - \rho_1 re^{-j\beta})\sin\theta \cdot e^{j\psi}\right|^2$$

(A.18)

$$p(\theta,\psi;r,\beta) = \frac{1}{1-r^2}\,(1 - r\sin 2\theta\cos(\psi-\beta))$$

The integral over W can be expressed in an alternate form by an obvious change of variable

$$\int_0^\infty W^3 I_0(2W\sqrt{\alpha})e^{-pW^2}\,dW$$

$$= \frac{1}{2}\int_0^\infty t\, I_0(2\sqrt{t\alpha})e^{-pt}\,dt \qquad (A.19)$$

From [8], p. 197,

$$\int_0^\infty t I_0(2\sqrt{t\alpha})e^{-pt}\,dt = \frac{1}{p}\,e^{\alpha/p} \qquad (A.20)$$

By differentiating (A.16) we find the pair

$$\frac{1}{2}\int_0^\infty t\, I_0(2\sqrt{t\alpha})e^{-pt}\,dt = \frac{-d}{dp}\left(\frac{1}{p}\,e^{\alpha/p}\right)\frac{1}{2} = \frac{1+\alpha/p}{2p^2}e^{\alpha/p} \qquad (A.21)$$

$$W(\psi;r,\beta,\rho_1,\rho_2) = \frac{1}{1-r^2}\exp\left(-\frac{\rho_1^2+\rho_2^2-2\rho_1\rho_2 r\cos\beta}{1-r^2}\right) x$$

$$\frac{1}{2\pi}\int_0^{\pi/2} \sin 2\theta\,\frac{1+\alpha(\theta,\cdot)/p(\theta,\cdot)}{p^2(\theta,\cdot)}\exp\left(\frac{\alpha(\theta,\cdot)}{p(\theta,\cdot)}\right)d\theta \qquad (A.22)$$

Consider some special cases. When the correlation coefficient is real, $\beta=0$, and the SNR's are equal, $\rho_1=\rho_2=\rho$.

$$\alpha(\theta,\psi;r,0,\rho_1,\rho) = \frac{\rho(1-r)}{[1-r^2]^2}\,(1+\sin 2\theta\cos\psi) \tag{A.23}$$

$$p(\theta,\psi;r,0) = \frac{1}{1-r^2}\,(1-r\sin 2\theta\cos\psi) \tag{A.24}$$

When the correlation coefficient vanishes

$$\alpha(\theta,\psi;0,0,\rho_1,\rho_2) = \rho_1^2\cos^2\theta+\rho_2^2\sin^2\theta+\rho_1\rho_2\sin 2\theta\cos\psi \tag{A.25}$$

$$\rho(\theta,\psi;0,0) = 1$$

Appendix B

OPEN LOOP ERROR VOLTAGES OF A PN RANGING RECEIVER

In this appendix we derive the open-loop response of the carrier and code loops of the PN receiver model. The channel model of Fig. 3.1 is assumed. We denote the open-loop error voltage of the carrier loop as $F(t_e,\theta_e)$ and that of the code loop as $G(t_e,\theta_e)$ where t_e and θ_e are the timing and phase errors, respectively, of the receiver measured relative to the direct path signal.

The channel and relevant elements of the code loop are shown in Fig. B.1a. The time constant of the receiver bandpass filter $H_{BP}(f)$ will be much shorter than the rate of fading of the time-varying channel represented by $T(f,t)$. As a result, the order of these operations may be reversed, as shown in Fig. B.1b. We use the notation $r(t)$ for the output of the bandpass filter $H_{BP}(f)$ when its input is $x(t)$.

In calculating $G(t_e,\theta_e)$ we consider first the component due to the direct path. In general, if the input complex envelopes to a mixer are $z_1(t)$ and $z_2(t)$, the real low-pass output waveform will be $\frac{1}{2}\,\mathrm{Re}\{z_1(t)z_2^*(t)\}$. In this case the envelopes are $r(t)$ and $y(t-t_e)e^{j\theta_e}$, so the mixer output is

$$\frac{1}{2}\, r(t)y(t-t_e)\cos\theta_e \tag{B.1}$$

The waveform $r(t)y(t-t_e)$ consists of a discrete d-c component and time-varying components whose bandwidth is on the order of the bandwidth of $r(t)$ and $y(t)$. The latter will not be passed by the low-pass filter $H_L(f)$, so we may write the direct-path

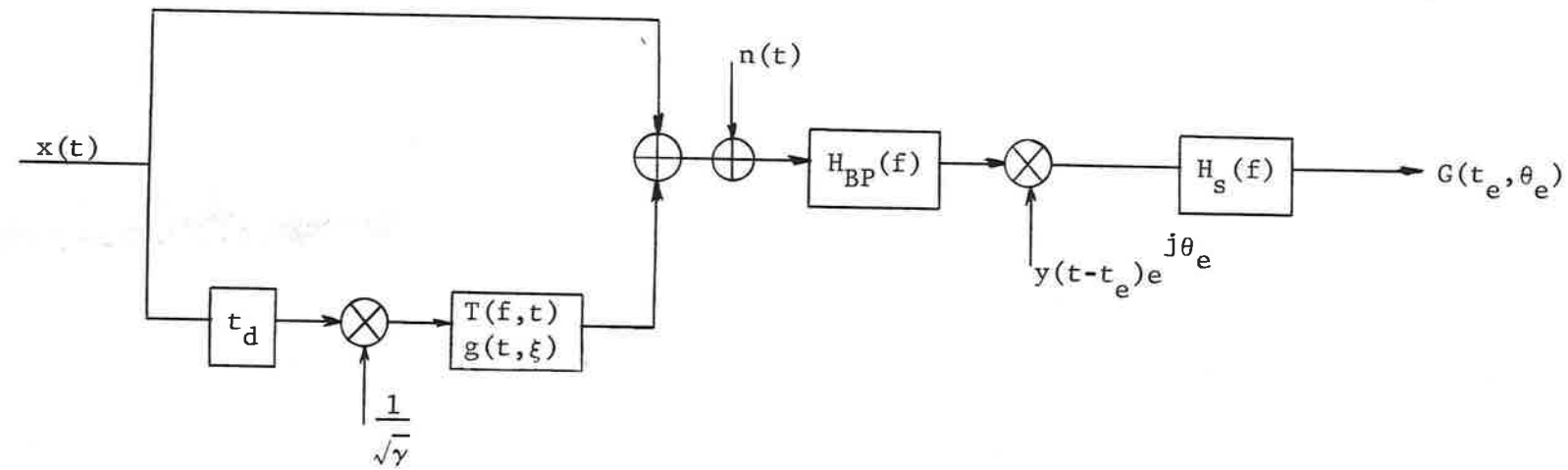

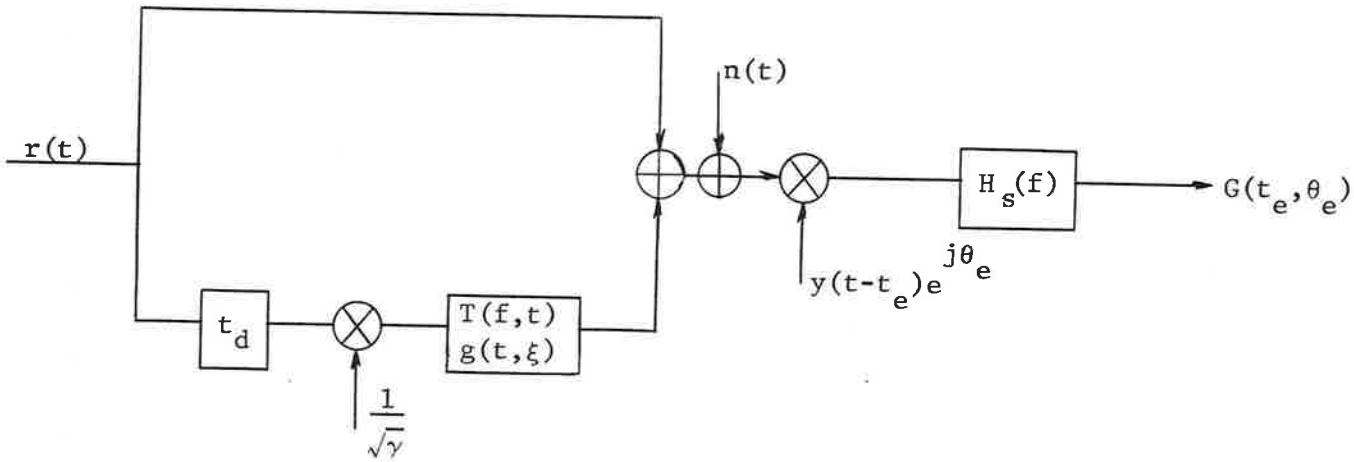

Figure B-1. Relevant to Open Loop Characteristics of PN Ranging Receiver

contribution to $G(t_e,\theta_e)$ as the d-c component of (B.1):

$$\frac{1}{2} S(t_e) \cos \theta_e \tag{B.2}$$

where we have defined the code loop error characteristic $S(t_e)$ by

$$S(t_e) = \int r(t)y(t-t_e)\, dt \tag{B.3}$$

Next we consider the contribution to $G(t_e,\theta_e)$ resulting from the scatter path. The channel input to the mixer is given by

$$\frac{1}{\sqrt{\gamma}} \int r(t-t_d-\xi)g(t,\xi)\, d\xi \tag{B.4}$$

and the mixer output is given by

$$\frac{1}{2\sqrt{\gamma}} \mathrm{Re}\{e^{-j\theta_e} y(t-t_e) \int r(t-t_d-\xi)g(t-\xi)\, d\xi\}. \tag{B.5}$$

Now we may move $y(t-t_e)$ inside the integral and replace the product $y(t-t_e)r(t-t_d-\xi)$ by its d-c component, as was done above. Thus the low-pass filter input may be written as

$$\frac{1}{2\sqrt{\gamma}} \mathrm{Re}\{e^{-j\theta_e} w_i(t)\} \tag{B.6}$$

where

$$w_i(t) = \int S(t_e-t_d-\xi)g(t-\xi)\, d\xi \tag{B.7}$$

Due to the assumed Gaussian nature of the channel, $w_i(t)$ will be a complex Gaussian random process; its auto-correlation is given by

$$\overline{w_i^*(t)w_i(t+\tau)} = \int S^2(t_e-t_d-\xi)Q(\tau,\xi)\, d\xi \qquad \text{(B.8)}$$

where use has been made of the fact that for a WSSUS channel

$$\overline{g^*(t,\xi)g(t+\tau,\eta)} = Q(\tau,\xi)\delta(\eta-\xi) \qquad \text{(B.9)}$$

The Fourier transform of the tap gain correlation function $Q(\tau,\xi)$ with respect to the τ variable is the scattering function $S(\xi,\nu)$. Therefore the power spectral density of $w_i(t)$ is

$$\int S^2(t_e-t_d-\xi)S(\xi,\nu)\, d\xi \qquad \text{(B.10)}$$

Now we define the low-pass filter output in terms of another complex Gaussian $w_o(t)$ by

$$\frac{1}{2\sqrt{\gamma}} \mathrm{Re}\{e^{-j\theta} w_o(t)\} \qquad \text{(B.11)}$$

Then the power spectral density of $w_o(t)$ is obtained by multiplying (B.10) by $|H_s(\nu)|^2$:

$$|H_s(\nu)|^2 \int S^2(t_e-t_d-\xi)S(\xi,\nu)\, d\xi \qquad \text{(B.12)}$$

Finally, the mean-square value of $w_o(t)$ is given by $\tilde{S}^2(t_e-t_d)$ where

$$\tilde{S}^2(t) \equiv \iint |H_s(\nu)|^2 S^2(t-\xi)S(\xi,\nu)\, d\xi\, d\nu \qquad (B.13)$$

The function $\tilde{S}(t)$ may be regarded as an average code loop error characteristic for the channel-perturbed signal. Now we may write the direct and scatter path contributions to the open-loop error voltage as

$$G(t_e,\theta_e) = S(t_e)\cos\theta_e + \frac{1}{\sqrt{\gamma}}\tilde{S}(t_e-t_d)\,\mathrm{Re}\{z_s(t)e^{-j\theta_e}\} \qquad (B.14)$$

In this expression $z_s(t)$ is a complex Gaussian process normalized to have unit mean-square, and a factor of 1/2 common to both terms on the right-hand side has been dropped.

The third contribution to the open-loop error voltage is that due to the additive noise. The noise term in the input to the mixer is the result of passing n(t) through the bandpass filter $h_{BP}(t)$:

$$\int h_{BP}(\tau)n(t-\tau)\, d\tau \qquad (B.15)$$

Thus the mixer output/filter input due to the additive noise is given by

$$\frac{1}{2}\,\mathrm{Re}\{e^{-j\theta_e}y(t-t_e)\int h_{BP}(\tau)n(t-\tau)\, d\tau\} \qquad (B.16)$$

Which we may write, as before, in the form

$$\frac{1}{2} \text{Re} \{e^{-j\theta_e} w_i(t)\} \tag{B.17}$$

where

$$w_i(t) = y(t-t_e) \int h_{BP}(\tau) n(t-\tau) \, d\tau \tag{B.18}$$

The autocorrelation of $w_i(t)$ is given by

$$\overline{w_i^*(t) w_i(t+\tau)} = \overline{y(t) y(t+\tau)} \left(\frac{N_o}{2}\right) \int h_{BP}^*(\lambda) h_{BP}(\lambda+\tau) \, d\lambda \tag{B.19}$$

Making use of the relationship $N_o/2 = 1/4\rho R$ this becomes

$$w_i^*(t) w_1(t+\tau) = \frac{R_y(\tau)}{4\rho R} \int h_{BP}^*(\lambda) h_{BP}(\lambda+\tau) \, d\lambda \tag{B.20}$$

where $R_y(\tau)$ is the autocorrelation of the waveform $y(t)$. Alternately, we may write the spectrum of $w_i(t)$ as

$$S_{w_i}(f) = \frac{1}{4\rho R} S_y(f) \otimes |H_{BP}(f)|^2 \tag{B.21}$$

where $S_y(f)$ is the power spectrum of $y(t)$.

The variable $w_i(t)$ will have a Gaussian distribution at any instant, but $w_i(t)$ is not a Gaussian process, due to the multiplication by $y(t-t_e)$. Therefore we cannot, in general,

state what the statistics of the filter output due to the additive noise will be. However, $w_o(t)$ will be zero-mean with spectrum given by

$$S_{w_o}(f) = |H_s(f)|^2 S_{w_i}(f) \tag{B.22}$$

Because the bandwidth of $H_s(f)$ is small relative to its input, we may replace $S_{w_i}(f)$ by its dc value, giving

$$S_{w_i}(f) = \frac{|H_s(f)|^2}{4\rho R} \left(S_y(f) \otimes |H_{BP}(f)|^2\right)\Big|_{f=0} \tag{B.23}$$

Therefore the variance of the filter output is given by

$$\overline{w_0^2(t)} = \frac{1}{4\rho R} S_y(f) \otimes |H_{BP}(f)|^2\Big|_{f=0} \int |H_s(f)|^2 \, df \tag{B.24}$$

Thus we may write the complete open-loop error voltage as

$$G(t_e,\theta_e) = S(t_e) \cos \theta_e + \frac{1}{\sqrt{\gamma}} \tilde{S}(t_e - t_d) \mathrm{Re}\{Z_s(t) e^{-j\theta_e}\}$$

$$+ \frac{1}{2} \sqrt{\frac{UB_{Ns}}{2\rho R}} n_s(t) \tag{B.25}$$

where the noise term $n_s(t)$ has unit variance, B_{Ns} stands for the noise bandwidth of the code loop

$$B_{Ns} = \int |H_s(f)|^2 \, df \tag{B.26}$$

and U is given by

$$U = S_y(f) \otimes |H_{BP}(f)|^2|_{f=0} \tag{B.27}$$

A completely parallel analysis can be made of the carrier loop. In this case the local input to the coherent detector is $x(t-t_e)e^{j\theta_e - \pi/2}$ and the relevant loop error characteristic is

$$R(t_e) = \int r(t)x(t-t_e) \, dt \tag{B.28}$$

Accordingly, the final result is

$$F(t_e,\theta_e) = R(t_e) \sin \theta_e + \frac{1}{\sqrt{\gamma}} \tilde{R}(t_e-t_d) \, \mathrm{Re}\{z_r(t)e^{-j(\theta_e-\pi/2)}\}$$

$$+ \frac{1}{2} \sqrt{\frac{TB_{Nr}}{2\rho R}} \, n_r(t) \tag{B.29}$$

Here we have defined an average carrier loop error characteristic for the channel-perturbed signal as

$$\tilde{R}^2(t) \equiv \iint |H_r(\nu)|^2 R^2(t-\xi) S(\xi,\nu) \, d\xi \, d\nu \tag{B.30}$$

and $z_r(t)$ is a complex Gaussian with unit mean-square absolute value. In general, the processes $z_r(t)$ and $z_s(t)$ are correlated; at any instant the cross correlation is given by

$$\rho_{rs} = \overline{z_r^*(t) z_s(t)}$$

$$= \frac{\iint S(t_e - t_d - \xi) R(t_e - t_d - \xi) S(\xi, \nu) H_r^*(\nu) H_s(\nu) \, d\xi \, d\nu}{\sqrt{\iint S^2(t_e - t_d - \xi) S(\xi, \nu) |H_s(\nu)|^2 d\xi \, d\nu \iint R^2(t_e - t_d - \xi) S(\xi, \nu) |H_r(\nu)|^2 d\xi \, d\nu}}$$

(B.31)

In writing the additive noise term, the following notation is used

$$B_{Nr} = \int |H_r(f)|^2 \, df \tag{B.32}$$

and

$$T = S_x(f) \otimes |H_{BP}(f)|^2 \Big|_{f=0} \tag{B.33}$$

where $S_x(f)$ is the power density spectrum of the waveform $x(t)$. The noise term $n_r(t)$ has unit variance and is uncorrelated with $n_s(t)$; that is,

$$\overline{n_r(t) n_s(t)} = 0 \tag{B.34}$$

Appendix C

ASYMPTOTIC SOLUTION OF THE LOOP TRACKING EQUATIONS OF A PN RECEIVER

In this appendix we consider the solution of the loop tracking equations in the high direct to scatter ratio case. The equations to be solved are,

$$F(t_e,\theta_e) = 0 \tag{C.1}$$

and

$$G(t_e,\theta_e) = 0 \tag{C.2}$$

where

$$F(t_e,\theta_e) = R(t_e) \sin \theta_e + \alpha_r \tilde{R}(t_e-t_d) \sin (\theta_e-\theta_r) + \beta_r \tag{C.3}$$

$$G(t_e,\theta_e) = S(t_e) \cos \theta_e + \alpha_s \tilde{S}(t_e-t_d) \cos (\theta_e-\theta_s) + \beta_s \tag{C.4}$$

In these equations the amplitudes α_r and α_s and phases θ_r and θ_s will represent the instantaneous values produced by a slowly varying scatter component. However, the solution to be obtained applies also to the case of a fixed multipath component in the sense that the absolute error is small. In the latter case the channel-perturbed error characteristics $\tilde{R}(t)$ and $\tilde{S}(t)$ would be replaced by the corresponding fixed-path characteristics $R(t)$ and $S(t)$. In either case we will assume that α_r and α_s are small compared to unity. Furthermore, we will assume that the additive noise contributions β_r and β_s will be small compared to unity. Due to the small values of t_e and θ_e which result, we may make the following approximations

$$\sin(\theta_e - \theta) \doteq -\sin\theta + \theta_e \cos\theta \tag{C.5}$$

$$\cos(\theta_e - \theta) \doteq \cos\theta + \theta_e \sin\theta \tag{C.6}$$

$$R(t_e) \doteq R(0) \tag{C.7}$$

$$S(t_e) \doteq t_e S'(0) \tag{C.8}$$

$$\tilde{R}(t_e - t_d) \doteq \tilde{R}(t_d) \tag{C.9}$$

$$\tilde{S}(t_e - t_d) \doteq -\tilde{S}(t_d) \tag{C.10}$$

(We have assumed that $R(t)$ and $\tilde{R}(t)$ are even functions while $S(t)$ and $\tilde{S}(t)$ are odd functions.) With these approximations Eqs. (C.3) and (C.4) become

$$F(t_e,\theta_e) \doteq R(0)\theta_e + \alpha_r \tilde{R}(t_d)[-\sin\theta_r + \theta_e \cos\theta_r] + \beta_r \tag{C.11}$$

$$G(t_e,\theta_e) \doteq t_e S'(0) - \alpha_s \tilde{S}(t_d)[\cos\theta_s + \theta_e \sin\theta_s] + \beta_s \tag{C.12}$$

We first consider the solution of Eq. (C.2) when $\cos\theta_s$ is not small; in that case the second term in the bracket of Eq. (C.12) may be neglected, giving

$$t_e \doteq \alpha \frac{\tilde{S}(t_d)}{S'(0)} \cos\theta_s - \frac{\beta_s}{S'(0)} \qquad \cos\theta_s \neq 0 \tag{C.13}$$

As noted, the approach applies only when $\cos \theta_s$ does not vanish. We consider this special case by setting $\cos \theta_s$ equal to zero in Eq. (C.12) and solving (C.2):

$$t_e \doteq \pm \alpha_s \theta_e \frac{\tilde{S}(t_d)}{S'(0)} - \frac{\beta_s}{S'(0)} \quad , \quad \cos \theta_s = 0 \qquad (C.14)$$

The first term of this result will be second-order due to the product of two small quantities α_s and θ_e. Therefore Eq. (C.13) holds approximately for all values of θ_s.

A similar analysis may be performed to show that the phase error θ_e is given by

$$\theta_e \doteq \alpha_r \frac{\tilde{R}(t_d)}{R(0)} \sin \theta_r - \frac{\beta_r}{R(0)} \qquad (C.15)$$

Appendix D

FLAT FADING SOLUTION OF THE TRACKING EQUATIONS OF A PN RECEIVER

D.1 Introduction

In the flat fading case the open loop error voltages for carrier and code tracking loops are

$$F(t_e,\theta_e) = R(t_e)\sin\theta_e + \alpha R(t_e-t_d)\sin(\theta_e-\theta_m) \qquad (D.1)$$

$$G(t_e,\theta_e) = S(t_e)\cos\theta_e + \alpha S(t_e-t_d)\cos(\theta_e-\theta_m) \qquad (D.2)$$

When both loops are locked both of these voltages may be considered zero. Thus, a solution of the simultaneous transcendental equations

$$F(t_e,\theta_e) = 0 \qquad (D.3)$$

$$G(t_e,\theta_e) = 0 \qquad (D.4)$$

gives a set of values (t_e^*,θ_e^*) for which both loops will be in lock. The stability of the loops will depend on the sign of the open-loop error voltage for small changes in the controlled parameter. Thus the stability of the carrier loop will be determined by the sign of

$$\left.\frac{\partial F(t_e,\theta_e)}{\partial\theta_e}\right|_{(t_e^*,\theta_e^*)} \qquad (D.5)$$

and the stability of the code loop will be determined by the sign of

$$\left.\frac{\partial G(t_e,\theta_e)}{\partial t_e}\right|_{(t_e^*\theta_e^*)} \tag{D.6}$$

The designation of which sign corresponds to stability is essentially a matter of convention. Consider the carrier loop in the absence of multipath; to preserve the meaning of θ_e we wish the stable point to be $\theta_e=0$ rather than $\theta_e=\pi$. This is accomplished by establishing the following condition for stability:

$$\left.\frac{\partial F(t_e,\theta_e)}{\partial \theta_e}\right|_{(t_e^*,\theta_e^*)} > 0 \tag{D.7}$$

The same reasoning may be applied to the code tracking loop; we will assume that the split-gate waveform consists of a positive pulse followed by a negative pulse so that $S'(0) < 0$. As a consequence the condition for stability of this loop is

$$\left.\frac{\partial G(t_e,\theta_e)}{\partial t_e}\right|_{(t_e^*,\theta_e^*)} < 0 \tag{D.8}$$

In this appendix we will consider numerical solutions to Eqs. (D.3) and (D.4) when $F(t_e,\theta_e)$ and $G(t_e,\theta_e)$ are given by Eqs. (D.1) and (D.2). We will take the point of view that θ_m is slowly varying with time. The rate of this variation

will be such that the two receiver loops track the received signal without loss of lock. Thus a continuous sequence of solutions to Eqs. (D.3) and (D.4) for values of θ_m between 0 and 2π is required.

In Solving Eqs. (D.3) and (D.4) we will use the correlation functions R(t) and S(t) derived in Section D.4. These assume that the local code and the output of the split-pulse generator are unfiltered, while the received sequence has passed through a Gaussian filter having an rf bandwidth equal to 1.5 times the chip rate.

D.2 Solutions in the Fixed Phase Case

In this section we examine tracking behavior when the two received signals have a fixed phase relationship; two cases are considered: $\theta_m=0$ and $\theta_m=\pi$. A detailed study of these cases will be useful later on, when solutions for other values of θ_m are required, as well as offering insight into loop behavior.

Substituting the value $\theta_m=0$ into Eqs. (D.1) and (D.2) gives

$$F(t_e,\theta_e) = [R(t_e) + \alpha R(t_e-t_d)] \sin \theta_e \qquad (D.9)$$

and

$$G(t_e,\theta_e) = [S(t_e) + \alpha S(t_e-t_d)] \cos \theta_e \qquad (D.10)$$

For the assumed Gaussian filter R(t) is positive (see Fig. D.7) for all values of t; therefore the only solutions to the equation $F(t_e,\theta_e) = 0$ are $\theta_e=0$ or $\theta_e=\pi$. The latter may be eliminated by taking the derivative of Eq. (D.9) with respect to θ_e and comparing with Eq. (D.7). Thus the only value of θ_e at which the carrier loop will track is

$$\theta_e^* = 0 \tag{D.11}$$

Substituting this result into Eq. (D.10) gives the open-loop error voltage of the code tracking loop:

$$G(t_e,0) = S(t_e) + \alpha S(t_e-t_d) \tag{D.12}$$

The stable tracking point(s) of the code loop will be given by the zero(s) of this function. From Fig. D.8 it is clear that the initial non-zero values assumed by S(t) are positive and that the final non-zero values are negative. The same must then be true of $G(t_e,0)$ as given by Eq. (D.12). As a direct consequence of this, the number of zeroes of $G(t_e,0)$ will be odd. Experience with the particular S(t) assumed indicates that only two cases actually occur.

1. One zero crossing with negative slope (stable)
2. Three zero crossings; two with negative slope (stable), separated by one with positive slope (unstable).

Whether case 1 or case 2 actually occurs is determined by the values of the parameters α and t_d. Graphs of $S(t_e,0)$ for two parameter choices which result in the two cases are shown in

Figs. D.1 and D.2. The first case is that of a relatively short delay (t_d = 0.5 bits) with the result that the correlation functions of the two paths overlap; the timing of the local sequence falls somewhere between the two received sequences. In Fig. D.2 the arrival times are separated enough (t_d = 1.2 bits) that it is possible for the receiver to track either of the received signals (with a small error due to the presence of the other). This tracking behavior may be summarized by plotting the code loop error t_e as a function of multipath delay, as in Fig. D.3. Note that for $t_m < 1.2$ bits only one stable tracking point exists, while for $t_m > 1.2$ bits two such points exist.

A similar analysis may be performed for the other fixed-phase case: $\theta_m = \pi$. In this case it can be shown that tracking points are related to the zeroes of the function

$$S(t_e) - \alpha S(t_e - t_d) \tag{D.13}$$

Two values of θ_e are possible, 0 and π. In the first case, the derivatives determining the stability of the tracking point are given by

$$\frac{\partial F}{\partial \theta_e} = R(t_e) - \alpha R(t_e - t_d) \tag{D.14}$$

and

$$\frac{\partial G}{\partial t_e} = S'(t_e) - \alpha S'(t_e - t_d) \tag{D.15}$$

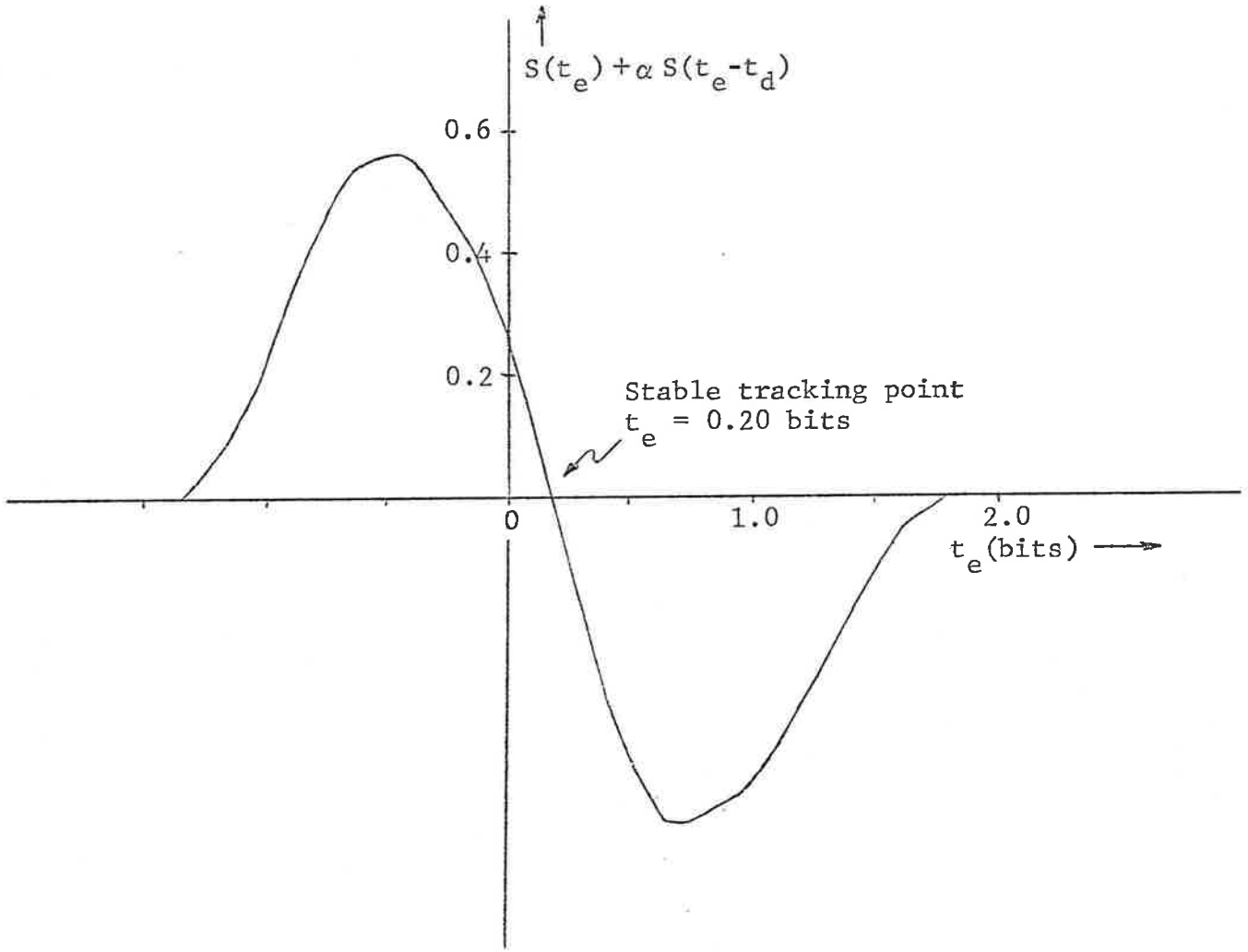

Figure D.1 Open Loop Error Voltage, α=0.7, t_d=1.2 bits, θ_m=0

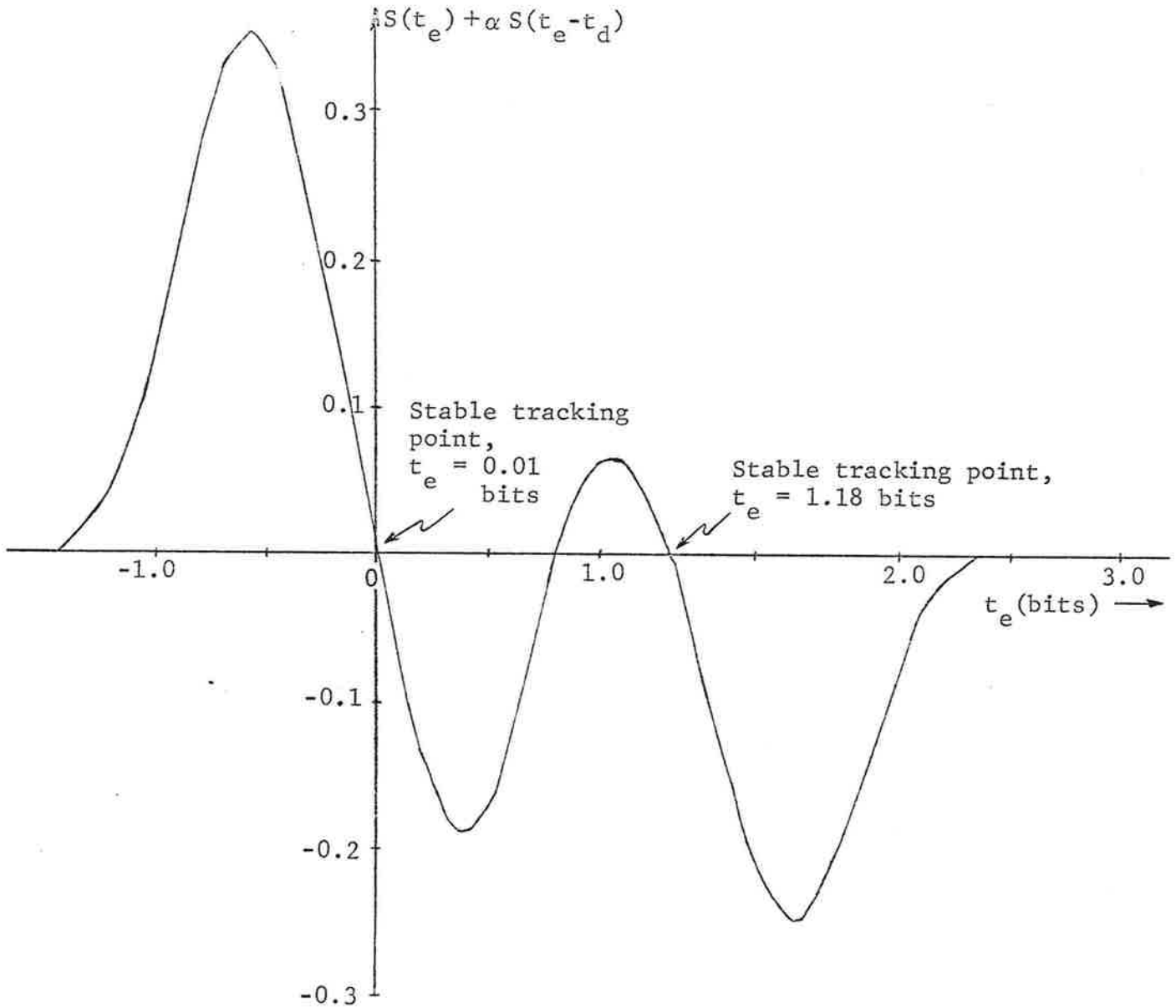

Figure D.2 Open Loop Error Voltage, α=0.7, t_d = 1.2 bits, θ_m=0

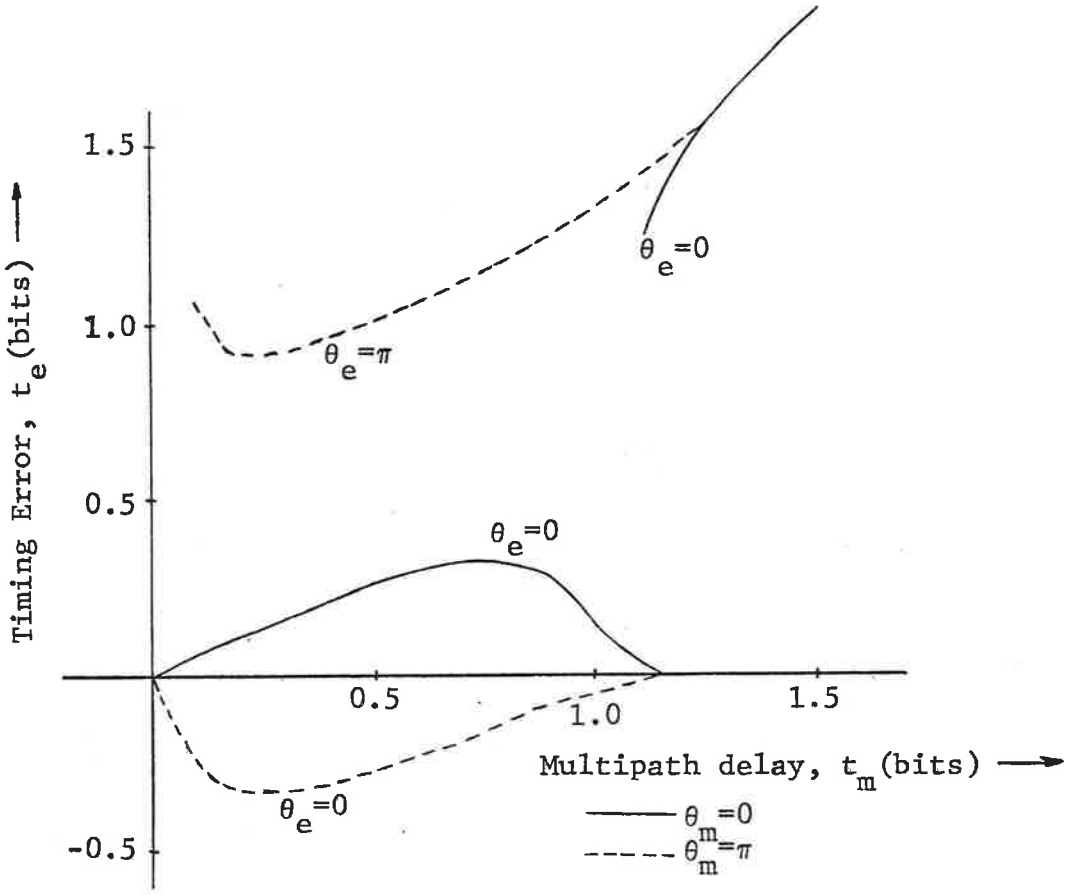

Figure D.3 Code Loop Tracking Error as a Function of Multipath Delay, for Fixed Multipath Phase (α=0.7)

In the second case, these derivatives are given by the same expressions with signs reversed. Experience with examples indicates that for most values of t_e, two stable tracking points exist, one with $\theta_e=0$ and another with $\theta_e=\pi$, as shown in Fig. D.4. The first value of θ_e is associated with negative values of t_e and the second with larger positive values of t_e. As t_d is increased and the correlation functions separate, the value of t_e corresponding to $\theta_e=0$ becomes zero (perfect tracking of the first signal) and the value of t_e corresponding to $\theta_e=\pi$ becomes equal to t_d (perfect tracking of the second signal). The behavior of these solutions as a function of t_e is also shown in Fig. D.3.

D.3 Solutions for Varying Phase

As discussed earlier, an actual receiver will encounter slowly varying phases, rather than fixed phases, as analyzed in the preceding section. If we assume that this variation is slow compared to the time constants of the loops involved, this implies timing and phase error functions

$$t_e(\theta_m) \quad \text{and} \quad \theta_e(\theta_m) \qquad 0 \leq \theta_m \leq 2\pi \tag{D.16}$$

which are periodic in θ_m, and which represent solutions to Eqs. (D.3) and (D.4) for all values of θ_m. In this section we numerically calculate such functions by means of the Newton-Raphson technique for solving simultaneous equations. It should be emphasized that this is not equivalent to simulating the exact loop behavior since it does not consider the loop dynamics. Thus consideration should be given to signal dynamics vis-a-vis loop bandwidths before applying these or subsequent results.

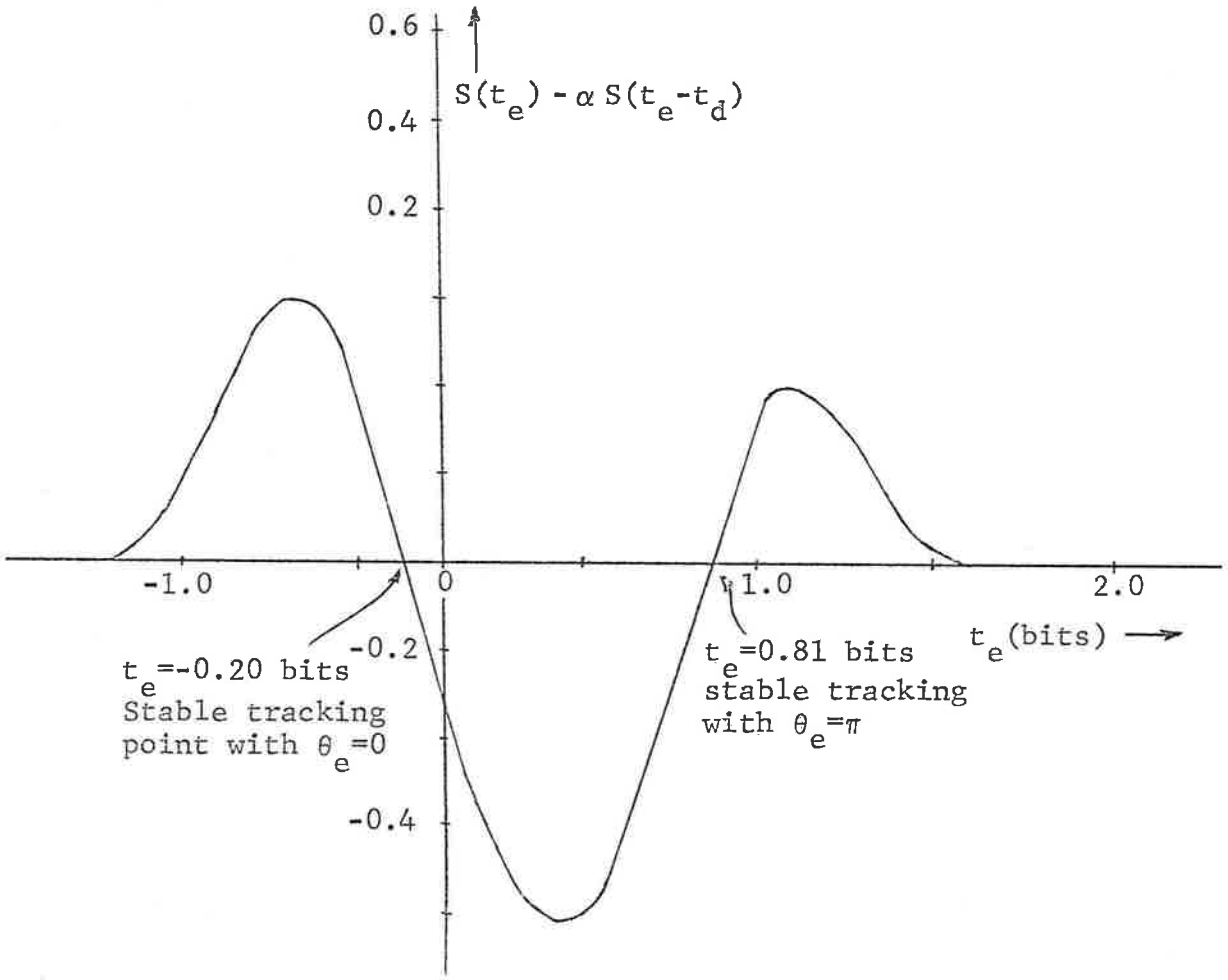

Figure D.4 Open Loop Error Voltage, α=0.7, t_d=0.5, θ_m=π

We will begin by referring back to Fig. D.3 which shows tracking points for fixed multipath phases. It is interesting to observe that for $0.1 \leq t_e < 1.1$ two tracking points exist for $\theta_m=\pi$ while only one exists for $\theta_m=0$. Clearly only one complete solution of the form of (D.10) can exist if there is only one fixed-phase solution at $\theta_m=0$. The presence of a second fixed-phase solution at $\theta_m=\pi$ indicates the presence of a partial solution to the varying-phase problem in the vicinity of $\theta_m=\pi$; however, this will not be considered further at present.

The technique used to calculate solutions of the form (D.16) is to begin with the known (fixed phase) solution at $\theta_m=0$. These values of t_e and θ_e are used as the starting point for computing a solution at $\theta_m=\Delta$ by means of the Newton-Raphson technique. The process is then repeated, using the solution at $\theta_m=\Delta$ as a starting point for finding a solution at $\theta_m=2\Delta$, and so forth. In the results to be presented, the step size Δ was chosen to be 10^o.

A set of solutions obtained in the above manner is shown in Fig. D.5. These solutions are for the case $t_d = 0.5$ chip. For small values of the relative amplitude α the solutions are approximately ellipses in the $\theta_e - t_e$ plane; this is the high direct-scatter approximation obtained in Appendix C. For larger values of α the trajectories are no longer elliptical.

D.4 Calculation of Correlation Functions

The detailed behavior of the carrier tracking loop in a PN receiver is determined by the correlation function R(t) of the received PN sequence and the locally generated replica.

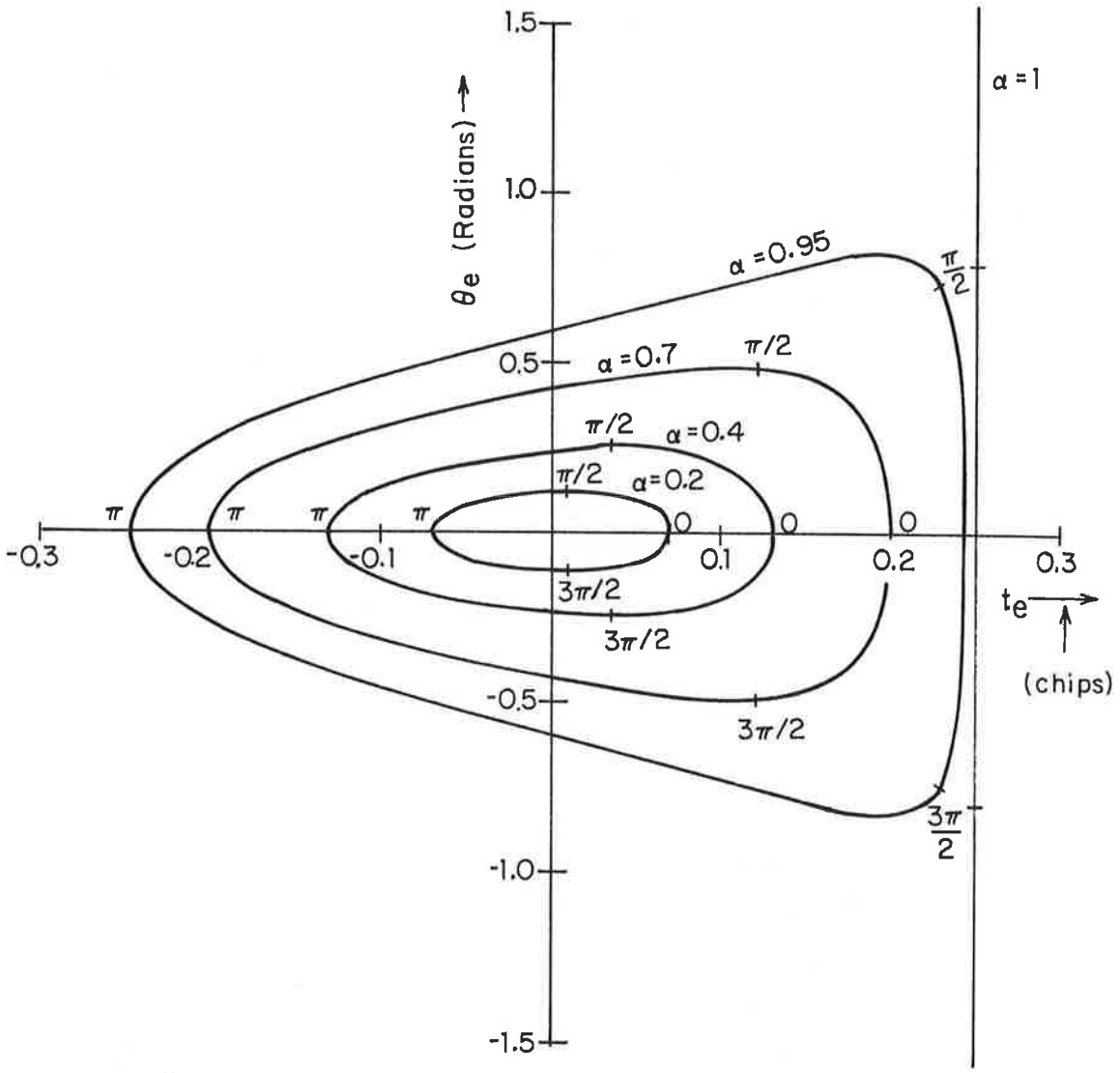

Figure D.5 Phase and Timing Error Trajectories ($t_d = 0.5$) (Points on the Trajectories Corresponding to $\theta_m = 0$, $\pi/2$, π, and $3\pi/2$ are Indicated)

Similarly, the behavior of the code tracking loop is determined by the correlation function S(t) of the received sequence and the output of the split-gate circuit. In this appendix we calculate these correlation functions for the case in which the received sequence has been passed through a linear filter with a Gaussian transfer function.

The receiver waveforms x(t) and y(t) are shown in Fig. D.6; x(t) is the PN output waveform and y(t) is the split-gate output waveform. The waveform r(t) of the received sequence is the result of passing x(t) through a linear filter with impulse response $h_{BP}(t)$; that is,

$$r(t) = x(t) * h_{BP}(t) \quad . \tag{D.17}$$

where

$$h_{BP}(t) = \frac{1}{2\sqrt{\pi\alpha}} e^{-t^2/4\alpha} \quad . \tag{D.18}$$

The transform of h(t) is given by

$$H_{BP}(\omega) = e^{-\alpha\omega^2} \tag{D.19}$$

The parameter α may be expressed in terms of the transfer function's 3 dB point:

$$\alpha = \frac{\log_e 2}{2\omega_{3\ dB}^2} \tag{D.20}$$

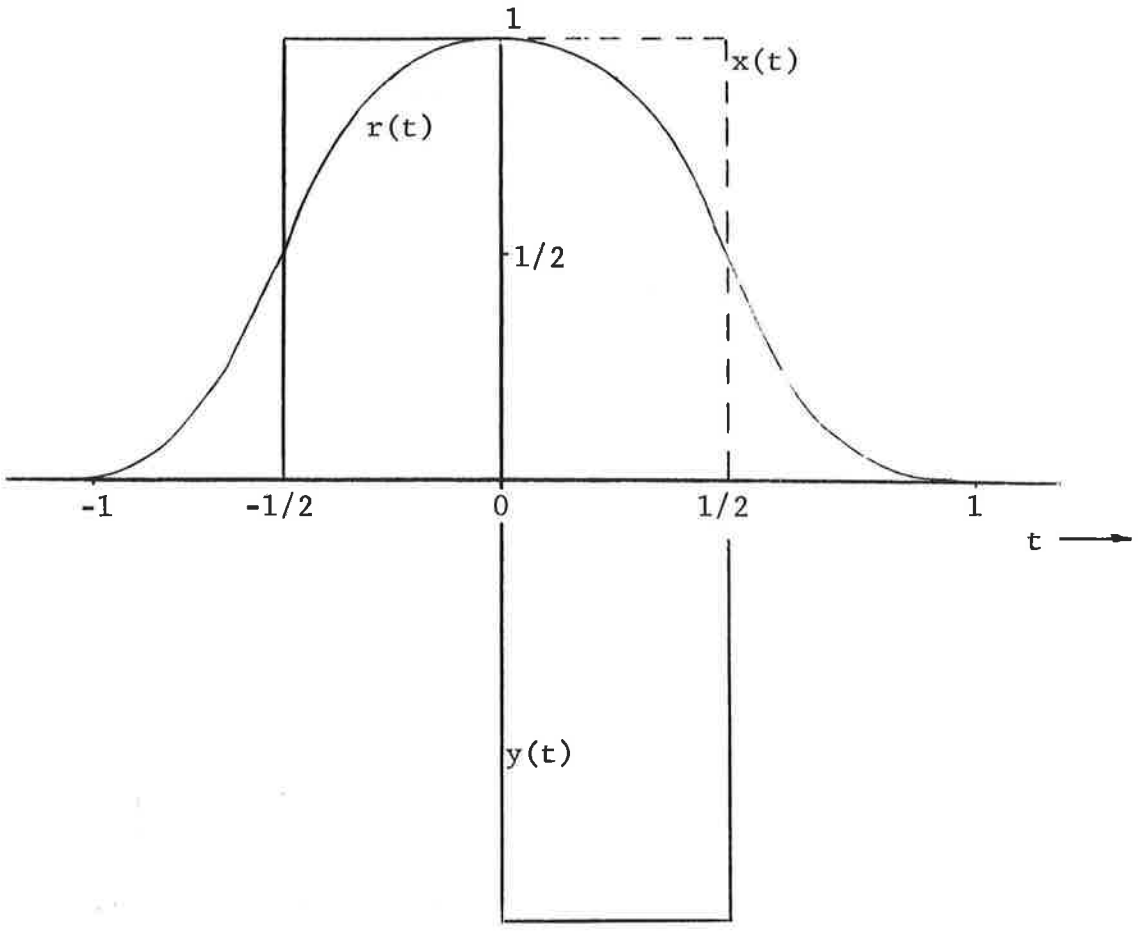

Figure D.6 Receiver Pulse Shapes

Substituting the transfer function of (D.19) into Eq. (D.17) it is readily found that

$$r(t) = \frac{1}{2}\left[\operatorname{erfc}\left(\frac{t-1/2}{2\sqrt{\alpha}}\right) - \operatorname{erfc}\left(\frac{t+1/2}{2\sqrt{\alpha}}\right)\right] \qquad (D.21)$$

where the complementary error function is defined by

$$\operatorname{erfc} x = 1 - \operatorname{erf}(x) \qquad (D.22)$$

where

$$\operatorname{erf}(x) = \frac{2}{\sqrt{\pi}} \int_0^x e^{-t^2}\, dt \qquad (D.23)$$

and

$$\operatorname{erf}(-x) = -\operatorname{erf}(x) \qquad (D.24)$$

The desired correlation functions are given by

$$R(t) = x(t) * r(t) \qquad (D.25)$$

and

$$S(t) = y(t) * r(t) \qquad (D.26)$$

Both of these may be evaluated by substituting the appropriate waveforms and carrying out the indicated convolution. The laborious details will not be presented; the results are:

$$R(t) = t\ \mathrm{erfc}\left(\frac{t}{2\sqrt{\alpha}}\right) - \left(\frac{t-1}{2}\right)\mathrm{erfc}\left(\frac{t-1}{2\sqrt{\alpha}}\right)$$

$$- \left(\frac{t+1}{2}\right)\mathrm{erfc}\left(\frac{t+1}{2\sqrt{\alpha}}\right) - \sqrt{\frac{\alpha}{\pi}}\left[2e^{-t^2/4\alpha} - e^{-(t-1)^2/4\alpha} - e^{-(t+1)^2/4\alpha}\right]$$

(D.27)

$$S(t) = (t+1/2)\ \mathrm{erfc}\left(\frac{t+1/2}{2\sqrt{\alpha}}\right) - (t-1/2)\ \mathrm{erfc}\left(\frac{t-1/2}{2\sqrt{\alpha}}\right)$$

$$+ \left(\frac{t-1}{2}\right)\mathrm{erfc}\left(\frac{t-1}{2\sqrt{\alpha}}\right) - \left(\frac{t+1}{2}\right)\mathrm{erfc}\left(\frac{t+1}{2\sqrt{\alpha}}\right)$$

$$- \sqrt{\frac{\alpha}{\pi}}\left[2e^{-(t+1/2)^2/4\alpha} - 2e^{-(t-1/2)^2/4\alpha} + e^{-(t-1)^2/4\alpha} - e^{-(t+1)^2/4\alpha}\right]$$

(D.28)

(These results are plotted in Figs. D.7 and D.8.)

In order to apply the Newton-Raphson technique to solving the simultaneous loop equations, expressions for the derivatives of these functions will be required. These are readily obtained by differentiating; the results are

$$R'(t) = \mathrm{erfc}\left(\frac{t}{2\sqrt{\alpha}}\right) - \frac{1}{2}\mathrm{erfc}\left(\frac{t-1}{2\sqrt{\alpha}}\right) - \frac{1}{2}\mathrm{erfc}\left(\frac{t+1}{2\sqrt{\alpha}}\right)$$

(D.29)

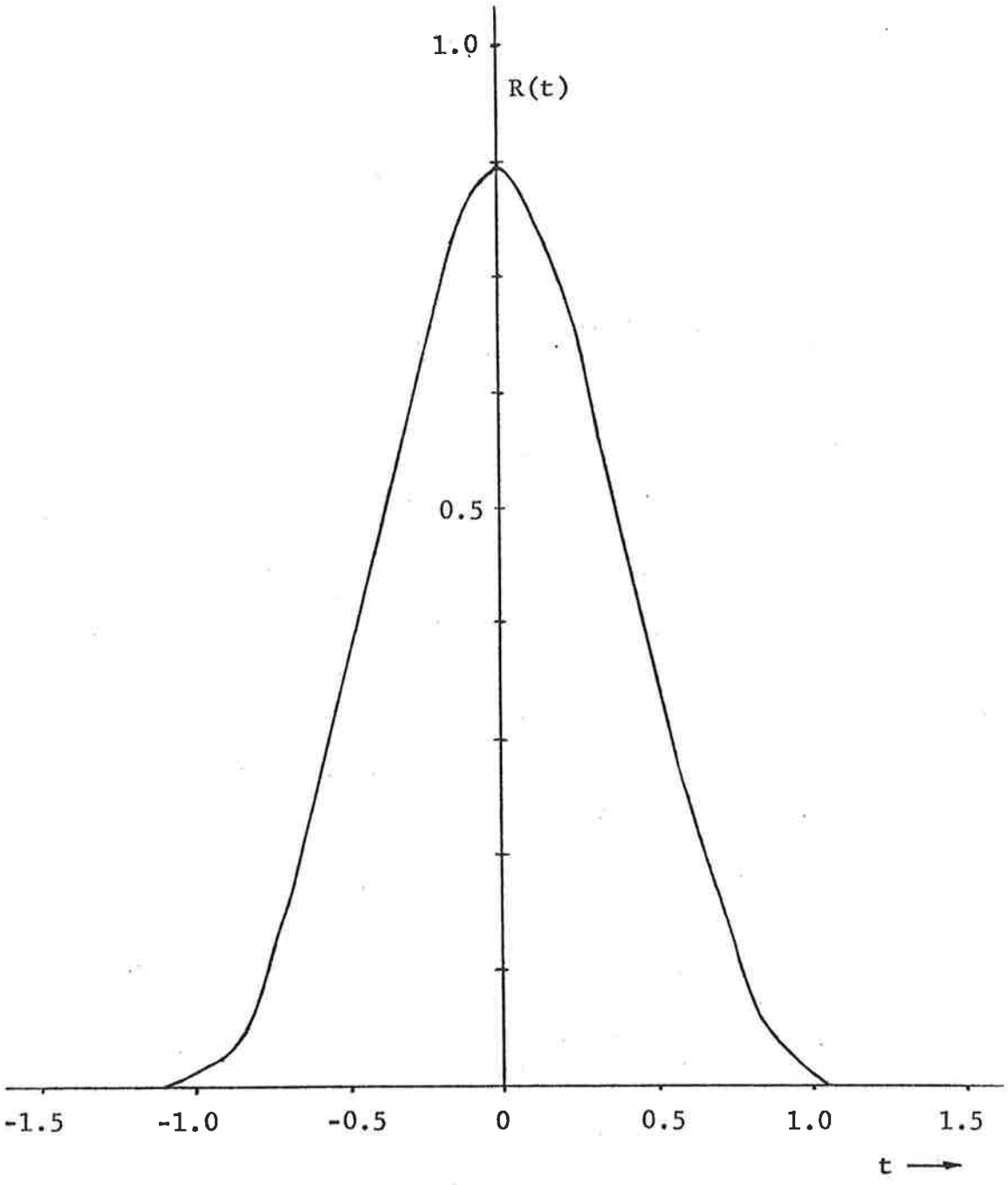

Figure D.7 The Correlation Function R(t)

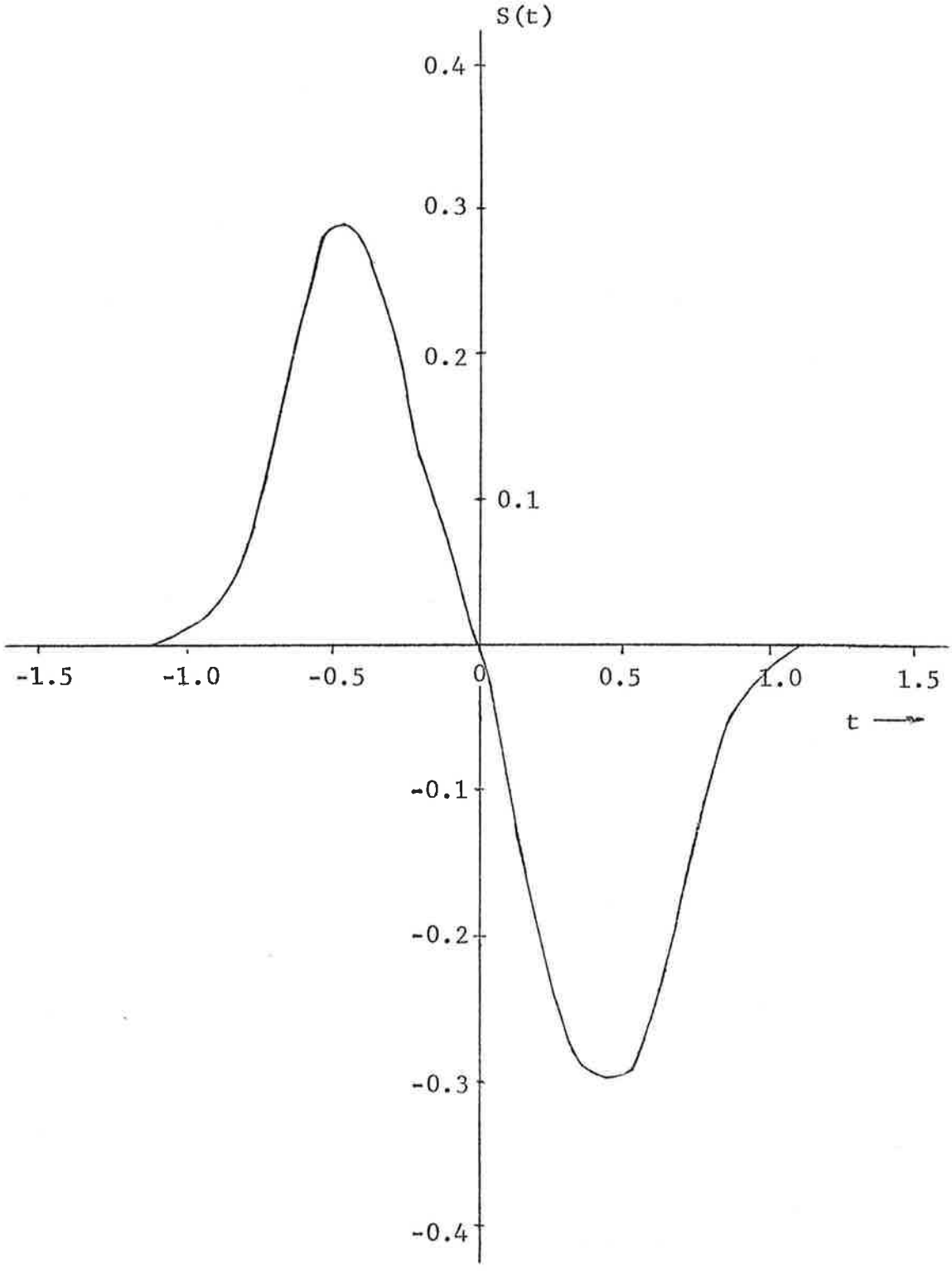

Figure D.8 The Correlation Function S(t)

and

$$S'(t) = \text{erfc}\ \left(\frac{t+1/2}{2\sqrt{\alpha}}\right) - \text{erfc}\ \left(\frac{t-1/2}{2\sqrt{\alpha}}\right) + \frac{1}{2}\ \text{erfc}\ \left(\frac{t-1}{2\sqrt{\alpha}}\right) - \frac{1}{2}\ \text{erfc}\ \left(\frac{t+1}{2\sqrt{\alpha}}\right) \tag{D.30}$$

In the analysis of additive noise performance another function appeared which depends on the receiver bandpass filtering. We calculate this function which is defined as

$$U = S_y(f) \otimes |H_{BP}(f)|^2|_{f=0} \tag{D.31}$$

where $S_y(f)$ is the power spectrum of the split-gate waveform $y(t)$ and $\otimes$ denotes convolution. It will be convenient to proceed from the alternate form

$$U = \int_{-\infty}^{\infty} R_y(\tau)(h_{BP}(\tau) \otimes h_{BP}(\tau))\ d\tau \tag{D.32}$$

The autocorrelation $R_y(\tau)$ is shown in Fig. D.9a; since $h_{BP}(\tau)$ is Gaussian, its self-convolution is Gaussian with twice the variance:

$$h_{BP}(\tau) * h_{BP}(\tau) = \frac{1}{2\sqrt{2\pi\alpha}}\ e^{-t^2/8\alpha} \tag{D.33}$$

The integral of Eq. (D.32) may now be carried out, giving

$$U = 1 - 2\,\mathrm{erfc}\left(\frac{1}{4\sqrt{2\alpha}}\right) + \mathrm{erfc}\left(\frac{1}{2\sqrt{2\alpha}}\right)$$

$$- \sqrt{\frac{\alpha}{2\pi}}\left(3 - 4e^{-1/32\alpha} + e^{-1/8\alpha}\right) \qquad \text{(D.34)}$$

The value of U decreases as the bandwidth of the filter decreases, as may be seen from Fig. D.9b.

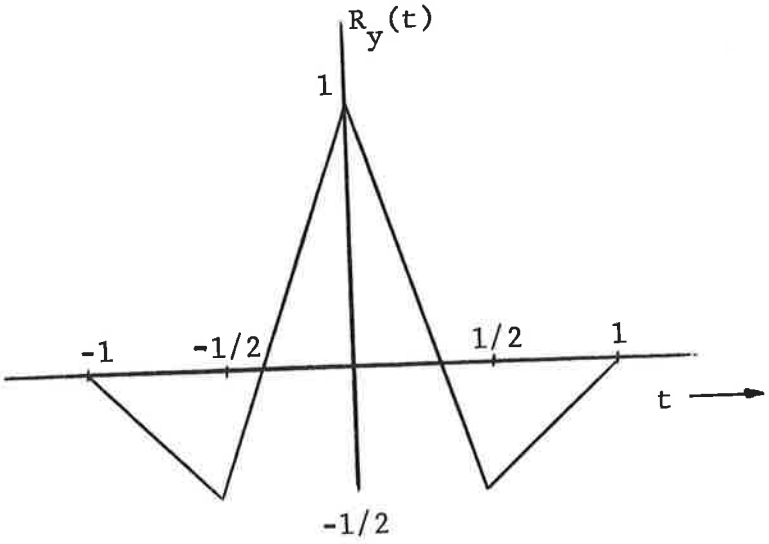

a) $R_y(t)$, The Autocorrelation of y(t)

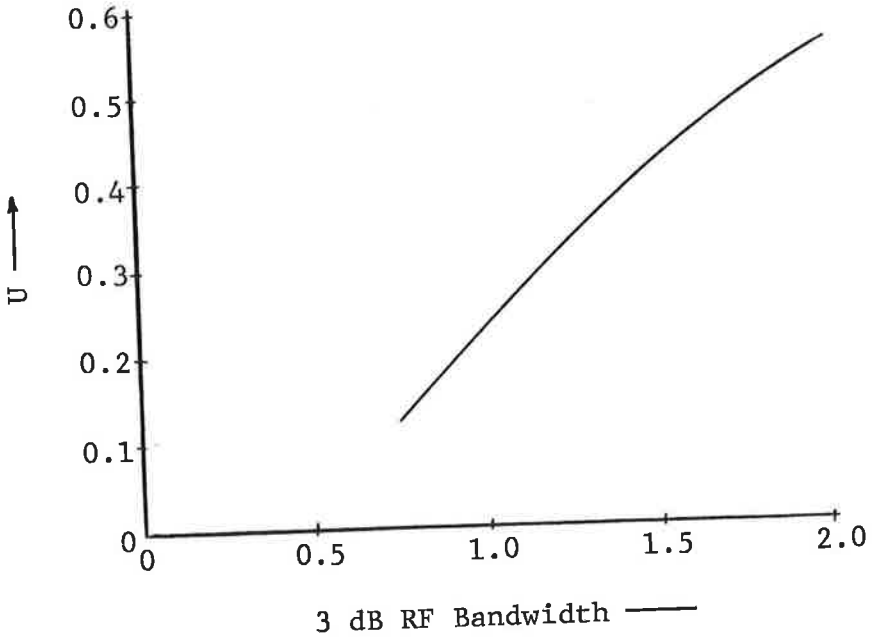

b) The Factor U as a Function of Filter Bandwidth

Figure D.9 Functions Related to Performance in Additive Noise

Appendix E

EFFECT OF GROUP DELAY TRACKING ERROR ON PLAYBACK CHANNEL SIMULATION*

E.1 Introduction

Playback channel simulation involves the measurement of the time variant transfer function of a communication channel for a limited time and bandwidth followed by a laboratory regeneration or playback of the previously measured transfer function. When there is relative movement between the terminals of the measured channel a time-varying group delay is produced. Provision must be made to accommodate this group delay variation in the playback and channel probing equipment. One may identify an active and a passive method of accommodation. In the passive case the equipment is designed as if the multipath spread were equal to the sum of the actual multipath spread plus the maximum variation in group delay. In the active case the equipment is designed for the correct multipath spread but compensating time-varying delays are introduced to effectively remove the time-varying group delay from the played back channel. In this appendix we investigate the effect of a group delay tracking error on playback channel simulation.

E.2 Channel Modeling With Time-Variable Group Delay

The channel is assumed to consist of a direct path plus reflections from a number of surrounding objects. Since the path delay associated with any reflection is always less than the direct transmitter-receiver path delay, one may express

*The material in this appendix was generated by P. Bello under Contract DOT-TSC-84. It is included here because of its general unavailability and its importance in the design of the prober.

the delay of each reflected signal as the sum of the direct path delay and a positive delay. Then the channel may be expressed conveniently as the cascade of two channels (or mathematical operations), a channel providing a pure time-variable delay equal to the direct path delay, and a hypothetical channel whose direct path has zero delay. If $\tau_d(t)$ denotes the time-variant delay associated with the direct path, then the corresponding pure-delay channel has a (low-pass equivalent) time-variant transfer function

$$H_d(f,t) = e^{-j2\pi f \tau_d(t)} e^{-j2\pi f_0 \tau_d(t)} \qquad \text{(E.1)}$$

where f_0 is the carrier frequency. The second exponential factor corresponds to the time-variant Doppler shift that would be observed on the direct path. The time-variant impulse response associated with the direct path channel is the Fourier transform

$$h_d(t,\xi) = \int H_d(f,t) e^{-j2\pi f \xi} \, df$$

or

$$h_d(t,\xi) = e^{-j2\pi f_0 \tau_d(t)} \delta(\xi - \tau_d(t)) \qquad \text{(E.2)}$$

where $\delta(\cdot)$ is the unit impulse function.

The second component channel with zero direct path delay is defined to have time-variant transfer function $H_0(f,t)$ and time-variant impulse response $h_0(t,\xi)$. With these definitions the actual channel time-variant impulse response is represented by the convolutions (on ξ)

$$h(t,\xi) = h_d(t,\xi) \otimes h_0(t,\xi)$$
$$= \delta(\xi - \tau_d(t))e^{-j2\pi f_0 \tau_d(t)} \otimes h_0(t,\xi) \quad \text{(E.3)}$$

E.3 Prober System Modeling

Figure E.1 provides a block diagram of the basic (complex-equivalent) operations of the prober system including the propagation channel (but not the additive noise which is not pertinent to the present discussion). The functions $h_T(\cdot)$, $h_R(\cdot)$ are the (complex-equivalent) impulse responses of the filtering operations in the transmitter and receiver, respectively. The complex envelope of the probing signal is $z(t)$. We denote the correlation operation of the receiver to produce the k'th tap output as a multiplication of the receiver output by $z^*(t-\tau_r(t)-k\Delta)$ followed by low-pass filtering. The time-variant delay $\tau_r(t)$ should equal $\tau_d(t)$ if the tracking or compensation is perfect.

Some simplification in the representation of the operation in Fig. E.1 is possible because the rate of variation of both the direct path delay $\tau_d(t)$ and the fading associated with Doppler shifts in the channel are negligible in a time interval of the order of the time constants of the transmitter and receiver filters and the multipath spread of the channel. Then one may conveniently lump the transmitter and receiver filters together and shift the direct path time-variant Doppler shift so that the prober signal processing operations appear as in Fig. E.2 where $e(\xi)$ is an equivalent filter combining the effects of the transmitter and receiver filters,

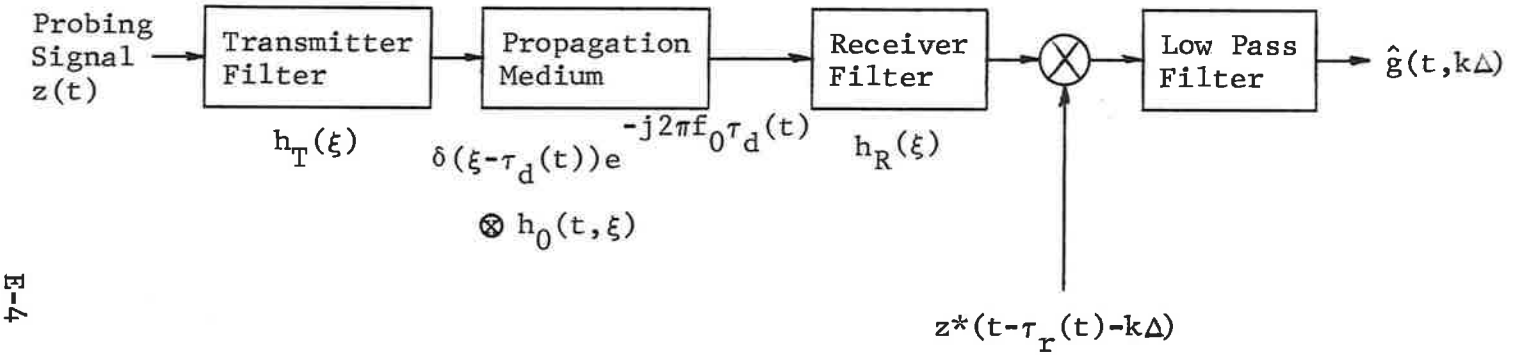

Figure E.1 Basic (Complex-Equivalent) Signal Processing Operations in Prober

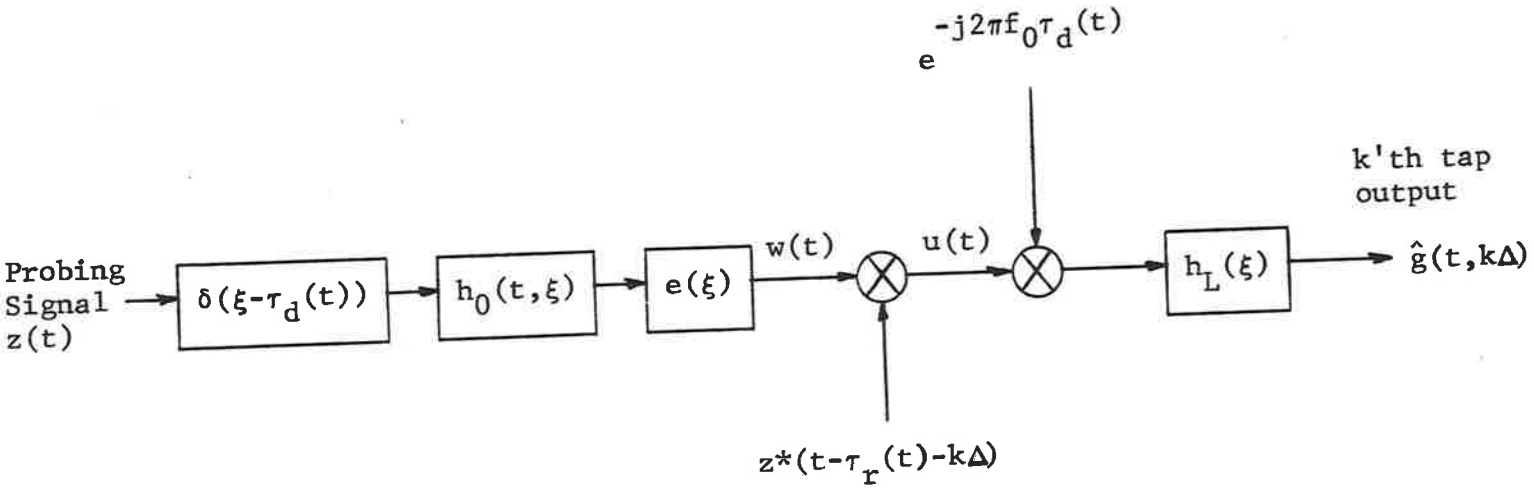

Figure E.2 Rearranged Signal Processing Operations of Prober

$$e(\xi) = h_T(\xi) \otimes h_R(\xi) \tag{E.4}$$

We further combine the "external" filter $e(\xi)$ with the channel $h_0(t,\xi)$, by defining

$$g(t,\xi) = h_0(t,\xi) \otimes e(\xi) \tag{E.5}$$

Then the prober output prior to correlation processing may be expressed as

$$w(t) = \int z(t-\xi-\tau_d(t))g(t,\xi)\, d\xi \tag{E.6}$$

After multiplication by the prober reference waveform, the result is

$$\mu(t) = \int z^*(t-k\Delta-\tau_r(t))z(t-\xi-\tau_d(t)g(t,\xi)\, d\xi \tag{E.7}$$

The probing signal is periodic with period T. Thus $z^*(t-\tau_1)z(t-\tau_2)$ may be shown to be periodic with period T with the Fourier series expansion

$$z^*(t-\tau_1)z(t-\tau_2) = \Sigma\, C_n e^{j2\pi \frac{n}{T} t} \tag{E.8}$$

where the Fourier coefficient is given by

$$C_n = X(\tau_1-\tau_2, \tfrac{n}{T})e^{-j2\pi \frac{n}{T} \tau_1} \tag{E.9}$$

and

$$X(\xi,\nu) = \frac{1}{T} \int_0^T z^*(t)z(t+\xi)e^{-j2\pi\nu t}\, dt \tag{E.10}$$

is the periodic complex ambiguity function of the probing signal.

Using (E.8) - (E.10) in (E.7) with

$$\tau_1 = k\Delta + \tau_r(t) \tag{E.11}$$

$$\tau_2 = \xi + \tau_d(t) \tag{E.12}$$

$$d(t) = \tau_r(t) - \tau_d(t) \tag{E.13}$$

we find that $\mu(t)$ may be expressed as a sequence of time functions which for $d(t) = 0$ occupy different zonal bands,

$$\mu(t,k\Delta) = \sum_{n=-\infty}^{\infty} e^{j2\pi \frac{n}{T}(t-k\Delta-\tau_r(t))} \int X(k\Delta-\xi + d(t), \tfrac{n}{T})g(t,\xi)\, d\xi \tag{E.14}$$

The n=0 term is the desired term and the other terms are cross talk or self noise. We shall develop conditions under which the self noise at the low pass filter output is negligible. However first consider the n=0 term,

$$\mu_0(t,k\Delta) = \int X(k\Delta-\xi + d(t),0)g(t,\xi)\, d\xi$$

$$= \int R(k\Delta + d(t) - \xi)g(t,\xi)\, d\xi \tag{E.15}$$

where

$$R(\xi) = \frac{1}{T}\int_0^T z^*(t)z(t+\xi)\, d\xi \tag{E.16}$$

is the auto correlation function of the periodic probing signal. Since the integral (E.15) is a convolution on ξ it may be expressed in the frequency domain as

$$\mu_0(t,k\Delta) = \int P(f)G(f,t)e^{j2\pi fd(t)}e^{j2\pi fk\Delta}\,df \qquad (E.17)$$

The output of the low pass filter is given by

$$\hat{g}(t,k\Delta) = \sum_{n=-\infty}^{\infty} \hat{g}_n(t,k\Delta) \qquad (E.18)$$

where

$$\hat{g}_n(t,k\Delta) = \mu_n(t,k\Delta) \otimes h_L(t) \qquad (E.19)$$

and

$$\mu_n(t,k\Delta) = e^{-j2\pi f_0\tau_d(t)}\, e^{j2\pi \frac{n}{T}(t-k\Delta-\tau_r(t))} \int X(k\Delta + d(t) - \xi, \tfrac{n}{T})g(t,\xi)\,d\xi \qquad (E.20)$$

Consider now the case n=0.

$$\hat{g}_0(t,k\Delta) = \mu_0(t,k\Delta) \otimes h_L(t)$$

$$= \int P(f)\{G_1(f,t)e^{j2\pi fd(t)} \otimes h_L(t)\}e^{j2\pi fk\Delta}\,df \qquad (E.21)$$

where we have let exp $[-j2\pi f_0\tau_d(t)]$ be absorbed in G(f,t), i.e.,

$$G_1(f,t) = G(f,t) \exp\,[-j2\pi f_0 \tau_d(t)] \qquad \text{(E.22)}$$

The low pass filter passband has been chosen wide enough to accommodate the Doppler spreads and shifts of the channel. As a consequence

$$G_1(f,t) \otimes h_L(t) = G_1(f,t) \qquad \text{(E.23)}$$

The presence of the factor exp [j2πfd(t)] in (E.20) prevents our making use of (E.23). In determining the effect of this exponential factor we must consider two cases

1. continuous delay tracking
2. discrete delay tracking.

For continuous delay tracking not only $\tau_d(t)$ but also $\tau_r(t)$ will be smooth slowly varying functions which have an essentially linear variation over intervals of time much longer than the time constant of $h_L(t)$. This means that d(t) produces a slowly time varying extremely small frequency shift on G(f,t) which is completely passed through the low pass filter, i.e.,

$$e^{j2\pi fd(t)} G_1(f,t) \otimes h_L(t) \approx e^{j2\pi fd(t)} G_1(f,t)$$

; continuous delay tracking

(E.24)

and

$$\hat{g}_0(t,k\Delta) = \mu_0(t,k\Delta) \;\text{; continuous delay tracking} \qquad \text{(E.25)}$$

In the case of discrete delay tracking a digital implementation attempts to vary $\tau_r(t)$ with small steps to approximate the smooth variation of $\tau_d(t)$. Then d(t) will contain jumps at the steps in $\tau_r(t)$. Note, however, that the time between jumps will be extremely large compared to the time constant of $h_L(t)$, and thus, except for the very small time intervals during which transient responses due to phase jumps in exp [j2πfd(t)] occur, Eq. (E.24) will still be valid. One may readily compute the effects of these jumps on $\hat{g}_0(t,k\Delta)$, but for the purpose of bounding the size of the error introduced in the played back channel, what is most important is the size of the change in phase of exp [j2πfd(t)] rather than the time for the change to take place, since the phase error lasts for a much longer time than the transient intervals. The low pass filter can be designed to assure a smooth transition without significant overshoot as the phase of exp [j2πfd(t)] jumps. To simplify our subsequent analysis we shall let the phase transition occur abruptly and ignore the smooth transition caused by the low pass filter. Thus, whether for continuous or discrete delay tracking we shall use

$$\hat{g}_0(t,k\Delta) = \mu_0(t,k\Delta) \tag{E.26}$$

in our error analysis.

We now consider the self noise terms. The typical self noise term is the time function $\mu_n(t,k\Delta)$ filtered by the low pass filter $h_L(t)$. As in the n=0 case, we must separately consider the continuous and discrete delay tracking cases.

When $d(t) = 0$, $\mu_n(t,k\Delta)$ will be a narrow-band process centered near the frequency n/T Hz. Its spectral width will be determined by the Doppler spread of the channel and its spectral location relative to n/T Hz will be determined by the Doppler shifts of the channel. Since these are known and since T was chosen so that there would be plenty of empty spectrum between $\mu_n(t,k\Delta)$ and $\mu_m(t,k\Delta)$, $m \neq n$, the low pass filter is readily designed to pass $\mu_0(t,k\Delta)$ and completely reject $\mu_n(t,k\Delta)$ = $n \neq 0$, when $d(t) = 0$. When $d(t) \neq 0$ but continuous tracking is used the bandwidth occupancy of the function $\mu_n(t,k\Delta)$ is not changed significantly from the case $d(t) = 0$. The low pass filter will then reject $\mu_n(t,k\Delta)$.

In the case of discrete delay tracking the function $\mu_n(t,k\Delta)$ differs in character from the case of continuous delay tracking only in the transient interval following the delay jump. This transient interval is of the order of the duration of the impulse response of the low pass filter. Outside the delay-jump transient interval $\mu_n(t,k\Delta)$ will be completely rejected by the low pass filter. As discussed before the time interval between jumps is orders of magnitude greater than the time constant of $h_L(t)$. Thus the vast majority of time the self noise will be suppressed. Let us bound the self noise occuring during the transient intervals.

The effect of the delay jump is to cause a sudden change in the complex amplitude of $\mu_n(t,k\Delta)$. The size of this change will depend upon the amount of delay jump. It is not difficult to see that the effect of a sudden change γ_n in the complex amplitude of $\mu_n(t,k\Delta)$ upon the output of the low pass filter may be estimated as the output of the low pass filter

produced by an input $\gamma_n \exp\left[j2\pi \frac{n}{T} t\right] U(t)$, where $U(t)$ is the unit step function. Approximating the spectrum of this input around f=0 by a constant over the passband of $h_L(t)$, this response becomes

$$p(t) = \frac{j\gamma_n}{2\pi n/T} h_L(t) \qquad (E.27)$$

We had previously normalized $H_L(f)$ to have unit amplitude at f=0, so that the area under $h_L(t)$ is unity. The peak value of $h_L(t)$ will then be of the order of the reciprocal time duration of $h_L(t)$ or the order of the bandwidth of $h_L(t)$. For a Gaussian shaped filter with an e^{-1} banewidth B (where the transfer function drops to e^{-1} of the zero frequency value), the peak value of $h_L(t)$ is $B\sqrt{2\pi}$. Thus

$$|\text{peak transient}| \approx |\gamma_n| \frac{1}{\sqrt{2\pi}} \cdot \frac{BT}{n} \qquad (E.28)$$

We now relate the size of γ_n to the size of the delay jump. First we note that γ_n, the jump in $\mu_n(t,k\Delta)$, is caused primarily by the change of d(t) in the integral of (E.20), since it may be shown that the product $2\pi \frac{n}{T} \tau_r(t)$ in the exponential factor will cause a negligible phase jump for the size of delay jumps in $\tau_r(t)$ that are anticipated (i.e., delay jumps of a small fraction of Δ).

The integral in (E.20) will be expressed in an alternate form to facilitate the analysis. By using (E.5) in (E.20) one may show that the integral in question can be expressed in the form

$$I = \int Y(k\Delta + d(t) - \xi, \frac{n}{T}) h_0(t,\xi)\, d\xi \qquad (E.29)$$

where $h_0(t,\xi)$ is the propagation medium impulse response and $Y(\xi,\nu)$ is the ambiguity function of a probing signal equal to the convolution of the original probing signal with the external filter impulse response e(t). Let us assume d(t) jumps from the value d_1 to $d_1 + \alpha\Delta$, where α is smaller than one. We may expand $Y(\cdot)$ in a Taylor series

$$Y(k\Delta + d_1 + \alpha\Delta - \xi, \frac{n}{T}) = Y(k\Delta + d_1 - \xi, \frac{n}{T}0 + \alpha\Delta \frac{\partial}{\partial\xi} Y(k\Delta + d_1 - \xi, \frac{n}{T}) + \ldots \qquad (E.30)$$

It follows that for small α,

$$|\gamma_n| \approx \alpha\Delta \left| \int \frac{\partial}{\partial\xi} Y(k\Delta + d_1 - \xi, \frac{n}{T}) h_0(t,\xi)\, d\xi \right| \qquad (E.31)$$

Note that γ_n is a random variable because $h_0(t,\xi)$ is a random process. The strength of γ_n is given by

$$\overline{|\gamma_n|^2} = \alpha^2\Delta^2 \iint \frac{\partial}{\partial\xi} Y^*(k\Delta + d_1 - \xi, \frac{n}{T}) \frac{\partial}{\partial\eta} Y(k\Delta + d_1 - \eta, \frac{n}{T}) \overline{h_0^*(t,\xi) h_0(t,\eta)}\, d\xi\, d\eta \qquad (E.32)$$

Since the channel is assumed WSSUS,

$$\overline{h_0^*(t,\xi) h_0(t,\eta)} = Q(\xi)\delta(\eta - \xi) \qquad (E.33)$$

we find that

$$\overline{|\gamma_n|^2} \leq \alpha^2\Delta^2 \operatorname*{Max}_{\xi} \left|\frac{\partial}{\partial \xi} Y(k\Delta + d_1 - \xi, \frac{n}{T})\right|^2 \int Q(\xi)\, d\xi \tag{E.34}$$

If the external filter produces only mild filtering of the probing signal, which is true in the present design, the ambiguity function $Y(\xi,\nu)$ will not differ significantly from $X(\xi,\nu)$. From the properties of $X(\xi,\nu)$ it may be deduced that

$$\operatorname*{Max}_{\xi} \left|\frac{\partial}{\partial \xi} X(\xi,\nu)\right|^2 \leq \frac{4}{N\Delta^2} \tag{E.35}$$

where N is the number of pulses in one period of the pseudo-random sequence. Thus (after normalizing the external filter to unity gain at midband) we bound

$$\overline{|\gamma_n|^2} \leq 4\alpha^2 \frac{1}{N} \int Q(\xi)\, d\xi \tag{E.36}$$

Using (E.28) the strengths of the peak transient due to the self noise component at n/T Hz is bounded by

$$\overline{|\text{peak transient}|^2} \leq \frac{\alpha^2}{2\pi} \frac{B^2T^2}{n^2N} \int Q(\xi)\, d\xi \tag{E.37}$$

There appears sufficient uncorrelatedness in the γ_n for different n to allow a summation of powers over n to compute the total bounding peak transient. Noting that

$$\sum_{n=1}^{\infty} \frac{1}{n^2} = \frac{\pi^2}{6} \tag{E.38}$$

we see that

$$P_{self} \equiv \overline{|\text{total peak transient}|^2} \leq \frac{\pi}{6} \alpha^2 \frac{B^2T^2}{N} \int Q(\xi)\, d\xi \tag{E.39}$$

The strength of the desired signal at the k'th tap output is

$$S_k = \Delta Q(k\Delta) \tag{E.40}$$

which leads to a signal to peak transient self noise bound of

$$\rho_{self} = \frac{S_k}{P_{self}} \geq \frac{6}{\pi} \cdot \frac{N}{\alpha^2 B^2 T^2} \cdot \frac{\Delta Q(k\Delta)}{\int Q(\xi)\, d\xi} \tag{E.41}$$

For uniformly distributed multipath over L seconds

$$\rho_{self} \geq \frac{6}{\pi} \cdot \frac{N}{\alpha^2 B^2 T^2} \cdot \frac{\Delta}{L} \tag{E.42}$$

We return now to a determination of the effect of delay jumps upon the output of the played-back channel. In this determination we assume that the self-noise has been reduced to an acceptable level by utilizing a sufficiently small value of α. The primary effect of the delay jump is then on the filtered tap output $\hat{g}_0(t,k\Delta)$. For reconstruction of the channel $\hat{g}_0(t,k\Delta)$ is used as the k'th complex gain on a tapped delay line. With an input s(t) having spectrum S(f) confined to a bandwidth over which the channel playback and

probing equipment has flat response, the playback channel output w(t) is given by (see Eqs. (E.21), (E.22), and (E.25))

$$w(t) = \int_{-\frac{W}{2}}^{\frac{W}{2}} S(f)G_1(f,t)e^{j2\pi fd(t)}e^{j2\pi ft}\,df \qquad (E.43)$$

where W is the bandwidth of the input. For

$$\pi W d(t) \ll 1 \qquad (E.44)$$

the exponential in (E.43) may be expanded in a Taylor series and the series integrated term by term to yield

$$w(t) = s_0(t) + d(t)s_0(t) + \ldots \qquad (E.45)$$

The strength of the first term relative to the second is given by

$$\rho_1 = \frac{1}{\frac{\pi}{3}\alpha^2\Delta^2W^2} \qquad (E.46)$$

for a rectangular input spectrum and a delay jump of $\alpha\Delta$.

Appendix F

EFFECT OF TAP CORRELATOR GAIN AND PHASE INSERTION ON STORED CHANNEL FIDELITY

F.1 Introduction

The measurement of a channel with the correlation technique involves the measurement of a sampled, complex, low-pass equivalent impulse response. We are concerned in this appendix with the effect of differential phase and gain insertions introduced by the set of correlators which attempt to sample the impulse response in time delay. These differential phase shifts and gains will cause errors in the transfer function of the stored channel techniques.

F.2 Analysis

We consider first the case of insertion phase errors and then proceed by analogy to the case of insertion gain.

The sampled impulse response of the channel can be expressed in the form

$$g(t,\xi) = \sum_{k=1}^{K} g_k(t)\delta(\xi-k\Delta) \qquad (F.1)$$

The effect of phase errors causes the measured impulse response to take the form

$$h(t,\xi) = \sum_{k=1}^{K} g_k(t)e^{j\theta_k}\delta(\xi-k\Delta) \qquad (F.2)$$

Since only phase insertion differences are of importance we express the phase errors in the form

$$\theta_k = \phi_k - \overline{\phi}_k \qquad \text{(F.3)}$$

where ϕ_k is the phase insertion of the k'th correlator and $\overline{\phi}_k$ is the average phase shift of the set of phase insertions.

Defining the transfer functions

$$G(f,t) = \Sigma\, g_k(t) e^{-j2\pi k\Delta f} \qquad \text{(F.4)}$$

$$H(f,t) = \Sigma\, g_k(t) e^{j\theta k} e^{-j2\pi k\Delta f} \qquad \text{(F.5)}$$

the error in the transfer function is

$$E(f,t) = H(f,t) - G(f,t)$$

$$= \Sigma\, g_k(t)(e^{j\theta_k} - 1) e^{-j2\pi k\Delta f} \qquad \text{(F.6)}$$

For small phase insertion difference this becomes

$$E(f,t) \approx \sum_1^K \theta_k g_k(t) e^{-j2\pi k\Delta f} \qquad \text{(F.7)}$$

If we assume that the channel gains are independent with strengths

$$\overline{|g_k|^2} = \sigma_k^2 \qquad \text{(F.8)}$$

then the mean squared value of the transfer function error becomes

$$\overline{|E(f,t)|^2} = \sum_1^K \theta_k^2 \sigma_k^2 \qquad \text{(F.9)}$$

which is independent of frequency. The average channel gain at any frequency is

$$\overline{|G(f,t)|^2} = \sum_1^K \sigma_k^2 \qquad \text{(F.10)}$$

Thus if the mean squared value of the transfer function error is normalized to the mean squared value of the true transfer function we obtain the normalized error

$$e = \frac{\sum_1^K \theta_k^2 \sigma_k^2}{\sum_1^K \sigma_k^2} \qquad \text{(F.11)}$$

If the delay power spectrum is uniform, i.e.,

$$\sigma_k^2 = \sigma^2 \qquad \text{(F.12)}$$

then the normalized error becomes

$$e = \frac{1}{K} \sum_1^K \theta_k^2 = \frac{1}{K} \sum_1^K (\phi_k - \overline{\phi}_k)^2 \qquad \text{(F.13)}$$

which is a finite sample estimate of the variance of the phase insertion error difference. For large K this estimate will be close to the true variance, i.e.,

$$e \approx \overline{(\phi - \overline{\phi})^2} \equiv \sigma_\phi^2 \qquad \text{(F.14)}$$

The cross correlation between the error transfer function and the correct transfer function is

$$\overline{E^*(f,t)G(f,t)} = j \Sigma \sigma_k^2 \theta_k \qquad \text{(F.15)}$$

and for equal strength paths the magnitude of the normalized correlation coefficient is

$$\rho = \frac{\overline{|E^*(f,t)G(f,t)|}}{\sqrt{|E(f,t)|^2 |G(f,t)|^2}}$$

$$= \frac{|\Sigma \theta_k|}{\sqrt{N \Sigma \theta_k^2}} \longrightarrow 0 \text{ for large } N \qquad \text{(F.16)}$$

Thus the error transfer function is essentially uncorrelated with the desired transfer function.

The analysis of the effect of differential insertion gain errors is entirely analogous because the impulse response with differential gain error may be expressed in the form

$$h(t,\xi) = \sum_{k=1}^{K} g_k(t) r_k \delta(\xi - k\Delta) \qquad \text{(F.17)}$$

and the error in the played back transfer function by

$$E(f,t) = \sum_{k=1}^{K} g_k(t)(r_k - 1)e^{-j2\pi k\Delta f} \qquad \text{(F.18)}$$

Since common tap gain changes are irrelevant we set

$$r_k = s_k - \bar{s}_k + 1 \tag{F.19}$$

which $\bar{s}_k$ is the average tap gain and define

$$r_k - 1 = \epsilon_k \tag{F.20}$$

as the differential gain error.

Thus

$$E(f,t) = \sum_{k=1}^{K} \epsilon_k g_k(t) e^{-j2\pi k\Delta f} \tag{F.21}$$

The mathematical form of (F.21) is identical to that of (F.7). Thus we may immediately express the normalized mean squared error in reproduction of the transfer function as

$$e = \frac{\sum_{k=1}^{K} \epsilon_k^2 \sigma_k^2}{\sum_{1}^{K} \sigma_k^2} \tag{F.22}$$

For a uniform delay power spectrum

$$e = \frac{1}{K} \sum_{1}^{K} \epsilon_k^2 \approx \sigma_\epsilon^2 \tag{F.23}$$

Also, by analogy, the error in the reproduced transfer function will be uncorrelated with the desired transfer function.

Appendix G
SCATTERING FUNCTION FOR GENERAL VELOCITY VECTOR

The scattering function for a general velocity vector is most easily derived by defining new variables

$$t = \frac{x}{S} \cos \Phi + y \sin \Phi \tag{G.1}$$

$$r = -\frac{x}{S} \sin \Phi + y \cos \Phi \tag{G.2}$$

where $S = \sin \theta$ and

$$\frac{\nu_y}{\nu_\theta} = \tan \Phi \tag{G.3}$$

In terms of these new variables the normalized delay and Doppler shift variables are

$$\delta = \frac{S}{2} [t^2 + r^2] \tag{G.4}$$

$$\omega = S\sqrt{\nu_y^2 + \nu_\theta^2}\, t \tag{G.5}$$

Using the random variable interpretation of x,y as zero mean unit variance Gaussian variables, t and r become zero mean correlated variables with joint density function

$$W_1(t,r) = \frac{1}{2\pi\sigma_t\sigma_r\sqrt{1-\rho^2}} \exp\left\{-\frac{1}{2(1-\rho^2)}\left(\frac{t^2}{\sigma_t^2} + \frac{r^2}{\sigma_r^2} - \frac{2\rho rt}{\sigma_r\sigma_t}\right)\right\} \tag{G.6}$$

where

$$\sigma_t^2 = \frac{\nu_\theta^2/S^2 + \nu_y^2}{\nu_y^2 + \nu_\theta^2} \qquad (G.7)$$

$$\sigma_r^2 = \frac{\nu_y^2/S^2 + \nu_\theta^2}{\nu_y^2 + \nu_\theta^2} \qquad (G.8)$$

$$\rho = \frac{-\cos^2\theta\ \nu_y \nu_\theta}{\sqrt{(\nu_\theta^2 + S^2\nu_y^2)(\nu_y^2 + S^2\nu_\theta^2)}} \qquad (G.9)$$

The Jacobian of the transformation between δ,ω and t,r is quickly found to be

$$J(\delta,\omega) = \frac{1}{S^2\sqrt{\nu_y^2 + \nu_\theta^2}\sqrt{\frac{2\delta}{S} - \frac{\omega^2}{S^2(\nu_y^2 + \nu_\theta^2)}}} \qquad G(.10)$$

Note that for each ω,δ there are two pairs of values t,r

$$t = \frac{\omega}{S\sqrt{\nu_y^2 + \nu_\theta^2}} \quad , \quad r = \pm\sqrt{\frac{2\delta}{S} - \frac{\omega^2}{S^2(\nu_y^2 + \nu_\theta^2)}} \qquad (G.11)$$

It follows that the scattering function

$$S_0(\delta,\omega) = J(\delta,\omega)\left\{W_1\left(\frac{\omega}{S\sqrt{\nu_y^2+\nu_\theta^2}}\ ,\ \sqrt{\frac{2\delta}{S}-\frac{\omega^2}{(S^2/\nu_y^2+\nu_\theta^2)}}\right)\right.$$

$$\left. + W_1\left(\frac{\omega}{S\sqrt{\nu_y^2+\nu_\theta^2}}\ ,\ -\sqrt{\frac{2\delta}{S}-\frac{\omega^2}{S^2/\nu_y^2+\nu_\theta^2}}\right)\right\} \qquad (G.12)$$

where $J(\delta,\omega)$ is given by (G.10) and $W_1(t,r)$ is given by (G.6) with the parameters (G.7) - (G.9).

Appendix H
REPORT OF INVENTIONS

After a diligent review of the work performed under this contract, no new innovation, discovery, improvement or invention was made.